

**Exploring the role of a neuro-repellent protein, Semaphorin3A, in functional muscle
regeneration through premature satellite cell activation**

**by
Nasibeh Daneshvar**

**A Thesis submitted to the
Faculty of Graduate Studies of the University of Manitoba
in partial fulfilment of the requirements of the degree of
DOCTOR OF PHILOSOPHY**

**Department of Biological Sciences
University of Manitoba
Winnipeg**

Copyright © 2021 by Nasibeh Daneshvar

Contents

Acknowledgements	6
List of Figures	8
List of Tables	9
ABSTRACT	10
1.0 INTRODUCTION	12
1.1 Muscle	12
1.1.1 Skeletal Muscle Structure	14
1.1.2 Muscle Contraction	17
1.1.3 Myokines.....	18
1.1.4 A model muscle, Tibialis Anterior (TA).....	19
1.2 Satellite Cells	20
1.2.1 Structure and Location – the SC “Niche”	20
1.2.2 Quiescence and Activation of SCs.....	22
1.2.3 Patterns of gene expression.....	24
1.2.4 Therapeutic Potential	26
1.3 Muscle Damage and Regeneration	28
1.3.1 Functional Impairment of Muscle.....	28
1.3.2 Muscle Repair	28
1.3.3 Phases of Muscle Regeneration	30
1.3.4 Models of Muscle Injury.....	35
1.3.5 The General Timing of Muscle Repair and Tissue Remodeling.....	37
1.3.6 Age-Related Alterations in Muscle Regenerative Capacity.....	38
1.4 Neuromuscular Junctions (NMJs)	43
1.4.1 Development of NMJs	46
1.4.2 Innervation	47
1.4.3 Motor Units.....	48
1.4.4 Motor Units and Activity-Related Alterations.....	49
1.4.5 Fiber Typing – Impact of Nutrition on Development	52
1.4.6 Neurotrophic Factors (Neurotrophins).....	55
1.4.7 Consequences of Denervation.....	56
1.4.8 Growth Cones and Guidance Cues	57
1.4.9 Terminal Schwann cells (TSCs)	58

1.4.10 S100B and p75	60
1.4.11 Wallerian Degeneration	61
1.5 Semaphorin 3A	63
1.5.1 Sema3A and Myogenesis.....	63
1.5.2 Actions of Sema3A	64
1.5.3 AchR Expression and Clustering	66
1.5.4 Sema3A and AchR Clustering	67
1.6 Nitric Oxide and Muscle Regeneration.....	68
1.6.1 NO-Based Treatments.....	68
1.7 Rationale and Hypotheses.....	70
2 RESULTS - 1.....	73
2.1 Introduction.....	73
2.2 Methods.....	76
2.2.1 Myotube growth.....	77
2.2.2 NMJ maturation	77
2.2.3 Protein expression.....	78
2.2.4 Pax7+ Cell DNA synthesis	79
2.3 Antibody Information	79
2.4 Statistical Analysis.....	80
2.5 Results.....	80
2.5.1 Myotube growth.....	81
2.5.2 NMJ maturation	84
2.5.3 Protein expression.....	90
2.5.4 Pax7+ satellite cell DNA synthesis	94
2.6 Discussion	97
3 RESULTS-2.....	102
3.1 Abstract	102
3.2 Introduction.....	103
3.3 Rationale and Hypotheses.....	107
3.4 Materials and Methods.....	108
3.4.1 Manitoba experiments.....	108
3.4.2 Antibody Information	109
3.4.3 In situ hybridization	109

3.4.4	In situ hybridization combined with immunohistochemistry.....	113
3.4.5	Statistical Analysis.....	117
3.4.6	Principal Component Analysis.....	118
3.5	Results.....	119
3.5.1	Expression of mRNA transcripts and cell localization	119
3.5.2	Observations from <i>in situ</i> hybridization experiments	120
3.5.3	Number of mRNA expression sites	124
3.5.4	Intensity (areal density) of mRNA expression sites.....	127
3.5.5	Diameter of mRNA expression sites.....	130
3.5.6	P75 by Immunostaining in combination with ISH.....	133
3.5.7	Principal Component Analysis (PCA).....	137
3.6	Discussion	140
4	RESULTS-3.....	145
4.1	Abstract	145
4.2	Introduction.....	146
4.3	Materials and Methods.....	150
4.3.1	Animal treatment and surgery	151
4.3.2	TA Sample collection.....	153
4.3.3	Western Blotting	153
4.3.4	Antibody Information	153
4.3.5	In situ hybridization	154
4.3.6	Principal Component Analysis (PCA).....	154
4.4	Results.....	156
4.4.1	Western Blotting	159
4.4.2	In situ hybridization (ISH)	162
4.4.3	Principal Component Analysis.....	170
4.5	Discussion	176
5	CONCLUDING DISCUSSION	184
5.1	Future research.....	193
6	REFERENCES	195
	Appendix	221
7	EXPERIMENTAL METHODS AND MATERIALS	221
7.1	Mice and surgery.....	221

Crush injury:	221
Cardiotoxin (CTX) injection:.....	222
7.1.1 Tissue handling	223
7.2 Hematoxylin and Eosin staining	224
7.3 NMJ maturation	225
7.4 Protein-expression studies using Western Blotting	226
7.4.1 Protein Isolation and Assay.....	227
7.4.2 Protein Sample Preparation.....	228
7.4.3 Gel Electrophoresis.....	228
7.4.4 Developing the Membrane.....	228
7.4.5 Quenching the Membranes	229
7.5 Immunostaining	229
7.6 Antibody Information	230
7.7 Fluorescence immunostaining	230
7.8 The generation of Sema3A-Cko Mice	231
7.8.1 Tamoxifen preparation.....	231
7.9 In situ hybridization	232

Acknowledgements

I Would like to thank several individuals for their support and guidance throughout the duration of my PhD project. I greatly appreciate the prayer, encouragement, and confidence; without your help and inspiration this thesis would not have been as enjoyable, and successful.

I must begin by thanking my amazing family. Mom, Dad, Ahmad and Zahra thank you for always supporting me and encouraging my decisions and my education every step of the way. Wayne, thanks for supporting me and listening to my practices. I hope to be able to be there for you, as you were for me, in your future accomplishments.

To the rest of my family and friends – thanks for always being supportive and understanding, and accommodating when I needed you there. I hope to be there to support you when you need it, too.

To my advisor, Judy Anderson. I cannot thank you enough for all of your help, both professionally and personally. Starting in my first year, your experience and knowledge taught me fundamental lessons in striving for perfection and not sacrificing quality in a profession. Your boundless energy, cheerful enthusiasm, your set of values as well as your dedication and care for your individual students had a strong impact on me that I will carry forward into my career for years to come. Having a teacher like you made me realize the importance of open- and fair-mindedness, respect and understanding, all helped me develop into the person I am today.

To my advisory committee – Dr. Peeler, Dr. Anderson and Dr. Cornish. Thanks for your help and guidance. It was an absolute pleasure working with, your contributions are gratefully acknowledged.

To Dr. Tatsumi- Thank you for all your support, help and mentorship during my stay in Japan and my PhD journey. It was such a pleasure to work with you and your wonderful group and I look forward to work with you again in near future.

Last but not the least, I must thank my lab-members and the department – Ziba, Arfa, Alison, Dave, Cass and others. Your friendship, company, and support were there every day. I know we will remain friends for years to come.

This work was supported through funding provided by the Natural Sciences and Engineering Research Council of Canada, Graduate Enhancement of Tri-Council, University of Manitoba Graduate Fellowship and Mitacs Globalink Research Award.

List of Abbreviations:

AchR – acetylcholine receptor

AchE – acetylcholinesterase

BrdU - bromodeoxyuridine

BTX - α -bungarotoxin

CNS – central nervous system

CTX – cardiotoxin

CR – crush injury

D – day

DNA – deoxyribonucleic acid

FITC – fluorescein isothiocyanate

HGF – hepatocyte growth factor

IgG H&L – immunoglobulin G, heavy and light chains

ISDN – isosorbide dinitrate

NMJ – neuromuscular junction

NO – nitric oxide

RNA – ribonucleic acid

SC – satellite cell

Sema3A – semaphorin 3A

TA – tibialis anterior muscle

TSC – terminal Schwann cell

List of Figures

Figure 1. Histological assessment of the time course of myogenic regeneration after muscle injury by cardiotoxin (CTX) or crush (CR).	83
Figure 2. Neuromuscular junction (NMJ) regions.	89
Figure 3. Western blot studies of semaphorin 3A (Sema3A), -acetylcholine receptor (-AchR), and S100B proteins in regenerating muscles after injury.	93
Figure 4. Bromodeoxyuridine (BrdU) labeling of DNA synthesis in Pax7 satellite cells.	96
Figure 5. In situ hybridization and Celleste software.	116
Figure 6. Combined fluorescent ISH/ICC.	123
Figure 7. Number of expression sites.	127
Figure 8. Intensity (areal density) of mRNA expression sites.	129
Figure 9. Diameter of mRNA expression sites.	133
Figure 10. Combined assay by in situ hybridization and immunohistochemistry (ISH/ICC assay).	135
Figure 11. Principal component analysis correlation circle.	139
Figure 12. Surgery plan.	152
Figure 13. ISH Staining.	158
Figure 14. Sema3A, γAchR, and S100B proteins after injury to nerve (NCr) or muscle (MCr), or control groups.	162
Figure 15. Box-whisker plots for expression studies by ISH.	167
Figure 16. Principal component analysis correlation circle for P75 NGFR, representing TSCs.	171
Figure 17. Principal component analysis correlation circle for Pax7, representing SCs...	175

List of Tables

Table 1. Experimental design for ISH combined with immune detection of P75.....	117
Table 2. A summary of statistical comparisons for assays of protein (A) and transcript expression (B) by Western blotting and in situ hybridization assays, respectively.	136
Table 3. Loading of variables on PCA Factors.	140
Table 4. The following summarizes the design of ISH-staining experiments.....	155
Table 5. A summary of statistical comparisons for assays of protein.....	168
Table 6 on data related to P75 in TSCs.....	171
Table 7 for PCA on data related to Pax7 in SCs. using.....	174

ABSTRACT

Communications between satellite cells (SCs) and their niche are important during regeneration after skeletal muscle injury. Semaphorin (Sema) 3A, a neuro-chemorepellent, is thought to regulate axon guidance to neuromuscular junctions (NMJs) during myotube differentiation. In this study I explored the NMJ reformation and the effect of Wallerian degeneration and SC-niche remodeling on SC-TSC interaction which may advance our ability to find new types of treatment for skeletal muscle diseases that could promote regeneration including NMJ restoration. The first part of this research tested whether "premature" SC activation (SC activation before injury) by a NO donor (isosorbide dinitrate) would disrupt early myogenesis and/or NMJs. NMJ maturation, classified by silver histochemistry (neurites) and acetylcholinesterase (AChE), and α -bungarotoxin staining (ACh receptors, AChRs) was delayed by pretreatment, consistent with a day-6 rise in the denervation marker γ -AChR. With the NO pretreatment, S100B from terminal Schwann cells (TSCs) increased at the post-synaptic area. Premature SC activation before injury both accelerated myogenic repair and disrupted NMJ remodeling and maturation, possibly by reducing Sema3A neuro-repulsion and altering S100B. Since active TSCs generate local cues, facilitating nerve terminal sprouting during re-innervation and muscle regeneration, the next part of my PhD examined whether the loss of SC-specific Sema3A expression would disrupt TSC gene and protein expression after nerve or muscle injury. *In situ* hybridization experiments were used to evaluate the transcript expression of Sema3A, S100B, P75NGFR and Pax7 with or without immunostaining to identify SCs and TSCs. Western blotting was used to assess levels of Sema3A, γ AChR, and S100B proteins. Measurement of expression sites (number, intensity, and diameter) generally confirmed western blotting findings for S100B and Sema3A protein expression with different changes in nerve vs. muscle injury over time. Different changes in nerve vs muscle injury especially for S100B, resulted from Sema3A knockout and increases in the number of TSC sites expressing Sema3A after muscle-crush injury vs. the no-surgery control. Colocalization studies analyzed by principal component analysis (PCA) of TSC and SC expression showed strong correlations of Sema3A protein and Pax7 intensity in SCs, and of S100 intensity and Sema3A protein in TSCs after Sema3A knockout. Findings suggest that the number of TSCs increased only with the loss of SC-derived Sema3A. Results, therefore, demonstrate the dynamic nature of TSC populations at the nerve terminal after injury, and their novel signaling with SCs using SC-derived Sema3A. Findings improve our understanding of

possible roles for Sema3A-mediated coordination of motor neurite connections to newly formed myofibers during the formation of NMJs. Moreover, these results open the door to future investigation of features in the SC niche that could be applied in designing novel therapeutic approaches to promote muscle regeneration and reinnervation that could improve successful rehabilitation in elderly individuals.

1.0 INTRODUCTION

1.1 Muscle

Muscle is a soft tissue which is generated during embryonic development by myogenesis and in the adult comprises almost 45% of human body mass. Muscle tissues have an important role in regulating body metabolism and movement [1], and muscles are distinguished through their function and location in the body, being subdivided into 3 types: cardiac muscle, skeletal muscle and smooth muscle [2]. Skeletal muscle is attached to bones by tendons and is utilized to perform skeletal movements including locomotion and to stabilize posture. Tendons help transmit the forces generated during muscle contractions, to the skeleton, enabling body movements and promoting body stability [3]. Although postural maintenance is controlled as an automatic reflex, it requires strong contraction by skeletal or voluntary muscles which also respond to intentional control.

Skeletal and cardiac muscles are comprised of cells that display sarcomeres (the origin of the term “striated muscle”) that can be seen by eye; sarcomeres are fixed arrangements of bundles of myofilaments inside the fibers (or cells); by comparison, the myofibrils inside smooth muscle cells do not have that fixed arrangement and thus are not striated [2, 4]. Even though the sarcomeres in cardiac muscle cells are organized in parallel, regular bundles, the cells join or bond at irregular, branching angles at structures termed intercalated discs [5]. The contraction and relaxation periods observed during force generation by striated muscle occur in intense and typically shorter bursts, while smooth muscle contraction is longer lived. Smooth muscle is located within the walls of structures and organs including the stomach, uterus, intestine, bladder, urethra, and esophagus. Unlike widely-dispersed smooth muscle, cardiac muscle is more similar in structure and organization to skeletal muscle, is located in the heart.

The muscle fibers in skeletal muscle are multinucleated syncytial cells; although fibers vary greatly in length among the many different muscles in the body, each fiber is attached to bone, tendon, or skin at both ends. However, individual muscles are not formed of homogeneous fibers; they are a mixture of slow- and faster-twitch fibers, collected in muscle-specific fiber-type proportions. There are two further elementary classes of skeletal muscle: fast-twitch or white fibers (fast glycolytic/Type IIB) and slow-twitch or red fibers (slow oxidative/Type I); each type has its own features and purposes [6, 7]. Slow-twitch muscle is supplied by a dense network of capillaries

and slow-twitch fibers contain large amounts of myoglobin which causes the red color that is characteristic of that type of muscle. These muscles also have a high content of mitochondria and depend on oxidative metabolism to produce energy in adenosine triphosphate (ATP) form. The contraction of slow-twitch fibers takes a relatively long time to reach a peak force, although that peak has a fairly low level compared to that of fast-twitch fibers. Slow-twitch fibers are known as fatigue resistant. Together these features are very appropriate for the utilization of slow-twitch fibers in activities where endurance is important. Fast-twitch muscle fibers that populate individual muscles by comparison, can be further divided into three main subtypes (IIa, IIx, and IIb); although all generate energy primarily through glycolysis, IIx and especially IIa muscle fibers also use oxidative metabolism. Therefore, the three subtypes of fast-twitch muscle differ in their properties of force generation and contractile speed, with IIb being the fastest and strongest type of fiber, and IIx being intermediate between IIb and the slower, less powerful and more fatigue-resistant type of fiber, IIa. The contraction of fast-twitch fibers is powerful and appropriate for fast bursts of strongly directed work, and fatigue more rapidly than slow-twitch fibers. Fast-twitch muscles (those muscles comprised of a majority of fast-twitch fibers) mostly contribute to the strength of muscle and have major potential for increases in mass that are called hypertrophy in response to exercise [8, 9].

The relative proportions of slow-twitch and fast-twitch myofibers in a particular muscle in the mammalian body are regulated by genetics and innervation, and differ among muscles; fiber-type composition, however, can be modified by changes in activity level and type, and may be accompanied by an increase in the level of matrix metalloproteinase (MMP)-9 during physical training. Raised levels of active MMP-9 result in hypertrophy in skeletal muscles of both dystrophin-deficient *mdx* dystrophic and normal mice. Moreover, particular hormones such as thyroid hormone can influence the size and type of myosin heavy chain (MyHC) expression in myofibers, MyHCs vary in concert with fiber type and subtype [10, 11].

In this thesis, the word “muscle” will be used to refer to skeletal muscle, unless otherwise indicated.

1.1.1 Skeletal Muscle Structure

As described above, muscles are typically attached to bones by bundles of collagen fibers known as tendons and are utilized to effect skeletal movement and contribute to the stability of the body. Histologically, tendons contain thick organized bundles of connective tissue (called fascicles) covered in lubricating sheaths of less dense connective tissue that allow tendons to move within the sheaths. Typical healthy tendons are made of parallel groups of collagen fibers densely bundled together. Tendons are typically the mechanism by which muscles attach to bone and transmit forces. Moreover, this connection enables tendons (along with the organization or pennation of fibers in a muscle) to passively modify force and its direction during locomotion, supplying extra stability with no active contractile function of their own. Since tendons have the ability to stretch and recoil elastically, a muscle can have less or in some cases no alteration in length while it contracts, thus potentiating the capacity for a muscle to transmit more force to a bony attachment than is generated directly by its contraction.

More than 600 muscles in the human body are continuously undergoing processes of growth, maintenance, degeneration, and repair [12]. Muscles are composed of muscle cells (or myofibers), vascular networks, axons for sensory and motor innervation, and connective tissues; they are considered as functionally and morphologically dynamic tissues. The ability of skeletal muscle to produce contractile force is provided by the sarcomeres that give their striated appearance. Sarcomeres are repeating units of muscle filaments (e.g., myosin and actin) and inside a fiber they are organized into long bundles known as myofibrils. Sarcomeres are known as the functional and structural unit of skeletal muscle. Around the contractile myofibrils, mitochondria, vesicles of the t-tubular system, nuclei and other organelles in each myofiber is the myofiber membrane (sarcolemma) which is comprised of the plasma membrane of each cell and an outer layer of polysaccharides. Myofibers, containing many thousands of sarcomeres in bundles and often many hundreds of post-mitotic nuclei, are each enclosed within a connective tissue layer termed the endomysium or basal lamina, which overlies sarcolemma. The endomysium supports nerve axons and capillaries and helps keep the tissue together; it also plays a role as a scaffold for the development of muscles during growth or repair [13].

Several to many myofibers come together to make up a fascicle or bundle, and hundreds of fascicles together, form the muscle belly. Fascicles are enclosed with a connective tissue sheath which is known as perimysium; a thicker layer called the epimysium surrounds the whole muscle

belly. The perimysium has some loose and more delicate collagen fibers that facilitate the penetration of blood vessels and nerve branches into the muscle fascicles for metabolic homeostasis and excitation-contraction coupling, respectively. The structural importance of connective tissue within the muscle is due to its resistance to stretch and the ability to evenly distribute forces and thus minimize the potential damage to the fibers during injury or strong contractions [9, 14].

Cytoskeletal proteins include integrins, dystrophin, sarcoglycans, and dystroglycans in the dystrophin-associated protein complex that spans the sarcolemma around myofibers; the arrangement and functional properties of cytoskeletal proteins form a strong mechanical link between connective tissue elements including laminins outside the fiber and the contractile component (filamentous actin and myosin in sarcomeres), non-contractile proteins (titin, myomesin, α -actin), and neuronal nitric oxide synthase (NOS-1) inside the muscle cells [15, 16]. The importance of that linkage is demonstrated by the large range of muscular dystrophies (both lethal and non-lethal, each with variable severity) that result from mutations in, or deficiency of any one of the many proteins in the dystrophin-associated protein complex.

Notably, the most common muscular dystrophy is a result of an X-linked mutation of the large dystrophin gene. Such mutation results in Duchenne or Becker muscular dystrophy, respectively due to absence of the protein (through a nonsense mutation) or expression of abnormal dystrophin that is often due to truncated translation or deletions in the exon sequence [17]. Although there are specific genetic differences between the many types of muscular dystrophy, individuals who have those diseases typically display a similar pattern of clinical presentation including progressive weakness of one or groups of muscles. Individuals with muscular dystrophy also share the phenotype of pathological myofiber degeneration, connective tissue and adipose tissue accumulation, and often focal or more widespread formation of new fibers. For this reason, there is a considerable body of literature on skeletal muscle damage and regeneration, as researchers investigated the causes of and potential treatments for dystrophy. Another outcome of the mutations of disease-relevant genes is disruptions in signaling pathways that are important in ongoing contraction and relaxation [18-20]. As well, the loss of dystrophin or disruption of the internal linkage of NOS-1 to the dystrophin-associated protein complex, dislodges NOS-I from its close proximity with the sarcolemma and overlying SCs [21, 22]. This structural disruption alters the nitric oxide signaling cascade, and affects the time-course and extent of muscle SC activation,

as discovered through early *in vivo* experiments by Anderson and colleagues and later confirmed using single muscle-fiber cultures [23-27]

Muscle is not only the largest organ (by mass) in the human body, it also contains multinucleated myofibers which are the largest cells in the body. The *in vitro* transition of myogenic cells in culture from a proliferative undifferentiated state into a mature, differentiated and syncytial myotube (in culture, seen as a web of tissue formed from the fusion of single myogenic cells), has been a research model for studying the *in vivo* processes of cell-lineage commitment and differentiation by myoblasts and myofibers.

Our understanding of the molecular processes involved in embryonic myogenesis (and also myogenesis in adult, regenerating muscle) was significantly advanced with the identification of myogenic regulatory factors (MRFs), specifically Myf5, myogenin, MyoD, and Mrf4, and experiments that tracked their expression in embryos and then adults of transgenic mice (an approach established in the late 1980s and early 1990s) [28-32]. The significant function of MRFs at various levels of myogenesis, including during hypertrophy, has been broadly assessed in knockout mouse models [33]. The importance of these factors in myogenic differentiation is demonstrated by realizing that expression of one (MyoD) or more of these regulatory genes *in vitro* in fibroblasts, is capable of converting non-myogenic cells into muscle cells that can fuse into myotubes *in vitro* and take on the phenotype of normal muscle [34].

Very early during muscle development in the embryo, signals from the mesoderm trigger development of neural tissue located in the overlying ectoderm; this results in formation of a neural tube and then neuronal migration and proliferation. Efferent axons originate from the embryonic spinal cord and elongate peripherally in the growing embryo, to a location where muscle fibers are forming. It is that location where the nerve axons create synaptic connections called the neuromuscular junctions (NMJs) with muscle fibers, and thus innervate each skeletal muscle. In mammals, each myofiber is typically innervated with a single motor axon (see below for development of NMJs); however, it is important to note that each motor neuron (located in the spinal cord) innervates multiple myofibers (more fibers per motor neuron in fast-twitch than slow-twitch muscles) and the group of fibers provided by a single motor neuron is defined as a motor unit [35].

Muscles also contain sensory organs known as muscle spindles that are specialized myofibers called intrafusal fibers; muscle spindles identify the extent of muscle stretch in a

stimulus (through Ia afferent sensory axons) and then, via synapses in the spinal cord, can rapidly trigger a response to that stimulus, either for the whole muscle to lengthen (and reduce tension) or for it to contract further (and take up the slack). In this manner, spindles arrange the length–tension relationship of muscles, through combining the proprioceptive report coming from their intrafusal fibers with voluntary motor signals coming from the nervous system. Remarkably, slow muscles are specifically sensitive to interactions with motor nerves [36] and grow mature arrangements of innervation [37] earlier in development than fast-twitch muscles [38, 39]. Moreover, motor nerve terminals have a flatter profile and less surface contact on slow-twitch fibers than on fast-twitch [40]. Such structural changes lead to the establishment of a fiber-type distribution and axon-branching structure that is stimulated by the shapes of motor-nerve firing frequency, duration, and voltage, and that are involved in contractile processes [41].

1.1.2 Muscle Contraction

The process of nerve signaling to muscle to induce contraction is called electrical-mechanical signal transduction. This signaling begins with a wave of membrane depolarization that travels down a motor nerve axon as an action potential. When the action potential reaches the end of an axon, calcium ions diffuse through calcium channels in the axon terminal membrane, into the terminal boutons. This rise in calcium concentration in the axon terminal triggers the fusion of synaptic vesicles with the plasma membrane of the terminal. This fusion process releases a neurotransmitter into the synaptic cleft, which is the region between the axon terminal and the NMJ in the underlying myofiber. In the case of mammalian motor nerve axons, the transmitter is acetylcholine (ACh). The released ACh binds to acetylcholine receptors (AChRs) at ligand-gated ion channels on the post-synaptic membrane of the myofiber, the region of the fiber sarcolemma that lies directly proximate to the axon terminals. This ligand binding triggers muscle contraction through the excitation-contraction (EC) coupling process [42]. Regular excitation-contraction coupling is effected through an increase in the concentration of cellular calcium inside the muscle cytoplasm; EC coupling also has a significant role in muscle weakness in myotubes of *mdx* dystrophic mice because calcium-specific leak channels are open more than the leak channels in myotubes of normal mice [43]. Moreover, increased levels of sarcoplasmic calcium ions can directly impair muscle function through elevating the action of calcium-dependent proteases including calpains which are able to split (degrade) proteins within myofibers [44].

The response to motor neuron action potentials is that the membrane around the myofibers become depolarized. This depolarization releases stored calcium ions from the t-tubules into the cytoplasm; in turn, this calcium release initiates a cascade that leads to contraction, in that, the heads of myosin filaments connect to the binding sites on actin filaments and form cross bridges which move in the presence of calcium. The action of cross bridges is called the power stroke, when myosin “slides along” actin; the power stroke shortens the sarcomere and leads to myofiber shortening, and ultimately, to muscle contraction [45].

Myofibers contain two important ‘classical’ or contractile type proteins, myosin (known as the thick filament) and actin (known as the thin filament); together, they form the basic contraction units, called sarcomeres. The interaction of myosin and actin through cross-bridge cycling (and proteins such as troponin and tropomyosin) results in sarcomere shortening. After re-uptake of calcium back into the smooth endoplasmic reticulum, the sarcomere once again lengthens (or relaxes). This contraction-relaxation mechanism of skeletal muscle is the basis of the now-classical sliding-filament theory [46, 47].

1.1.3 Myokines

Myokines are one subset of the family of small cell-signaling proteins (cytokines) that are synthesized and released by myocytes during muscle contraction. They may have paracrine, autocrine and/or endocrine signaling effects, depending on how they are released from cells (i.e., to the muscle interstitium or into blood vessels). Myokine receptors are on muscle and many other types of cell, including pancreas, bone, liver, fat, heart, brain and immune cells. Multiple myokines participate in the metabolic alterations that follow exercise, as well as in tissue maintenance (the regular turnover of healthy tissue during function, remodeling, and aging), tissue regeneration, cell signaling and immunomodulation [48, 49]. In 2008, myostatin, was found as the first myokine (it acts to inhibit muscle growth) while interleukin 6 (IL-6) was the first secreted myokine identified in the blood stream following muscle contractions [50]. As well, different types of myofibers release different groups of myokines during muscle contraction [12]. Although brain-derived neurotrophic factor (BDNF) is a myokine, it is not released into blood circulation. BDNFs and their receptor, tyrosine kinase receptor B (TrkB), are expressed widely in the brain and skeletal muscle tissue and the signals from BDNF binding have beneficial effects on neuronal function, neuronal development and the modulation of synaptic plasticity (see section 1.4.6). The activation

of skeletal muscle via exercise also has an effect on increasing the secretion of BDNF in the brain [51]. Chronic muscle exercise increases the level of BDNF and insulin tolerance in a TrkB-dependent manner [52], in addition to having endocrine effects on the brain as part of an ongoing feedback system between the two tissues [53].

1.1.4 A model muscle, Tibialis Anterior (TA)

The tibialis anterior muscle (TA) is found in the leg; it originates from a large area of attachment from the lateral surface of the tibia and joins into a large tendon in the middle of the muscle belly. The tendon passes distally in a tendon sheath, under the medial part of the transverse and cruciate ligaments of the extensor retinaculum of the ankle, inserts into the medial and dorsal aspects of the cuneiform bone before finally inserting into the base of the first metatarsal bone of the foot. The TA belly overlies the blood vessels that supply it, and also over its innervation, the deep peroneal nerve in the leg. Fibers take origin from the area of the lateral tibia known as the lateral condyle and also the lateral surface of the tibia itself. Some fibers also take origin, especially in athletic or physically active individuals, from nearby regions of the interosseous membrane (between tibia and fibula) and even from the connective tissue (epimysium) that separates the TA from the extensor digitorum longus (EDL) muscle. This so-called circumpennate muscle (where fibers attach around the circumference of a tendon that forms deep in the muscle belly) has myofibers that run parallel to the insertion plane and that end in a tendon on the anteromedial side of the dorsal part of the foot. The TA muscle is the most medial muscle of the anterior aspect of the leg. The TA controls the dorsiflexion movements of the foot (lifting the foot upward in stance) and assist with inverting the ankle [54, 55].

The TA is the primary antagonist of the soleus, tibialis posterior and gastrocnemius muscles on the posterior leg. Innervated by the deep peroneal nerve, the TA muscle helps in walking, kicking a ball, running, hiking on uneven ground, and the other activities that require the leg to move the foot. It has a major role in stabilizing stance. The motor endplates, where axon terminals of the deep peroneal nerve synapse with TA myofibers, are located at approximately the middle of the length of individual myofibers, and typically form a broad inverted-V shaped chevron when visualized by staining methods [56].

1.2 Satellite Cells

Satellite cells are muscle precursor or stem cells of skeletal muscle, and are essential to the remarkable capacity of muscle for regeneration from injury and disease [57-61].

1.2.1 Structure and Location – the SC “Niche”

The adjacent microenvironment of stem cells, also called the stem cell “niche”, preserves the “stemness” and characteristics of tissue-specific stem cells through biochemical and structural cues. Currently, stem cells, each within a corresponding niche, are detected in many tissues, such as brain, liver, intestine, heart, white fat, skin and bone marrow. Like these cells, adult stem cells in skeletal muscle exist in an extremely specified niche, which contains the ECM, the underlying myofibers on which SCs reside, neural and vascular networks, and various kinds of adjacent cells. The expression of cell membrane associated proteoglycans including glypican-1 and syndecan-4 play a crucial role in managing the extracellular environment in the SCs niche, cytoskeletal structure, cell-to-cell adhesion, signal transduction and SCs migration. Moreover, SCs *per se*, affect each other through cell-to-cell interaction and paracrine or autocrine processes. The interactions between SCs and their niche adjusts the activity of SCs from quiescence to proliferation, and then into differentiation. Thus, the “tuning” or adjustment prevents the excess growth of muscle and also the potential to atrophy (such as with inactive SCs), while the pool of SCs is preserved during the sequence of events that SCs undergo during regeneration. SCs receive many signals from the regenerative microenvironment which direct cells through the process of cell activation and the induction of differentiation to stimulate regeneration of damaged muscles. Released necrotic cues from damaged myofibers, secreted cytokines through the inflammatory infiltration growth factors, soluble proteins, free radicals and changes in the ECM alter the SCs niche [62-64].

Studying the communications between SCs and their niche is important for finding new types of treatment of skeletal muscle diseases that could promote regeneration. It is understood that angiogenesis is essential for muscle repair and the relationships between SCs and blood vessel cells govern myogenesis, myogenic cell expansion and angiogenesis. For instance, during muscle regeneration, endothelial cells stimulate myogenic cell growth and differentiating myogenic cells help angiogenesis. Other studies also show that M2 macrophages improve SCs differentiation and the formation of myotubes, to maintain a niche that is proper for the regeneration of skeletal

muscles. Moreover, additional parameters such as aging cause changes to the niche and affect the fate of SCs through changes in environmental cues, causing aged SCs to fail to return to quiescence state, abnormally entering senescence and/or failing to inhibit fibrosis. Aging also makes some changes in the SC niche, such as modifying electrical-mechanical activity, neural-related trophic factors and systemic factors in the environment. A better understanding of the elements present in the SC niche and their effects on the SCs will accelerate the future development of therapeutic interventions designed to improve the activity of SCs, promoting growth and/or regeneration, as well as improving the response of the tissue to injury or inactivity in elderly individuals [51, 65-75].

Mauro was the first to utilize electron microscopy to observe mononucleated cells which were called satellite cells (SCs) because of their direct juxtaposition, like a “satellite” in association with the sarcolemma. The location of myofibers and SCs raised a hypothesis of participation of these cells in the regeneration and growth of muscles. Using tritiated-thymidine tracing together with the assessments of electron microscopy, research showed that while SCs experience mitosis, they have a cytoplasm-enriched morphology. [3H]thymidine assessments also displayed that SCs are quiescent in mature adult muscle and only begin dividing after a muscle injury; after that the precursors are called proliferating myoblasts, which then form multinucleated myotubes [76]. More studies on the behaviors of SCs during regeneration *in vitro* [77], indicated that myofiber necrosis after injury is associated with the outgrowth of SCs beyond the external lamina surrounding a myofiber, and future myoblast fusion to develop striated regenerated myotubes that can return muscle function. These results emphasize the contribution of SCs (instead of the myonuclei inside myofibers) in muscle repair and growth after injury. Several early research reports focused on the regulatory mechanisms of SCs to investigate SC function in muscle regeneration; those by Bischoff provided very clear insight into the process, as experiments utilized muscle that was separated into single or bundles of myofibers. One of Bischoff’s experiments found that quiescent SCs were activated by a mitogen derived from crushed muscle [78]. Other investigators discovered that the differentiation and proliferation of myoblasts in culture occurred by a dose-dependent reaction to different growth factors [79, 80]. Further studies showed that the proliferation of SCs throughout the regeneration of muscle was affected by hormones, vasculature, nutrition, innervation, and the degree of tissue injury [81-84]. Early electron microscopy observations that initially identified SCs as likely precursors for muscle,

revealed the morphological characteristics of SCs, tiny cells that could take on a “wedged” appearance; the SCs described by Mauro had a small condensed nucleus during interphase and very few organelles [85]. Mauro has been heralded as making a pivotal discovery in the timeline of research on skeletal muscle regeneration [86].

By comparison to lengthy electron microscopy studies of SCs in a tissue, current identification of SCs in adult skeletal muscle relies on the expression of specific biomarkers including Pax7, Pax3, M-cadherin, c-met, integrin, CD34, syndecan-3, and syndecan-4, often by fluorescence microscopy using immune-detection methods or *in situ* hybridization. Moreover, bioluminescence imaging techniques can be used to visualize the SC population *in vivo*. However, numerous studies have revealed that population of SCs vary, in the particular at the molecular level, as well as at the structural or population level in relation to the quantity of SCs (density per muscle fiber) that differs among different types of myofiber and muscle, and during development. The molecular distinctions among SCs are known as features of SC heterogeneity [87] [88, 89].

Regarding the size of SC populations in adult muscle, there are at least twice the proportion of SCs (as a ratio with myonuclei inside fibers) in the soleus (slow-twitch) muscle than that in the EDL or TA muscles (fast-twitch); since mammalian muscles typically have a mixture of fiber types, there is a similar difference between muscle fiber types (i.e., more SCs on slow type I myofibers than on fast type IIB and IIA myofibers) [90-92]. These differences illustrate fundamental heterogeneity of SCs on various myofibers and specify that myofibers regulate SC populations to some extent.

1.2.2 Quiescence and Activation of SCs

The regeneration of muscles can be summarized from the perspective of SCs and muscle precursors, as comprising various overlapping steps in myogenesis including activation, proliferation, differentiation, and self-renewal; these steps are described in detail below (section 3.3). Appropriate progression through these various stages needs careful regulation of the cell cycle. However, the initial degeneration of muscle after an injury or strenuous exercise, starts with the necrosis of injured myofibers (or segments of fibers) and results in enhanced permeability of the myofiber sarcolemma, enhanced calcium release from the sarcoplasmic reticulum (SR) and then calcium influx into the cytoplasm of the myofiber; the resulting localized contraction of sarcomeres in this area leads to further changes that initiate extensive tissue degeneration [44].

Myofiber necrosis also induces inflammatory responses which subsequently cause the chemotactic attraction of circulating leukocytes to regions of local damage [93]. Infiltration of inflammatory cells like neutrophils can be observed 1 to 6 hours after exercise as well as after experimental muscle injury induced by myotoxin [93], or within minutes of a crush injury [23].

Muscle regeneration can be illustrated through the description of a number of morphological characteristics detected through histological staining and immunofluorescence studies. Overall, it is important to remember that newly generated myofibers can be characterized by their centrally located myonuclei and small caliber; their size increases as regeneration continues. As well, the central myonuclei transfer to the periphery of the myofiber after the regeneration process in human muscle diseases, although central nucleation is permanent in mouse muscle and therefore still an excellent indicator of regeneration in experiments on mice [94-98], likely as mice are more short-lived than humans.

In adult muscles, SCs exist in a state of quiescence (G0) and their ability to preserve this resting condition is crucial for the preservation of the SC pool. The fast re-entry of SCs into the cell cycle that occurs rapidly after muscle injury shows that the quiescent condition represents a 'ready' situation for activation in most SCs. However, there are SCs with a slower response that constitute a more stem-like subset of the SC population [27], and others that reportedly "idle" in a state of readiness for subsequent activation [99]. Any losses in the capability of SCs or their niche on fibers to preserve their quiescent status, will decrease the self-renewal capability of SCs (as stem cells) and jeopardize the success and/or magnitude of a muscle-regeneration response especially if it is required on a long-term or repeated basis such as in muscular dystrophy [27, 100, 101]. The Notch pathway has a key role in regulating SC quiescence; Notch signaling shows higher action in quiescent SCs than in activated myogenic cells [102]. Remarkably, inactivation of Notch leads to SC differentiation, signifying that Notch has a double function in preserving the progenitor condition. The downregulation of Notch is required for the progression of the myogenic cell lineage during regeneration, [103], and Notch impairment in SCs from muscle of 24-month-old mice (compared to those from muscle of two to four-month-old mice) also affects the ability of muscle stem cells to enter and complete mitosis [104]. Although many aspects of the transition from quiescence to activation (and even back toward quiescence) are reported, the regulation of the transition is still not clear [105].

It has been known for decades, that mitogenic factors are released post-injury that stimulate quiescent SCs to re-start the cell cycle [106]. Damaged muscles also liberate various growth factors which later activate signaling pathways engaged in SC entry into the cell cycle. For example, the expression of FGF2 in regenerating muscle activates different pathways such as MAPK and ERK1/2 (Mapk3/1) which are critical for the transition of G1 to S phase in SCs [107]. Additional experiments demonstrated the unique ability of HGF to activate SC cycling and cell division *in vitro*, whereas FGF2 will not shift SCs from quiescence to activation [108]. Once activated and having finished nuclear division then cell division, SCs exit the cell cycle and either undergo differentiation or return to quiescence. This exit needs the upregulation of cyclin-dependent kinase inhibitors. The activation of Notch signaling is also critical for the return of SCs to the quiescent condition. Activation of Notch also raises Pax7 expression and prevents MyoD expression, therefore preserving the primitive (undifferentiated) state of SCs [109]. Furthermore, the loss of Notch is thought to result in a problem in the positioning of SCs to their typical location on the sarcolemma, because of the failure of SCs to produce various extracellular matrix (ECM) proteins, including collagen and integrin and cell adhesion molecules (CAMs) such as the dystroglycan complex components [110].

1.2.3 Patterns of gene expression

As mentioned earlier, SCs are mitotically quiescent and can be distinguished by Pax7 expression but not Myogenin. Upon receiving signals from an injured area, SCs initiate cycling toward proliferation by becoming activated. Proliferating SCs and their progeny are called myoblasts. It is also known that SCs outside the location of damage, will become activated; this is due to signaling along a damaged fiber and niche-related factors. As an example, many of the SCs along the length of a myofiber become activated under some circumstances, when only one end of the myofiber is damaged; subsequently, many of the activated SCs move toward the area of damage to begin repair of the fiber. There are studies that show that SCs can migrate across basal lamina and through layers of connective tissue as muscle grows, remodels, and regenerates [111]. Lately, sialomucin, also called CD34, which is highly expressed on quiescent SCs sharply decreased after activation and was shown to inhibit SC adhesion with other cells, essentially easing the movement and proliferation of activated SCs at early steps of the regeneration of muscles

[112]. Moreover, the regulation of ephrin ligands and Eph receptors in regenerating myofibers and activated SCs have been shown to direct SCs migration [113].

Precursor cells are distinguished by the MyoD expression as a myogenic transcription factor [114-116] and Myf5 [117]. The presence of MyoD, Myogenin and desmin in a subpopulation of SCs was detected approximately 12 hrs post-injury [118]. In contrast, most of the SCs express either Myf5 or MyoD around 24 hrs after damage [117, 119] and co-express both transcription factors by 48 h [117, 120] which suggests different functions for these factors in adult myogenesis. The regeneration of muscle is also diminished in MyoD^{-/-} mice, leading to a larger number of myoblasts in the injured area [121] which fail to fuse into myotubes. These reports show that MyoD expression is a significant factor in regulating myogenic proliferation and differentiation since without MyoD, activated myoblasts have a tendency to proliferate rather than differentiate and form fibers [122].

In contrast, Myf5^{-/-} mutant mice display a hypertrophy in the myofiber [123]. These findings indicate a disparate role for Myf5 compared to MyoD: Myf5 is important in the proliferation of myoblast, whereas MyoD is important for differentiation. In particular, different roles of MyoD and Myf5 during the regeneration of muscle suggest a hypothesis that SCs start various myogenic settings depending on whether MyoD or Myf5 expression leads [124]. The higher expression of MyoD would cause early differentiation, as demonstrated by myoblasts from Myf5^{-/-} transgenic mice [125], while higher expression of Myf5 would enhance proliferation and delay differentiation, as shown in MyoD^{-/-} myoblasts [122].

MyoD expression is maximal at the mid-G1 stage of the cell cycle in myoblasts, while the expression of Myf5 peaks in the G0 and G2 phases [126]. Thus, interruptions to the changing Myf5/MyoD ratio were suggested to control SC fate determination and myogenic programs in development, growth, and regeneration. In addition, observing the progression of SCs during culture exposed that some MyoD⁺/Pax7⁺ myoblasts could eventually return to quiescence [127]. The findings showed that Pax7 reduces the transcription, stability, and activity of MyoD, while Myogenin controls the transcription of Pax7 [128] and so the ratio of Pax7/MyoD is important in determining SC fate, or rather the fate of myoblasts that originate from SCs [129]. According to the 2007 paper by Olguin et al. [129], a high ratio of Pax7 to MyoD (as observed in quiescent SCs) would cause SCs to stay in their quiescent stage. A medium Pax7/ MyoD ratio allows the SCs to proliferate without differentiating. A low Pax7/MyoD ratio starts differentiation, and an extra

decrease in the level of Pax7 is observed after Myogenin activation. After a few rounds of proliferation, most myoblasts will differentiate and start to fuse to generate new myofibers.

Early experiments with the tool of *in situ* hybridization to localize gene-transcript expression showed that the beginning of differentiation initiates with the expression of Myogenin and Myf6 [120, 130-132]. The expression of Myogenin is mainly influenced by MyoD and also increases the expression of a group of genes that has been already started by MyoD [133] including the genes encoding myosins, troponins and actin. The expression of these so-called structural genes is critical for the morphology, function and formation of skeletal muscle and therefore several mechanisms are involved in their regulation [134]. Others have reported MRF gene expression using *in situ* hybridization in context of muscle regeneration represented by the immune localization of developmental myosin heavy chain, in dystrophic mouse diaphragm muscle [135].

The transcriptional regulation of Myogenin and MyoD are first noted by post-transcriptional modifications. The transcriptional regulation of Myogenin is controlled by protein kinase C and A [136]. Myogenic gene expression of MRFs is also controlled by protein inhibitors. The transcriptional role of MRFs depends on heterodimerization with E proteins, a process that is adjusted by a set of DNA-binding proteins called Ids (Id1, Id2, Id3, and Id4). The heterodimerization of Id proteins with E proteins will stop the E-protein linkage with MRFs, thus revoking the expression of myogenic gene [137]. Similarly, the sequestration of E proteins can also inhibit the activity of MyoD [138].

Other factors are also engaged in myogenic differentiation. Micro-RNAs (MiRs) which repress translation and function to decrease the constancy of their mRNAs. Experiments showed that MRFs including Myogenin, Myf5 and MyoD, trigger the expression of a group of myogenic microRNAs (miR-1, miR-133, miR-206) which control the expression level of myogenic regulators and transcription factors including Pax7 [139, 140] and c-met [141] during SCs proliferation, activation and differentiation. More recently, a large number of circular, non-coding RNAs have been shown to interact with MiRs and other molecules, and further regulate SC differentiation and repair of skeletal muscle [142, 143] and muscle development [144, 145]

1.2.4 Therapeutic Potential

There have been many trials testing the use of mouse, primate, and human stem cells as possible treatments for muscle diseases. Unfortunately many trials were not successful, either in the short or longer term, due to early problems with limited stem-cell migration [146], fibrosis

[147], immune rejection [148] or the need to establish normal SCs on whatever fibers are generated from the implanted cells [88]. Interestingly, types of stem cells that did not come from skeletal muscle were also investigated for potential use as therapy for muscle diseases, as stem cells can be guided in their differentiation by the complex influence of surrounding tissues they may encounter. For example, bone marrow cells (BMCs) are well characterized in relation to the hematopoietic cell lineage that produces all our blood cells. Intravenous injection of BMCs into a damaged area or direct intramuscular injection of BMCs into damaged muscles resulted in the integration of those cells into newly generated myofibers in regenerating muscles. Adult bone marrow has both stromal and hematopoietic stem cells (HSCs). The HSCs are able to join into newly generated myofibers and support muscle regeneration. These results highlight the role of the muscle microenvironment on the specification of stem cells including SCs. Other studies have tested applications of muscle stem cells for use in supporting repair or regeneration of damaged cardiac muscle [149-152]. Further investigations are needed to describe the subpopulation(s) of BMCs which exhibit myogenic potential *in vivo*, mainly for potential treatment of muscle diseases [153-155].

A population of cells, known as muscle-derived stem cells (MDSCs), could be isolated from muscles, although they are not necessarily retrieved from a satellite position on myofibers. The isolation of MDSCs is based on specific characteristics including their capacity to sustain long-term proliferation in culture. Using fluorescence-activated cell-sorting analyses to isolate MDSCs showed that these cells are positive for expression of Flk-1, desmin, and Sca-1, and do not express M-cadherin, CD34, or CD45, which distinguishes them from hematopoietic cells and SCs. MDSCs can participate to reform myofibers, merge into the SC niche, and also differentiate into neural and endothelial cells [51], so they are clearly distinct from SC-derived myoblasts. Skeletal muscle also contains an exclusive population of cells called skeletal muscle side-population cells (SPCs), first identified by isolation methods using fluorescence-activated cell sorting. These cells are characterized by expression of Pax7, CD45, the ATP-binding cassette subfamily G member 2 (ABCG2), desmin (a muscle-specific structural protein) and Myf5. SPCs were identified as located in the muscle interstitium, adjacent to blood vessels and separate from SCs that live next to myofibers in the satellite-cell niche. SPCs can also differentiate into myogenic cells through forced expression of MyoD or Pax7 or following co-culture with primary myoblasts. The nuclei of SPCs rafted into muscle were also observed within myofibers and in cells in the SC niche, after direct

injection to regenerating muscles, which shows that the SPCs can impact muscle regeneration in an experimental study. Nevertheless, the particular role of the SPC phenotype in the muscle regeneration process *in vivo* is still unclear [156-158].

1.3 Muscle Damage and Regeneration

1.3.1 Functional Impairment of Muscle

Impairment of muscle function can be caused by aging, disease, toxicity, and injury; these conditions all influence life quality, and can impair or prevent individuals from performing their daily activities and staying independent [49, 159, 160]. Skeletal muscle injuries are common, since there are many factors that affect the integrity of muscle structure. Muscle damage can be caused by either external or internal events including myofibril damage, traumatic tearing of the muscle belly or even excessive lengthening contractions during exercise. Muscle necrosis (cell death) can be caused by external traumatic events if the nerve and/or blood supply is compromised during the injury.

Different experimental models of muscle damage such as denervation and devascularization, crush injury, lengthening contractions and toxin injection, *in vitro*, and *in vivo* have been utilized to develop our knowledge about the events during muscle repair [161]. Based on the severity and mechanism of injury, damage to a muscle can disrupt an entire myofiber or involve only a segment or short region of a few sarcomeres along the length of a single fiber.

1.3.2 Muscle Repair

More acute muscle damage typically triggers segmental or global necrosis of myofibers which sequentially provokes the characteristic response observed as muscle regeneration mediated mainly by SCs. As mentioned earlier, SCs proliferate and differentiate after muscle injury, and repair is accompanied by myotube formation and/or fusion of myoblasts with undamaged regions of some myofibers, before the appearance of mature myofibers [162, 163]. Even when an injury is limited to the myofiber and does not directly affect the surrounding basal lamina of the myofiber, the active contribution of other cell types in this regeneration process is still required. Monocyte-derived macrophages specifically are attracted to muscle injury site, are strongly involved not only in disposal of necrotic debris, but also in growth factor release which supports or limits the

proliferation and differentiation of myogenic cells [164]. Ultimately, functional recovery needs the return of motor innervation to the regenerated fibers to forming new or remodeled neuromuscular junctions (NMJs) to re-establish the electrical-mechanical linkage that enables voluntary contraction [165].

The ability to repair or regenerate is one of the most interesting (and vital) characteristics of striated muscle and has captured the attention of researchers for many years. Note, that reports in the literature variously use the terms “regenerate” and “repair” interchangeably, whereas others distinguish myogenic regeneration from the overall repair of skeletal muscle tissue. An early experiment on muscle repair illustrated that, regardless of the experimental approach to injuring muscle, the subsequent damage and repair processes follow a similar plan to restore the muscle [166]: first inflammation, then proliferation of precursors and formation of fibers, followed by fiber growth while inflammation resolves. Nevertheless, each experimental approach to injury (model) shows distinct differences in the levels of degeneration and repair, related to the timing and the nature or extent of each of: the immune response, the damage, and the need for vessel and nerve formation [58].

Even in less serious injuries, the process of repair may not be totally effective, hence, a better understanding of features engaged in the pathology and the processes of muscle regeneration, including formation of neuromuscular junctions on myofibers, would improve our ability to promote regeneration to restore function. Several growth factors including insulin-like growth factor 1 (IGF-1), hepatocyte growth factor (HGF), fibroblast growth factor 2 (FGF2) and members of the transforming growth factor- β family (TGF- β) sequentially interact with molecules in the basal lamina and with SCs during skeletal muscle regeneration, triggering muscle to reform new myofibers at a particular timepoint after injury. Muscle denervation also affects the production of many growth factors including leukemia inhibitory factor (LIF), which is a part of the cytokine family. LIF is a proliferative component for myoblasts and shows upregulated expression during denervation, but whether it participates directly in mediating the myogenic reinnervation process is not clear [167].

Most typical injuries to muscle include physical trauma with no substantial loss of muscle tissue from the site of injury. Under these circumstances, muscle has a robust regeneration capability through the activities of SCs. In fact, in animal experiments, a muscle can be entirely removed, chopped and put back into the original muscle “bed” of connective tissue and will

subsequently form myotubes; those myotubes will mature into myofibers, and may ultimately regain the ability to contract and generate voluntary force depending on the success of the reinnervation process, and in some cases regain essentially the full strength of the original, intact muscle [168]. Nevertheless, the capability of a muscle to self-repair after damage is reliant on the severity and type of the injury [167, 169]. When muscle injury is accompanied by trauma, such as occurs in a crush injury, the capability of a muscle to repair is reduced compared to injury by a chemical that is toxic to the fibers or a freezing injury where the muscle fiber architecture is not disrupted by trauma; in cases with more than 20% of a muscle injured, the normal repair procedure will often fail, especially in the central “core” of the muscle belly; this will lead to deposition and maturation of fibrotic scar tissue, which can prevent reinnervation of distal muscle fibers and result in functional impairment [170]. Therefore, there is still an obvious need for therapeutic approaches to improve the innate capability of skeletal muscle to regenerate after localized or major trauma and/or to stimulate *de novo* development of new “replacement” tissue that will function as voluntary muscle.

1.3.3 Phases of Muscle Regeneration

Muscle regeneration encompasses significant cellular events, including degeneration and inflammation, activation of satellite cells (SCs), proliferation of SCs and their daughter cells called myoblasts, and the formation of new myofibers [171]. Regardless of the severity or type of injury, muscle regeneration is commonly divided into three phases or chapters: a degeneration chapter that is described by necrosis and disruption of myofibers and inflammation; a repair chapter that launches SC activation and myogenesis, angiogenesis for revascularization, and connective tissue deposition. Regeneration also overlaps (in time) with the degeneration chapter, and with a remodeling chapter (third) that includes the maturation of regenerating myofibers, connective tissue remodeling (possibly into a scar) and the restoration of voluntary muscle function as fibers become innervated [172, 173].

SCs also affect each other due to cell-cell interactions and paracrine or autocrine signals released respectively by other cells or SCs themselves. SC activities including quiescence, proliferation, and differentiation are regulated by a many factors contained in structural features of the SC “niche”, discussed above (section 1.2.1) as an exclusive site in muscle tissue where SCs can live for an unlimited time and generate progeny cells [65]. Secreted products from other cells

such as those in the microvasculature, the interstitium, the immune system, and NMJs are also inherent in muscle structure [51]. The activation of SCs is not limited to the injured area of the muscle, in fact, local injury at one site of a myofiber (called segmental injury due to its localization at one part of a longer myofiber) results in the activation of essentially all SCs on that myofiber as well as migration of these SCs toward the regeneration area. Moreover, the activation of SCs is associated with widespread cell migration [174]. It has been reported that SCs can migrate or move between muscles and to myofibers in different fascicles of a muscle through barriers of connective tissues and basal lamina all through muscle growth, development, and regeneration [111]. It has also been demonstrated that sialomucin, also called CD34, which has high expression in quiescent SCs and is dramatically reduced expression during SC activation, works as an anti-adhesive molecule to assist migration and help SC proliferation during early phases regeneration in the muscle [175].

1.3.3.1 Degeneration Phase

Injuries change or breach (break) the myofiber sarcolemma and cause an interruption of the calcium equilibrium; this initiates the degeneration chapter in an injured muscle. Inflammation is also triggered by cytokines that are released from the myofiber after a breach or change in the sarcolemma. During a typical period of muscle degeneration, injured and necrotic myofibers are degraded and initially eliminated by immune cells, such as pro-inflammatory macrophages and neutrophils. Through the second, repair chapter, necrotic myofibers and cellular debris continue to be removed through phagocytosis. The degeneration chapter, which normally starts within the first minutes post injury, can continue for up to 2 weeks [176] depending on the muscle properties (size and shape), type and extent of injury, age, activity, and vascularity (original and surviving injury). For example, if blood flow is restricted or the inflammatory immune response is less than effective during degeneration, debris removal will be slower. If an animal has a chronic myositis (as modelled by the SJL/J mouse strain), the response to an acute traumatic injury to muscle can be faster than normal [177, 178] [179-181], in part as the SCs in an inflamed muscle can be activated before a direct injury to muscle [182].

During this degenerative chapter, several mononuclear inflammatory cells including monocytes which act as “wound hormones”, display chemotaxis to injured sites of muscle [93]. Differentiation of monocytes into pro-inflammatory macrophages (M1) happens after monocytes

have infiltrated the injured area from residence in non-injured tissue. These M1 macrophages then enclose the injured site and eliminate muscle debris by phagocytosis. The activity of monocytes during inflammation and debris removal is crucial for effective regeneration [164]. Somewhat later, another set of monocytes besides those residents ones in the muscle, is attracted toward the site of muscle injury to move through capillary walls into the interstitium. That population then differentiates into anti-inflammatory macrophages (M2 macrophages) that secrete growth factors such as HGF into the injured site to finalize muscle degeneration and help the procedures supporting muscle formation and regeneration through the activation of SCs and further regulation of SC process [183, 184]. HGF signaling through its receptor c-met, plays an important role during the initial, early stage of repair since the level of HGF that is released from damaged fibers and their surrounding basal lamina, decreases over time. The activation of SCs via HGF in the initial phase of muscle regeneration is caused by both HGF release from the ECM and activation of HGF transcription in SCs; thus HGF functions in both paracrine and autocrine ways to stimulate the proliferation of SCs [185]. This HGF stimulus is magnified by the increase in expression of c-met that occurs very rapidly upon injury, supporting the idea of c-met as an early, immediate gene [27]. The HGF released from M2 macrophages also plays a role in stimulating SCs engaged in proliferation and early differentiation, to produce semaphorin 3A (Sema3A), although this is not mediated through HGF-c-met binding (see sections 6.1 and 6.2) [186].

The two predominant inflammatory cells (M1 and M2) macrophages invade the injured muscle sequentially and reach their highest concentration 3 days after injury. Levels of macrophages decrease after 7 days and return to baseline 14 days post-injury [187]. The M1 (CD68⁺) macrophages secrete proinflammatory cytokines such as tumor necrosis factor (TNF) and interleukin-1 (IL-1) which have roles in removing cellular debris from an area of injury. M2 (CD163⁻/CD206⁺/CD68⁻) macrophages reach a peak population between days 2 to 4 post injury and secrete anti-inflammatory cytokines; M2 macrophages linger in injured muscle until the inflammation resolves. A subclass of M2 macrophages (CD163⁺/CD206⁺/CD68⁻) can inactivate the M1 macrophages to reduce muscle damage, and help myofiber growth and membrane repair [188]. Subsequent stages of the muscle regeneration process consist of extensive proliferation of SCs to provide an adequate supply of myonuclei and the cellular building blocks for the restoration of myofibers [189-191].

1.3.3.2 Repair Phase

During the repair procedure, muscle cells, nerves and blood vessels infiltrate the injured parts of the tissue. The repair phase can be said to begin with the activation of SCs, described above as a heterogeneous group of adult stem cells that are “sandwiched” between the basement membrane and sarcolemma of the myofiber [159, 192]. SCs need to transition from a quiescent to an activated state (G0 to G1 in the cell cycle) before they can proliferate in response to myofiber damage and/or stretching (see below for details of activation).

Once SCs are activated, they become myoblasts that proliferate, differentiate and fuse to the injured myofibers or gather together to generate new myofibers [163, 193]. Nevertheless, SCs are not the only progenitor cells that contribute to the repair of muscles. There is considerable controversy and interest in the involvement of other types of muscle-derived stem cells and progenitor cells including cells derived from bone marrow, in the formation of new muscle either by myogenic differentiation or through secretion of paracrine factors which influence those nearby cells.

In any injury to muscle, such as induced by cardiotoxin (snake venom) or trauma (muscle-crush injury), many pro-inflammatory macrophages and increasing numbers of proliferating myoblasts (derived from activated SCs) are apparent by 2 days post-injury [54, 194]. For example, some snake venom toxins have phospholipase A2 activity and induce a rapid and widespread necrosis of myofibers that is followed by a sequence of regenerative events [195]. Regenerated myofibers begin to develop quickly by the addition of new ‘lengths’ of muscle between the two remnant ends of the fiber segments that survived the injury (i.e., into the region of injury and degeneration within the length of a damaged fiber); this starts at about 2-3 days post-injury [196]. Parallel to new muscle formation, scar tissue from repair of the connective tissues in the muscle, forms connections between the residual functional myofibers and maintains the capacity for some level of transduction of force along the muscle. In less severe injuries, this tissue scar acts like a channel or scaffold that can assist myofiber formation. In more severe injuries, the tissue scar is large, and its maturation can block migration of the myoblasts, vascular endothelial cells, and axons that are required for effective regeneration.

Newly regenerated regions of a myofiber can be identified by their centrally located myonuclei, a hallmark of regenerated myofibers and myofiber segments [197, 198]. These new myofibers (called myotubes) are formed after the fusion of myoblasts that were produced by

proliferation of activated SCs. The new myotubes grow in diameter and in length (by further fusion events and through the expansion or growth of the cytoplasmic domains around each nucleus from a former myoblast); this process is thought to contribute to muscle repair for up to 10 days post-injury [199]. As young (immature) myotubes lengthen and extend across the damaged area of the muscle, they can attach and fuse laterally (side by side) to one another or at their ends to undamaged segments of broken myofibers, and also can extend by further growth and myoblast fusion toward the tendons where they will insert. Finally, the myonuclei located in the central-core region of regenerated myotubes are thought to shift to the periphery of the myofiber in long-lived tissue in human muscle; however, in mouse muscle, the central nuclei are stable in regenerated myofibers [200]. This process of myogenesis thus shapes a regenerated skeletal myofiber.

1.3.3.3 Remodeling Phase

Finally, the remodeling step of regeneration is an extension of the repair process in which the freshly formed myofibers (shaped by fusion of progenitor cells) mature further, grow in diameter and length, and form strong attachments to the adjacent extracellular matrix, tendons and/or bones to which the muscle attaches. Functional muscles need the parallel arrangement of myofibers, the development of a functional vascular supply and the appropriate innervation to generate regulated and controllable forces [186]. There has been considerable research investigating the development of vascularization in the site of a muscle injury [160, 169, 195, 201]. The stimulation of angiogenesis can activate resident SCs and the vascular tree will supply a channel for the migration of myogenic progenitor cells [202].

A critical stage in regenerative medicine for skeletal muscle tissue is the restoration of motor innervation and the development of robust motor endplates that deliver appropriate nerve action potentials to the regenerated myofibers. These motor endplates present not only functional control to the newly generated muscles, but their stimulatory effects also influence myofiber size, fiber-type distribution, and fiber alignment. The failure of neuromuscular connections to be re-established will lead to the development of atrophic muscles due to myofiber denervation.

The significance of nerve activity in the regeneration of muscles has been clearly shown after use of a myotoxin called bupivacaine to stimulate muscle injury. Bupivacaine stimulates necrosis of whole myofibers but leaves SCs, blood vessels and nerves intact. Using this injury model, the formation of new myotubes commenced after about 3 days. Regardless of structural

differences shown by regenerated muscles, significant myosin synthesis in the regenerates started to increase at day 4 post-injury. The regenerated muscles already displayed the same pattern as that of control muscles, with fast development of fresh motor endplates which lead to rapid muscle tissue maturation and the restoration of function [203].

Experiments *in vitro* using co-cultures of myoblasts, SCs and neurons have displayed that in comparison to muscle-only structures (myotubes formed in culture), nerve-muscle structures produce greater contractile force after electrical stimulation. Successful reinnervation was also characterized in an experimental model using the small intestinal submucosa (SIS)-ECM-mediated repair of gastrocnemius muscle. As an ECM scaffold, SIS-ECM has the ability to modify the microenvironment of a wound through the release of growth factors that act as chemo-attractants for myogenic precursor cells. In this SIS-ECM model of muscle repair, newly formed nerves occupy the injury site within 2 months of inserting the SIS-ECM scaffold and develop the pre-synaptic aspect of motor endplates that extend towards regenerated muscle fibers. Ultimately, the motor endplates are reconnected functionally with the sciatic nerve, as verified by documenting action potentials were produced to depolarize the muscle after nerve stimulation. Skeletal muscles showed vascularization and innervation similar to normal muscle in the site of ECM-scaffold implantation within 6 months [204].

1.3.4 Models of Muscle Injury

Different types of muscle injury are usually utilized to study particular processes and time period of muscle repair that take place after damage to fibers (plus or minus other types of tissue in a muscle belly). Some of these models, such as injection of a myotoxin, are reported as only disrupting myofibers themselves, including the sarcolemma and then the sarcomeres [203]. Other models such as a traumatic crush injury, affect all types of cells in a muscle, including the basal lamina around myofibers [205, 206] plus connective tissues (e.g., tendon, epimysium, and perimysium), blood vessels, nerve axons, NMJs, and sensory innervation. A noticeable disruption of the basement membrane and connective tissue patterning in a skeletal muscle, such as occurs after a crush injury, results in a slow or gradual process of muscle regeneration, often accompanied by fibrosis and scar formation in larger muscles [207]. By comparison, myotoxic injury stimulates a faster and quite complete regeneration of a muscle [208].

The many types of experimental injury that have been utilized to examine the regeneration capacity of skeletal muscle, the process of SC activation, the properties of stem cells, and the roles of many paracrine, endocrine, and autocrine factors, can be grouped into those models that: include myotoxins and chemicals (e.g., barium chloride) that directly damage myofibers; traumatic injury of various forms such as muscle crush, muscle chopping, needling of a tiny volume, eccentric lengthening or over-stretching, overload injury, and freezing; auto-transplantation; and denervation-devascularization. Other types of injury used to investigate muscle regeneration have examined damage-repair processes in a number of neuromuscular disease models such as X-linked and autosomal dominant forms of muscular dystrophy.

Regardless of the model of muscle damage that is employed in an experiment, the progression of myogenic regeneration includes the same overall phases, although different timing, duration, extent, and/or outcome. The consistent feature in all types of muscle injury is the involvement of SCs in the process of muscle regeneration. As early as a study by Carlson [209] and other reports, investigators noted that the duration of muscle regeneration and the fundamental properties of regenerated muscles are influenced by many factors including the availability of SCs inside damaged muscle, the preservation of the structures of extracellular matrix in the endomysial sheath around fibers after fiber damage, and the magnitude of the damage to nerves, axons, axon boutons, and blood vessels. Very early in the research timeline on muscle regeneration, it was determined that basement membrane preservation is a key factor that enables the rapid orientation of new myotubes during regeneration in the process of damage recovery [207]. A major disruption of the ECM and the basal lamina after crush injury may also influence the production (synthesis and release) of a broad variety of growth factors [210].

Fibro-adipogenic progenitors (FAPs) are multipotent cells which comprise 2–3 % of the mononuclear cells that could be isolated from skeletal muscle. FAPs provide support to myogenic progenitors during the myofiber development and regeneration that is required for fiber maturation and specification. Moreover, FAPs are a main source of fibrosis during conditions of a degenerative disease, showing their importance as a potential target for anti-fibrotic muscle treatments [211]. While evidence shows the important role for FAPs in tissue degeneration and normal regeneration, the signals controlling their survival, growth, and differentiation are still under investigation. Nonetheless, the multipotent FAPs have been identified as having a potential for use in the reparative treatment of a range of disorders, such as ectopic bone formation,

adipocyte accumulation, and fibrous tissue deposition. Effective methods to culture purified and identify FAPs are critical research steps for understanding physiological functions of these cells, and are under investigation through application of cell culture, gene expression studies, transplantation, and single-cell experiments [212]. One study utilized a model of acute muscle damage to show that inhibition of FAP expansion using a pharmacological tyrosine kinase inhibitor (Nilotinib), has a damaging effect on myogenesis during regeneration. This study also confirmed the inhibitory effect of Nilotinib on damage-induced expansion of SCs *in vivo*, signifying a non-cell-autonomous effect. [213]

Among the many types of experimental muscle injury, trauma (e.g., by crush) and myotoxin injection are the two main models reported in the literature. Key differences in the repair process between crush and myotoxin include the timing of new myofiber formation, the extent and duration of inflammation, the timing or restoration of myofiber contractile properties, and the extent of fibrosis remaining after regeneration. In addition, the rapid restoration of innervation to new myotubes after myotoxic injury, either inside preserved endomysial sheaths or produced *de novo* around myotubes regenerated after phagocytosis of damaged tissues, and the sustained integrity of microvasculature within the ECM are important in the fast recovery after damage to myofibers by a myotoxin [214]. In contrast, since a traumatic injury such as a muscle crush is associated with severe damage to nerve-terminal boutons, NMJs, small and larger branches of the vasculature, and myofibers, the functional innervation of new myotubes is considered to be impaired for quite some time. The slow re-establishment of the functional innervation of new myotubes thus delays the expression of slower MyHC isoforms (i.e., MyHCIIa, MyHCI) and the recovery of typical patterns of oxidative enzymes after crush injury compared to the rapid regenerative patterns following myotoxin injury that include the persistence of fast MyHC isoforms expressed in the regenerated muscle [208, 215].

1.3.5 The General Timing of Muscle Repair and Tissue Remodeling

At the same time as myofiber restoration (by myogenesis) is progressing, myofibers need to receive oxygen and nutrients and be cleared of metabolites. This occurs through the ingrowth of new blood capillaries (vascularization). The formation of scar tissue (fibrosis) is also launched during the early phase of regeneration, and the elements of loose connective tissue (fibroblasts, collagen, laminin, and adipose tissue) can often seem to fill the interstitial space between residual

myofibers and new myotubes. Myogenesis and the vascularization of regenerated myofibers via capillary ingrowth normally peak at about 1 week after injury and then decline, although they continue for the following 2-3 weeks post-injury. By comparison the deposition of fibrous connective tissues (e.g., collagen bundles) starts around 2 to 3 weeks post-injury and subsequently matures into fibrotic scar tissue in the longer term, depending on the rate and effectiveness of myogenic regeneration and vascularization during repair of the muscle [216]. Essentially, the regeneration of connective tissues, including fibroblasts and adipocytes via their respective precursors, is directly involved in the timing and success of muscle regeneration and the return to function [213]. Indeed, animal experiments have demonstrated that even in dystrophic muscles of the *mdx* mouse, reduction of fibrotic connective tissues using an anti-fibrosis drug called halofuginone, can markedly improve the function of those regenerated and dystrophic muscles (skeletal and cardiac) even in the long term, and also reduce the susceptibility of myofibers to further dystrophic injury during exercise [217, 218]. Thus, there are many interactions among all the different types of cells in a muscle, that determine the speed and effectiveness of regeneration after a muscle injury.

1.3.6 Age-Related Alterations in Muscle Regenerative Capacity

It is well understood that during aging in humans and animals, muscles demonstrate reduced volume and mass, smaller fiber cross-sectional area (CSA), decreased strength and impaired contractile function; these changes are collectively known as sarcopenia. Similar findings are reported in other conditions. For example, patients with diabetic polyneuropathy have reduced muscle quality and strength as well as contractile slowing [219]. However, the impact of such age-related changes on muscle capacity for regeneration is not as clear, likely due to the many models and outcome measures that are used to conduct such research. By means of various *in vitro* and *in vivo* methods, it has been revealed that SC function is influenced by aging in both animals and humans. Cell-intrinsic and extrinsic triggers have been associated with this drop in SC function. Among the intrinsic factors (i.e., those inherent within single cells), somatic mutations are known to accumulate in the genome of SCs through aging, and are associated with defects in proliferation and differentiation. More modifications in the epigenome and transcriptome in addition to the progressive deterioration of cellular metabolic components and changes in signaling pathways that adjust the capacity for self-renewal in SC progenitors, gradually compromise the function of SCs

in older humans. In parallel, extrinsic factors including hormonal, immune and extracellular matrix modifications further reduce the functional ability of SCs to be activated [220], proliferate and differentiate. Under the pressure of the collection of intrinsic and extrinsic factors, SCs tend to enter a condition of senescence and the numbers of functional (responsive) SCs increasingly declines in the muscle. Consequently, aged skeletal muscle exhibits a decreased capacity to recover the original muscle mass after negative incidents such as immobilization, injury or inactivity. Notably, that conclusion applies to large muscles in humans; there is evidence of significantly greater capability for muscle regeneration in the much smaller muscles of mice after significant age-related atrophy toward senescence [169]. However, the muscle environment in older people does preserve the ability of SCs to react to stimuli such as strenuous exercise and can progress through muscle remodeling [221, 222]. Exercise routines therefore need tailoring in features such as exercise type, intensity, and volume to reduce, delay or even stop the intrinsic and extrinsic negative events that can occur in SCs with aging [223].

The physiological actions of both SCs and immune cells deteriorate through ageing, thereby blunting or changing the ability of skeletal muscle to regenerate. The age-related decrease in muscle repair efficiency causes development of sarcopenia which is one of the most crucial factors of disability in elderly people. Preserving muscle regeneration capacity, in part through physical activity and/or potential treatment with blood-borne paracrine regulatory factors including myokines [48, 62, 224-226] would slow the development of this syndrome. Aging also causes a decrease in capillarization of muscles. Inadequate vascularization of myofiber could be a key factor of impaired regulation of SCs in older adults. It was shown that the distance between capillaries and SCs for type II myofibers is more in older adults. The bigger distance between capillaries and SCs in older adults could cause dysregulation in the activation of SC and damage the ability of muscle to remodel and regenerate. Even though there is controversy on the actual contribution of SCs to the development of sarcopenia in later life, maintaining or increasing exercise activity remains a potent strategy for older individuals, to reduce the effects of sarcopenia. Other approaches have proved that nutrients such as polyphenols, vitamin D and amino acids can improve the regeneration of skeletal muscle through targeting main functions of muscle cells and/or immune cells [227-229].

The function of SCs is influenced by oxidative stress, which also increases during aging. This change likely contributes further, to the way that SCs on sarcopenic myofibers react to

stressors including disuse, exercise, or rehabilitation. Nutritional intervention affords one therapeutic approach to develop the systemic factors and SCs niche in ways that could improve the function of SCs in aging myofibers. Even though older individuals consume various nutraceuticals, many of those compounds have not been well tested using scientific methods, and the impression that they could have on SC function and sarcopenia is not clear evidence of a real benefit. One study examined the responses and function of SCs in aging skeletal muscles, in testing the effects of three compounds including green tea catechins, resveratrol, and β -hydroxy- β -methylbutyrate on regulating SC function by following whether they decreased sarcopenia or increased muscle mass in aged skeletal muscles. The results showed that using these nutraceutical compounds can boost the function of SCs throughout rehabilitative loading in aged animal models of muscle regeneration. Even though these compounds have not been examined in humans, findings from studies of aged animals present a basis for performing a human study to determine whether such nutraceuticals can overcome the muscle loss, or benefit regeneration in sarcopenic muscles of older humans through improved SC function [63].

The use of healthy SCs to produce new myofibers, and/or reform existing fibers, can be considered one way to fix the defects that cause muscle wasting by aging, as additional fibers would restore muscle mass and force, and rejuvenation of the sarcopenic muscle. One study showed that transplanting SCs into injured muscle of young mice caused growth in muscle mass and an increase in force that persisted as the mice aged. In this model, the lifelong persistence of enhanced muscle mass came from a rise in the number of myofibers and their progressive hypertrophy [230].

SCs and other types of myogenic progenitor-cells have been successfully utilized to repair the effects of degenerative muscle diseases triggered by genetic conditions. Effective engraftment with the methodology utilized in preclinical trials, to deliver cells that will engraft to the muscle, needs a concurrent injury; this is not a practical approach for treating sarcopenia. Besides, the local and chronic inflammation in old organisms represents another problem which would worsen engraftment, survival and the myogenic ability of transplanted progenitor cells.

Age-related dysregulation of the immune system and inflammation have been consistently shown to have a negative effect on SC function, reducing their myogenic capacity and regenerative potential, promoting the development of sarcopenia. One study used myoblast implantation in a model of Duchenne muscular dystrophy (DMD), to deliver signals that would support expansion

of myoblasts before differentiation is started [231]. These studies, together with the use of pharmacological involvements that help myoblast migration, demonstrated the possibility of modulating the activity of a muscle progenitor to promote muscle repair. Successful cell therapy methods for sarcopenia require the progress of concurrent interventions to supply the pro-repair signals produced by the injury and to progress myogenesis and the following phases of muscle regeneration that are limited by pro-inflammation. In DMD models, the injury signal generated by exercise boost the success of engraftment of muscle progenitor, eliminating the need for a concurrent injury caused by chemicals or toxins. Nevertheless, physical exercise is not sufficient to stimulate myofiber hypertrophy in the old muscles but can enhance the responses of SCs in injury models. Therefore, it is possible that in aged models, the capability of doing exercise to stimulate pro-repair and pro-growth signals is not completely functional. A recent study on young mice showed an increase in the levels of apelin after exercise. Apelin is a novel exercise-induced myokine that increases both stem cell function and muscle cell metabolism during aging and is used in promoting research on skeletal muscle hypertrophy. Low apelin levels are related to sarcopenia and apelin signaling helps fiber hypertrophy and SC-mediated muscle repair, it is possible that the impairment of apelin-induced muscle development in aged models would diminish the useful effects of exercise in advancing myoblast engraftment [232]. Thus, it is critical to find other factors that mediate the effects of exercise and that could be utilized in muscle cell therapy in sarcopenia. A study by Richchetti demonstrated that during aging, SCs switch to a condition of permanent or highly persistent cell-cycle senescence which stops their activation. The senescence of SCs is due to defective autophagy which regulates the mechanism that degrades damaged organelles and proteins. Molecular damage is caused by oxidative stress that also helps epigenetic modifications which trigger the expression of genes that ensures senescence [233].

In response to stimuli, SCs are activated and proliferate and then have two different fates: progeny may repopulate the SC niche or differentiate to regenerate myofibers. Regardless of the fate of SC daughter cells, both the ability to regenerate and replace lost fibers and the ability to repopulate the SC niche drop with aging. This loss of performance seems to result from extrinsic alterations in the niche, such as modifications to signaling or changes in the ECM, combined with intrinsic epigenetic alterations that could also affect the fate of the cells and cause the drop in regenerative capacity. In the aged niche, SCs transfer from a quiescent to an active phase without a regenerative signal [71]. TGF β - and Wnt-dependent growth of fibrosis in skeletal muscles

interrupts the architecture of the basal lamina. Dysregulation of FGF, Wnt, p38 α / β and Notch signaling results in a loss of cell polarity and stops asymmetric division of cells that enables renewal of stem-like and myogenic populations of SCs. Age-related persistence of TGF β activity and loss of Notch activity produce epigenetic modifications that induce expression of p16INK4A and de-repress the CDKN2A locus; this drives SCs away from their typical cell fate (differentiation or self-renewal) and pushes them to age-related senescence. In genome-wide linked research, the p16INK4A locus is genetically related to the peak amount of age-associated pathologies. Reestablishing regenerative ability to aged skeletal muscle may be as easy as switching aged SCs with young SCs, and/or altering signaling pathways to preserve alterable quiescence. This means that skeletal muscle aging could be reversed only by controlling the epigenetic memory of SCs and returning the aging clock back to zero [71].

The study by Lee and colleagues [161] examined muscle regeneration capacity using three models of muscle injury in mouse: injection of the myotoxin called notexin (which kills fibers but does not damage satellite cells or the neurovascular supply to muscle), denervation-devascularization (DD, which traumatically disrupts all vessels and nerves as well as fibers in a whole muscle without damaging the basement membrane or connective tissue proteins), and freezing (with localized injuries to muscle, nerve and blood vessels without structural disruption until later inflammation and disposal of necrotic tissue). Comparison of muscle regeneration capacity between young, old and senescent mice injured with each of the three models of muscle damage, was used to assess whether there are age-related alterations in regenerative capacity of muscle to restore normal function. The results demonstrated by muscles 30 days post-injury at all three ages (young, old and senescent mice) showed that regeneration after notexin injury (to muscle only) was fully effective, even in the very oldest group of mice (28 months of age), as shown by both physiology (contractility), histological and morphometric analyses. While freeze injury generated regional damage and structural regeneration of muscle with slightly lower restoration of function after 30 days (compared to age-matched controls and notexin-induced injury). In further contrast, after DD injury (which disrupts myofibers, nerves and blood vessels), muscles displayed delayed regeneration compared to the other two types of injury, greater collagen deposition, and less contractile strength and lower fatigue resistance. Results therefore, showed that SCs in muscles of old and even senescent mice retain the capacity for muscle regenerative

responses to injury which are similar to those from muscle in young animals, such that the result of regeneration did not differ significantly between freezing or notexin injury [161].

Thus, even though important steps have been made in studying the importance of SCs in the progression and treatment of sarcopenia, the idea that the function of SCs is a therapeutic target that will cure sarcopenia still requires clarification.

1.4 Neuromuscular Junctions (NMJs)

It is impossible to discuss skeletal muscle structure without including NMJs which connect the muscular system and the nervous system. These structures pass signals including the neurotransmitter, acetylcholine (Ach) released from the nerve ends or terminals of myelinated motor-nerve axons in the pre-synaptic region, across the synapse or synaptic cleft to bind acetylcholine receptors (AchRs) in the post-synaptic area on each myofiber. NMJs thus convey the motor stimulus for contraction to myofibers.

Nerve terminals, myofibers and terminal Schwann cells (TSCs) establish the cellular apparatus of the synapse. Many aspects of these cells and their interactions have been used as a focus when studying the stability and pathology of NMJs, since there can be disease- or disruption-related changes in the preservation of cellular synaptic compartments, the location and number of AchR clusters on a myofiber, the number of nerve-terminal boutons per myofiber, the number and configuration of non-myelinating TSCs covering the nerve boutons as they reach across the synaptic cleft toward the myofiber, and the basal lamina near the synaptic clefts.

The proper functionality of NMJs controls crucial and complex processes including body movements and breathing. Therefore, deficient formation of NMJs with abnormally developed synapses or improper maintenance of NMJs later, may each create several neurodegenerative diseases. Since NMJs are fairly large regions on myofibers, and reasonably easy to stain histologically, investigators have developed many tools for studying their structure and function in modeling synaptogenesis and the interactions between nerves and muscles [234]. The initial growth of a NMJ needs the development of a motor axon bouton to reach close to a specific muscle fiber. Growth cones at the tip of the axons, are chemical sensors of molecular guidance cues that exist in target cells including myofibers. Even though the mechanisms engaged in the guidance of motor axons to muscle targets in many species including human, mouse, *Drosophila*, and *C.*

elegans are well described, there are fewer reports focused on the cues involved in the stabilizing NMJs during life.

During postnatal development, there are significant events that take place at the postsynaptic area of the NMJ. First, the function of the NMJ derives from the role of AchRs of the nicotinic type. AchRs form within the myofiber sarcolemma; initially AchRs are distributed on the whole membrane in early development and later they cluster at the region that will become the post-synaptic membrane on the myofiber. AchR morphology also changes, and gradually stabilizes during maturation. Therefore, the overall maturation process involves changes in the shape of the NMJ containing AchRs, and alterations in the relative levels of the subunits (see below) of each receptor complex within the motor-endplate region.

In the neonatal mammal, AchR clusters exhibit a simple plaque shape; these plaques are transformed into “pretzel-like” more complex plaques that show multiple perforations” formed by the many intricate nerve-terminal branches passing over the region of post-synaptic specializations or clefts of the myofiber surface. A huge density of AchRs at the synapse is the hallmark of mature NMJs.

Each AchR is composed of five protein subunits (each a transmembrane protein) arranged evenly around a central pore through the sarcolemma of a myofiber [235]. These subunits are named alpha, beta, gamma, delta, and epsilon. Alpha and beta subunit proteins have multiple sequence variants which results in many alternate forms of nicotinic AchRs. At the neuromuscular junction, an AchR has two alpha subunits, one beta, one delta, and one gamma or epsilon subunit in the pentamer channel. Moreover, AchRs themselves, change during synapse maintenance and maturation. First, the embryonic gamma (γ)-subunits of AchRs are replaced by the more adult isoform, epsilon (ϵ)-subunits, during early postnatal development, as post-synaptic myonuclei collect under the NMJ plaque. This shift increases the calcium permeability of the receptor (“magnifying” the signal), and is also crucial for the developmental growth of junctional folds in the NMJ and the maintenance of AchR clusters in the synaptic site [236-238].

AchRs on a myofiber change during the stages of maturation and with the innervation status of a fiber. The AchRs in fetal and denervated muscles express the gamma subunit, while AchRs in normal adult and innervated muscles express the epsilon subunit. An improvement of receptor function results from a shift from AchRs containing the gamma subunit to those comprising the epsilon subunit. Moreover, the composition of AchRs on the sarcolemma is also

modified during the process of fiber innervation, itself. Maturation of the NMJ region is accompanied by a shift from linearly and dispersed AchRs to the clustering of AchR complexes. With denervation, AchRs return over time, to the more immature, linear and dispersed arrangement.

The structural hallmarks of denervation in skeletal muscle can be distinguished by approaches that study the location and relative amount of fetal and adult subunits of AchRs and the physical components of AchRs at the NMJs. One study showed that experimental knockout of a chemorepellant protein called semaphorin 3A (Sema3A) using Sema3A-siRNA treatment on myoblast cultures caused a reduction in the expression of mRNA and protein for AchR subunits gamma and epsilon, and of myogenin; these findings display the role of Sema3A in the production and stabilization of AchR clusters [239]. Another study on human muscle cells after rotator-cuff injury (RCI) displayed a consistent interaction between AchR clustering and Sema3A levels by showing an increase in the ratio of gamma:epsilon (γ : ϵ) subunits of AchRs in the sarcolemma [240].

In the presence of complex guidance cues during nervous system development, motor neurons proliferate and differentiate in the spinal cord, and develop into fast and slow neuronal subtypes. These classes of motor neurons allow the maintenance of NMJ-specific contractile functions. Similar to myofibers, motor neurons are classified into three main subtypes including: fast-twitch fatigable or fatigue-sensitive, slow-twitch fatigue-resistant and fast-twitch fatigue-resistant, based on their electrical properties [241], which ultimately drive the metabolic distribution of fiber-types in the muscle itself (see below). Generally, it is the neurons that develop first and connect to the developing fibers, but the muscle precursor myoblasts that develop in the embryo very quickly begin to show features of faster or slower muscles, in part because of their position in a limb or body region [242]. The more superficial muscles are generally faster twitch than the deep muscles close to the bone and the joints that the muscles cross over. While it can be considered a little different in regeneration (compared to development from the start). In regeneration, the muscle phenotype is driven by the SCs that are available to respond and divide and the neurons that will connect via NMJs [243]. In development the timing of expression of MRF genes is really crucial [244], and this overlays with the complexity of neuronal development and their separation into fast or slower neurons.

Synaptic formation initiates as a fundamental property of axonal terminals, through the creation of active zones on the terminals. The active zones, located at the pre-synaptic area of terminal swellings or boutons, are the sites of the release of synaptic vesicles containing Ach, and have key roles in the pathology and function of NMJs.

There is, therefore, a complex interaction between axons, TSCs and the differentiating myofibers, creating a “multilateral” neuromuscular (NM) synapse during development, meaning that myofibers signal neurons, neurons signal myofibers, and closely adjacent TSCs signal (and presumably receive signals from) both proximate neurons and myofibers. Terminal Schwann cells contact axon boutons while they cover the regions on myofibers that will become NMJs. Myofibers send signals to regulate the function of motor neurites through agrin and the Wnt signaling pathways. Wnt ligands are secreted molecules that adjust different aspects of embryonic development such as axon guidance, formation of synapses, AchR aggregation and clustering and differentiation of the pre- and postsynaptic components of the NMJ [245]. Wnt glycoproteins are also necessary in adjusting the function of stem cells in adult tissues as well as in regulating the differentiation during myofiber development. In the adult, Wnt signaling is required for the myogenic commitment of SCs in muscle tissue after acute damages [246].

1.4.1 Development of NMJs

During body development, there are three germ layers in the growing embryo. Myoblasts arise in the mesoderm and fuse to form multi-nucleated myotubes. Shortly after or during the formation of each myotube, motor neurons in the neural tube extend axons toward the areas of developing muscle, and these axons form the initial contacts with the newly developed myotubes.

During NMJ development, laminin and nerve-derived agrin protein stimulate AchR clustering in aneural (non-innervated) myotubes. This process is also relatively related to the activation of the tyrosine kinase MuSK receptor that works through a rapsyn-dependent mechanism. Rapsyn plays several roles in skeletal muscle. Rapsyn not only co-targets with AchRs to the post-synaptic region, it also can self-associate to stimulate AchR clustering. Moreover, rapsyn is necessary for the formation of AchR clusters and transduction of the MuSK phosphorylation signal to AchRs that is evoked by agrin. Lastly, rapsyn makes connections between the cytoskeletal complex associated with the protein utrophin and AchRs, which is needed to stabilize AchRs and during maturation of the NMJ [247].

Agrin is crucial for AchR clustering and supports other facets of post-synaptic differentiation during the formation of synapses. There are two different modes of NMJ maturation in reference to agrin: influences that are insensitive to agrin inhibition and those that are sensitive. The agrin-insensitive type is restricted to the small number of NMJs that develop function in the early phases of innervation. The majority of NMJs only become contraction-competent in the final phases of development. These latter NMJs transmit the motor-function signal on condition that the action of agrin is uncompromised [236, 238]. Myogenin, one of the muscle-specific transcription factors, also has a key role in controlling AchR gene expression and robust AchR clustering, in addition to its role in myoblast differentiation. Although MuSK can also launch a signaling cascade that causes AchR clustering, MuSK and myogenin are not sufficient to induce AchR clustering in early muscle development without the innervation of myofibers [248].

Even though skeletal muscle patterning is assumed to be dependent on the signals delivered by motor nerves, it has been demonstrated that expression of AchR and clustering are localized in the middle area of an embryonic skeletal muscle long before myofiber innervation. Nerve-supplied agrin is not essential during this step of AchR expression, but interestingly, MuSK is necessary to launch this so-called “pre-patterning” of AchRs. These observations all suggest that initially muscle is patterned without innervation, which highlights the probability that spatial cues that confine axon growth to a particular region on a myofiber and enhance synapse development might be supplied by molecules which are also pre-patterned in muscles [172]. Such a suggestion is consistent with even early reports on muscle development and regeneration showing that myogenesis per se, is initially independent of innervation [249-256].

1.4.2 Innervation

As introduced above, early in development of the mammalian embryo, myofibers display connections with more than one nerve axon which is known as polyneuronal innervation. During later development, these connections between myofibers and motor neurons are modified or ‘pruned’, such that in mature muscle, every myofiber is innervated by only one axon (mononeuronal innervation). The pattern of pruning or axon retraction, which occurs through Eph-ephrin signaling, accounts for development of mono-neuronal innervation. Prolonged blockade of neuromuscular transmission results in longer persistence of polyneuronal innervation in development [257].

Studies have displayed that remodeling of NMJs and their AchR areas in the peripheral nervous system is more considerable when there is a delay in reinnervation post-injury to muscle. The “contest” between multiple axons trying to reinnervate the same NMJ region was long ago proposed to cause this remodeling [258]. The difference between slow and rapid reinnervation was the level of polyneuronal innervation of myofibers throughout the reinnervation procedure. Polyneuronal innervation was then proposed to be caused by the reinnervation of a NMJ by escaped nerve axons coming as extra branches from a nearby, fully innervated NMJ; that process was thought to “chase” TSC processes connecting the two NMJs [259]. During reinnervation, the number of NMJs with multiple-neuronal innervation is less than the number of NMJs that display a loss of postsynaptic receptors. This finding suggests other reasons for the elimination of synaptic areas than competition between several axons innervating the same NMJ [260].

1.4.3 Motor Units

A motor unit in skeletal muscle includes a single motor neuron, its axon and axonal branches, and all the myofibers innervated by that neuron, including their respective NMJs [261]. Myofibers in adult mammals generally display only a single NMJ and are innervated by one motor neuron. Thus the motor unit forms a functional entity, since by a single impulse discharge through the nerve fiber, the myofibers of that whole motor-unit group are excited together [261]. By increasing the number of myofibers in a motor unit, impressive movements are possible (e.g., one motor unit can supply more than a thousand myofibers), and by intermingling the fibers of different motor units, contractions can be smooth and controlled.

Recent studies illustrated the presence of different sub-types of neuromuscular synapses in muscles that vary in the spreading of fiber types among the population of fibers. Differences among motor neurons result in three major types of motor units in mammalian muscle, since a single unit of myofibers will demonstrate quite uniform metabolic and contractile features. Slow fatigue-resistant, fast-fatigable and fast fatigue-resistant myofibers result, with each type expressing a particular distribution of the isoforms of MyHC protein including type I, type IIa, and type IIb, respectively. Type IIx MyHC is expressed in fibers in transition from one type of Type II fiber to another. The different types of motor unit vary in their anatomical plasticity, physiological properties and vulnerability to loss of neuromuscular connectivity. Slow-type fatigue-resistant synapses, in contrast with fast-fatigable-type synapses, show widespread sprouting of motor

nerve. Moreover, fast-fatiguable synapses are more vulnerable to loss in motor neuron diseases [236, 238]. The axon that extends from a motor neuron, along with its innervating branches to myofibers, also is subject to pathologies including toxicity, intracellular-transport defects, trauma, and loss of the protective, insulating myelin sheath. Axons are supported by a structural framework of neurofilaments (NF) that form a cytoskeleton, which is also involved in controlling axon diameter. NFs and other axonal proteins are synthesized in the neuronal cell body and move down the axon to their destination [262].

1.4.4 Motor Units and Activity-Related Alterations

There are three main contractile features of motor units: fatigability, contraction speed and maximal force. Modifications in typical steps of physical activity can affect these features.

Skeletal muscle displays an amazing plasticity, and is able to adjust to a range of external stimuli including changes in: the level of contractile activity including endurance exercise training, the prevailing environmental situations such as thermal stress, loading state such as resistance exercise training and substrate availability such as macronutrient supply. Even though this level of plasticity is regular to all vertebrate muscle, there is a vast difference in the extent of adaptability across species, and among individuals in a species. This flexibility partially clarifies the variations in features of physical functioning including strength or endurance among individuals [8].

The properties of elevated physical activity vary per the duration and intensity of the activity. The performance of short-term periods of high-intensity contractions a few times weekly improves motor unit force and contraction speed, while prolonged sets of low-intensity contractions decrease the fatigability of the motor unit. Physical activity routines that include such variances are regularly defined, respectively, as strength and endurance training. It has been revealed previously that running endurance training in young subjects may reduce the area of type I and type II myofibers. For instance, a study displayed that marathon training decreased fast-twitch and slow-twitch myofiber size but that it improved the functional profile of these myofibers [263]. Nevertheless, the impacts of endurance training on skeletal muscle highly depends on the volume, intensity, and mode of training. Furthermore, several studies have displayed that resistance exercise training decrease the expression of MyHCIIx in human skeletal muscle and enhance the expression of MyHCIIa, while the expression of MHCI is unaffected by the resistance exercise. This is a highly solid observation and a general consensus on this point exists among people working in the field. Likewise, cessation of resistance

training will induce, or re-induce MyHCIIx at the expense of MyHCIIa. Whether the number of myofibers expressing MyHCI is increased or decreased following strength training is arguable, but most likely, there is no subtle changes in the number of myofibers expressing MyHCI. Therefore, the overall rule of the plasticity of MyHC isoform in human skeletal muscle could be an increase in the amount of resistance training leads to an increase in MyHCIIa or decrease in MyHCIIx whereas a withdrawal in resistance training causes an increase in MyHCIIx and decrease in MyHCIIa, while MyHCI is relatively unaffected [264]. Also studying the effect resistance exercise training on transcript levels of MyHC isoforms for 3 months revealed that an age-related decrease in the transcript levels of MyHCIIa and MyHCIIx did not change by exercise, while exercise results in a higher synthesis rate of MyHC and an increase in MyHCI isoform transcript levels [265]. Another study showed that the cross-sectional area of type I, IIa and IIb myofibers increased in vastus lateralis muscle of middle-aged men after 21 weeks of strength training. An increase in the CSA of the muscle also suggested muscle hypertrophy after strength training. Architectural changes such as changes in pennation angle of the myofibers, may also have taken place during the strength training period. The findings also specify the important role of the nervous system to maximal strength development during strength training periods which could be due to an increase in motor unit recruitment, number of active motor units and/or in their firing frequency [266, 267]. The endurance and resistance training might induce various types of signaling pathways after electrical stimulations. The main challenge for exercise biochemists is directly linking the metabolic and intracellular signaling events that happen after different durations, types, and intensities of exercise to particular changes in the expression of gene and protein in skeletal muscle. This will be difficult through the fact that these pathways are not linear, but rather establish a complicated network with lots of cross-talk, feedback regulation, and transient activation [268, 269].

Modifications in the profile of contractile features of motor units can occur through alterations in the biochemical properties and structural specializations of myofibers. For example, the increase in contraction speed triggered by strength training is accompanied with an improvement in the highest shortening velocity of a myofiber triggered by the improved enzymatic molecules (involving troponins and tropomyosins) that enable adjustment of the speed of myosin-actin interaction of the myosin molecules in the myofiber. Likewise, an improvement in the most rapidly produced force is accompanied with an increase in intrinsic force capability and

enlargement of myofiber size via an increase in the density and number of contractile proteins. Changes in the fatigability of a myofiber, can be triggered by various adaptations including alteration in capillary density, the number of mitochondria, metabolic capabilities of the myofibers and excitation-contraction coupling. Endurance exercise can elevate mitochondrial biogenesis and improve the oxidative capacity of a myofiber, thus decreasing its fatigability. Even though the adaptive capabilities of myofibers are reduced by aging, muscles are still capable of responding to exercise due to the up-regulation of diverse signaling and gene regulatory pathways necessary for metabolic and functional adaptations. A reduction in muscle activity such as happens during bed rest, aging, space flight or limb immobilization, decreases the maximal potential of contractile features of motor units [15]. A previous study addressed skeletal muscle atrophy due to non-weight-bearing as a fundamental issue associated with spaceflight deconditioning and a microgravity environment. This study used weight-bearing aerobic exercise in rats exposed to simulated weightlessness via hindlimb suspension to investigate whether muscle atrophy could be reduced. The results displayed that hindlimb-suspended (HS) rats with exercise showed greater muscle mass than HS groups without exercise. Therefore, the moderate aerobic exercise reduced muscle atrophy as a result of simulated weightlessness, nevertheless, its effectiveness varied between different tissues and anatomical sites [270].

There are also age-related changes in motor units. The number of myofibers innervated by a motor unit rises with age, in part as a motor axon can branch into a neighboring motor unit and provide “backup” innervation when a myofiber loses its original nerve supply. This process is described as compensation for progressive partial denervation in aging [271, 272]. The recruitment pattern of motor units changes due to age-related shifts in muscle synergies within a muscle compartment. The threshold at which motor nerves generate an action potential through depolarization and repolarization of the membrane are reported to depend on the metabolism of neurons, axons and nerve terminals [273-275]. As well, at the level of the spinal cord, the interaction of sensory afferents, descending nerve signals from the spinal cord and brain, and motor neurons are also modified with age [276, 277]. Interestingly, many of the alterations with aging of motor neurons and NMJs are closely mirrored by the pathology of the NMJs and motor systems in amyotrophic lateral sclerosis (ALS), and there is considerable debate about whether a loss of motor units in ALS occurs before or after pathological changes in the NMJs in ALS [278]. However, the extent to which the many types of alteration relates to early-onset aging [279], or is

increased by declining physical activity during aging (or other conditions such as depression) is not known.

In advanced age, the capability for reinnervation wanes, leading to persistent denervation that accelerates muscle atrophy and impaired muscle contractility. Alterations in muscle fibers and motoneurons are both likely involved in driving denervation through destabilization of the NMJ. In this way, mitochondria are implicated in aging and age-related neurodegenerative disorders, and are also likely key to age-related muscle changes through their direct effects on muscle fiber energetics and metabolism, and through secondary effects mediated by mitochondrial impairments in motor neurons. Indeed, the large abundance of mitochondria, especially in slow muscle fibers and in motor neurons, that is further concentrated on both sides of the NMJ, likely reduces NMJs especially vulnerable to age-related mitochondrial dysfunction. Manifestations of mitochondrial dysfunction with aging include impaired respiratory function, elevated production of reactive oxygen species, and increased susceptibility to permeability transition-pore opening, which together contribute to reduced ATP-generating capacity, oxidative damage, and apoptotic signaling [280].

1.4.5 Fiber Typing – Impact of Nutrition on Development

Proportions of the various fiber types in muscles are the key to understanding many properties of skeletal muscle such as metabolism (glycolytic and oxidative, resistance to fatigue), contractility (slow- and fast-twitch), and its attributes as muscle (differential contents and fat deposition). Consequently, the study of mechanisms regulating these properties and their influence is important for human health. Even though the effect of motor-nerve impulse frequency and the transcriptional circuitry involved in innervation are well established, the molecular mechanisms that affect fiber-type composition during muscle adaptation or under different nutritional states are still under investigation.

Nutritional supplementation can affect fiber-type distribution in adult muscle, as introduced above. For instance, one recent study displayed that an 8-week dietary intake of 5% apple polyphenol (an extract of apple peel) increased the levels of MyHC type IIx/IIb and myoglobin in rat muscle. Two reports from Tatsumi and colleagues [228, 281] also demonstrated that there was an accompanying increase in fatigue resistance that occurred along with a decrease in the maximum isometric force of plantar-flexor contraction produced after tibial nerve

stimulation. Results related to the biochemical content of muscles in the treated rats showed the intimate relationship between fiber-type distribution and the contractile, sensory, and metabolic properties of the muscles. Another study also investigated the effect of a high-fat diet-induced obesity on the repair process of skeletal muscle and SC function. The muscle regeneration process in obese mice subjected to CTX injury was attenuated, as displayed by delayed expression of Myogenin and MyoD, prolonged necrosis, increased collagen content, and persistent embryonic MyHC expression. Although no considerable differences were observed in SC content, SCs from obese muscles did not activate normally and did not respond to exogenous HGF. Also, injured muscle showed less HGF release than control mice that were fed with standard food. This study showed deficits in muscle repair in obese mice and the impairments in the function of SCs due to the altered HGF/c-met signaling resulted in the delayed regeneration [282].

Other studies have explored the impact of numerous nutritional supplements to increase fatigue resistance and/or strengthen muscle in athletes, exercising individuals, and/or untrained sedentary young or older individuals. For example, a study by Cornish and Chilibeck on the effects of alpha-linolenic acid (a largely omega-3 fatty acid) on older adults during a resistance training program showed that this supplement decreases Interleukin-6 only in older men and has a minimal effect on muscle strength and mass during the exercises. Other reports by Cornish showed a combination of conjugated linoleic acid, creatine and whey protein was beneficial for increasing lean tissue mass and strength and during resistance training while it has no changes in kidney function or oxidative stress [283, 284]. As well, using creatine supplementation combined with resistance training improved physical performance factors such as muscle strength, endurance, and average power as well as lean tissue mass in older men [285].

Many mechanisms are involved in the generation of different myofiber types during development. Early muscle differentiation of fiber-type patterning needs an interaction between patterning systems which contain the *Hox* and *Wnt* gene families and effects on different myoblast populations. Expression studies of the marker molecules involved in adult myofiber typing showed that environmental factors can play a role in the determination of fiber type.

Through later phases of muscle differentiation, hormones, innervation, and functional need increasingly act to regulate fiber type, while individual muscles still preserve an innate commitment to develop specific fiber types. Myofiber types drastically vary in their response to the same stimulus. Regarding nutrient deprivation, fast muscles, are more sensitive to starvation

compared to slow muscles which could be related to the various sensitivity of slow and fast muscles to corticosteroids. Starvation reduces the generation of protein and increases degradation of proteins in both slow and fast muscles in rats [286]. Classic studies demonstrated that exchanging a nerve from a slow muscle to innervate a fast muscle causes a transformation to a slow phenotype in the muscle and vice versa, which can be explained through the various firing patterns of slow and fast nerves [287, 288]. Another study showed that denervation in the diaphragm muscle in rat results in the atrophy of type IIb myofibers, and shows no change in type IIa. Similar changes were found in other fast muscles; however, the type-I myofibers of the slow soleus do show atrophy after denervation, suggesting that the same type of fiber may experience different changes in different muscles [289].

Recent studies showed that three key factors are responsible for the development of the adult fiber types. The first is NMJ maturation through the removal of polyneuronal innervation and the formation of motor units. Slow and fast motor neurons undergo a parallel maturation during the same period of time, and motor-neuron firing arrangements are formed so that the slow and fast motor neurons are matched to the myofibers they innervate [243, 290-295].

Even though the mechanism that first establishes fiber types in mammalian muscles and typically regulates that distribution in uninjured muscle (through innervation patterns from fast and slow motor neurons) is quite well known, the procedure by which the original composition of fiber types in a muscle that is regenerated after a chemical insult (for example by cardiotoxin (CTX) injection) or after muscle trauma (for example after a muscle-crush injury) is not well understood. For example, myosin changes in muscle regeneration are characterized by transformation of immature (neonatal) isoforms of MyHC into adult fast isoforms in fast-twitch muscle, and via the oxidative form of fast isoforms, finally into the adult slow MyHC isoform in slow-twitch muscles [203, 296]. The contractile and metabolic properties of muscles and the myofibers within them, are adjusted during muscle regeneration in this sequence, in adaptation to the functional requirements on the muscle at that time. Creatine kinase and lactate dehydrogenase are two important metabolic enzymes which also have isoforms, and these enzymes also contribute to establishing the metabolic capabilities of new myofibers in the fiber-type proportions that develop during repair. However, it is interesting that the numerous studies of muscle regeneration after injury have focused on myofibers and their ultimate function rather than on the process of reinnervation that restores the functional capacity to respond to voluntary nerve impulses.

Fairly recently, a series of reports by Tatsumi and colleagues, demonstrated that SCs considerably upregulate the expression and secretion of a molecule called Semaphorin3A (Sema3A) that is a chemorepellent to motor neurites (see section 1.5, below, for further information on Sema3A). Tatsumi's research demonstrated that a burst of Sema3A that is secreted from myoblasts signals muscle to express MyHC type I and to form slow-twitch fibers. As well, Sema3A secretion by activated, proliferating SCs occurs exclusively at the early differentiation step of myogenic regeneration. This timing was investigated using cultures of primary myoblasts (derived from SCs) that were treated *in vitro*, with hepatocyte growth factor (HGF) and *in vivo* experiments using crush or CTX injury to muscle [194, 297]. Cultures of SC-derived myoblasts from adult rat soleus muscle were found to secrete more Sema3A than those isolated and cultured from the fast-twitch EDL muscle after HGF treatment, and a burst of Sema3A from myoblasts signaled the expression of MyHC type I by myotubes forming in culture, and the formation of slow-twitch fibers *in vivo* [298]. It is interesting that SCs of slow and fast muscles from rats vary in the molecular mechanisms inducing their differentiation, such as higher expression of Sema3A upon treatment with HGF in cultures of slow-muscle SCs (from soleus muscle) in comparison to SCs from fast muscles like extensor digitorum longus muscle (EDL) [299]. These results are further evidence that fiber-type distribution in skeletal muscle can be modified by localized input from secreted factors derived from SCs (which may or may not be affected by physical activity), in addition to signals related more directly to innervation, aging, and activity.

1.4.6 Neurotrophic Factors (Neurotrophins)

The innervation provided to muscle by neurons developing in the spinal cord and extending toward a muscle in the body periphery, is regulated through the secretion of different neurotrophic factors which promote axonal or neurite elongation toward a target cell. These factors are crucial for neuron survival, function and development. Brain-derived neurotrophic factor (BDNF), also called NGF or nerve growth factor was identified as a 119 amino acid polypeptide in embryonic rats that protects sensory neurons from naturally occurring cell death. Neurotrophins 3 (NT3) and 4 (NT4, also known as NF5) with protein structures like BDNF, are all produced by myofibers and can rescue motor neurons from natural cell death in the embryo, and from cell death following axotomy (cutting of an axon) in the adult. High-affinity neurotrophin receptor complexes on motor nerve terminals act to mediate the biological actions of neurotrophins. Ciliary neurotrophic

factor (CNTF) is also released abundantly during nerve injuries that are accompanied by muscle damage. CNTF has a significant role in promoting neurotransmitter synthesis. Earlier studies showed that the protein and mRNA of CNTF are generated in Schwann cells of adult peripheral nerves. The administration of CNTF supports the viability of myogenic progenitor cells in vitro and myotube differentiation during muscle regeneration [216, 261].

1.4.7 Consequences of Denervation

As mentioned earlier, muscle injuries normally will not repair without scar tissue development, a process that can also involve distal muscle denervation. Therefore, an important phase in regenerative-medicine approaches to tissue damage, is the restoration of nerves and the development of new motor endplates in the regenerating muscle.

Newly formed motor endplates not only present functional control to the myofibers but their stimulatory and chemotropic influences also effect myofiber type, size and alignment. Any failure in the re-establishment of neuromuscular connections will cause atrophy in the regenerating muscle. When a motor unit is denervated, the transmission of action potentials from the neuron to the myofibers is disrupted completely. This prevents contraction of that motor unit, and thus, results in muscle weakness. Denervation is probably the most remarkable kind of atrophic stimulus [300], although atrophy can certainly happen for several other reasons including toxicity, traumatic injury, lack of use, infection, auto-immune processes, or loss of vascular supply [301]. The processes ensuing after a motor nerve is cut or injured involve retraction of the motor axon from the fiber. Retraction may progress to involve damage to the neuron cell body, itself, in the spinal cord. Overall, this process is known as Wallerian degeneration [302]. Aside from loss of muscle function, a reduction in muscle mass (atrophy) is the most visibly notable consequence of denervation; in the longer term, denervation-induced atrophy can be accompanied by fatty infiltration and fibrosis (especially in human muscle) and subsequent changes in myofiber-type composition (shifting toward faster, more fatigable fibers) and gross appearance [9].

After a denervation event severs a motor axon, the reinnervation of a myofiber is classically described to include regrowth of the initially damaged axon toward the myofiber that was its original target. The effectiveness of this regrowth depends, in significant part, on the proximity of the proximal outgrowing neurite (closest to the spinal cord) and the surviving distal aspect of the original nerve pathway to the muscle (comprised of Schwann cells, myelin, and an empty ‘tunnel’ where the axon was originally located) [303].

1.4.8 Growth Cones and Guidance Cues

After axotomy (and also in development), the proximal part of the nerve axon that extends distally toward a myofiber, has a growing tip called a growth cone that “sniffs out” the extracellular area, “looking for” instructional signals to guide the direction of growth. These instructional signals are called axon-guidance cues (or more simply, guidance cues), and can either attract or repel axons [9, 304]. Axon guidance is facilitated by the impacts of repellent and attractant guidance signals on the cytoskeleton of axons. Through development, axon retraction is a significant feature of the pruning of improperly targeted axons following repellent guidance signals. Therefore, clarifying the mechanism of repellent cue-induced axon retraction is of significance to comprehend the pruning of axonal pathways and axon guidance. The mechanism of guidance includes the growth cone detecting cues when protein ligands from nearby cells bind to receptors such as integrins on the growth cone, itself. Once bound, the receptors activate different signaling molecules within the nerve, which in turn regulate growth cone elongation (neuritogenesis) toward or away from the source of the guidance signals [305].

After denervation of myofibers, axon growth is guided by the growth cone which provides a random contact near the location where nerve fibers enter the muscle mass. Synaptic transmission happens within 1 to 2 hours after the axon terminal makes first contact with a myofiber. This fast onset is managed by the spontaneous release of Ach by the growth cone, mediated by signals from the growing myofibers to the axon terminal. Alternatively, there is another process by which denervated fibers can be innervated: new axonal branches can sprout toward a denervated myofiber from other healthy axons in the surrounding muscle tissue [261]. This process enlarges the size of a motor unit, as the supplying neuron would subsequently innervate one or more additional fibers compared to its original pattern of myofiber innervation. Peripheral nerve impairments can trigger partial or complete paralysis as well as sensory disorders, but fortunately, this kind of functional injury is frequently temporary, due to the effective regeneration of damaged axons. However, the time needed for efficient recovery of innervation following myofiber denervation is slower with increasing age, since the process that damaged nerves use to clear up debris is slowed in old animals as there are more obstructions to regenerating axons within the endoneurial tubes of old animals [306].

1.4.9 Terminal Schwann cells (TSCs)

Plasticity, maintenance and regeneration of NMJs rely on terminal Schwann cells (TSCs) [307, 308]. Like most chemical synapses, the vertebrate NMJ is comprised of three closely joined cellular regions, including the presynaptic nerve terminals or boutons, the postsynaptic specialized area of a myofiber, and perisynaptic TSCs that cover the nerve terminals like a bridge between nerve terminals and the myofiber. The concept of the tripartite synapse came from a study on glial cells at synapses [309], which illustrated that glial astrocytes in the CNS and TSCs in the peripheral nervous system (PNS) are integral and active partners of vertebrate chemical synapses. In CNS cultures, astrocytes have displayed an important role in the maintenance and formation of synapses and the adjustment of synaptic function. Only during the last few decades has the role of TSCs in synapse formation, remodeling, function, and regeneration begun to be appreciated [310]. Thus, to have a broad understanding of how an NMJ forms, functions and is maintained, it is essential to continue investigating the interactions among TSCs, nerve terminals and myofibers [311].

In the PNS, injured motor axons regenerate and reform NMJ structures [312] as long as the nerve endoneurial tubes are preserved in the damaged areas [258, 313]. Regenerating axons reach the formerly established synaptic areas through these endoneurial tubes [312]. TSCs usually cover the axon terminals at NMJs, they also are located above the AchR areas on the myofiber membrane, and therefore are in close apposition to the myofiber surface that contains synaptic folds. However, TSCs begin to abandon portions of these areas post denervation, causing synapse remodeling and receptor loss in those areas.

The regenerating axons normally follow TSC processes after denervation, making connection with the receptor surface, and reoccupying at least some postsynaptic receptor regions without the help of TSCs [314, 315]. A study of the behavior of regenerating axons in denervated mouse sternomastoid muscle showed that the configuration of TSC processes at the time a regenerating axon reaches the myofiber, predicts the axonal branching pattern and whether an axon will arrive at a myofiber from the original direction as it reaches a previous synaptic area. Although the majority of myofibers will be reinnervated by an axon sprouting and extending through the endoneurial tube of TSC processes, some segments might be reinnervated by an axon coming from a different direction; in the end, parts of the synaptic area that lack TSCs will lose their AchRs [316, 317]. The frequency of these alterations in the branching of axon terminals as well as the direction of reinnervation depend on the length of the denervation period that the muscle has

experienced. Further experiments using a variety of methods to denervate the sternomastoid muscle in the anterior neck, showed that synapse reinnervation typically started sooner (4 days after nerve crush when the crush was very close to the muscle) and took longer to start when the nerve crush was further from the muscle (6 days) or there were two crushes close together (9 days) [317].

In the human PNS, the time required for regenerating axons to reach the denervated synaptic areas (due to the long paths of motor axons between the spinal cord and limb muscles, for instance) causes a suboptimal recovery after nerve injuries. Long-term denervation triggers a shrinkage of the formerly established synaptic area of the NMJ, and this shrinkage is thought to decrease the potential for functional recovery after nerve injury; the reduction is even more severe in aged individuals due to the slower rate of axon regeneration that occurs with aging [260, 318-320]. Furthermore, NMJs in old animals are fragmented and muscle strength is reduced due to sarcopenia which means that more receptor-rich areas on the denervated myofibers disappear during reinnervation than would be the case in younger animals [321]. Aging also has an impact on the cell-to-cell signaling that is required for effective synapse reinnervation, since in old animals, there is less ability for appropriate pruning or degradation of the atypical axon sprouts that can form distal to nerve terminals or extend to non-denervated myofibers outside the original motor unit [322]. Indeed, as Apel and colleagues indicated, “age is the most important predictor of clinical outcome after peripheral nerve injury” [323]. It is interesting that a slow process of partial denervation, where an increasing fraction of myofibers in a large motor unit becomes less and less sensitive to nerve impulses and ultimately lose their nerve supply, is considered as an underlying factor in the degree of sarcopenia in aging. That factor may account for the reduced response to physical activity by muscle in older animals including humans [324]. Findings of increased gamma-AchR subunits and hyper-responsiveness of SCs in muscle-explant cultures to NO-induced activation, suggested partial denervation could be part of the pathology in rotator cuff injury and contribute to the high rate of surgical failure in rotator cuff repair [240, 325].

TSCs in the region of a denervated motor synapse respond by sending multiple cellular processes outward from the region of the NMJ; this occurs at the same time as other Schwann cell processes within the synapse are pulled back. The extent of these two processes increases with denervation time. The second of these processes is part of the mechanism that recruits motor axons to reinnervate the NMJ. The removal of processes from non-terminal Schwann cells is thought to

accelerate the procedure of axonal return to the NMJ region, which is beneficial for overcoming partial denervation. Nevertheless, the same process may have a harmful effect in injuries where there is prolonged denervation, as it results in a decreased opportunity for functional recovery of NMJs after reinnervation. The development of treatments for injuries that leave NMJs denervated for a long time might be finding the components that attract axons to the NMJ site [317].

The slow improvement in our understanding the role of TSCs in the past was partly due to the lack of suitable probes for specifically labeling these cells. Although the lineage of Schwann cell has been extensively explored, and variances in molecular profile between non-myelinating and myelinating Schwann cells have been identified [326, 327], there were few probes to distinguish TSCs from other types of Schwann cell. The frequently utilized Schwann cell probe, is an original antibody to a calcium-handling protein (S100B) [328]. Antibodies to glial fibrillary acidic protein, (GFAP) [329], NCAM [330], and growth-associated protein-43 (GAP-43) [331] will label all non-myelinating Schwann cells. Besides, anti-GAP-43 labels Schwann cells only after blockade of activity or nerve injury [332-334]. Thus, none of the usually accessible Schwann cell probes were able to specifically label TSCs through many years of research. Moreover, the lack of specific promoters and markers for TSCs has restricted approaches for the selective knockout of TSCs (or TSC-specific molecules) in genetic models that would facilitate studies of the function of these cells *in vivo*. Another limitation regarding probes for TSCs has been that they could not be utilized for detecting perisynaptic Schwann cell dynamics *in vivo* [307].

The usage of vital dyes to label nerve terminals, TSCs [335] or transgenically labeled molecules in synapses [317] has enabled direct study of nerve terminal dynamics at NMJs over time and *in vivo*. Observations displayed that TSC-associated ECM often spreads ahead of nerve terminals during synaptic remodeling in frogs [336]. Another study also showed that the nerve terminal processes occasionally follow the guidance of TSC processes *in vivo* are constantly remodeling through the regression and formation of processes [337].

1.4.10 S100B and p75

Numerous markers have been used to investigate different elements of the synapse, such as neurofilaments (NF) to study the nerve endings, S100B and neurotrophic factor receptor p75 (known as p75^{NTR}) to study TSCs, and (described below, section 1.5.3) α -bungarotoxin to elucidate the muscle side of the NMJ. The p75^{NTR} is expressed by immature Schwann cells, and is suppressed in myelinating Schwann cells while is reactivated again in injured nerves. During

Wallerian degeneration (see below, section 1.4.11), the loss of the myelin sheath and the return of a group of protein markers of immature cells including NCAM and p75NTR represents obvious similarities between immature cells in developing nerves and denervated cells [338].

The expression of S100B varies during TSC development, and different markers of TSCs such as P75 are used to further illustrate this phenomenon [339, 340]. Studies show that P75-positive TSCs extended ahead of nerve boutons at the leading edge of a growth cone. The contact area between TSCs and myofibers was greater than that between nerve boutons and myofibers.

S100 proteins play a role in a range of events including apoptosis, energy metabolism, and the regulation of inflammation, proliferation and differentiation. These events are interceded through interactions with some cytoskeletal subunits, target enzymes, receptors, nucleic acids and transcription factors. S100 proteins regulate the activities of neurons, macrophages, neutrophils, myoblasts and Schwann cells, thereby participating in immune responses, tissue development and repair and tumor cell [341]. S100 protein itself, is a member of a family of calcium-binding proteins and is identified as having A and B subunits. Antibody against S100 stains Schwannomas, astroglomas, ependymomas and almost all kinds of malignant melanoma, and is used in diagnostic pathology [342]. S100A proteins are found in skeletal myofibers and cardiomyocytes [341] Antibody against the S100B subunit identifies TSCs [303, 315]. In the following chapters, use of the term S100 refers specifically to S100B.

1.4.11 Wallerian Degeneration

Wallerian degeneration is described as a degeneration procedure that happens after crushing or cutting nerve fibers; it is the degeneration of the axon section distal to the injury. Wallerian degeneration occurs after axonal injury in both the PNS and the CNS and typically begins (from a histological perspective) during 24–36 hours post damage, although the process begins much more quickly in relation to electrical and molecular events. The distal part of the cut axon tends to be very electrically excitable before the degeneration is completed, which could be due to the effects of electrical stimulation on the expression of nerve growth factors in the neurons, while the axonal skeleton collapses and the axonal membrane breaks apart. Axonal degeneration is continued by degradation of the myelin sheath and infiltration by macrophages which clear the degeneration debris in association with Schwann cells [343, 344].

Even though most injury responses include some signaling related to calcium influx into damaged cells, axonal injuries primarily result in an acute axonal degeneration that occurs within the first 30 minutes post injury causing separation of the proximal and distal ends. A brief period of inactivity happens in the distal part of the axon, during which it remains electrically excitable and physically intact. Then, the Wallerian degeneration process continues as granular fragmentation of the axonal cytoskeleton and takes around 24 hours in the PNS (even longer in the CNS). The early alterations contain accumulation of mitochondria at the site of injury which is followed by degradation of the endoplasmic reticulum and disintegration of mitochondria. The depolymerization of microtubules is followed by the degradation of neurofilaments and other cytoskeletal elements which together cause the complete fragmentation of the axon [319]

The rate of Wallerian degradation depends on the type of injury and is slower in the CNS than in the PNS. Another important feature in degradation rate is the axon diameter: larger axons need a longer time for the cytoskeleton to respond to damage and degenerate [345].

Schwann cells also react to axonal damage through downregulation of myelin genes, dedifferentiation and proliferation in the PNS. The distal end of the nerve fiber that is most proximal to the injury site sends out axon-terminal sprouts which are then attracted by growth factors generated by Schwann cells; the axon-terminal sprouts can grow to reach and reinnervate the target tissue. While the axonal regeneration process is effective in the PNS, with close to full recovery in case of injuries close to the nerve terminal, recovery is hardly seen in the spinal cord and CNS [346].

Myelin is a multi-layered configuration of phospholipid-rich Schwann-cell membranes that are wrapped around axons and insulate their transmission of action potentials. Myelin is generated by Schwann cells in the PNS and by oligodendrocytes in the CNS. Myelin clearance, the next step in Wallerian degeneration after axonal degeneration in the PNS is different from that in the CNS. The cleaning up of myelin debris following PNS injuries to nerve axons is much faster and more efficient than in the CNS. Moreover, the permeability to proteins and migratory cells increases via the distal stump in the PNS while the barrier disruption is only limited to the injury site in the CNS [347].

1.5 Semaphorin 3A

Repellent guidance cues can drive neuronal growth cones through development and inhibit regeneration of mature axons. A family of glycoproteins in the chick brain, called semaphorins, were first identified as a suitable candidate for providing repellent guidance cues [348]. Semaphorins are a class of membrane-bound and secreted proteins that mostly operate as short-range inhibitory signals that work via multimeric receptor complexes. Even though different types of semaphorin utilize different receptors, their principal receptors are plexins. The ‘turning away’ function that repels a growth cone involves regulation of actin-microtubule interactions and so-called “collapse” of the growth cone. More than 20 different types of semaphorin have been detected up until now, and they have various roles, including functions in cardiogenesis, angiogenesis and immune regulation [349].

Semaphorin 3A (Sema3A, also referred to as collapsin) is a class-3 secreted semaphorin in vertebrates and is characterized as a potent growth-cone collapse-inducing factor. It was first characterized as a neural chemorepellent for neurons of the dorsal root ganglion in the sensory system. Sema3A acts as a chemorepellent for sensory, sympathetic, and motor axons. Constant expression of Sema3A receptor components, including class A plexins and neuropilin-1 mediates the collapse of growth cones [350].

1.5.1 Sema3A and Myogenesis

In 2009, Tatsumi and Anderson gave the first indication that Sema3A was involved in myogenesis and regeneration processes in muscle [194]. There was a remarkable dose-dependent up-regulation of Sema3A mRNA expression and protein in response to treatment of myoblasts in culture, with HGF to induce activation. Other growth factors had little to no effect on Sema3A expression or production. Sema3A was also identified by immunostaining, in SCs located in their resident position on single isolated myofibers in culture, and in SCs in their niche on the sarcolemma of myofibers in cross-sectioned tissue. Sema3A was produced in the early phase of differentiation by myoblasts in culture, as identified by the levels of myogenin expression and incorporation of bromodeoxyuridine into DNA in the cycling cells. While HGF activates SCs through binding to its receptor, c-met protein, treatment of HGF-treated myoblasts with neutralizing antibody to c-met did not block upregulation of Sema3A expression, pointing to

involvement of a receptor that was not c-met, as mediating this response. The assay in rat muscle SCs isolated from muscle regenerating after crush injury showed that *Sema3A* expression increased in those activated SCs during the first 4 days post-injury, peaked at 6 days post-injury, plateaued between 8-12 days, and then declined to a baseline level by 30 days post-injury [186].

Another report highlighted the time-dependent regulation of *Sema3A* expression and signaling mediated by FGF2, HGF, and TGF- β s in dose-dependent responses, with peak *Sema3A* secretion and expression at the early stage of cell differentiation by myoblasts *in vitro* [351]. In order to advance this concept, a further study described that mRNA expression of the transmembrane proteoglycan receptors, syndecan-2 and 4 (but not syndecan-1 and 3), in early-differentiated myoblasts was sufficient for FGF2 and HGF to induce an increase in *Sema3A* expression; the *in vitro* knock-down of syndecan-2,4 also reduced *Sema3A* expression to a baseline level in myoblast cultures [352].

SCs from slow-twitch soleus muscle express higher levels of *Sema3A* than SCs isolated from the fast-twitch EDL muscle. The clear up-regulation of myogenin, a muscle regulatory protein expressed in differentiation, by treatment of cultured SCs with *Sema3A* protein involved mediation of the signal through plexin-A2 and neuropilins [299] and signaling of the myogenic regulatory gene, MyoD, at 4–12 days post-injury [353]. This finding highlights the dynamic role of SCs in coordinating *Sema3A* expression during their key role as precursor cells for muscle regeneration.

1.5.2 Actions of *Sema3A*

Sema3A is identified as one of the main aspects of the regulatory system responsible for axon guidance through the regulation and development of neuron-neuron connections in the nervous system [348]. RhoA-ROCK signaling is a key factor in the balance between protrusive activity (axonal extension) and cellular contractility (retraction) during axon guidance and extension; multiple cues balance this process by organizing the activity of myosin II in coordination with the F-actin cytoskeleton in axonal extensions. The functions of myosin II and RhoA-kinase in axon retraction and growth cone collapse in response to *Sema3A* were also investigated, and results demonstrated that *Sema3A* manages the myosin II activation by producing an F-actin-bundle cytoskeleton which works as a substratum for force generation by myosin II during axonal retraction. Moreover, ROCK is indicated as a downstream effector of

Sema3A signaling, shutting down F-actin polymerization and resulting in protrusive activity, leading to growth cone collapse. Myosin II might have a role in growth cone collapse through producing contractile forces that can direct improved retrograde flow of F-actin in response to semaphorin 3A in growth cones [354].

Another study also established an interesting role for Sema3A, as Sema3A expression was increased in clones of chondrocytes seen in association with the repair of damaged cartilage and inhibition of cell migration in osteoarthritis (OA) cartilage [355]. Sema3A is also involved in regulating bone formation and resorption, as well as angiogenesis via vascular endothelial growth factor (VEGF). The Sema3A signaling network may arrange a repulsive guidance signal, providing the nerve fibers ability to grow to their targets in the bone tissue, regulating the development of bone innervation and other features of bone remodeling and development. VEGF affects both blood vessels and peripheral nerves and opposes the Sema3A effect. VEGF increases endothelial cell mobility and survival and enhances neural survival and axonal outgrowth *in vitro*. In contrast, Sema3A prevents endothelial cell survival and mobility as well as axonal outgrowth *in vitro* [356].

The most interesting action of Sema3A relevant to this thesis, is its role as a neural chemorepellent for motor axons [357, 358], since Sema3A is also found in skeletal muscle tissues and has potential for a similar chemorepellent function in regenerating skeletal muscle. This finding opens the door to studies of a possible role for Sema3A in myogenic processes including the coordination of motor neurites making NMJ connections to newly formed and differentiating myotubes, as first proposed by Tatsumi and colleagues in 2009. This notion is supported, for example, in experiments where nerve-muscle connections are remodeled (in growth, after paralysis or in nerve regeneration), Sema3A expression is up-regulated in Schwann cells in close proximity to muscle SCs at the NMJ [303]. Another study using C2C12 cells (a murine myoblast cell line) found that during differentiation, Sema3A protein increased early and then decreased, while Sema3A mRNA expression remained fairly constant through the same period and only showed a slight decline later in differentiation [359].

Semaphorins are expressed by brain tissue and several non-neuronal tissues, where they play various roles in processes such as regulation of inflammation and angiogenesis, as introduced earlier. Sema3A is also a member of secreted group of semaphorins that guides axons as well as the growth and migration of many cell types [360, 361]. In denervated muscle, TSCs are suggested

as regulating the guidance of regenerating axons to their initial NMJs. Interestingly, a subgroup of TSCs in type IIb myofibers (fast-glycolytic fibers) upregulates *Sema3A* after muscle denervation. Firstly, this shows that the microenvironment which manages these procedures differs at the level of the single myofiber. Secondly, this observation displays the need for another cell type to manage the reinnervation procedure. Research has shown the critical role of *Sema3A* in guiding intramuscular neuritogenesis during muscle regeneration. De Winter's investigations utilizing gastrocnemius muscle denervation, showed the selective expression of *Sema3A* message in TSCs at NMJs of fast-twitch (type IIb/IIx) myofibers, but not in slower-twitch fibers (types I and IIa). The same research study displayed that upregulation of *Sema3A* expression in TSCs was not detected in the denervated soleus muscle that lacks fast, type IIb/x myofibers [303]. While these observations support the idea that denervation induces *Sema3A* expression in myofibers in a fiber type-specific manner, the detailed mechanism underlying the findings is not fully understood. However, the receptors for *Sema3A*, HGF and FGF2, show distinct differences in expression in the different types of muscle [297, 352, 362]

Since *Sema3A* inhibition can enhance recovery of nerve-nerve connections during recovery from spinal cord injury [165], it may have a parallel role in mediating nerve-muscle connectivity in regenerating muscle. It is proposed that *Sema3A* may regulate the timing of a motor nerve axon making a new or renewed connection with a regenerating fiber, by temporarily preventing that reconnection until the myofiber has undergone sufficient differentiation to receive the neurite into a developing synapse [186]. This has not yet been directly demonstrated.

1.5.3 AchR Expression and Clustering

Both the expression and clustering of Ach receptors (AchRs) at NMJs on the post-synaptic membrane of fibers, are intricately sensitive to innervation status. According to the method described by Kummer et al. [256], α -bungarotoxin (BTX) is an acetylcholine antagonist and attaches specifically to single or clustered AchRs. Thus, we can use cytochemistry by staining with a fluorescent form of BTX to visualize the status of AchR clustering [363]. Calcium ions act as second messengers and trigger many cellular processes such as secretion, metabolism, contraction, cell growth and cell division. Calcium receptor proteins change the intracellular calcium levels and make alterations in the function of cells. These alterations change the expression and function

of calcium-binding proteins in human neurodegenerative disorders. S100B is a Schwann-cell-specific calcium-binding family of proteins that can be utilized to identify regenerating axons and Sema3A-expressing cells by immunostaining methods [303]. S100 proteins play a role in a variety of processes including energy metabolism, apoptosis, and the regulation of proliferation, differentiation and inflammation. These processes are mediated through interactions with several target enzymes, cytoskeletal subunits, receptors, transcription factors and nucleic acids. S100 proteins thus, have a regulatory effect on neurons, monocytes, macrophages, microglia, myoblasts, neutrophils, vascular smooth muscle cells, and Schwann cells, and thereby contribute to immune responses and tissue repair and development [341].

1.5.4 Sema3A and AchR Clustering

A recent study on cultured myotubes (lacking nerve supply in the culture dish) was used to study the effects of Sema3A knock-down on expression of genes related to synapse development and muscle differentiation (Do and Tatsumi, personal communication). Sema3A knock-down via siRNA transfection considerably inhibited AchR clustering. The following experiment was developed by two-day transfection of Sema3A siRNA and resulted in reduction in AchR subunits (ϵ and γ) on aneural (non-innervated) myotubes. The transfection to knock down Sema3A had no effects on the expression of MRFs, myogenin and MyoD, or on rapsyn, MuSK genes and other AchR subunits (β , α , δ). Interestingly, at day 3 post-transfection, there were considerable decreases in expression levels of AchR subunits γ and ϵ and myogenin, but no effects on other AchR subunits (α , β , and δ), MyoD, rapsyn and MuSK were observed in Sema3A knock-down cultures. To study the role of myogenin activity during myogenic differentiation and fusion, myogenin knock-down experiments in those myotube cultures were performed using myogenin siRNA transfection. Results showed considerable reduction was evident in γ -AchR subunit expression but myogenin knock-down had no effect on AchR clustering or the expression of the other AchR subunits. Notably in *in vivo* studies in Sema3A knockout mice (where the knockout is directed specifically to satellite cells), morphological abnormalities in NMJs, such as uncontrolled branching of intramuscular nerve terminals and decreased development of acetylcholinesterase (AChE) in the post-synaptic region were detected. These preliminary findings [364] emphasize an unexplored function of Sema3A secreted from SCs; that function is related to the regulation of NMJ development through the interaction of motor neurite connections with regenerating muscle fibers.

The results of these *in vitro* and *in vivo* experiments presented evidence of SC involvement in nerve formation, but again, the specific action of Sema3A and the timing of the effects that might mediate a change in AchR clustering is not known in detail (Do M-KQ and Tatsumi R, unpublished observations, personal communication).

1.6 Nitric Oxide and Muscle Regeneration

In 1998, an experiment introduced HGF as a significant extracellular modulator of the activation of quiescent SCs in response to muscle injury [108]. SC activation was subsequently found to occur through a series of mechanically-transduced alterations to chemical signaling in a myofiber [365]. This cascade of events that activates SCs begins by an influx of calcium ions [366] mediated by a release of nitric oxide (NO) from myofibers [367]; this signal induces a release of HGF, which interacts with the c-met receptor on SCs [365, 366].

1.6.1 NO-Based Treatments

NO is a diffusible gas that functions as a signaling and neurotransmitter molecule; it was first identified in cellular processes in 1988 as a vascular relaxation factor [368-370]. As discovered by Dr. Anderson [23] SC activation after muscle injury is mediated by NO and thus, manipulation of the NO signal was proposed by Anderson (2000) as a potential treatment for enhancing muscle repair and/or growth. This idea was supported by later reports from our lab and others. For example, the role of NO and HGF as regulators of SC activation has been revealed by distinctive methods using cultured myofibers [21, 25-27, 371, 372], dispersed cultures of myogenic cells [373-375] and *in vivo* experiments [376-384] [385]. Representative reviews of NO roles in regeneration of muscle are found in the following references [384, 386, 387].

Several studies about NO-mediated SC activation and proliferation displayed that increased levels of NO in muscle promote regeneration of dystrophic and normal muscle [377, 388]. As well, isosorbide dinitrate (ISDN), a NO-donor drug that has the ability to deliver NO to tissues without the need of NO synthase (NOS) activity, was proposed as a potential treatment that would promote muscle regeneration [23] and foster the regeneration of muscles in *mdx* dystrophic mice [23, 389].

Interestingly, the NO level in skeletal muscle has a significant effect on the fusion of myogenic precursors to the remnant stumps or myotubes of damaged fibers. This is demonstrated by findings that with a low level of NO *in vivo* in regenerating muscle, the branched phenotype of myotubes prevails over the normal slender cylindrical form of myotubes [23, 200]. Other work from our lab showed that NO manipulation using ISDN (a NO-donor drug) to treat normal mice, in combination with voluntary exercise, attenuated age-related muscle atrophy, promoted a notable 25% increase in fiber diameter in response to exercise that typically would enhance atrophy in old animals, increased SC proliferation and increased the contribution by SC in the growth of myofibers [23, 160]. This research extended our understanding of the impact of NO and NO-based treatments to stimulating SC activation and proliferation *in vivo* and promoting muscle growth and regeneration in normal or aged muscle tissue.

Treatment of muscles in adult mice with a new NO-releasing compound (guaifenesin dinitrate, GDN) designed and developed in Dr. Anderson's lab, has potential for promoting skeletal muscle proliferation, growth and muscle regeneration [390]. Our lab demonstrated that both ISDN and a novel NO-donor molecule (MyoNovin) improved the status of muscle (and its regeneration) in the muscle most severely affected by X-linked dystrophy in the *mdx* mouse, the thoracic diaphragm muscle [377]. Findings in this study were interpreted to suggest that the new NO donor decreases the need for SC activation as part of a repair response to dystrophy, while it helps the fusion of precursors into regenerating myofibers. SC activation was higher than normal in myofibers with dystrophin deficiency and NOS1 due to low levels of NO. Variances in the two NO donor drugs likely influenced their effects on the efficiency or speed of regeneration and reestablishing the balance of SC quiescence and activation. MyoNovin decreased proliferation in dystrophic muscle, consistent with effects on activation in normal muscle, while treatment with ISDN increased the area proportion of regeneration. Most relevant to this thesis, in an experiment on groups of young-adult and mature-adult mice, daily NO-donor treatment with ISDN reduced or prevented the development of important features of muscle atrophy in hindlimb muscles. Since NO mediates the activation of SCs and stimulates hypertrophy with exercise in old mice, this study examined whether a NO-donor drug (ISDN) treatment, during hind limb suspension would decrease atrophy. Mice were suspended with or without daily ISDN (66mg/kg) for 18 days and then tested for atrophy (fiber diameter, weight), myostatin (inhibits myogenesis), regulatory changes in atrogen-1 (a negative regulator of muscle mass), and SC proliferation; and metabolic

responses in MyHCs, hypothalamic gene expression and liver lipid. Suspension attenuated weight relative to body weight and muscle weight between 25-55%, and gastrocnemius myofiber diameter vs. controls. The ISDN treatment in young-adult mice, reduced atrophy by half or more, prohibited the suspension-induced increase in atrogen-1 in quadriceps and decreased myostatin precursor. The ISDN treatment also reduced the alterations in MyHCs I and IIb detected in unloaded muscles without treatment. Moreover, fatty liver was decreased by ISDN in suspended young-adult mice while higher hypothalamic expression of the orexigenic agouti-related protein, *Agrp* was observed in suspended young mice than control group. A suspension-induced reduction in the proliferation of SCs by 25-58% was also completely inhibited (young mice) or reduced (in young-adult mice) through ISDN treatment. This study showed that NO-donor drug treatment has potential to diminish metabolic changes and atrophy; inhibit regulatory alternations during disuse and hinder wasting in space travel and sarcopenia. Furthermore, increases in the proliferation of precursors resulting from ISDN treatment would also intensify benefits of exercise and physical therapy [378].

1.7 Rationale and Hypotheses

It is well established that SCs play a key role in the molecular and cellular processes of muscle formation called myogenesis. The activation of SC underpins muscle repair, as activation that pushes SCs into the cell cycle from their normally quiescent state in adult muscle is required to form new myofibers. Restoring muscle function after myogenesis requires the reinnervation of new myotubes. SC activation is mediated by NO, a signaling free-radical that is released upon fiber stretching or injury. Interestingly, after injury, during early differentiation in repair, SC-derived myoblasts also up-regulate expression of *Sema3A* which is thought to mediate the growth of axons toward regenerating myotubes. After injury with a myotoxic drug, motor axons normally reconstitute NMJs in the region of original synapses by following the remnant nerve sheaths toward myofibers.

After traumatic injury, new NMJs must be formed in order to re-establish voluntary muscle control. Moreover, during synapse formation, the clustering of new AchRs is stimulated by axon terminals that have followed Schwann cell processes that form in the absence of innervation. The redistribution of some of the new AchRs will fail due to a lack of Schwann cells in the

reinnervation process. As well, slow-twitch myofibers are particularly sensitive to disruption of their connections with motor nerves. In repairing from a muscle-crush injury, slow fibers form mature arrangements of AchRs later than fast-twitch fibers. By comparison to reinnervation after traumatic muscle injury, muscle denervation experiments reported that *Sema3A* mRNA was selectively expressed in TSCs at NMJs of fast-twitch myofibers and not in slow-twitch fibers. Since *Sema3A* also promotes differentiation of slow-twitch myofibers, and slow muscles develop mature patterns of innervation later than fast muscles, the disruption of fundamental features such as the structural pattern of NMJs, motor nerve axon terminals, and fiber-type distribution will have a major impact on muscle function. In meat-producing animals, changes in the proportion of slow fibers (expressing MyHC1) would affect the quality of meat.

Hypothesis 1 of this PhD project, was that disruption of the timing of SC activation in muscle regeneration, induced by pre-activation of SCs before injury, would impact the restoration of NMJs on new myofibers by effects on myogenesis, *Sema3A* production, and motor neuritogenesis compared to normal regenerating muscle without premature SC activation. Hypothesis 2 was that the impact of premature SC activation would differ between two models of muscle injury, depending on the extent of involvement of nerves in the tissue damage. We designed this hypothesis to complete the characterization of nerve muscle contraction by looking at the timing of nerve supply restoration between those two models of injury with and without NO pre-treatment.

Hypothesis 3 for this dissertation was that elimination of *Sema3A* production by SCs prior to injury by muscle crush and/or nerve crush, would show that SC-derived *Sema3A* is essential to restoration of NMJs on myofibers.

Experiments started by manipulating the behavior of SCs by using a NO-donor treatment (isosorbide dinitrate, ISDN) to pre-activate SCs before muscle injury by a traumatic crush or CTX injection. A variety of assays employing protein biochemistry were used; gene expression (mRNA transcripts) and histochemistry techniques such as Western blotting, immunostaining, and in situ hybridization were used. In situ hybridization experiments were done to detect the source of expression of *Sema3A* and *S100B* (a marker of terminal Schwann cells) in regenerating muscle, as well as a combined ISH-histochemical staining method for neurites, acetylcholine receptors and acetylcholinesterase activity at NMJs.

My interest in TSC behavior at the NMJ during reinnervation from damage, grew immensely during this project, as it appeared that TSCs respond to Sema3A made by SCs. My passion to further explore the role(s) of Sema3A and S100B in growth, regeneration, and disease led to the aim of my next chapter, to examine these markers in muscle regenerating from crush and from nerve damage, in conditional knockout of Sema3A expression by muscle cells.

Hypothesis 4 was therefore, that SC-derived Sema3A is essential to TSC function and gene expression at NMJs and around neurites. I predicted that terminal Schwann cell function would be disrupted by the loss of SC-derived Sema3A, even though Schwann cells themselves, express Sema3A. I specifically changed the experimental protocol to include the surgical model by using nerve crush injury to investigate whether the impact of Sema3A knock-down in SCs on NMJs would be different after nerve injury compared to muscle injury. This was important because interruption of the nerve in the area (lack of repolarization of the nerve and a significant drop in the number of action potentials) can affect NMJ reinnervation. Neurite extension is essential in forming axon terminals at NMJs during repair of nerve, with or without the additional need to repair muscle tissue to receive innervation. I anticipated NMJ formation and TSC activities would be disrupted by the specific loss of Sema3A expression by SCs in the fast-twitch muscle, TA.

Early experiments with Sema3A knock-down *in vivo* were conducted using mice generated in Dr. Tatsumi's lab (Kyushu University, Japan) that has a SC-specific Sema3A conditional knock-out. The cre/loxP system was used to induce transgene expression (Sema3A) that was controlled through tamoxifen administration (utilized to control the recombination timing).

This thesis is structured as a “sandwich-style” thesis (with an abstract, general introduction and literature review, followed by a rationale and hypotheses, general reporting of all methods, a series of published papers or drafted manuscripts, and concluded by an overall discussion). The first results chapter is published work [391] which was designed by Dr. Anderson and Nasibeh Daneshvar and she (Daneshvar) performed the assays at the University of Manitoba. Following the results chapters, an overall discussion chapter is used to summarize the thesis project and consider future directions of research.

1 RESULTS - 1

Premature satellite cell activation before injury accelerates myogenesis and disrupts neuromuscular junction maturation in regenerating muscle

Daneshvar N, Tatsumi R, Peeler J, Anderson JE. Am J Physiol Cell Physiol. 2020 Jul 1;319(1):C116-C128. doi: 10.1152/ajpcell.00121.2020. Epub 2020 May 6. PMID: 32374678 [391]

1.1 Introduction

Repair of muscle tissue after injury relies on the coordinated interactions of many types of cells [392] and ultimately results in the development of new fibers (myogenesis) and restores motor innervation and an appropriate vascular supply. The extent of damage and inflammation, the need for nerve and vessel formation, and the time-course of repair vary by the type and extent of damage [169, 393]. Two injury models, myotoxic fiber damage [117, 394, 395] and traumatic crush injury [54, 396], are often used to understand steps in myogenic repair; however, the involvement and responses by other tissues such as nerves in a muscle is often overlooked [397]. Regardless of the mechanism of injury, muscle-resident satellite cells (SCs) and their rapid activation, proliferation and myoblast fusion after injury, are essential to fiber regeneration, particularly, in the first 5-7 days after injury [191, 194, 398].

The morphological sequence of steps in myogenic repair and the rapid time-course of nitric oxide (NO) signaling that initiates SC activation are well described [23, 27, 108, 384, 387, 399, 400]. NO mediates SC activation by stretch and exercise, as well as macrophage activity in inflammation [21, 26, 27, 400-403]. NO is generated by NO synthase-1 in the dystrophin-associated cytoskeleton [404] in response to mechanical forces. Increased NO was proposed as a potential SC-directed treatment to attenuate disuse atrophy [378] and rotator cuff injury [240, 325], restore SC regulation and improve regeneration in muscular dystrophy [21, 23, 405, 406], and support exercise-induced hypertrophy in age-related sarcopenic muscle [160].

By comparison to myogenic repair, relatively little is known about the processes involved in the restoration of neuromuscular junctions (NMJs) on newly regenerated fibers that display central nuclei (myotubes). In normal development, nerve-terminal contacts, post-synaptic specialization of the fiber sarcolemma, and pre-synaptic gutters of acetylcholinesterase (AChE) activity each form in relation to the patterning, distribution, density, and sprouting of motor

neurites [303, 407]. Similarly, acetylcholine receptors (AChRs) develop and cluster at the post-synaptic membrane and are gradually stabilized. The immature NMJ is a simple plaque of AChRs containing immature gamma (γ)-subunits, while mature NMJs have a complex “pretzel-like” shape containing more of the adult epsilon-AChR subunit [237]. Since this shift is crucial for forming junctional folds and maintaining AChR clusters at the synapse [237, 238], the expression of γ -AChR can be used as a marker of NMJ immaturity and/or denervation [235, 240, 325, 408]. Precisely when these changes occur in myogenic repair is not clear, although the sequential timing of each step is assumed to vary among diverse types of muscle injury.

Motor neurite growth toward myotubes during muscle regeneration, a critical step in injuries involving nerve axons, and the timing to re-establish synaptic contact are not as well understood as normal NMJ development [297]. The processes of moto-neuritogenesis are not fully available from experiments using myotoxic injury where axons and axon terminals are commonly taken to be preserved during the primary myotoxic injury as muscle fibers are rapidly regenerated and functional [397, 409]. However, there is evidence that myotoxic injury can damage post-synaptic gutters, disrupt AChR clustering and AchE localization, and induce endplate fragmentation that persists for at least 6 months after cardiotoxin injection in mice [394, 409, 410]. The timing of NMJ restoration on myotubes formed after a traumatic crush injury that includes direct nerve injury, is even less well understood, in part due to challenges associated with tracing the stages of fiber and presumably also axonal repair in different regions of an injured muscle over time [54, 411-413]. However, for reinnervation to restore function, motor axons need to regrow to former synapses and/or reinnervate AChR areas that lack nerve connection or induce formation of new AChRs and the pre- and post-synaptic apparatus. The timing and extent of these processes depend on the degree of collective injury to muscle fibers, axons and myelin sheaths in nerves, and vessels, as well as inflammation.

Interestingly, SCs are implicated in the processes of restoring motor supply to regenerating muscle fibers. Early electron microscopy studies showed an enrichment of SCs at pre-synaptic regions of non-injured human and rat fibers, suggesting their involvement in NMJs due to their proximate location [414]. Successful remodeling and restoration of NMJs are known to depend on the spatiotemporal expression of repulsive and attractive factors and their receptors [415, 416], from research that has explored NMJs on the basis of previous findings on central nervous system (CNS) synaptogenesis. One such factor, Semaphorin 3A (Sema3A), modulates neuritogenesis in

the CNS, as well as angiogenesis and immune responsiveness in many tissues [361, 417, 418]. Sema3A is implicated in regulating motor neurite ingrowth during muscle repair [194]. Sema3A is secreted by differentiating myoblasts at the early-differentiation phase of regeneration *in vitro* and *in vivo* [194] and interestingly, also by terminal Schwann cells (TSCs) [303] directly proximate to both the fiber sarcolemma and axon terminals at NMJs. Sema3A acts on growth cones of motor neurites through a chemo-repulsive process [238, 416, 419-421]. S100-B is a calcium-binding, “calcium-sensor” protein [422] expressed by TSCs [303] at higher levels than expressed by the non-terminal Schwann cells that form myelin sheaths around nerve axons [423]. S100B changes in response to synaptic activity and NMJ maturation, and S100 (including A and B forms of S100) is thought to help regulate muscle repair [424]. The benefit of increased SC activity in accelerating myogenic repair itself, is well established. The impact of changes in SC activity at the time of muscle injury, on the extent and timing of NMJ formation and maturation has not been tested as an experimental approach to test the role of SCs or their products in restoring nerve connections to muscle. Such knowledge could help find new therapeutic targets to promote successful rehabilitation and the early return of function following injury.

This study tested the effects of NO-induced premature SC activation before muscle injury by cardiotoxin or traumatic crush, on myotube regeneration and the early changes in and establishment of NMJs. Experiments induced premature SC activation in mice using 2 days of daily pretreatment with the non-specific NO-donor, isosorbide dinitrate (ISDN), previously shown to activate SCs *in vitro* [372, 425] and *in vivo* [378, 425], and followed muscle regeneration, Pax7+ SC proliferation, pre- and post-synaptic changes during early NMJ maturation, and the expression of Sema3A, γ AchR, and S100B proteins for 0, 4, 6, 8, and 10 days post-injury. Results were applied to test the hypothesis that activating SCs before injury will affect the timing and extent of both myogenic repair and NMJ restoration, and that there would be model-specific disruptions in NMJ restoration and the timing of myogenic regeneration between myotoxic and traumatic injuries to muscle.

1.2 Methods

Adult male C57BL6 mice (10 weeks old, n=84) were housed and handled according to regulations set by the Canadian Council on Animal Care as approved by the University of Manitoba, protocol F14-015. Half the mice received a daily oral dose of ISDN (66 mg/kg in canola oil; at a volume of 2.7 μ l/g body weight) for 2 days [378, 405] as “pretreatment” before surgery (24 hr after the second dose). Animals were assigned to receive either crush (CR, n=40) or cardiotoxin injury (CTX, n=40) such that half of each injury group received pretreatment with ISDN and the other half did not.

After inducing anesthesia (isoflurane inhalation), removing hair from the left lower hindlimb, and cleaning and opening the skin, the left tibialis anterior muscle (TA) was injured by either CR [54] or injections of CTX, venom from the *Naja mossambica* snake [407]. The CR caused injury to the entire tissue mass of the muscle “belly” through a focal region (approx. 1mm wide) across the mid-region of the TA after fully exposing the muscle by a lateral skin incision. Blunt-end forceps were carefully passed beneath the mid-belly of the TA (below its attachment to the tibia) to separate it from surrounding and deeper muscles, avoiding damage to the nerve and blood supplies entering the proximal, deep aspect of the muscle. After withdrawing the forceps, one blade of a small hemostat was passed beneath the TA mid-belly and closed over the TA (to one click) for 5 seconds, as reported [162, 426]. After releasing the hemostat and checking for blood loss, the skin was closed using 3-4 absorbable monofilament sutures (3-0 monocryl, Ethicon, USA). Mice were allowed to recover under Meloxicam analgesia (1mg/kg, Boehringer Ingelheim, Japan) daily for 2 days, to control pain.

For the CTX injury, mice were anesthetized and prepared for surgery exactly as for CR. After exposing the muscle through an incision in the cleaned skin, a total volume of 0.1ml of 10mM CTX (Sigma-Aldrich, Mississauga, ON, Canada) was injected by even distribution to 4 sites spaced evenly along the proximo-distal axis of the TA. Again, skin was closed by sutures, and mice recovered under analgesia.

Two hours before euthanasia, mice were injected with bromodeoxyuridine (BrdU; 100mg/kg intra peritoneal, B5002, Sigma Aldrich) to label DNA synthesis. This protocol thus established 4 treatment groups: crush (CR) and cardiotoxin injury (CTX), both with and without ISDN pretreatment, with n=4 mice per time point and treatment group, for each type of injury.

Four additional littermate mice were available as untreated controls for the studies of NMJ patterning and myofiber diameter and had no injury, surgery, or treatment with ISDN or BrdU.

Animals were euthanized by cervical dislocation under isoflurane anesthesia at days 0 (within 10 minutes of injury, while still under anesthesia), 4, 6, 8 and 10 post-injury (n=4 mice per time point, for each treatment group). At each time-point, half the mice in each CTX and CR group had received pretreatment with ISDN. TA muscles were quickly dissected from limbs, bisected longitudinally, and prepared for cryosectioning of paraformaldehyde-fixed (4%) tissues or protein isolation for Western blotting, as reported [160, 240, 427]. Samples and sections were coded. In order to minimize observer bias; data were decoded for analysis after observation, measurement and/or photography.

1.2.1 Myotube growth

One set of muscle sections was stained with hematoxylin and eosin (H&E) for histologic assessment of tissue damage, regeneration, and fiber morphometry. Myotubes were photographed within the mid-belly of the TA after CTX injury and in the regenerating zone one 20X field proximal to the directly-crushed region in the CR muscles [54]. Ten non-overlapping fields (200X) were photographed using an Olympus BH-2 microscope, and myotube diameter was measured in the first 100 myotubes in each section using calibrated NIH ImageJ software, as previously reported [378]. Muscle fiber diameter was also measured in day-0 injured muscles and in TAs of untreated control animals, as a baseline.

1.2.2 NMJ maturation

An overview of post-synaptic configurations on new myotubes was examined using coded slides of regenerating muscle and direct-fluorescent staining for AchRs [428], as reported for developing [429] and pathological muscle [240]. Sections were fixed with acetone, air dried, and incubated overnight at 4°C with fluorescein-conjugated α -bungarotoxin (BTX, 1:200 in PBS; Invitrogen, Carlsbad, CA). Coded slides were scanned and the first 20 regions of fluorescence in areas of regeneration were photographed at 100X (with observer blinded to source group) using a Zeiss Apotome (Jena, Germany). The configuration of the fluorescent regions, ranging from linear to “pretzel-like” patterns, was assessed over the time-course of regeneration in the 4 treatment groups.

Pre-synaptic regions of AchE activity and the configuration of motor neurites and nerve terminals were detected with histochemistry and silver staining in muscles at day 8-10. AchE sites form a plaque on the fiber membrane in mature NMJs while silver staining of intramuscular pre-synaptic motor neurites typically shows one or more branches emanating from an axon toward a smaller AchE plaque [56, 429]. Sections were incubated in fresh 2.6 mM acetyl-thiocholine iodide (A5751, Sigma-Aldrich) mixed in 0.1 M sodium hydrogen maleate buffer (pH 6.0) containing 0.1 M sodium citrate, 30 mM copper sulphate and 5 mM potassium ferricyanide. After rinsing in distilled water, sections were incubated in 0.5 M potassium ferricyanide, rinsed again, and incubated (60 min) in aqueous 10% silver nitrate (209139, Sigma Aldrich). Sections were rinsed, saturated with Bodian's developer (5.0 g sodium sulfite and 1.0 g hydroquinone in 100 ml DW), rinsed in 1% glacial acetic, dehydrated in ethanols, and coverslipped. Images from 10 non-overlapping fields were captured at 400X magnification on a Zeiss Apotome (location). The number of silver-stained plaques, either mature ovals of AchE plus neurites (\pm terminal boutons) or smaller, immature AchE plaques with neurite branches, was counted in each field of regenerating fibers. The mature proportion of total silver-stained plaques was compared across groups.

A combination of BTX direct-fluorescent staining and silver-staining histochemistry (processed in that order) was applied to sections from a subset of slides (approximately half the mice per group) and used as for in-depth assessment of NMJ maturity. NMJ regions were scored according to the presence or absence of colocalized post-synaptic AchRs (BTX+) plus pre-synaptic silver staining for AchE plaques and motor neurites. The distribution of NMJ regions with BTX+ regions, silver staining (neurites+AchE), or both (neurites+AchE+BTX) was determined by counting all stained regions in 10 non-overlapping fields of regenerating myotubes photographed at 400X.

1.2.3 Protein expression

The levels of Sema3A, γ AchR, S100B, and a loading control (β -actin) were assayed using Western blots of muscle-protein extracts using standard protocols for extraction, electrophoresis, blotting, and chemiluminescence detection, as previously reported [160, 240, 430]. Membranes were probed with primary antibody mixed in immunoreaction enhancer solution1 then secondary antibodies mixed in Can Get signal solution2 (TYB-NKB-101, Cosmo Bio Ltd., Toyobo, Osaka,

Japan) to detect the protein of interest [421] before probing for the loading control to standardize quantification. In one lane of each gel, 1 μ L of Western protein molecular weight standards (MagicMark XP, LC5602, Fisher) was loaded to provide direct visualization of the standard on the blot.

1.2.4 Pax7+ Cell DNA synthesis

The proliferative activity of Pax7+ SCs was visualized as previously described, by detecting BrdU incorporation into nuclei synthesizing DNA [240]. Slides were incubated overnight at 4^oC in a solution of rabbit anti-Pax7 and mouse anti-BrdU in buffer, then incubated at room temperature in buffer containing Dylight650-conjugated goat anti-rabbit IgG and FITC-conjugated goat anti-mouse IgG H&L. Sections were coverslipped and photographed at 400X in 10 non-overlapping images per section for fluorescence and differential interference contrast (DIC) using a Zeiss Apotome. Pax7+ SCs were counted as labeled (BrdU+) or not (BrdU-) and the labeled proportion of SCs was calculated and compared among groups.

1.3 Antibody Information

Blocking antibodies in double immunofluorescence staining included: unconjugated Fab Fragment goat anti-mouse IgG (115-007-003, Jackson ImmunoResearch, 1:200), and unconjugated Fab Fragment goat anti-rabbit IgG (11-007-003, Jackson ImmunoResearch, 1:200). Primary antibodies used in double fluorescence staining included: rabbit anti-Pax7 (ab34360, Abcam, 1:150) and mouse anti-BrdU (11170376001, Roche, 1:200). Secondary antibodies included: goat anti-rabbit IgG DyLight650 (ab96902, Abcam, 1:200), goat anti-mouse IgG conjugated with DyLight488 (ab96879, Abcam, 1:200) and goat anti-mouse IgG conjugated to horseradish peroxidase (HRP) (A2304, Sigma, 1:200). DAPI was used to counterstain nuclei (D9542 Sigma, 1:10000).

For western blotting, primary antibodies included: rabbit anti-Semaphorin 3A (ab23393-50, Abcam, 1:5000), rabbit anti- γ AchR (sc-13998, Santa Cruz, 1:300), rabbit polyclonal anti-S100B (orb228251, Biorbyt, 1:3000), and mouse anti- β -actin (sc-81178, Santa Cruz, 1:1500).

Secondary antibodies included: HRP-conjugated goat anti-rabbit IgG H&L (ab97057, Abcam, 1:5000) and HRP-conjugated goat anti-mouse (A-2304, Sigma, 1:5000). Recombinant mouse Semaphorin3A Fc chimera protein (5926-S3-025/CF, R&D Systems) served as a positive control.

1.4 Statistical Analysis

Data were compiled in spreadsheets using Microsoft Excel (Microsoft Office Professional Plus 2016), decoded by treatment group and time point (days post-injury), and analyzed using Excel, JMP (SAS, Cary, NC), or Jamovi v1.1.9 open-access software [431]. For score data, main factors, injury type (CR, CTX), regeneration time (days 0, 4, 6, 8, 10), and ISDN pretreatment, and interaction effects (time*injury, treatment*injury, time*treatment, and time*injury*treatment) were determined, where appropriate, by three-way analysis of variance tests for unbalanced design using type II Sum of Squares (ANOVA); post hoc Tukey's means tests were used to compare two groups, as appropriate. Frequency distributions were examined using Chi-square statistics. Data are reported using box-whisker plots representing first and third quartiles, median, mean, maximum, and minimum for scored data. In all cases, a probability of $p < 0.05$ was used to establish significance.

1.5 Results

This study investigated the effects of premature SC activation (pre-activation) on myogenesis and NMJ regions on newly formed myotubes after either CTX-myotoxin or crush (CR) injury. Histological assessment (Fig. 1) showed that muscles collected at day 0, within 10 minutes of injury, were not overly disrupted. As expected, the observed pattern of regeneration differed between CTX-injured and CR-injured muscles (compare Fig. 1A vs. 1B). After CTX injury, essentially the whole muscle was involved in necrosis and inflammation. Inflammation had mostly resolved by day 4 as many new, basophilic myotubes formed and grew quickly at a very uniform diameter. By day 8, myotubes extended the length of the CTX-injured muscle.

In contrast, CR injury induced a band of segmental necrosis and inflammation in the region of direct trauma in the TA. The necrotic region was bordered, both proximally and distally, by bands of basophilic inflammatory cells. Further proximally and distally, were segments of remnant fibers that had survived the initial injury and the later secondary inflammation [54]. By day 4,

small centrally nucleated, basophilic myotubes were observed within the zone bordering the crushed region. By day 6, myotubes had elongated further, and gradually spanned the necrotic region as inflammation declined, typically between 6-8 days. In comparison to CTX-injured muscle, myotubes appeared shorter and smaller in diameter in CR-injured muscle.

The overall histological sequence of necrosis, inflammation, and regeneration was similar with or without ISDN pretreatment for each of the CR and CTX-injured groups. However, in both injury models, observations revealed that inflammation resolved about 2 days earlier in mice that had received ISDN pretreatment compared to the respective untreated group, and myotubes appeared to be subjectively larger and more numerous in pretreated than untreated groups.

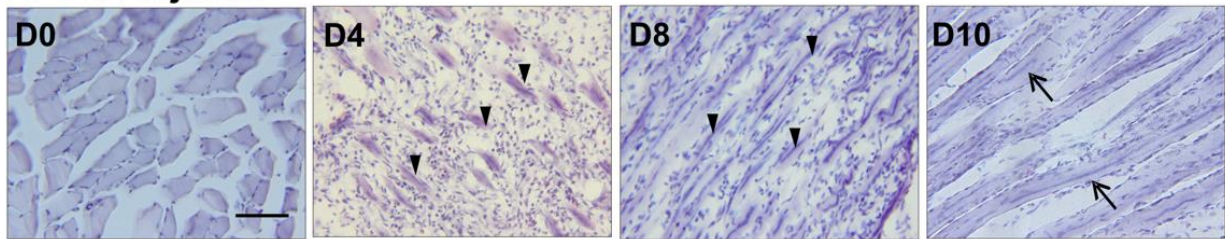
1.5.1 Myotube growth

Myotube diameter measurements confirmed histological observations. The three main factors, time ($F(df=4) = 139.23, p < 0.001$), treatment ($F(df=1) = 20.01, p < 0.001$), and type of injury ($F(df=1) = 90.27, p < 0.001$), showed significant effects on myotube diameter by 3-way ANOVA, as did all interactions ($0.048 < p < 0.001$). CTX-injured muscles displayed larger myotubes than CR-injured muscles (time*injury interaction, $F(df=4) = 24.59, p < 0.001$, Tukey's $p = 0.003$). Separating this into pairwise comparisons, results showed that without pretreatment, myotube diameter increased between days 4 and 10 following both CTX (Tukey's tests, $p < 0.001$, Fig. 1Ci) and CR injury (Tukey's tests, $0.001 < p < 0.05$; Fig. 1Cii). In CTX-injured muscles, myotube diameter at day 10 was larger than that in control mice without treatment (Tukey's, $p < 0.01$) or littermate-control muscle without any injury (t-test, $p < 0.01$). After ISDN pretreatment, myotubes regenerating in CTX-injured muscles were larger in diameter at each time point post-injury compared to those in muscles of untreated CTX-injured mice at the same time point (time*treatment interaction, $F(df=4) = 4.52, p = 0.004$, Tukey's $0.01 < p < 0.05$), indicating that pretreatment accelerated myogenic regeneration.

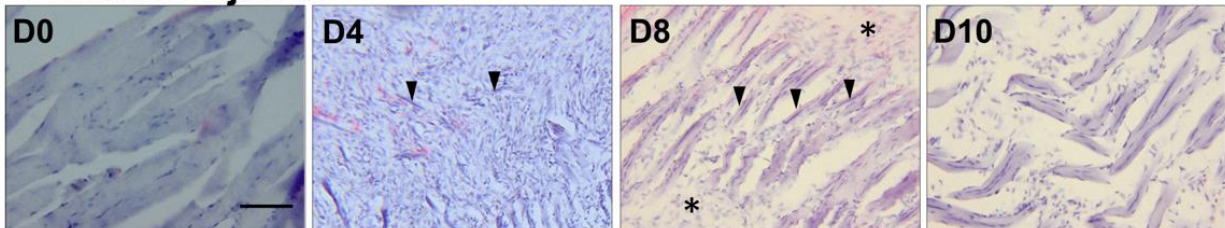
Myotube diameter also increased after CR injury, occurring between days 4 and 10, although the increase was smaller than after CTX injury at comparable time points (time*injury interaction, $F(df=4) = 24.59, p < 0.001$). However, by day 10 after CR, myotube diameter remained smaller than in muscle at day 0 immediately after CR (Tukey's; $p < 0.05$) or control muscle (t-test; $p < 0.05$). Pretreatment before CR injury reduced myotube diameter between days 4-6 compared to untreated CR-injury groups (time*treatment interaction as above, Tukey's test, $p = 0.05$).

In addition, in both CTX and CR injured muscles, fibers were larger at day 0 (immediately after injury), in the pretreated group compared to fibers in the respective untreated (Tukey's tests, $p < 0.05$) and control (t-tests, $p < 0.05$) groups.

A. CTX-injured



B. CRUSH-injured



C. Myotube growth

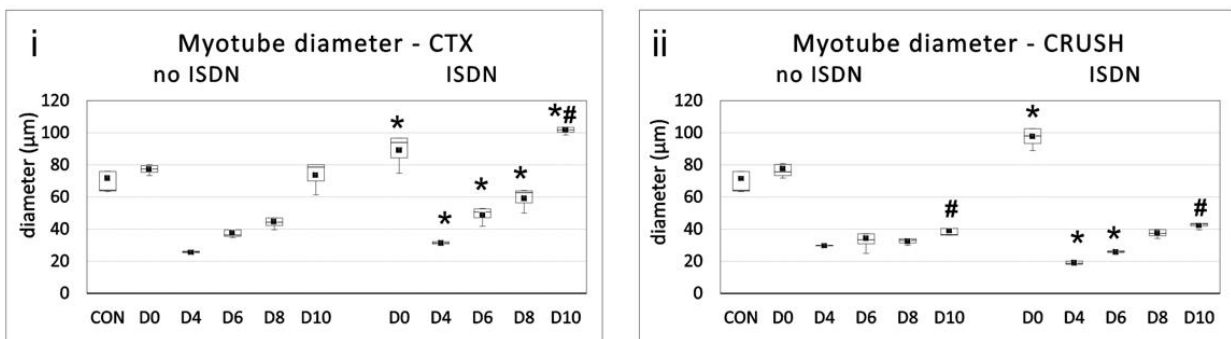


Figure 1. Histological assessment of the time course of myogenic regeneration after muscle injury by cardiotoxin (CTX) or crush (CR). Representative micrographs are shown in A and B. Box-whisker graphs of myofiber or myotube diameter from day (D) 0 to D10 after injury are shown in C (n=4 male mice/group after unilateral injury to the tibialis anterior muscle). A: after CTX, large myofibers with peripheral nuclei are observed at D0, apparently undamaged. At D4, necrotic fibers are mostly removed, and short myotubes (arrowheads) are present. By D8, inflammation is much reduced, and myotubes (arrowheads) are longer. At D10, a few inflammatory cells around vessels run between large, centrally nucleated myotubes (arrows). B: after CR at D0, myofibers show little evidence of damage. By D4, a few myotubes (arrowheads) appear in fields of mononuclear cells. By D8, myotubes have grown and elongated among the mononuclear cells. Two relatively acellular regions display incomplete resolution of CR-damaged tissue (*). By D10,

myotubes are larger, and the inflammatory cell infiltrate is reduced. Hematoxylin and eosin staining. Bar=100 m, consistent across all images (A and B). C: box-whisker plots of the diameter of myofibers (D0) and myotubes (D4 to D10) as a function of regeneration time for muscles injured by CTX (Ci) and CR (Cii) in mice that were untreated (no ISDN) or pretreated with ISDN for 2 days before injury (n 4 male mice/group). Fiber diameter in control uninjured, untreated littermate mice is included for reference (CON). Data were analyzed by three-way ANOVA, with significance as reported in the text. Myotube diameter increased with time between D4 and D10 for both CTX and CR-injured groups, was greater in CTX- than in CR-injured groups, and was increased by ISDN. For CTX injury (Ci), myotube diameter was greater after pretreatment than without from D4 to D10. By D10, myotube diameter in the CTX ISDN group was greater than fiber diameter at D0 immediately after injury. For CR injury (Cii), myotube diameter was lower at D4 and D6 after pretreatment compared with the untreated CR-injured groups. On D10, the diameter of myotubes in CR-injured groups (with or without ISDN pretreatment) was less than for fibers at D0. Symbols indicate a significant difference (Tukey's $0.05 < P \leq 0.001$) from untreated group at same time point (*) or from D0 of the same injury-and-treatment group (#).

1.5.2 NMJ maturation

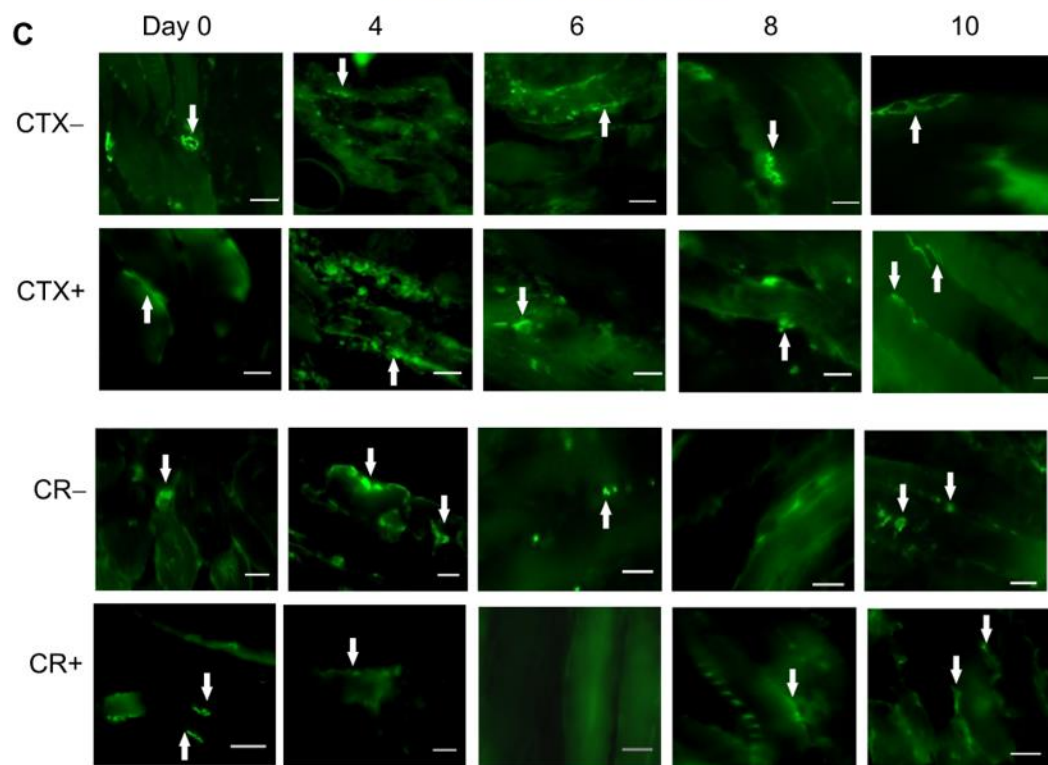
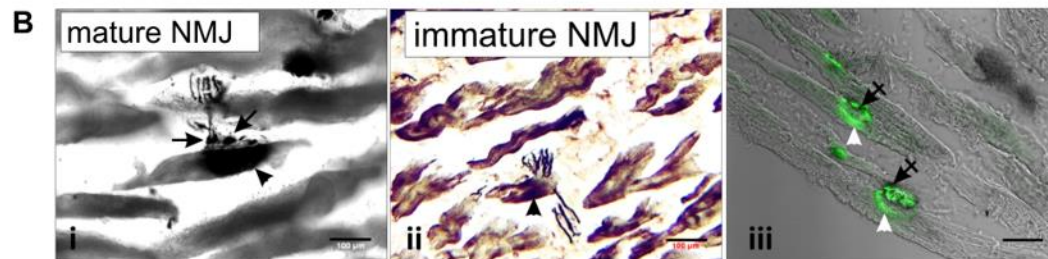
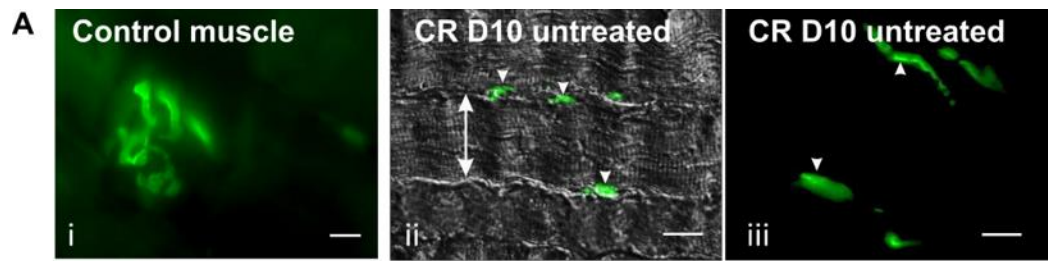
NMJ maturity was classified using three approaches to document structural details in the complex junctional regions (Fig. 2): 1. direct fluorescence for BTX bound to AchRs (Fig. 2Ai-iii); 2. histochemistry (by silver-impregnation staining) to visualize pre-synaptic AchE activity, motor neuron terminals, and neurites and the effect of ISDN pre-treatment on them (Fig. 2Bi-ii); and 3. combined BTX and silver staining to visualize the colocalization of respective post- and pre-synaptic areas in NMJ regions (Fig. 2Biii). Post-synaptic AchRs demonstrated complex pretzel-like configurations in non-injured control muscle (Fig. 2Ai). BTX+ regions on myotube membranes during regeneration (at least 132 regions per group) showed differences in the arrangement of AchRs at different time points. At day 0, immediately after injury, occasional segments of damaged fibers had small to medium-sized pretzel-like regions with fluorescent

staining; a similar pattern appeared on some new myotubes at days 8-10 (Fig. 2C, CTX-). By contrast, up to day 10, BTX staining for AchRs appeared only as spots or lines of fluorescence on damaged fibers and small myotubes in the CR muscles of treated and untreated mice, and in the CTX-injured muscles in treated mice,

The combination of pre-synaptic silver-staining and histochemistry for neurites and AchE activity respectively, displayed a range of patterns. Staining showed large oval plaques of AchE adjacent to nerve terminals that were typical of a mature NMJ (Fig. 2Bi) as well as small or fragmented plaques of AchE with branched neurites, more typical of immature NMJ regions (Figs. 2Bii-iii, 2C). Pre-synaptic patterning, assessed as a distribution of immature vs. mature features, was statistically different between pretreated and untreated groups, and the difference between pretreated and untreated groups reached significance at different time points in the two models of injury (Fig. 2D). After CTX injury, the pattern was more immature after pretreatment at day 10 (Chi-squared $\chi^2=16.73$, $df=2$, $p=0.018$). After CR injury, the immaturity after pretreatment was significant at day 8 (Chi-squared $\chi^2=8.049$, $df=2$, $p<0.001$). Interestingly, control muscle (without surgery or pretreatment) exhibited both the mature and immature NMJ configurations; this observation, likely a sectioning artifact, evidenced a fairly coarse resolution of NMJ changes by this assay. Overall, at least half of all NMJ regions in regenerating muscles in all groups were classified as having immature pre-synaptic patterning. There was no difference in the pattern at day 10 between CTX- and CR-injury models.

Since the second assessment of NMJs had relatively coarse resolution, further analysis was conducted by combining staining with BTX (for post-synaptic AchRs), and histochemistry and silver staining for pre-synaptic structures (AchE plaques, neurites, and terminal boutons). This tripartite assessment classified the proximity of these structures such that full overlap of the three stains (fluorescence, silver and histochemical) indicated a mature NMJ configuration. Results provided further evidence of a model-dependent time course to changes in NMJ configuration, and of the difference due to ISDN pretreatment (Fig. 2E). Of the NMJ regions observed in muscles from days 0-4 after injury, 30% of CTX-injured muscles and 20% of CR muscles showed a mature configuration of AchRs, AchE and neurites, likely areas that survived the direct injury to myofibers. That proportion did not change over the 10 days of regeneration that were examined in CTX-injured muscles. By contrast the mature proportion of NMJ regions in CR-injured muscles was lower than in CTX injury. Only about 10% of regions were classified as mature by days 8-10,

and a much larger frequency of NMJ regions (about 80%) stained only with BTX (i.e., localizing AchRs without proximate AchE and neurites) by 8-10 days compared to CTX-injured muscle. The distribution of staining patterns was more immature for CR than CTX (Chi-squared $\chi^2=34$, $df=10$, $p<0.01$). Pretreatment did not affect the distribution after CTX injury (Chi-squared $\chi^2=14$, $df=10$, $p=0.18$). By contrast, pretreatment before CR injury shifted the distribution toward the immature pattern during regeneration (Chi-squared $\chi^2=80$, $df=10$, $p<<0.0001$).



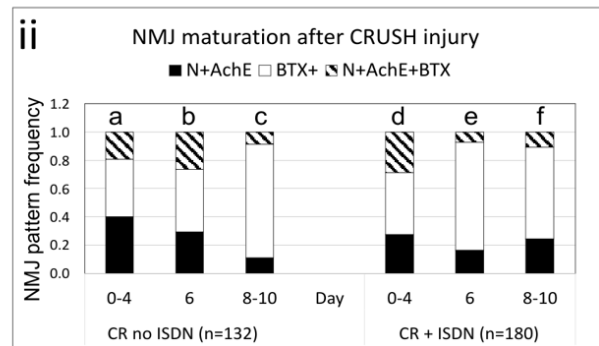
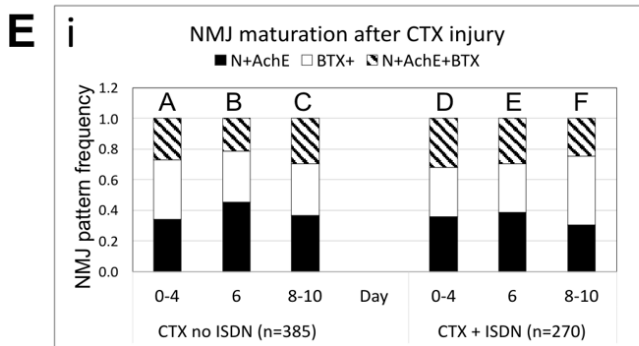
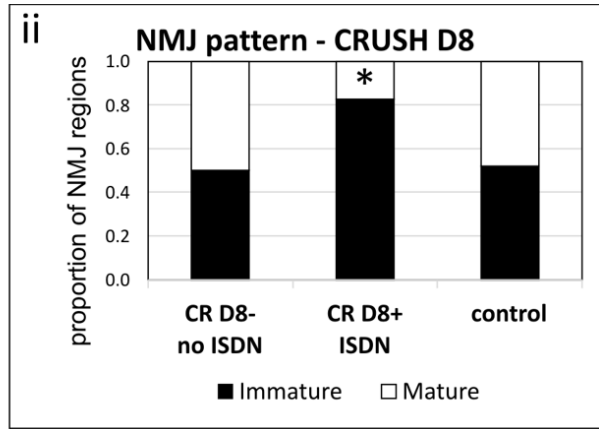
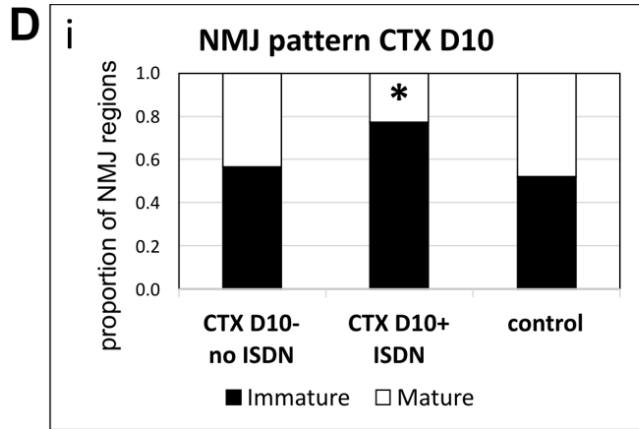


Figure 2. Neuromuscular junction (NMJ) regions. A: representative images of FITC-conjugated -bungarotoxin (BTX) staining for postsynaptic acetylcholine receptors (AChRs). Ai shows a mature “pretzel-like” configuration of BTX staining on a myotube membrane in a control (untreated, noninjured) muscle. Aii and Aiii show linear patches of fluorescence (arrowheads) typical of immature or denervated NMJs located along myotube membranes in two untreated muscles 10 days (D10) after crush (CR) injury. Myotube diameter in Aii is spanned by a double-headed arrow in a merged image of fluorescence staining and differential interference contrast (DIC). Bar in A 10 μ m. B: silver-staining histochemistry for acetylcholinesterase (AChE) and neurites shown in representative images. Bi shows the configuration representative of the presynaptic region of a mature NMJ, including terminal boutons (black arrows) and a large, oval AChE plaque (arrowhead). Bii illustrates an immature NMJ configuration of branches and a small AChE plaque (arrowhead). Biii shows immature NMJ regions with colocalized staining for AChRs (green BTX-fluorescence; white arrowhead) and AChE (black silver-staining histochemistry; crossed arrows) without neurite branches. Bar in B 25 μ m. C: panel of representative images of BTX-FITC staining of AChR regions on disrupted myofibers and myotubes from days 0 to 10 in muscles regenerating from cardiotoxin (CTX) or crush (CR) injury in untreated mice (CTX and CR) and mice pretreated with isosorbide dinitrate (ISDN) 2 days before injury (CTX and CR) (n 4 mice/group). White arrows indicate irregular patches or lines of AChR clusters. Pretzel-like configurations, more typical of mature NMJs, are seen only in muscles of untreated CTX mice at days 0 and 10. Bar in C 10 μ m. D: graphs of the distribution of mature and immature configurations for silver staining in regenerating muscle with and without ISDN pretreatment (n 4 male mice/group for each time point). Di and Dii: stacked-bar graphs show that the proportion of the immature NMJ pattern was higher in pretreated muscles regenerating 10 days (D10) after CTX injury and 8 days (D8) after CR injury compared with respective untreated groups with the same injury. *Significant difference (Chi-square) between pretreated vs. untreated and control groups. Note that silver staining of control muscles (no pretreatment, no injury) also showed presynaptic NMJ regions with an immature staining pattern. E: distribution of NMJ configuration from combined silver staining for presynaptic neurites and AChE (N AChE) and bungarotoxin (BTX) staining for postsynaptic AChRs after 0 – 4, 6, and 8 –10 days regeneration following (Ei) CTX injury or (Eii) CR injury with or without ISDN pretreatment. The number of male mice/group for this analysis was n 8 (days 0–4), n 4 (day 6), and n 8 (days 8–10). Counts of colocalized (N AChE BTX; cross-hatched bars) and single-pattern neurites (N AChE; black) or AChRs (BTX; white) were made from coded slides. Staining was imaged on myotubes with DAPI-stained central nuclei in 132–385 NMJ regions/treatment group. Bars are topped with a capital (CTX; A–F) or lowercase letter (CR; a–f) for reference. The distribution of mature colocalized and immature single-stained regions did not change during regeneration from CTX injury either with or without ISDN pretreatment. From D0 to D10 after CR injury, the frequency of immature (single-stained) NMJ regions

increased (Chi-squared, $P < 0.0001$, i.e., c vs. a, f vs. d). The frequency of immature NMJ regions was higher in untreated CR than in untreated CTX muscles at comparable time points (Chi-squared, $P < 0.001$, i.e., a vs. A, b vs. B, and c vs. C) and higher in pretreated CR than in pretreated CTX muscles at the same time point (Chi-square tests, $P 0.001$, i.e., d vs. D, e vs. E, and f vs. F).

1.5.3 Protein expression

Levels of three proteins, the 65kD form of Sema3A referred to as Sema3A-65, γ AchR, and S100B were detected by Western blotting (Fig. 3A). Band optical density in each blot was normalized to β -actin in the same lane.

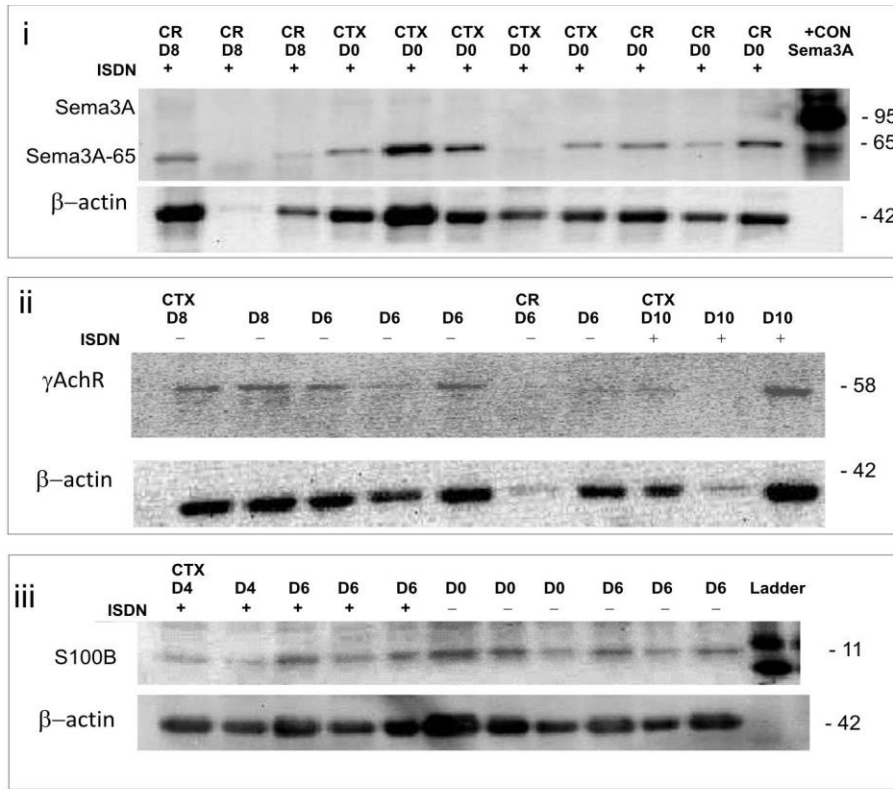
The level of Sema3A-65, also reported as SemD [432], was significantly affected by regeneration time ($F(df=4) = 6.55$, $p=0.001$) and a time*injury*treatment interaction ($F(df=2) = 3.07$, $p=0.05$). Sema3A-65 dropped from day 0 to day 6 in CTX injury without pretreatment (Fig. 3Bi), then increased starting at day 8 (Tukey's test $t(df=39) = 3.27$, $p=0.018$). Pretreatment before CTX injury increased Sema3A-65 at days 8 and 10 compared to untreated groups at the same time point. In CR-injured muscles without pretreatment (Fig. Ci), Sema3A-65 was lower at day 10 than at day 0 (Tukey's $t(df=39) = 4.009$, $p=0.002$). Sema3A-65 was higher at day 0 after pretreatment before CR injury, than at other time-points, and also higher than Sema3A-65 in untreated CR-injured muscles (Tukey's tests, $0.01 < p < 0.05$).

The level of the γ AchR subunit, a marker of early NMJ development and denervation, differed was significantly affected by regeneration time ($F(df=4) = 5.17$, $p=0.002$), the type of injury ($F(df=1) = 7.427$, $p=0.009$), and a time*injury*treatment interaction ($F(df=4) = 7.195$, $p < 0.001$), meaning γ AchR differed between CTX- and CR-injured groups, and was affected by ISDN pretreatment. Gamma AchR did not change over time after CTX injury or after pretreatment (Fig. 3Bii). By contrast, after CR injury in untreated mice, γ AchR was higher at day 4 and 8 than at other time points (Tukey's $p=0.01$). Pretreatment before CR injury reduced γ AchR at days 4 and 8 compared to untreated groups at the same time points (Tukey's tests, $p < 0.01$).

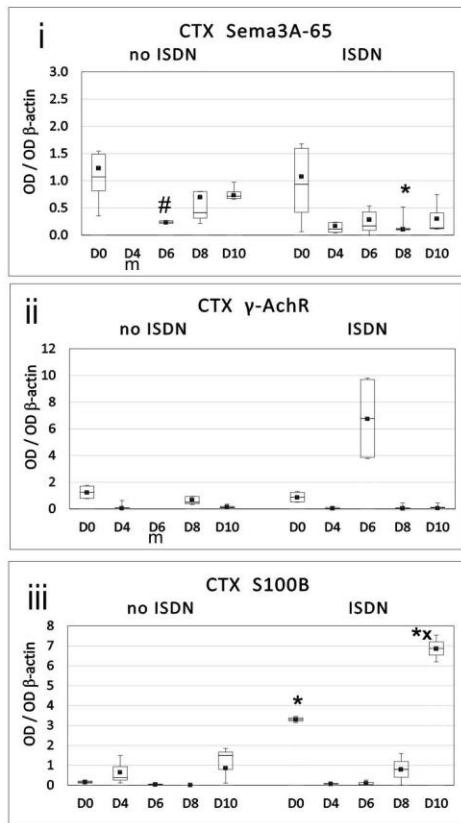
As a first step in understanding the potential impact of muscle injury and premature SC activation on TSCs during regeneration from CTX and CR injury, S100B was assayed in the regenerating muscles. Blots for this protein show more than one band above the 11 kDa band for S100B, possibly S100B homodimers, S100B/S100A1 heterodimers [433] or potential cross-

reactivity of the polyclonal antibody with S100A proteins [434]. S100B was significantly affected by regeneration time ($F(df=4)=27.95$, $p<0.001$), pretreatment ($F(df=1)=56.63$, $p<0.001$), and type of injury ($F(df=1)=70.5$, $p<0.001$), and interactions (time*injury, $F(df=4)=28.87$, $p<0.001$), time*treatment ($F(df=4)=35.8$, $p<0.001$), injury*treatment ($F(df=1)=10.85$, $p<0.001$), and time*injury*treatment ($F(df=2)=5.17$, $p=0.014$). After CTX injury without pretreatment, S100B was low between days 0-10 (day 8 included only $n=1$ sample). Pretreatment increased S100B at days 0 and 10, 10- and 20-fold, respectively, compared to untreated groups at the same time points (Tukey's $t(df=24) =8.76$, $p<0.001$). In CR-injured muscle, while S100B did not change during regeneration without treatment (day 6 included only $n=1$ sample), pretreatment before CR injury increased S100B at day 6 of regeneration (Tukey's $t(df=24) =3.162$, $p<0.003$). In contrast with CTX injury, pretreatment did not increase S100B at day 0 (Table .1).

A



B



C

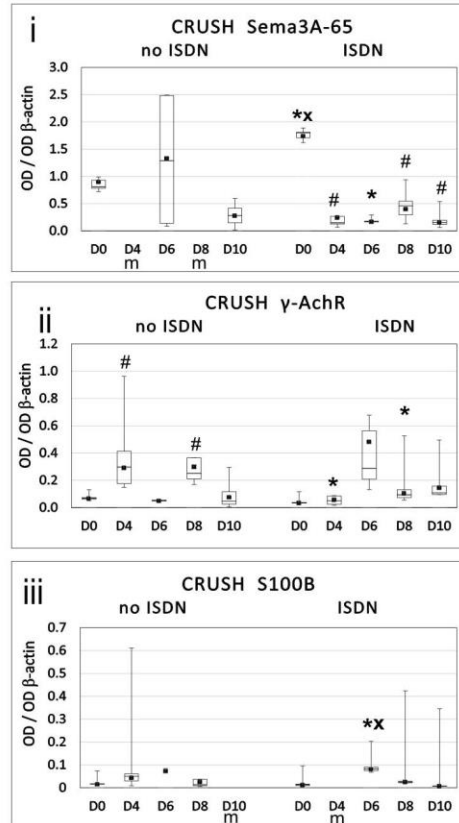


Figure 3. Western blot studies of semaphorin 3A (Sema3A), acetylcholine receptor (AchR), and S100B proteins in regenerating muscles after injury. A: representative Western blots for: Ai, Sema3A-65 (65 kDa); Ai, the α -subunit of AchR (58 kDa); and Aiii, S100B (11 kDa), each with the respective blot for the loading control, β -actin (42 kDa). Labels above each lane indicate type of injury [crush (CR); cardiotoxin (CTX)], the day (D) postinjury (D0 –D10), and sample origin from untreated (–) or ISDN-pretreated (I) mouse. B and C: box-whisker plots of protein level [optical density (OD) standardized to β -actin] in groups of muscles regenerating after CTX (B) or CR (C) injury without treatment or after 2 days of isosorbide dinitrate (ISDN) pretreatment. Bi and Ci, Sema3A-65; Bii and Cii, α -AchR; and Biii and Ciii, S100B. Data were analyzed by three-way ANOVA, with significance as reported in text. *Significant difference (Tukey's 0.05 <P <0.001) from untreated group at the same time point; #significant difference from D0 with the same treatment; X significant difference from all other time points in the same treatment (n 1– 4 male mice/time point in each treatment group); “m” below x-axis indicates missing data from this group.

1.5.4 Pax7+ satellite cell DNA synthesis

SCs were identified as cells with Pax7+ nuclei, located directly adjacent to fibers (at day 0) and myotubes (days 2-10). BrdU+/Pax7+ cells are reported as the proliferative proportion of total SCs cells, omitting interstitial Pax7+ myoblasts (Fig. 4A). Occasionally, BrdU+ nuclei observed by DAPI counterstaining appeared fragmented (Fig. 4Aviii-ix). The proliferative proportion of SCs was significantly affected by regeneration time ($F(df=4) = 5.65$, $p=0.001$) and the type of injury ($F(df=1) = 19.56$, $p<0.001$), with time*injury ($F(df=4) = 2.853$, $p<0.05$) and treatment*injury ($F(df=1) = 3.966$, $p=0.05$) interactions. After CTX injury without pretreatment, the proliferative proportion of SCs increased after day 0 (Tukey's tests, $0.001<p<0.02$) (Fig. 4Bi). Pretreatment before CTX injury increased SC proliferation at day 0 compared to the CTX-injured group without pretreatment (Tukey's $p=0.04$). SC proliferation continued through the 10-day interval of regeneration in both types of injury. Pooling data for days 0-10, SC proliferation was higher overall in CR- than in CTX-injured muscle (Fig. 4Bii vs. 4Bi) (Tukey's $t(df=32) = 4.47$, $p=0.001$). Pretreatment before CR injury decreased SC proliferation at day 0 and day 10 compared to untreated groups at the same time points, and increased SC proliferation between day 0 and days 4, 6, and 8 (Tukey's tests $0.01<p<0.05$). SC proliferation was higher at days 8-10 in muscle from untreated mice after CTX injury, and higher at days 4-8 in muscle from pretreated mice after CR injury (Tukey's tests, $0.02<p<0.05$).

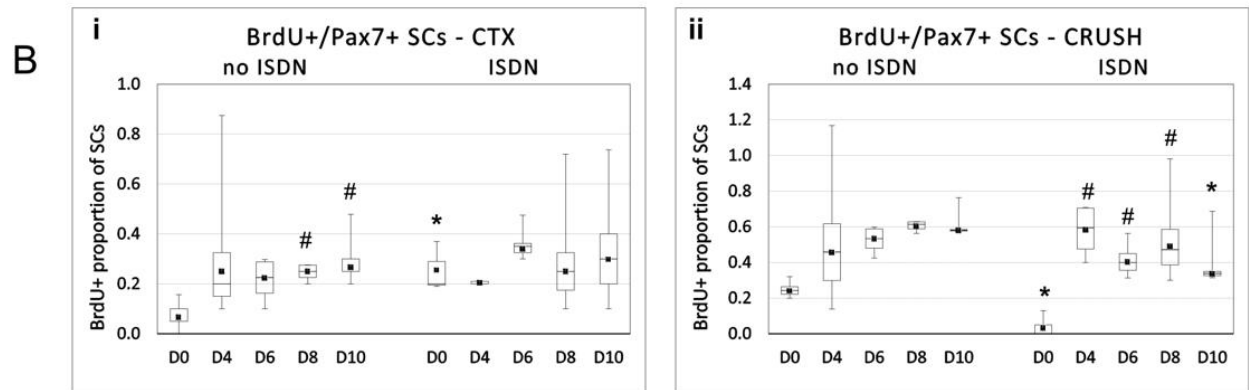
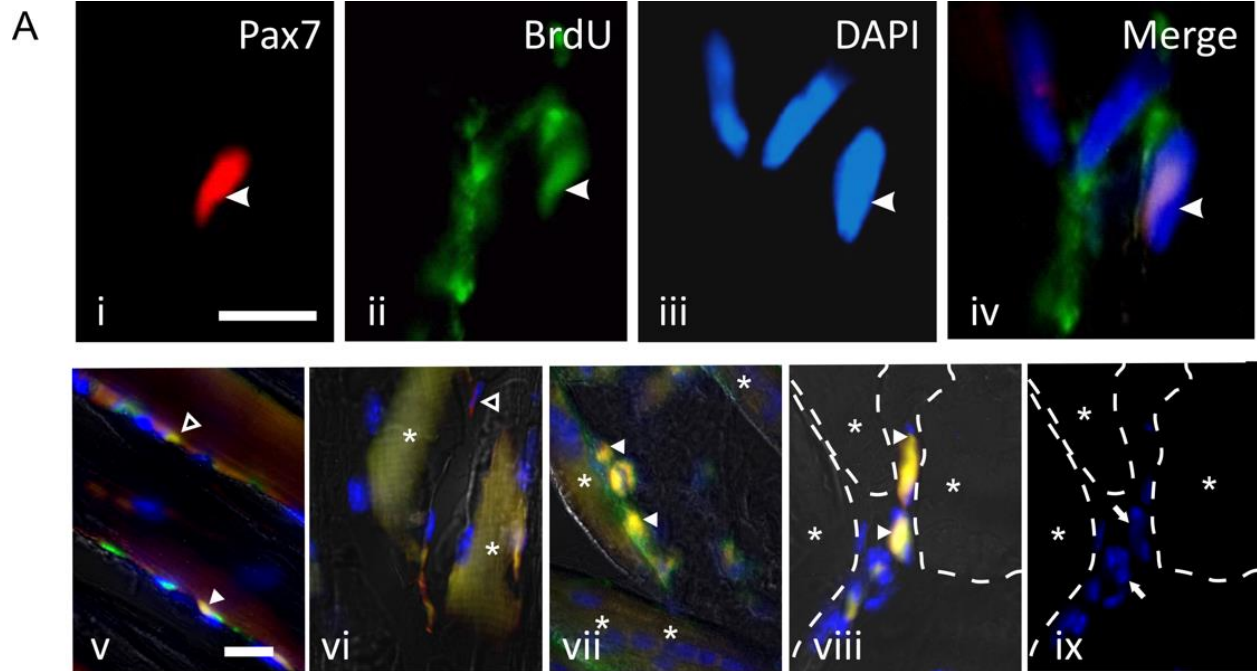


Figure 4. Bromodeoxyuridine (BrdU) labeling of DNA synthesis in Pax7 satellite cells. A: representative images of nuclei immunostained for: Ai, Pax7 (red); Aii, BrdU incorporation (green, arrowhead); Aiii, DAPI counterstain (blue); and Aiv, merged image showing a BrdU/Pax7 satellite cell (SC) nucleus (arrowhead) in a muscle at day 4 post-cardiotoxin (CTX) injury in a mouse pretreated with isosorbide dinitrate (ISDN) (Bar 20 m). Images in Av–ix show examples of Pax7 nuclei in a satellite position on fibers or myotubes that are BrdU or BrdU in: Av, control uninjured muscle; Avi, crush (CR)-injured muscle at day (D) 0; Avii, CTX-injured muscle at D8; Aviii–Aix, CTX-injured muscle at D0 with apparently fragmented nuclei, indicated by arrows in a merged image (Aviii), and Aix, DAPI staining (dashes outline fiber margins). Asterisks indicate fibers or myotubes. Outlined arrowhead indicates a Pax7/BrdU SC nucleus. Solid arrowheads indicate BrdU/Pax7 nuclei. Bar 20 m. B: box-whisker plots of the proliferative proportion of satellite cells (BrdU/Pax7 cells as a proportion of total Pax7 satellite cells; n 4 male mice per time point in each group) in: Bi, CTX-injured and Bii, CR-injured muscles from D0 to D10. There were 20–25 cells counted per time point, observed in 10 fields/muscle, 1 muscle/animal from mice with or without ISDN pretreatment; data were analyzed by three-way ANOVA, with significance as reported in text. The proportion of proliferative SCs at D0 after CTX injury was greater after ISDN pretreatment and was lower at D0 ($P < 0.01$) and D10 in pretreated CR-injured muscle compared with untreated groups with the same injury at the same time point. SC proliferation was higher at days 8–10 in muscle from untreated mice after CTX injury and higher at days 4–8 in muscle from pretreated mice after CR injury. *Significant difference (Tukey's $< P 0.05$) from untreated group at the same time point; #significant difference (Tukey's $P < 0.05$) from D0 with the same treatment.

1.6 Discussion

Experiments tested the effects of premature SC activation before two types of muscle injury, on myogenic regeneration and NMJ formation and remodeling, since SCs are implicated as regulating motor neuritogenesis via *Sema3A* production. Premature SC activation was induced by 2 days of oral ISDN before either myotoxic injury by CTX or traumatic injury by CR. Myogenesis and NMJ maturity were tracked for the first 10 days after injury through established peaks in SC proliferation and *Sema3A* production [84, 194, 396, 417]. Without pretreatment, myogenic regeneration was earlier after CTX than after CR injury, as anticipated. NMJ regions also matured earlier after CTX than after CR injury, including AchR configuration, neurite branching, AchE plaques, and colocalization of pre- and post-synaptic structures. There were model-specific differences in protein expression in the absence of pretreatment: *Sema3A-65* dropped at day 8 after CTX; γ AchR increased at day 4 and 8 after CR, and S100B rose markedly at days 0 and 10 post-CTX. Pretreatment increased SC proliferation immediately after CTX injury, consistent with ISDN-induced SC activation before injury. Pretreatment also decreased NMJ maturation during myogenic repair in both models, especially after CR injury. By contrast, premature SC activation before CR initially reduced SC proliferation (day 0), reduced myotube growth, increased *Sema3A-65* and S100B at day 6, and decreased γ AchR. Pretreatment also reduced SC proliferation at day 10 after CR injury compared to untreated CR-injured muscle. Findings open a new perspective on the timeline of tissue repair in these two models of injury. Results also demonstrate differential effects of the type of muscle injury on S100B protein, and implicate TSCs and SCs in the spatiotemporal synchrony of NMJ/synaptic remodeling and myogenic repair. Evidence of this structural synchronization provides a new basis for research on acute injury responses and later motor neurite/NMJ remodeling and maturation during myotube growth and regeneration, since altered SC activity at the time of injury disrupted the timing of both myogenesis and motor-neuritogenesis during early regeneration. Results open the potential of finding new targets for interventions that both promote and synchronize these two processes for successful rehabilitation.

ISDN effects on myogenesis and myotube growth were anticipated from previous reports that ISDN established exercise-induced muscle growth in old female mice [160] and reduced

suspension-induced muscle atrophy by at least half [378]. In those reports, SC activation was increased by ISDN, promoting hypertrophy and attenuating atrophy compared to respective controls. In the current study, premature SC activation was evidenced by noting increased SC proliferation with ISDN pretreatment before CTX injury compared to controls without ISDN. Since SC daughter cells stop dividing before fusing into new myotubes, declining SC proliferation from days 4-10 after CTX injury without pretreatment vs. ongoing SC proliferation from days 4-10 after CR injury without pretreatment, is consistent with the earlier appearance and more rapid growth of myotubes after CTX vs. CR injury. However, since ISDN is a non-specific NO-donor drug, SC-independent effects of ISDN on injury responses by vascular, immune, or nervous tissues [435, 436] may also be implicated in current findings. It is not known whether pretreatment with MyoNovin, a novel NO-donor designed to target skeletal muscle more specifically [405, 425], would have a different impact than ISDN on NMJ regions.

Surprisingly, right after injury, the DNA-synthesis index of SC proliferation without treatment was higher within 10 minutes after CR injury than after CTX injury. CTX affects muscle fiber membranes and macrophages [437], while CR affects all tissues in the muscle. While SCs are rapidly activated and mobilized after CR injury [23], the increase in BrdU uptake observed so soon after CR injury was puzzling. Since BrdU labeling at day 0 in untreated CR muscles suggests the possibility of early apoptotic changes and rapid DNA repair from DNA damage [438] which requires DNA synthesis [439]. Studies including TUNEL staining would determine whether DNA synthesis at day 0 in CR muscle was uncoupled from S-phase and due to apoptosis, as previously reported [438]. Myogenic cells have inherent susceptibility to DNA damage [438] and a DNA-repair deficiency [440], so cells labeled at day 0 would not likely survive to contribute to later proliferation or myotube formation, as shown in the now-classical studies of SC proliferation after muscle damage [54, 84, 162]. Non-proliferative DNA synthesis is reported for injured Purkinje in an ischemia-hypoxia model of stroke [441], in allylamine cardiotoxicity [442], and in rapid ultraviolet light damage of cultured myoblast and myotube nuclei [443]. The higher BrdU uptake by SCs in CR- and CTX-injured muscle of untreated mice at day 0 may also relate to enhanced proteolytic activation of hepatocyte growth factor (HGF) by traumatic CR, as shown for hepatic tissue injury [108, 444].

The effect of ISDN pretreatment to decrease BrdU uptake at day 0 after CR injury compared to untreated CR muscle was also puzzling. Very few reports track SC proliferation

immediately after injury. Traumatic free-radical release by CR injury may increase after ISDN pretreatment, and could abrogate DNA polymerase activity in DNA repair. While it is not clear how SC activation by injury could involve S-phase so soon after injury, high or low measures of BrdU uptake by SCs resident on fibers and myotubes are consistent with the U-shaped dose-response curve proposed for NO-mediated SC activation [27]. Such changes are also consistent with reports that high HGF [194], traumatic preparation of HGF-containing crushed muscle extract [26, 445], and observations that Marcaine (another myotoxin), inhibited SC activation on cultured fibers [445]. Possible CTX effects on damage-associated DNA repair [438], if confirmed, could help decipher the interactions of injury type, SC pre-activation by ISDN, and relative contributions of DNA repair and S-phase in SCs in the current study.

CTX induces primary muscle-fiber damage, and initially spares fiber-supporting structures including neurites, Schwann cells, connective tissue and vasculature [169, 397, 407]. However, secondary changes in NMJs and neurites after exposure to myotoxic venoms are reported [394, 409, 410, 446]. Examination of the potential impact of altered Sema3A during muscle repair thus required use of an injury model such as traumatic crush, with more extensive nerve damage than CTX [397]. Since TSCs also secrete Sema3A [303], a comparative time-course study of NMJs during muscle repair after two types of damage was useful in identifying model-specific histological differences in advance of future studies of changes in Sema3A and S100B expression at the level of individual cells.

Formation of NMJs after CR injury was delayed by ISDN pretreatment according to two structural indices. NMJ patterns of neurites and AchE plaques shown by silver-staining histochemistry, and colocalized distribution of pre- and post-synaptic NMJ specializations were both more immature after pretreatment. By contrast after CTX injury, only pre-synaptic patterning was immature, albeit transiently at day 8. The model-dependent impact of premature activation on NMJ maturation was consistent with indications of denervation-type immaturity since γ -AchR was reduced by pretreatment before CTX injury and increased during regeneration after CR injury (peak at day 6).

SCs produce Sema3A in the early-differentiation phase of myogenic repair [194, 407], and SC-specific knockout of Sema3A expression interferes with NMJ formation by inducing uncontrolled branching and reducing AchE [397]. Thus, it was surprising that premature SC activation did not advance the time of increased Sema3A early in myotube formation. Even after

CTX injury, where myotubes formed and grew faster after pretreatment than without ISDN, Sema3A did not increase sooner after injury. Further, the 97-kD Sema3A moiety reported to increase in early differentiation [194] was not detected in any samples. Instead, a Sema3A-65 kD moiety was present, and changed differently during regeneration with treatment in both models of injury. Possible ISDN effects on Sema3A proteolysis are unlikely to persist for 10 days, and would only affect pretreated groups, so a toxicity mechanism does not account for the different moiety. A positive-control, recombinant Sema3A was detected at both 97 and 65 kD. However, since Sema3A-65 (also called SemD) is a processed form of pro-semaphorin that is proteolytically activated to become chemorepulsive [432], finding only Sema3A-65 suggests there may be an injury-dependent timing of proteolytic Sema3A processing in SCs (and/or other cells) in injured muscle tissue. As well, the smaller form of Sema3A is less chemorepulsive and allows greater neurite extension toward a target than the larger Sema3A moiety [432]. Since early in-growth of motor neurites will disturb the timing of terminal boutons appearing near regions where AchE and AchR cluster on new myotubes, that change alone would disrupt NMJ maturation.

These experiments assessed NMJ changes on early myotubes regenerating after only 2 days of premature SC activation, induced 48 and 24 hr prior to injury. Determining whether premature SC activation could promote longer-term NMJ restoration and remodeling after traumatic CR (more physiological damage than CTX damage) would better test the potential role of Sema3A signaling in motor reinnervation. This unresolved question is particularly important given a recent report that the reduced chemorepulsive activity of K108N-mutant Sema3A [447] produced by TSCs at NMJs does not abrogate normal motor-neurite sprouting on type IIB fibers after denervation by botulinum toxin [448]. This observation is fascinating, as sensory and motor pathways plus non-neural and non-myogenic tissues are also affected in mutant and Sema3A-null transgenic models [201, 397, 449]. TSCs on fast-twitch fibers express Sema3A during reinnervation [303] as well as S100B. TSC involvement in synaptic plasticity after nerve crush [303], aging [260, 450], botulinum toxin denervation, and during neurite sprouting in amyotrophic lateral sclerosis [451] suggests TSCs are important contributors to regulating moto-neuritogenesis. TSCs may also integrate cues from SCs during myogenic regeneration, since S100 proteins regulate activities of macrophages, neurons, neutrophils, Schwann cells, and myoblasts [424, 452].

Motor-nerve terminals were rapidly disrupted by injury and largely disappeared from muscle 2-4 days after fiber damage in the current study. Muscle is potently trophic in maintaining

nerve terminals at NMJs; reciprocally, nerve terminals sustain post-synaptic receptors on the fiber sarcolemma [258]. By comparison to changes in these trophic interactions after different types of muscle injury, TSCs retain S100B expression and remain functional for ~10 days after nerve injury [453]. Thus, there is a highly complex interplay among a regenerating myotube, its NMJ and motor axon terminals, and adjacent TSCs and SCs. Concurrent effects of pretreatment on Sema3A-65 and S100B that differed between CTX and CR injuries suggest that both the guidance and the elongation of neurites by TSCs may be affected by premature activation of SCs (and possibly ISDN), and secondary effects on the multiple sources of Sema3A [417] during NMJ restoration and remodeling. Localizing the sources of Sema3A expression, processing, and secretion through the time-course of muscle regeneration requires further investigation.

In summary, premature SC activation before muscle damage had distinctive impacts on regulating muscle and synapse regeneration. Results highlight the exquisite importance of synchronous myogenesis and NMJ restoration in shaping the outcome of regeneration, since disrupted synchrony affected the outcome of muscle-tissue responses to injury. TSCs are important in guiding motor axons to reconstitute NMJs in the region of original synapses after nerve injury. Further understanding of TSC support for the maintenance and repair of synapses during muscle-tissue repair will advance our ability to interpret how damage to fibers, neurites, and NMJs each factor into the overall regenerative process, or whether NO-based pretreatment to activate SCs might promote re-innervation after nerve injury. The detailed interplay of Sema3A (from SCs and other tissues) and S100B (from TSCs) in restoring motor and sensory innervation in muscle now awaits careful injury experiments that can perturb the level or source of Sema3A in a genetic or disease model to study the impact on pre- and post-synaptic NMJ compartments [41, 160] and fiber types [228, 397, 420]. Such research, and an advanced knowledge of venom-specific toxicities [454] are important for applying new insights on nerve-muscle interaction to developing ways to sustain or promote muscle function and growth with the rehabilitation approaches used to manage muscle injury, aging, and disease.

2 RESULTS-2

Preliminary studies of gene-expression patterns in satellite cells and terminal Schwann cells in muscle regenerating from crush or CTX-induced injury.

2.1 Abstract

Terminal schwann cells (TSCs) have active roles in the formation, maintenance, function and repair of the neuromuscular junctions (NMJs). TSCs also have an important role in guiding motor axons in the region of original synapses to reconstitute NMJs following muscle injury. To extend knowledge about how TSCs support the maintenance and repair of synapses during muscle regeneration and reinnervation, the effect of a NO-based pretreatment to activate SCs before injury in promoting reinnervation was investigated after muscle injury by cardiotoxin (CTX) or crush (CR). Previous results showed that premature activation of SCs disrupted NMJ remodeling and maturation while accelerating myogenic regeneration and caused a decrease in Sema3A-induced neuro-repulsion and time-dependent changes in S100B. Therefore, since TSCs may be involved in disrupting NMJs during muscle regeneration after premature SC activation, I examined whether TSCs can also selectively confine anatomical plasticity at fast-fatigable (type IIb) synapses during muscles regenerating after either traumatic CR or CTX treated with or without ISDN-induced preactivation. These samples were available at day 0 (crush and CTX) immediately after injury, day 6 (CTX), and days 8 and 10 (crush). The findings showed that the number of Sema3A and S100B expression was each positively correlated with regeneration time (Pearson's $r = 0.598$: $P < 0.007$ and Pearson's $r = 0.705$: $P < 0.001$, respectively). The results related to ISH/ICC assay showed that pretreatment before CR injury decreased the expression of both S100B and Sema3A transcripts compared to the group without pretreatment, at both day 0 and day 10 (t-test, $p < 0.05$). This PCA was run to examine the localization of P75NFGR expression in TSCs and study the relationships among variables for the combined ISH/ICC staining experiments. The PCA study of the expression of Sema3A, S100B and P75NGFR in TSCs in the CR and CTX regenerating muscles with and without pre-treatment suggested them as key regulators during both muscle and nerve regeneration following muscle injury. In summary, the ability to separate the contributory roles of gene expression by TSCs and SCs will advance our understanding of the signaling

interactions of nerve and muscle in the neuromuscular systems and could be applied to promote muscle regeneration and reinnervation following injuries.

2.2 Introduction

P75, expressed in satellite cells (SCs) and terminal Schwann cells (TSCs) is one of two types of receptors for an important family of proteins, called neurotrophic factors. Those neurotrophic factors facilitate survival, neurite outgrowth, differentiation and functional plasticity in several neuronal populations in the central (CNS) and peripheral nervous systems (PNS). TSCs also produce S100B, as reported in the results of Chapter 2 as a first look at the possible interaction of TSCs in mediating myogenic regeneration and motor neuritogenesis during disruptions to repair caused by premature activation of SCs.

Results in Chapter 2 identified that the level of S100B in muscle was significantly affected by regeneration time, the model of muscle injury, and isosorbide dinitrate (ISDN), a nitric oxide donor molecule, to prematurely activate SCs before injury; these findings resulted from analysis of protein extracts from muscles regenerating after either traumatic crush injury (CR) or cardiotoxin injury (CTX) treated with or without ISDN-induced preactivation. With ISDN pretreatment, S100B from TSCs rose markedly (10-20-fold) right after injury (day 0) and at day 10 during regeneration from CTX injury. S100B was twice as high as in untreated controls after CR injury and ensuing regeneration. The ISDN-induced preactivation of SCs before injury also caused disruption of motoneuritogenesis between 8 and 10 days after CTX injury, as evidenced by the reduced colocalization of pre- and postsynaptic features of NMJs, and increased levels of *Sema3A-65*. That work [391] showed that premature SC activation accelerated myogenic repair while disrupting NMJ remodeling and maturation, suggesting that the reduced chemorepulsion of neurites from expression of a lower-potency form of *Sema3A* as its 65kD form, *Sema3A-65*, would allow neurites to grow too early, toward new myofibers, out of synchrony with the formation of new muscle and other post-synaptic remodelling enabled at least in part by TSCs.

The above interpretation suggested that brief NO effects that changed the timing and type of *Sema3A* effects on SCs, also involved TSC production of S100B. Experiments in the current chapter further investigated the involvement of TSCs in NMJ development and remodelling on new myotubes using samples collected from the animal experiments in Chapter 2.

The neurotrophin family in mammals, consists of brain-derived neurotrophic factor (BDNF), nerve growth factor (NGF), and neurotrophin (NT)-3, 4/5. Neurotrophins as a family of proteins, mediate their cellular influences through binding to two groups of membrane receptors which act together in “bidirectional crosstalk”, including tyrosine receptor kinase (trk) family, and the P75 NGF receptor (NGFR) [455]. While all neurotrophins bind P75 NGFR with similar affinity, the trk receptors are more specific; the dual binding of neurotrophins to two types of receptor forms a multi-subunit receptor, and the NGF interaction with this complex provides flexibility in the impact of the signal, either promoting SC activities in NMJ formation and development, or truncating their involvement by promoting cell death. In relation to Trk binding, NGF binds to trkA, NT-3 binds to trkC and trkA, and BDNF and NT-4/5 bind to trkB [456, 457]. Due to the ability of neurotrophins to advance embryonic axonal growth *in vivo* [458], and an observed up-regulation in their expression in muscle and in the non-neural cells of the distal nerve stump after peripheral nerve injury, neurotrophins have been suggested to be involved in the regeneration processes of the PNS.

As described earlier, muscle growth and regeneration after injury resemble embryonic myogenesis to some extent and are mediated by myogenic stem cells known as satellite cells (SCs) located between the cell membrane and the basal lamina of myofibers [23, 87]. Muscle injury in adult mammals (before such time as they would be considered aged or senescent) activates quiescent SCs. Those SCs then re-enter the cell cycle, proliferate and differentiate followed by their fusion to each other to form new myofibers and/or to other or broken fibers to repair those damaged by the injury. A minority of SCs return to the quiescent state to preserve the pool of progenitor cells. This preservation of the SC pool is crucial for maintaining regeneration capability, and so the niche also supplies cues for SCs to return to quiescence once regeneration is finished. [459, 460]. Many gene-signaling pathways are responsible for regulating myogenesis, such as MyoD (and other myogenic regulatory genes), MEF2 transcription factors, and extracellular agonists including insulin-like growth factor (IGF), transforming growth factor (TGF), and fibroblast and hepatocyte growth factors (FGFs and HGF) [461, 462].

The expression of NGF has been studied both in human and animal models of myogenesis. NGF is expressed in developing muscle [463] and is up-regulated during pathological conditions such as muscular dystrophy [464] and amyotrophic lateral sclerosis [465]. Indeed, mice with

functional knockdown of NGF signaling display signs of muscle dystrophy [466]. The effect of NGF is mediated by an interaction with a low-affinity receptor, a 75 kDa glycoprotein, P75NGFR [467]. In addition, P75NGFR is expressed in Pax7-expressing muscle satellite cells [468] and human primary myoblasts and myotubes [467], and its expression is reportedly mediated by MyoD [469]. Activity of the P75NGFR gene is implicated in processes in the nervous system such as neuronal survival, axonal elongation, and cell death [470-472].

Skeletal muscle needs the innervation of motor nerves to yield voluntary muscle contractions and to prevent muscle atrophy. Cellular interaction between motor neurons and their target myofibers creates a chemical synapse, known as the neuromuscular junction (NMJ). Excited motor neurons release acetylcholine (ACh) from nerve terminals, which diffuses across the synapse and binds to nicotinic acetylcholine receptors (nAChRs) on the postsynaptic area of the muscle. Proper organization and development of NMJs are essential for effective neuromuscular transmission [473]. Injured skeletal muscle and peripheral nerve both have a distinctive ability to regenerate tissue and function [474, 475]. Even though regenerated NMJs are mostly developed at original synaptic sites of the skeletal muscle [476], there is growing evidence to demonstrate that NMJs are also formed by regenerated axons and on regenerated myofibers [260, 477].

Previous studies displayed many markers that were, at least initially, thought to be specific to Schwann cells, including neural cell adhesion molecule (NCAM), Sox10, Oct6 and Sox2 and the most frequently used proteins, S100B and P75NGFR. In addition, anti-GAP-43 and anti-P75 immunostaining studies also reported finding that these antibodies label Schwann cells, although only after nerve injury or blockade of nerve activity [332]. The level of P75NGFR protein in motor neurites, axons and Schwann cells increases during Wallerian degeneration [478]. A study on two models of motor neuron injury using P75^{-/-} mice displayed that this up-regulation of P75NGFR during Wallerian degeneration was not essential for motor neurite survival; to the contrary, it in fact enhanced the sensitivity of motor neurons to cell death [479, 480]. In relation to muscle, denervation leads to increased NGF production by skeletal muscle 4 days after nerve injury [481].

In skeletal muscle, NGF binds to P75NGFR and the expression of both NGF and P75NGFR is upregulated during primary myoblast differentiation *in vitro*, and this upregulation functions to trigger morphological changes involved in myoblast fusion. Research indicates that neurotrophic factors act in an autocrine fashion to regulate SC behavior and muscle regeneration. Thus, it is

conceivable that systematic release of neurotrophic factors after denervation has a similar impact on SC activation and differentiation. Moreover, denervation can trigger secondary effects on SCs by influencing the physiological properties of myofibers [51], which in turn will impact a fiber's mechanical interactions and signaling to closely adjacent SC, such as release of nitric oxide from the mechanosensitive enzyme, neuronal NO synthase, at the start of the SC activation cascade during stretching or exercise [482].

The reaction of neurons to neurotrophins is regulated through the expression of two sets of cell surface receptors including P75 NGFR and TrkA receptor tyrosine kinase. The related TrkB receptor tyrosine kinase binds both neurotrophin-4 and BDNF while TrkC receptor binds only neurotrophin-3. The P75 NGFR binds to all neurotrophins with similar affinity, but the binding character of different neurotrophins shows diverse kinetics; thus, the neurotrophins can engage two distinct receptors, which can interact with each other or act independently. The Trk sub-family of tyrosine kinase receptors is characterized by immunoglobulin-C2 domains which are rich in cysteine and leucine residues in their extracellular area, a tyrosine kinase domain, and a short cytoplasmic tail. By comparison, the P75 receptor comprises four negatively charged extracellular repeats, and a cytoplasmic domain which is highly preserved among species. There are no sequence resemblances in cytoplasmic domains or ligand-binding regions between the P75 and Trk receptors. Further, the P75 receptor is a member of a super family of receptors, demonstrated by tumor necrosis factor (TNF) receptors. The TNF-receptor family is identified by canonical cysteine-rich regions in the extracellular area. Other members of the TNF-receptor family include the lymphoid cell-specific receptors such as CD27, CD30, CD40 and other proteins such as CAR-1 [483]. All of these transmembrane proteins contain a cysteine-rich motif in their extracellular sequence that covers 40 amino acids and is replicated two to six times. Each group of receptors experiences ligand-induced dimerization that activates several signal transduction pathways. Neurotrophin binds to Trk members and generates biological reactions by activating tyrosine kinase domains. This results in a rapid increase in the phosphorylation of certain effector enzymes, such as phosphatidylinositol 3X-kinase (PI3-K), phospholipase C-g, and PI3-K SHC. The second messengers for neurotrophin Trk receptors, PI3-K SHC and phospholipase C-g adaptor proteins are used by several tyrosine kinase receptors [455].

Research findings presented in the previous chapter showed that, premature SC activation before muscle damage had distinctive impacts on regulating muscle and synapse regeneration

[391]. Those results highlighted the exquisite importance of synchronous myogenesis and NMJ restoration in shaping the outcome of regeneration, since disrupted synchrony affected the outcome of muscle-tissue responses to injury. TSCs are important in guiding motor axons to reconstitute NMJs in the region of original synapses after nerve injury. Further understanding of how TSCs support the maintenance and repair of synapses during muscle-tissue repair will advance our ability to interpret how damage to fibers, neurites, and NMJs each factor into the overall regenerative process, or whether NO-based pretreatment to activate SCs before injury might promote re-innervation after nerve injury. Such a scenario may ensue in a surgical intervention, where pretreatment in the form of “prehabilitation”, could help advance the post-surgical outcome of rehabilitation.

2.3 Rationale and Hypotheses

Previous literature indicates that signals started by TSCs upon denervation work as a guidance substrate for regenerating motor neurites, and can induce the formation of new motor boutons at synapses after denervation [259]. As well, results from the first chapter of this thesis indicated that after two days of premature SC activation, S100B from TSCs increased 10-20-fold at very early (day 0) and at day 10 after cardiotoxin injury whereas S100B had only doubled by 6 days after traumatic crush injury following 2 days of premature SC activation. Premature SC activation thus disrupted NMJ remodeling and maturation while accelerating myogenic regeneration, and results suggested this involved a reduction of Sema3A-induced neuro-repulsion and time-dependent changes in S100B [391].

Therefore, since active TSCs generate local cues, facilitating nerve terminal sprouting during re-innervation and muscle regeneration, and TSCs may be involved in disrupting NMJs in regenerating muscle following premature SC activation, in the second part of my thesis research, I examined whether TSCs can also selectively restrict anatomical plasticity at fast-fatigable (type IIb) synapses during these processes.

To test the hypothesis, I first studied the expression of Sema3A and AchR γ subunit in SCs and S100B in TSCs in the CR and CTX regenerating muscles with and without pre-treatment using sections from the same animal experiments described in Chapter 2.

The significance of these experiments is that repair from crush injury requires the whole architecture and signaling of nerve-muscle interactions to be remodeled to restore muscle function. The ability to dissect the contributory roles of gene expression by TSCs and SCs in that restoration using in situ hybridization will advance our understanding of the complexity of systems involved in the functional outcome of treatments for traumatic and disease conditions of the neuromuscular system.

2.4 Materials and Methods

The described experiment in this chapter was conducted utilizing tissue sections available from experiments conducted at the University of Manitoba, as described in the first Results chapter [391].

2.4.1 Manitoba experiments

As described earlier [391], adult C57BL6 mice (10 weeks old, n=84) were housed and treated according to regulations set by the Canadian Council on Animal Care as approved by the University of Manitoba, protocol F14-015. Half the mice received a daily oral dose of ISDN (66 mg/kg in canola oil; at a volume of 2.7 μ L/g body weight) for 2 days [378, 391, 405] before muscle-injury surgery 24hr later. Under anesthesia, mice received an injury to the left tibialis anterior muscle (TA) by either a traumatic crush (CR) or percutaneous injections of cardiotoxin (CTX) (Sigma-Aldrich, Mississauga, ON, Canada) evenly spaced at 4 sites from the proximal to distal TA [391]. A further group of 4 mice served as untreated controls for the NMJ study and had no injury or surgery. This protocol established 4 treatment groups: crush (CR) and cardiotoxin injury (CTX), each with two sub-groups with and without ISDN pretreatment (n=20 mice per injury-and-treatment group).

Animals were allowed to recover before euthanizing for 0 days (within 10 minutes of injury, while still under full anesthesia), or 4-10 post-injury; at each time point, half the euthanized animals in each of CTX and CR groups had received pretreatment with ISDN. In order to minimize observer bias, data were not decoded until after observation, measurement, or photography.

2.4.2 Antibody Information

Blocking antibodies in double immunofluorescence staining included: unconjugated Fab Fragment goat anti-mouse IgG (115-007-003, Jackson ImmunoResearch, 1:200), and unconjugated Fab Fragment goat anti-rabbit IgG (11-007-003, Jackson ImmunoResearch, 1:200).

Primary antibodies used for fluorescence staining included mouse anti-NGFR P75 antibody (sc-271708, Santa Cruz, 1:1500). Secondary antibodies included: goat anti-rabbit IgG DyLight650 (ab96902, Abcam, 1:200), goat anti-mouse IgG conjugated with DyLight488 (ab96879, Abcam, 1:200) and goat anti-mouse IgG conjugated to horseradish peroxidase (HRP) (A2304, Sigma, 1:200). DAPI was used to counterstain nuclei (D9542 Sigma, 1:10000).

2.4.3 In situ hybridization

In situ hybridization experiments (ISH) were performed to detect the level of expression of various mRNA transcripts (S100B, Sema3A and P75) in muscle sections. The *in situ* hybridization protocol (ISH) was applied to detect multiple transcripts in one section using fluorescence detection with RNAScope® Multiplex Fluorescent Assay v2 products (equipment and reagents), as established by the manufacturer and available through Advanced Cell Diagnostics (ACD, Hayward, CA). Sections were typically counterstained with 4',6-diamidino-2-phenylindole (DAPI, which fluoresces blue) to identify the location of cell nuclei. To address particular research questions, additional application of immunostaining methods allowed supplementary identification of a second cell type; this was useful when the number of fluorescently tagged probes exceeded the 3-probe capacity of the RNAScope™ multiplex system that was purchased. Negative- and positive-control probes are provided with the kit to standardize the protocol for a user and to confirm that the level of detection provided from that user's technique and particular type of sample (which can range from frozen or fixed-frozen specimens or paraffin-embedded specimens, to isolated cells or cell pellets and cultured cells). In these experiments, only paraformaldehyde-fixed, frozen sections were used for ISH studies according to manufacturer's instructions (see above, section, 2.9, *in situ* hybridization).

NIH ImageJ software was used to determine two-probe pairs that generated visible signals. In this study, 10 pairs for each probe were selected to generate near-ideal signals (high signal-to-noise ratio) and to add robustness against partial RNA degradation and variations in target

accessibility within the samples. The sequences of target probes, preamplifier, amplifier, as well as label probes are available through open access at <http://jmd.amjpathol.org> [484] and supplied through Advanced Cell Diagnostics (Hayward, CA). Probes were constructed by the manufacturer for fluorescent detection of Sema3A, S100B and P75 (Molecular Probes; Invitrogen, Eugene, OR). Transcripts were detected on sections of muscle from samples (slides from animals after crush and CTX injury (with and without pre-treatment). These samples were only available at day 0 (crush and CTX) immediately after injury, day 6 (CTX), and days 8 and 10 (crush) due to previous work in the same experiment having exhausted the supply of slides as described in the previous results chapter.

2.4.3.1 In situ hybridization Procedures

All reagents identified in this protocol (named in capital letters) were provided by RNAScope® product catalog as a kit (V2 multiplex fluorescent detection reagent kit, ACD, 323100) unless otherwise noted. The assay protocol began (day 1) by turning on the HybEZ™ Oven (Advanced Cell Diagnostics, Hayward, CA) and setting the temperature on 40°C. The tray was warmed for 30 minutes at 40°C before use. A humidifying paper was placed in the Humidity Control Tray and wet completely with distilled water. The covered tray was inserted into oven and the oven door was closed to keep the temperature constant. Fresh RNAScope® 1X Target Retrieval Reagent (200 mL) was prepared by adding 180 mL distilled water to 20 mL of 10X Target Retrieval Reagent. Slides were placed on the cleaned, covered bench and 1 drop (100 µL) of RNAScope® Hydrogen Peroxide was added onto each slide to cover the entire section; slides were then incubated for 10 minutes at RT. The Hydrogen Peroxide solution was removed from one slide at a time by tapping and/or flicking the side of the slide onto absorbent paper. The slide was taken immediately into a slide rack submerged in a staining dish filled with distilled water. A one-tier steamer (model no. HS2241WD, Black & Decker,) was used to perform target retrieval; two slide holders were placed in the steam bowl (each filled with 200 mL of 1X Target Retrieval Reagent and 200 mL of distilled water). The timer was set to heat for 95 min with temperature of at least 99°C. The slides were added to the container containing distilled water for 10 seconds to acclimate slides and then moved to the container of Target Retrieval Reagent. Slides were removed from the steamer after 5 minutes, transferred to a separate rinse container with 200 mL of distilled

water and rinsed for 15sec. The slides were then transferred in to 100% alcohol for 30 minutes and then dried in 60°C incubator (or at RT). A barrier was drawn 2–4 times around each section with the Immedge™ hydrophobic barrier pen (Vector Laboratories, Burlingame, CA) and allowed to dry completely (1 min or overnight at RT).

Dried slides were placed on the ACD EZ-Batch™ Slide Rack, and 1 drop (100 µL) of RNAscope Protease Plus was added to entirely cover each section. The HybEZ™ Humidity Control Tray was removed from the oven and the slide rack was placed in the tray. The lid was closed, sealed, and the tray was inserted back into the oven and incubated at 40°C for the standard time. Each slide was taken, one at a time from the slide rack and excess liquid removed before being placed in a Slide Rack submerged in a Staining Dish filled with distilled water immediately. The slides were then washed 3–5 times by moving the slide rack up and down in the distilled water. Prepare 1X Wash Buffer. The excess liquid was removed from the slides, placed in the HybEZ™ or EZ-Batch™ Slide Rack and 1 drop (100µL) of the probe mix was added to entirely cover each slide and the slide rack containing the slides was inserted into the HybEZ™Oven for 2 hrs at 40°C. The slides were washed in 1X Wash Buffer for 2 minutes at RT. One drop (100 µL) RNAscope® Multiplex FL v2 Amp 1 was added to entirely cover each slide and then slides were returned into the oven for 30 minutes at 40°C. Next, one drop (100 µL) RNAscope® Multiplex FL v2 Amp 2 was added to entirely cover each slide, and slides were returned into the oven for 30 minutes at 40°C. The slides were washed in 1X Wash Buffer for 2 minutes at RT. A drop (100 µL) RNAscope® Multiplex FL v2 Amp 3 was added to entirely cover each slide, the slides were returned to the oven for 15 minutes at 40°C and then were washed in 1X Wash Buffer for 2 minutes at RT.

TSA Plus fluorophores were then prepared. To develop an HRP-Channel1 signal, 1 drop (100 µL) of RNAscope® Multiplex FL v2 HRP-C1 was added to entirely cover each slide, and slides were inserted into the HybEZ™Oven for 15 minutes at 40°C, washed in 1X Wash Buffer for 2 minutes, the excess liquid was removed and 150–200 µL of diluted TSA® Plus fluorescein was added to each slide followed by a 30-min incubation at 40°C. After a 2- min wash in 1X Wash Buffer, 100 µL) of RNAscope® Multiplex FL v2 HRP blocker was added to slides which were then incubated at 40°C for 30 min before washing with 1X Wash Buffer for 2 minutes at RT. During next step and to develop the HRP-C2 signal, 1 drop (100 µL) of RNAscope® Multiplex

FL v2 HRP-C2 was added to each slide, and slides were incubated for 15 min at 40°C before washing in 1X Wash Buffer for 2 min at RT. Next, 150–200 µL diluted TSA® Plus tetramethyl rhodamine was added to each slide and slides were incubated for 30 minutes at 40°C and then washed in 1X Wash Buffer for 2 minutes at RT. After removing excess fluid, this was followed by adding 100 µL RNAscope® Multiplex FL v2 HRP blocker to each slide, incubating 15 mins at 40°C and washing for 2 min at RT in 1X Wash Buffer. At the last step, excess liquid was removed from slides, 100 µL of DAPI was added to each slide, and slides were incubated for 30 min at RT. After 30 min, liquid was removed and 1-2 drops of ProLong Gold Antifade Mountant were placed on each slide before applying 24 mm x 50 mm glass coverslips. Slides were dried for 30 min to overnight in the dark. Images of cell morphology and staining were captured during observation at 40X magnification using an Olympus IX71 fluorescent microscope and a PXL37 CCD camera (Photometrics, Tucson, AZ). The measured level of mRNA transcript expression revealed by use of the RNAScope® technology was based on the count, intensity, and area of fluorescent spots identified in microscopic images captured at 40X.

The method provided by the manufacturer was studied in detail while preparing for at least two practice sessions or “dry runs” of the full 2-day protocol that were conducted prior to the appropriate quality-control experiments in which the results were reproduced well. Staining quality from applying the protocol exactly as prescribed was evaluated carefully prior to any full experiments with research samples. The *in situ* staining signal was tested for non-specific background staining (little to none was present) and for detection sensitivity using positive- and negative-control slides provided by the manufacturer specifically for the probes of interest. After consultation with the technical resource expert at Advanced Cell Diagnostics, the full protocol was then run on test slides of muscle sections prepared in house (paraformaldehyde-fixed, cryosections); these sections were known from earlier work to contain NMJ regions. A second consultation with ACD experts (with exchange of images) found the results to be of excellent quality, high sensitivity and specificity, and reproducible. Therefore, slides were subsequently processed for *in situ* hybridization, as described in the above protocol. Slides were processed in groups of 10 selected from among the different treatment groups.

In all cases, expression was determined using the same (default) calibration of colour and intensity provided by the software. Thus, the number of punctate sites of expression, the size of

each expression site, and the density of staining at each site was assessed for each gene transcript of interest in each captured image. The statistical comparisons related to each dataset are provided in the relevant text and Figure legend.

Each of the three features of expression sites that was measured (number/field, intensity, and diameter) is used to indicate expression level in some fashion [485], while the *in situ* technique itself, localizes the site of expression and identifies the transcript(s) that are expressed.

2.4.4 In situ hybridization combined with immunohistochemistry

In situ hybridization (ISH) was performed as described above, omitting the mounting medium and coverslips. Then, to identify the TSCs in sections in combination with the ISH protocol for S100B that is not produced by SCs, slides were washed 3 times for 2 mins each with Tris-buffered saline containing 0.1 % Triton-x100 (TBST). After rinsing, slides were processed for immunohistochemical detection of P75 using a mouse anti-P75 primary antibody overnight. After washing again in TBST 3 times for 2 mins each, slides were incubated in the fluorochrome-conjugated secondary antibody (Alexa488 anti-mouse IgG, diluted 1:500) for 2 hrs at RT. After rinsing 3 times in TBST, coverslips were mounted over sections, and slides observed under a fluorescence microscope Zeiss Apotome (Jena, Germany).

The Sema3A-positive proportion of cells expressing both S100B and P75, was determined by observing a minimum of 200 Sema3A-positive cells in sections of muscle from each group and time-point of interest. This area is referred to as the P75 colocalization area (i.e., colocalization with S100B and Sema3A). Images were analysed for the number of expression sites per field, the intensity (areal density of fluorescence) of expression sites, and the diameter of expression sites for each sequence/protein using Celleste Image Analysis Software v 5.0 (InVitrogen, Thermo Fisher Scientific, Waltham, MA). Colocalization of various gene or protein combinations was also determined. These were: (“com” indicates the number of overlapping spots for two factors such as S100 &P75 and P75&Sema3A. The “S&S “stands for the number of overlapping spots for Sema3A and S100B; and also “All3 com” indicate the number of overlapping spots for Sema3A, S100B and P75NGFR in samples. Coloc P75 indicates the number of overlapping areas with the RNA expression of S100B, Sema3A and P75NGFR in TSCs.

Celleste software employs a set of visualization and image analysis tools in a format designed for efficiency and usability. The software provides streamlined set of tools by which to process and analyze images. An auto-alignment feature allows the overlay of two images (e.g., from two different fluorescence wavelengths) and eliminate background noise. Other tools are available for labeling images based on color or intensity level. Celleste™ also contains the capability for outlining areas for colocalization analysis. Colocalization results can be adjusted to adjust the intensity threshold for each channel to be above background fluorescence. After counting the fluorescent objects, images were sorted and displayed based on particle size and other parameters (Figure 5).

In these preliminary studies with *in situ* hybridization (ISH), muscle sections from mice were available for staining at day 0 and 6 after cardiotoxin (CTX) injection and at days 0, 8 and 10 after muscle-crush injury (ISDN pretreated, and untreated mice). The colocalization of RNA expression of S100B (red) and Sema3A (green) in TSCs was detected via the ISH method. In addition, in the combined fluorescent-ISH/ICC assay (indicated by naming the variable by using “com” for “combined”, after a particular gene or protein name), TSCs were identified through the colocalization of the expression of S100B and Sema3A transcripts (by ISH) with the P75NGFR protein (by ICC), together in a single cell. The number of areas of colocalized expression was tabulated in the 10 fields imaged per slide/sample, and formed a variable representing TSCs (S100B + Sema3A + P75NGFR) for the PCA. Representative images from the staining experiments illustrate the ISH signals and areas of colocalization that were used to identify TSCs and SCs.

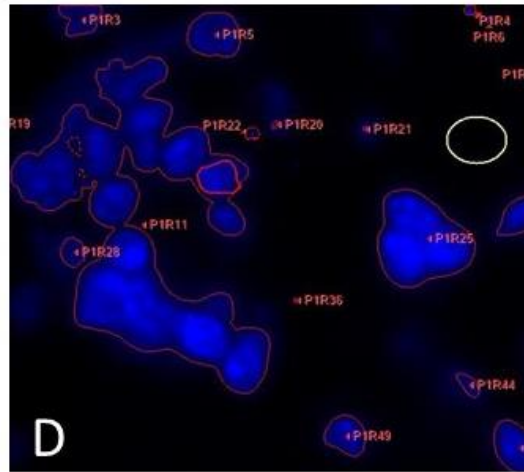
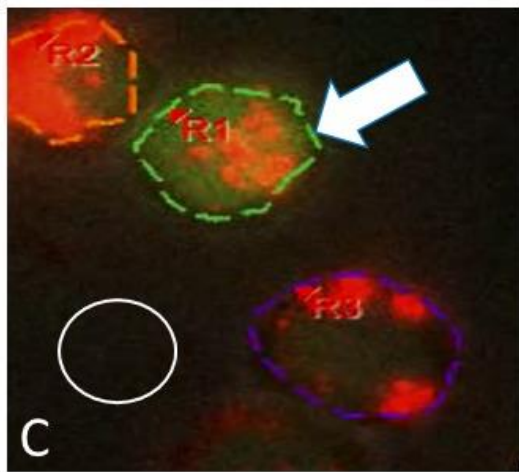
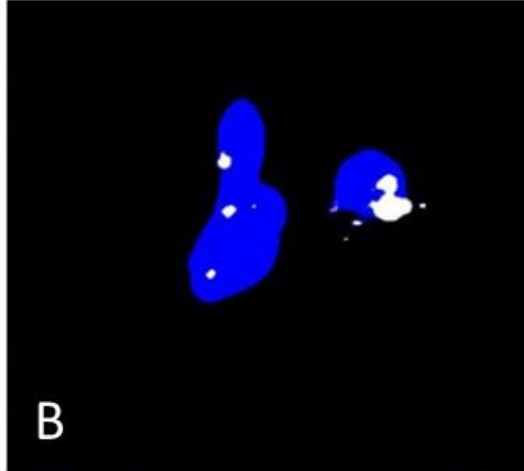
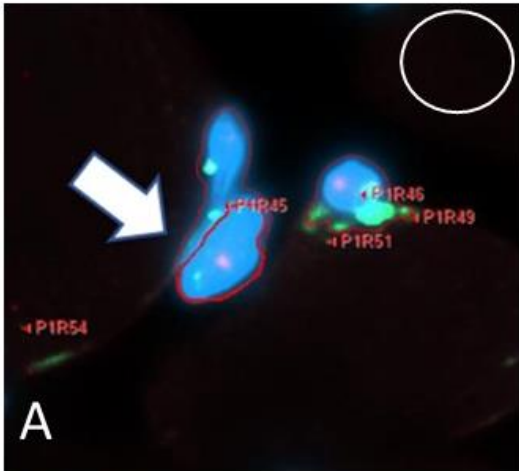


Figure 5. In situ hybridization and Celleste software. The level of mRNA expression in regions containing NMJs was assessed by identifying the number of expression sites of a particular fluorescent colour, determining the overall intensity of fluorescence (areal density) of those regions, and measuring the size (diameter) of each of those regions. A. In this example, regions of blue fluorescence (outlined by red lines, one is indicated by the white arrow), green fluorescence, and a representative region of background (white circle) are identified and drawn in an image using the “smart segmentation” tool in Celleste software. The fluorescent regions are automatically counted and labelled by the software. A region of background was selected in an area that did not overlap any other region selected for measurement. The density (areal intensity) of the background region was subtracted by the software, from the intensity measured in each region of fluorescence. From each fluorescent region, the irregularly shaped region of fluorescence was counted as a single expression site, and the density (areal intensity) of that region of expression was measured (not including non-fluorescent pixels inside the outline). Finally, the maximum diameter of the fluorescent region was measured. In this example, regions of blue fluorescence are overlapping with regions of green fluorescence. B. The Celeste “colocalization” feature was used to identify and measure the spatial overlap between two (or more) different fluorescent-color labels and count the number of overlapping sites. In this example, the colocalization feature identifies the regions of overlap between blue and green in A, as white regions, which then were counted and measured by the software. C. An example representing ISH containing a field with three outlined sites of red fluorescence (irregular fluorescent regions are outlined by dashed red lines, one indicated by white arrow). One of these sites overlaps with green fluorescence from a second probe. A region selected for background subtraction is identified by the white circle. D. A representative field illustrating the counting feature of Celleste software applied to a single fluorochrome. Each region of fluorescence is outlined and then labelled on the image with a unique-identifier alpha-numeric label. Original magnification by oil immersion X40 objective lens.

The various staining combinations available from the above experiments are tabulated below. Cells positive for all three markers of interest in a particular experiment, either from *in situ* hybridization or the *in situ* approach combined with immunohistochemistry were identified as follows. Cell positive for S100B, P75 (protein or mRNA) and Sema3A were considered to be TSCs. Cells positive for S100B and P75 (but not Sema3A) were categorized as non-terminal Schwann cells. Other cells positive for Sema3A expression but not labeled by other *in situ* probes or immunohistochemistry, were not counted. Groups and assays are summarized in Table 1. ISH was conducted on (CR and CTX injured, with or without ISDN pretreatment) samples to detect the expression (+ sign) of Sema3A and S100B transcripts and P75 protein using immunostaining.

Table 1. Experimental design for ISH combined with immune detection of P75

assay	Sema3A (mRNA)	S100B (mRNA)	Pax7 (mRNA)	P75 (protein)
groups				
Muscle crush	+	+	-	+
CTX				

2.4.5 Statistical Analysis

Data were compiled in spreadsheets using Microsoft Excel (Microsoft Office Professional Plus 2016), decoded by treatment group and time-point (days post-injury), and analyzed using Microsoft Excel 2016 or Jamovi v1.1.9 open access software. For score data, the main factors (effects) were: injury type (muscle crush and CTX), pretreatment with ISDN (vs. control), and regeneration time, with interaction effects and *post hoc* means tests, as appropriate. Data are reported using box-whisker plots representing first and third quartiles, median, mean, maximum, and minimum for scored data. Correlation analyses for possible associated parameters, such as the RNA expression of Sema3A, S100B, Pax7, P75NGFR and regeneration time were performed by

linear regression analyses (Pearson). In all cases, a probability of $p < 0.05$ was used to establish significance.

2.4.6 Principal Component Analysis

Principal component analysis (PCA) was used to decrease the dimensionality of the multivariate results of the study down to two- or three-dimensional data and facilitate graphical visualization of the complex dataset. PCA was used to identify those variables that make the largest contribution to explaining the overall variability in the dataset (somewhat like the explanation of variation (by R^2) in a two-variable regression). Although other statistical analyses such as t-tests are used to assess hypotheses related to only one variable, PCA offers a comprehensive test by creating a few new components (factors). These new components, therefore, attempt to explain most of the variation in the original data through use of a smaller number of factors (or principal components) that maintain correlations among the variables.

Graphical illustration of significant PCA findings is known as a biplot or loading plot and is useful for choosing those components that maintain the most critical information in the dataset. The new components are known as principal components (PCs) and are developed as collections of variables in the initial set of data. PCs (shown in this thesis as “factors” or “F”s) are obtained by linear transformation of data into correlation matrices or eigenvectors of covariance, with the biplots graphically showing the variability in the data. The first new variable is known as PC1 (also known as F1), and is the component or vector or dimension that comprises the most variance in the dataset; the following PCs or Fs explain the next highest levels of variation, designated as F2 and F3 in decreasing order of importance [486]. Correlation coefficient is represented as R for a sample statistic and that R^2 is the amount of variability explained by a particular variable. Correlation coefficients are used to assess the direction and strength of the linear relationships among pairs of variables [487]. The loading coefficients > 0.5 were considered strong relationships in this research. All data in the PCA studies were organized for PCA by means of the R programming language within the Jamovi software.

PCA findings are interpreted in terms of angles either between variables or between variables and PCA dimensions. Angles ranging from less than 45 degrees (highly acute) or greater than 135 degrees (highly obtuse) are interpreted as indicating larger positive or negative correlations.

As part of the analysis, an assumption regarding sphericity needs to be examined. Sphericity essentially checks that the variables in the dataset are correlated with each other so that they can potentially be summarized with a smaller set of factors. Bartlett's analysis for sphericity tests whether the detected correlation matrix differs significantly from a zero-correlation matrix. So, if Bartlett's test is significant, this shows that the observed correlation matrix is significantly different from the Null hypothesis that the variables are not correlated. Regardless of treatment group, all the animal data were included for the PCA. A few terms require definition, in advance of reporting PCA findings. The term “com” in PCA tables and plots, indicates the number of overlapping spots or sites of transcript expression for two factors, such as S100 plus P75 or P75 plus Sema3A. The term “S&S” stands for the number of overlapping spots of mRNA expression for Sema3A and S100B. The term “All3 com” indicates the number of overlapping spots of mRNA expression for Sema3A, S100B and P75NGFR altogether, in ISH experiments. All the data for every animal in the experiments, regardless of treatment group, were included in the P75 PCA run for the limited number of samples that were available for study by in situ hybridization (N=20).

2.5 Results

The purpose of this research was to advance our understanding of the processes and time period of muscle repair and reinnervation, including dependence on SC-derived Sema3A during those processes that must occur on newly repaired myofibers to enable them to function and work by voluntary contraction. This exploration was conducted using two models of injury including CTX injection and muscle crush.

2.5.1 Expression of mRNA transcripts and cell localization

As a first step in understanding the potential differences in gene expression among different treatments after muscle injury by crush or cardiotoxin, the level of expression of each transcript (mRNAs of Sema3A, S100B, and P75NGFR) was assessed in each image by counting the number,

the overall intensity (areal density), and the size (diameter) of expression sites per 40X field containing NMJ regions.

2.5.2 Observations from *in situ* hybridization experiments

Observations under fluorescence (often with the aid of differential interference contrast, DIC), showed that sections serial to those previously identified from histology studies (Chapter 2) as containing a region of one or more NMJs, also displayed one or more cells expressing one or more transcript of interest. DAPI staining of nuclei helped identify the general density of individual cells and often their alignment or collection (e.g., in myotubes or at NMJ regions). DAPI staining also enabled the confirmation of muscle fibers as regenerated (i.e., centrally nucleated myotubes) or not (i.e., all nuclei at the fiber periphery). Images were captured at 400X from 10 fields of myotubes per section (1 section per muscle per mouse).

Representative images (Figure 6) show the range of variation in the number of expression sites per field, the intensity (areal density) of staining representing expression in that field of muscle tissue, and the size (diameter) of expression sites.

A single cell could contain one “dot” or punctum of fluorescence ranging from a clear although modestly fluorescent spot, to an intensely bright fluorescent dot. These dots are termed sites of expression, where transcripts of interest are located inside cells, in the following descriptions of results per field. The number of dots per field ranged widely across a given field, and was assessed over 10 imaged fields per section.

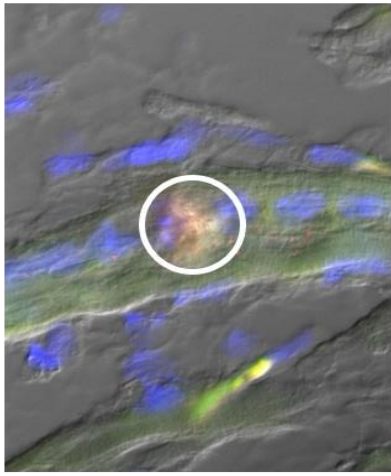
In addition, there was a very wide distribution of brightness of their intensity also ranged widely among and within sections. This variability was related to the histological region that was imaged, and the number of NMJs in a particular field, as well as the architecture of NMJs and other cells in the particular field and section. The overall distribution was measured as the intensity (meaning “areal density”) of expression.

The third parameter, the diameter of expression sites, was evaluated as sites ranged from small puncta to collections of puncta, to much larger areas that sometimes appeared to fill entire cells. The size of the expression site relates to the extent of expression by the population of cells in a tissue, and the size range can show the evenness (homogeneity vs. heterogeneity) of expression

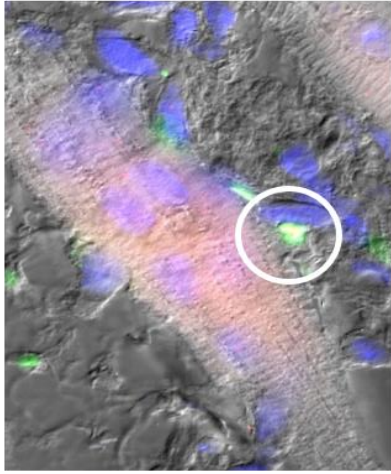
levels by one or more cell type (if they are identifiable), as an assessment of the cellular level of expression activity.

The findings related to ISH/ICC assay on disrupted myofibers and myotubes from days 6 to 10 in muscles regenerating from cardiotoxin (CTX) or crush (CR) injury in untreated mice (CTX and CR) and mice pretreated with isosorbide dinitrate (ISDN) 2 days before injuries showed more sites with colocalized staining for Sema3A and S100B RNAs and P75NGFR protein at TSCs in CTX samples than in CR muscles with or without pretreatment at the same time points. While levels of P75NGFR protein and Sema3A and S100B mRNAs appeared subjectively to increase over time post-injury, the fluorescent signals appeared greater in samples without pretreatment in both CTX and CR groups (Figure 6).

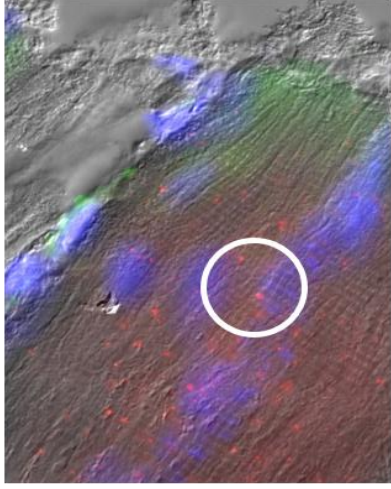
A.



CTX- / D6

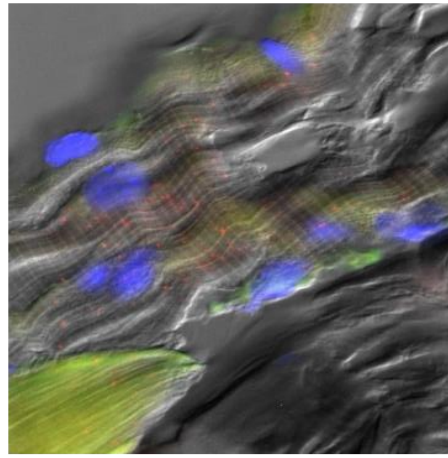


CR- / D8



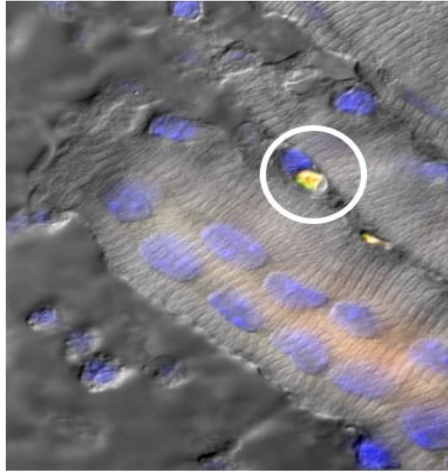
CR- / D10

B.



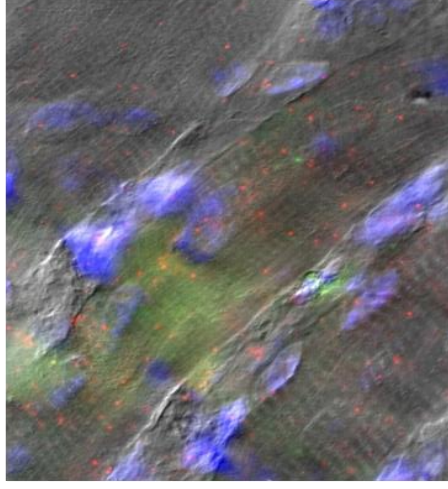
CTX+ / D6

D.



CR+ / D8

F.



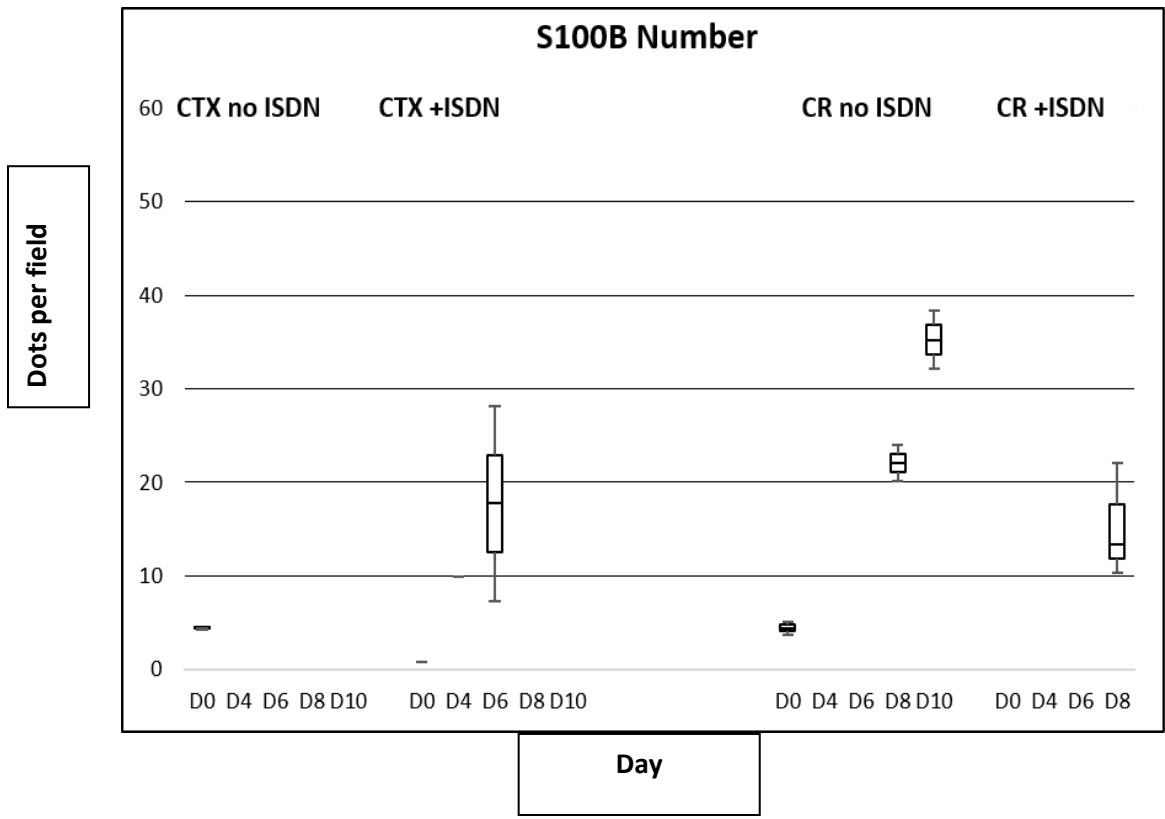
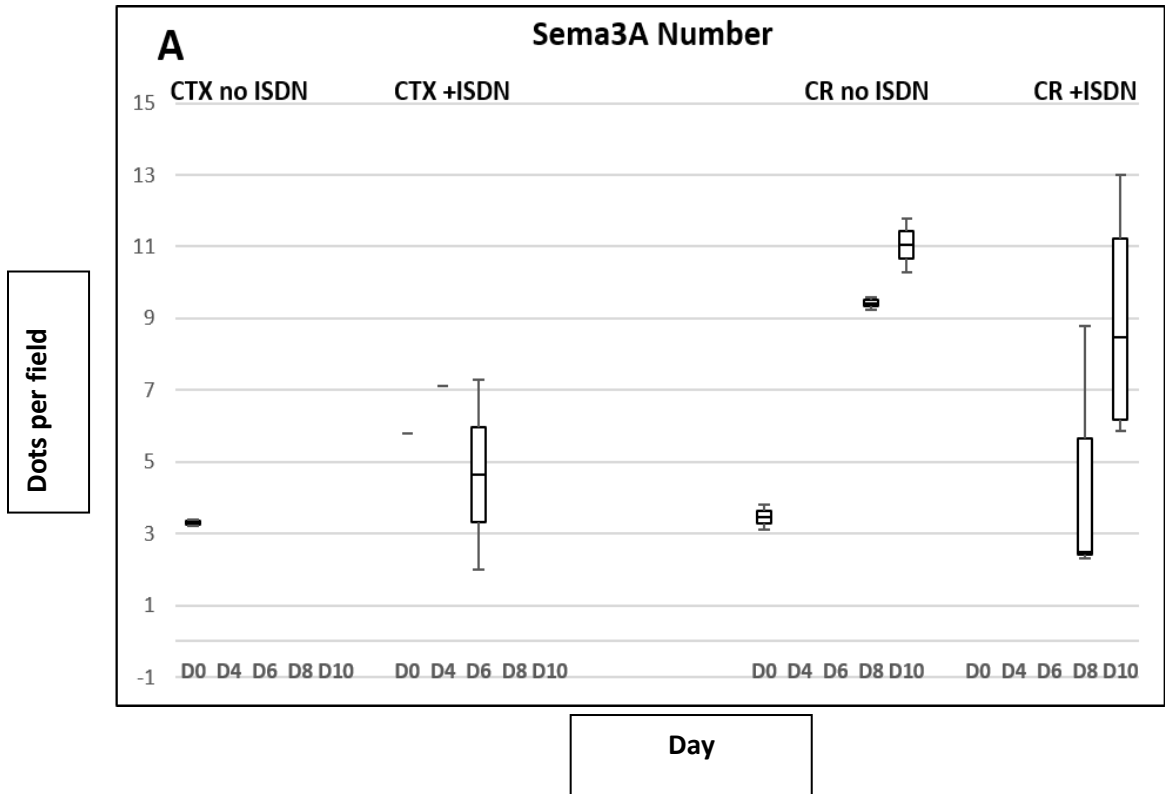
CR+ / D10

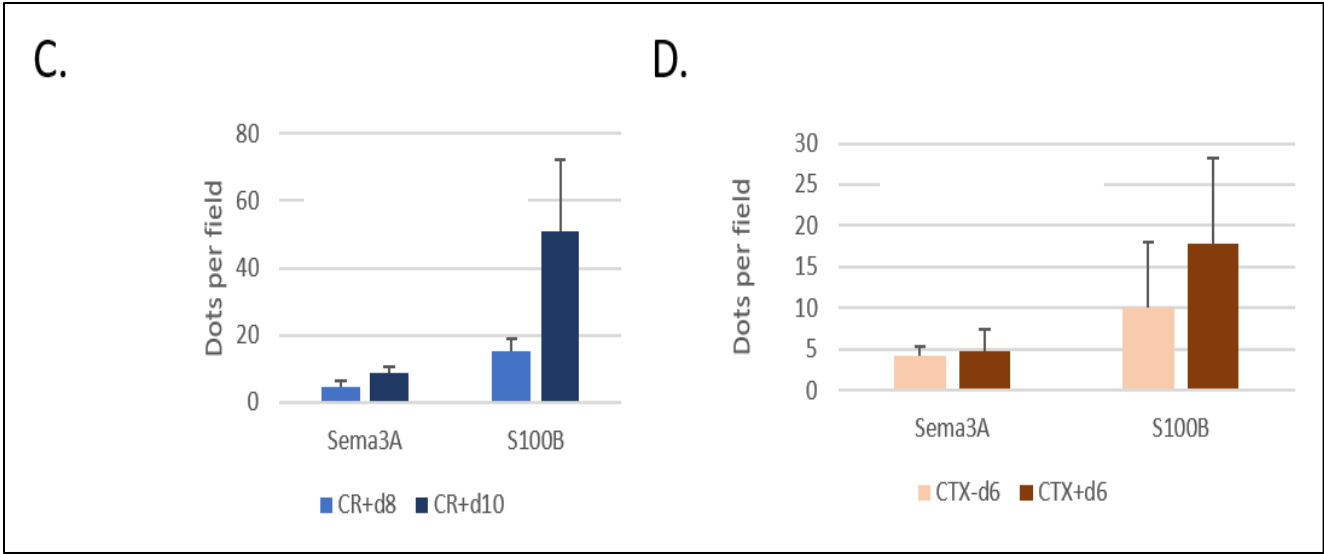
Figure 6. Combined fluorescent ISH/ICC. To determine the cellular origin of Sema3A (green) and S100B (red) mRNA expression and P75 (white) protein in the TA muscle at different time points after cardiotoxin (CTX) and muscle-crush (CR) injury. A combined fluorescent *in situ* hybridization and immunostaining method was used. A. shows the Sema3A (green) and S100B (red) mRNA expression in CTX- at day 6 post injury. B. shows the colocalization of Sema3A (green) and S100B (red) RNA expression and P75 (white) protein in TSCs in CTX+ at day (D) 6 post injury (white circle). C. shows the Sema3A (green) mRNA expression in SCs in CR- at D8 post injury (white circle). D. illustrates the colocalization of Sema3A (green) mRNA expression and P75 (white) protein in SCs in CR+ at D8 post-injury (white circle). E and F. show the S100B (Red) mRNA expression in CR+/- at D10 post-injury in Schwann cells. CTX+ and CR+ indicate groups that were pretreated with ISDN; “CTX-” and “CR-” indicate groups that were not pretreated. Original magnification by oil immersion X40 objective lens.

2.5.3 Number of mRNA expression sites

Box-whisker plots of the number of mRNA expression sites per field as a function of regeneration time after CTX and CR injury with or without ISDN pretreatment (n=4 male mice per group) are shown in Fig. 7. A.

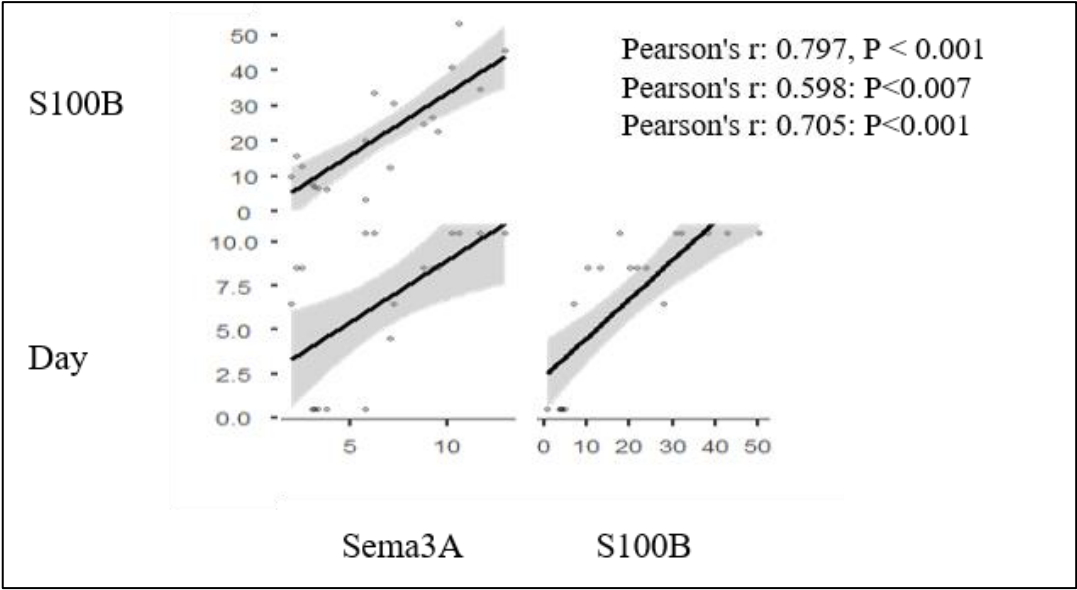
Crush-injured muscles without pre-treatment, displayed a higher number of S100B mRNA expression sites per field at day 10 than day 8 (t-test, $p < 0.05$, Fig. 7. A). There was no significant effect of regeneration from CTX, either with or without pretreatment, in the number of expression sites for S100B or Sema3A at those time points post-surgery. The number of Sema3A and S100B expression sites per field was each positively correlated with regeneration time (Pearson's $r = 0.598$: $P < 0.007$ and Pearson's $r = 0.705$: $P < 0.001$, respectively). Also, the number of S100B mRNA expression sites per field was positively correlated with the number of Sema3A mRNA expression sites (Pearson's $r = 0.797$, $P < 0.001$, Fig. 7. B). Asterisks (*) indicate significant difference (t-test, $p < 0.05$) from untreated group at the same time point.





Type of injury

Independent variables



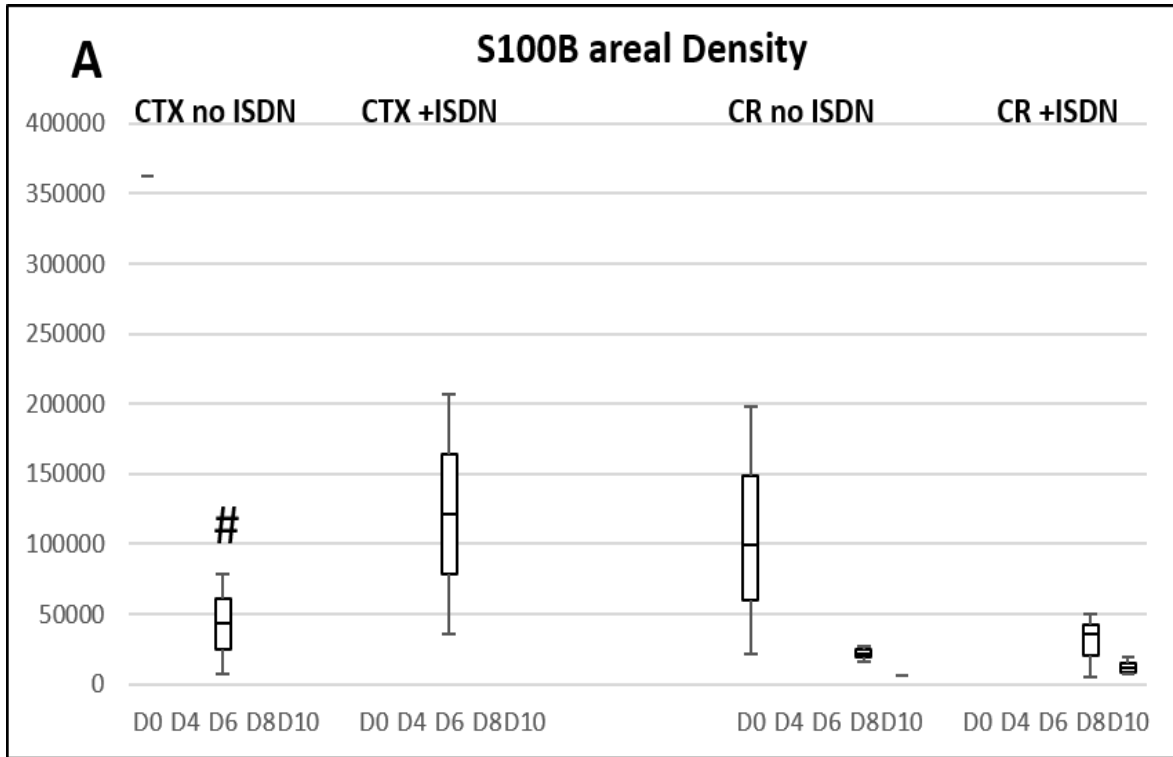
Dependent variables

Figure 7. Number of expression sites. A. Number of staining sites for DAPI, Sema3A, and S100B for CR (blue) and CTX-injured (orange) muscles over time, in mice after ISDN pretreatment or not (none). B. Linear regressions of the number of mRNA expression sites showed positive correlations of S100B and Sema3A with regeneration time (Pearson's $r = 0.598$; $P < 0.007$ and Pearson's $r = 0.705$; $P < 0.001$, respectively), and between S100B and Sema3A (Pearson's $r = 0.797$, $P < 0.001$). C. Crush-injured muscles with pre-treatment, displayed a higher number of S100B mRNA expression sites at day 10 than day 8 D. The results did not show any significant effect of regeneration from CTX, either with or without pretreatment, in the number of expression sites for S100B or Sema3A at those time points post-surgery.

2.5.4 Intensity (areal density) of mRNA expression sites

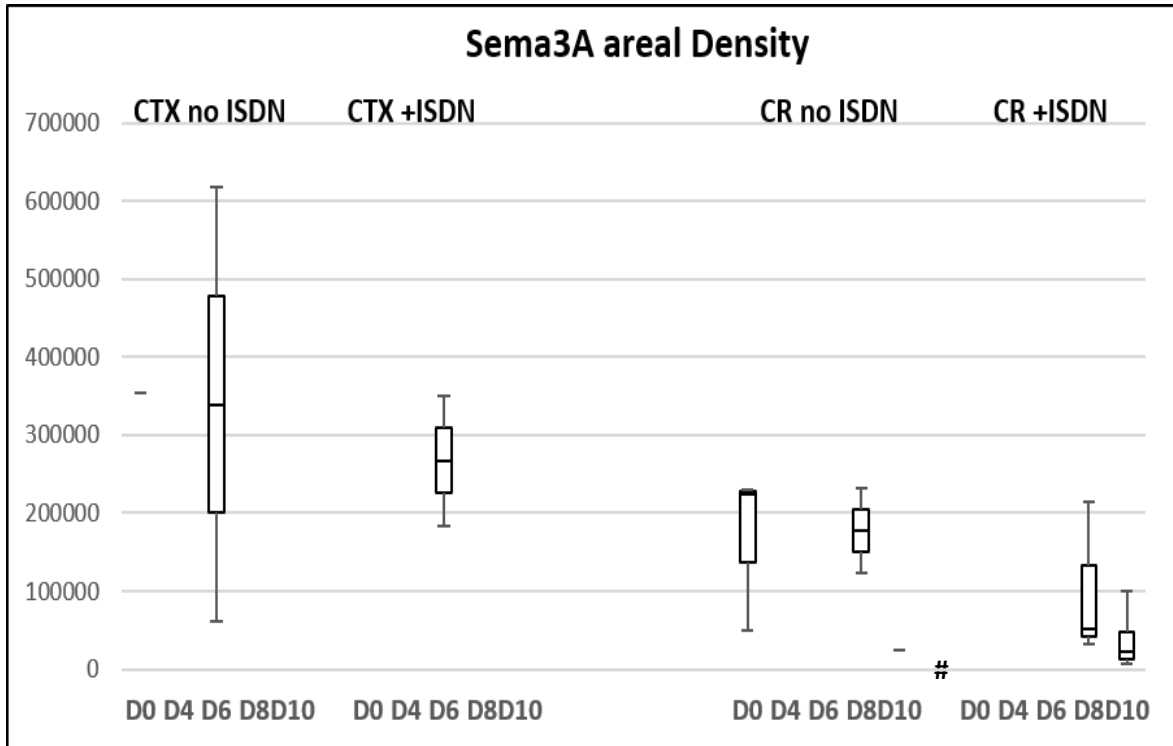
Results for the intensity of the expression sites showed that pre-treatment increased the intensity of S100B mRNA expression sites also increased after CR injury, occurring during day 8 to 10, although the increase was smaller than after Sema3A mRNA expression sites at comparable time points. However, by day 10 after CR, myotube diameter remained smaller in muscle. In addition, in untreated CTX-injured muscles, the intensity of S100B mRNA expression sites was lower at day 6 compared to day 0 (Tukey's, $df = 10$, $p = 0.044$) (Figure 8. A). The intensity of S100B mRNA regions was negatively correlated with time and decreased with increasing time (Pearson's $r = -0.649$, $P < 0.004$). However, regression analysis between the intensity of Sema3A and S100B RNA regions and time did not reveal significant correlations (Fig. 8. A. B).

Region: Areal Density (Mean)



Day

Region: Areal Density (Mean)

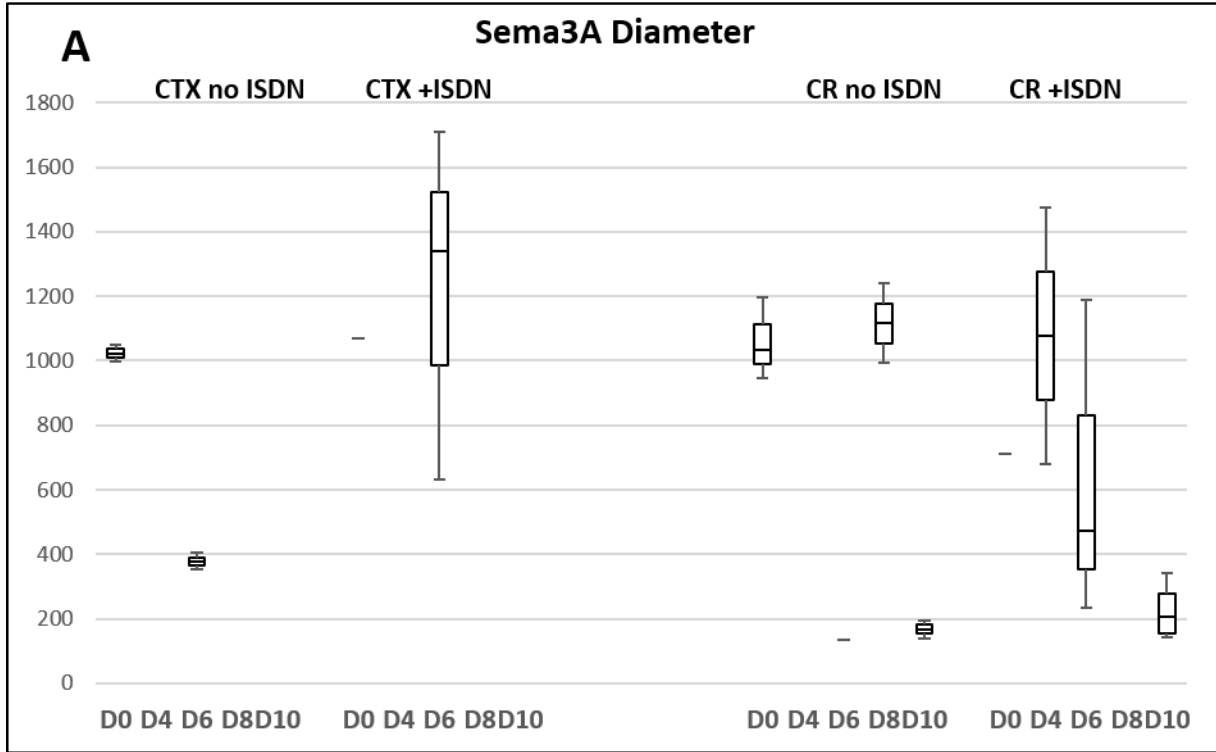


Day

2.5.5 Diameter of mRNA expression sites

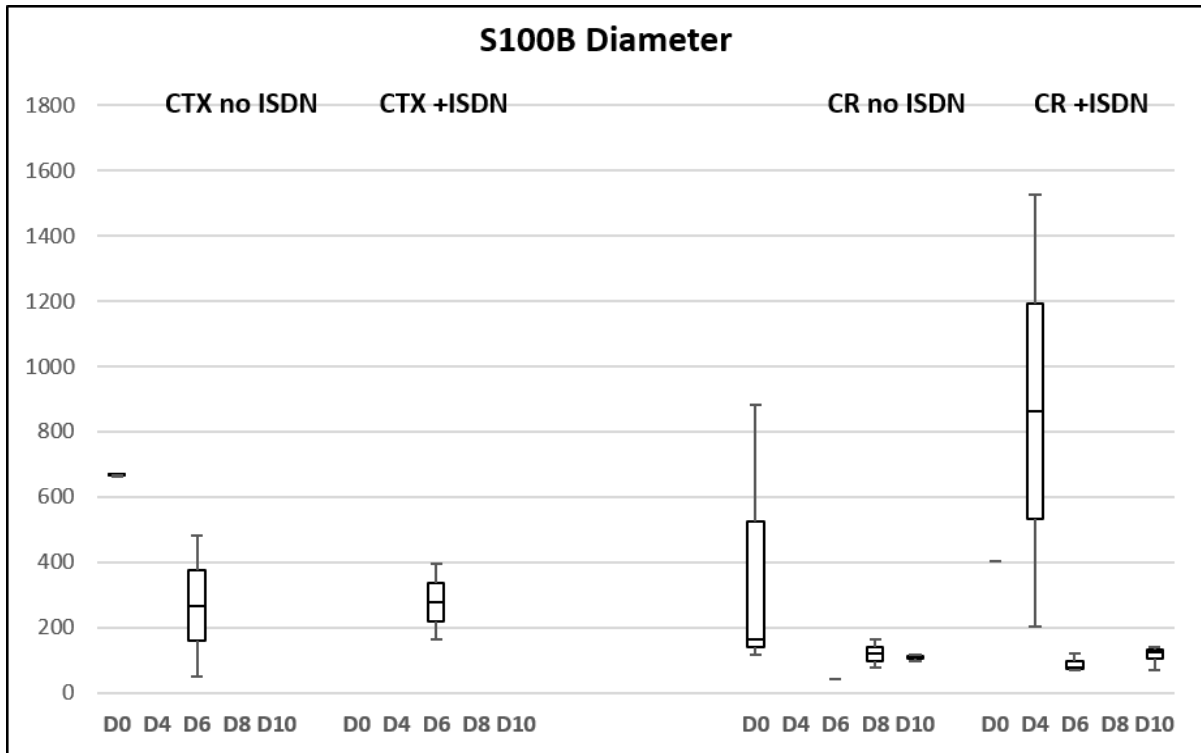
The diameter of S100B mRNA expression sites was significantly affected by regeneration time and showed an increase after CR injury with pre-treatment, occurring between days 8 and 10 (t-test, $p < 0.05$, Fig. 9. C). The diameter of Sema3A mRNA expression sites was significantly affected by a day*treatment interaction (Anova, $p < 0.041$) and decreased at day 10 compared to day 8 in CR injury with pre-treatment. Also, pretreatment before CTX injury increased the diameter of Sema3A mRNA expression sites at day 6 compared to the CTX-injured group without pretreatment. Also, the diameter of S100B and Sema3A mRNA expression sites were negatively correlated with time and decreased with increasing time (Pearson's $r = -0.475$, $P < 0.017$ and Pearson's $r = -0.530$, $P < 0.005$, respectively). The slopes of linear regression lines and the R^2 suggested that 56% of the variation is explained in this correlation ($R^2 = 0.568$, $F = 3.19$, $p = 0.024$).

Region: Diameter (area %)



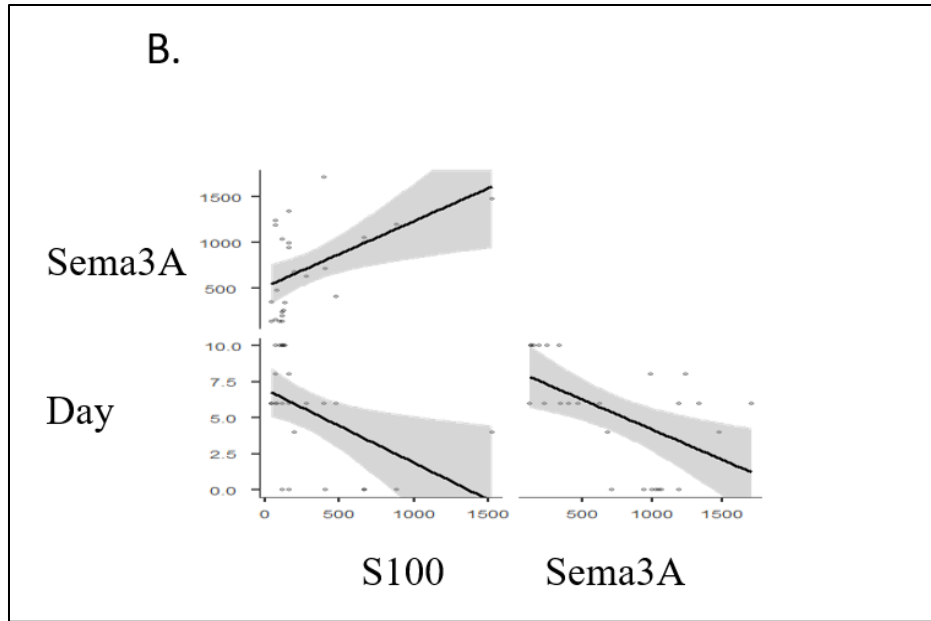
Day

Region: Diameter (area %)



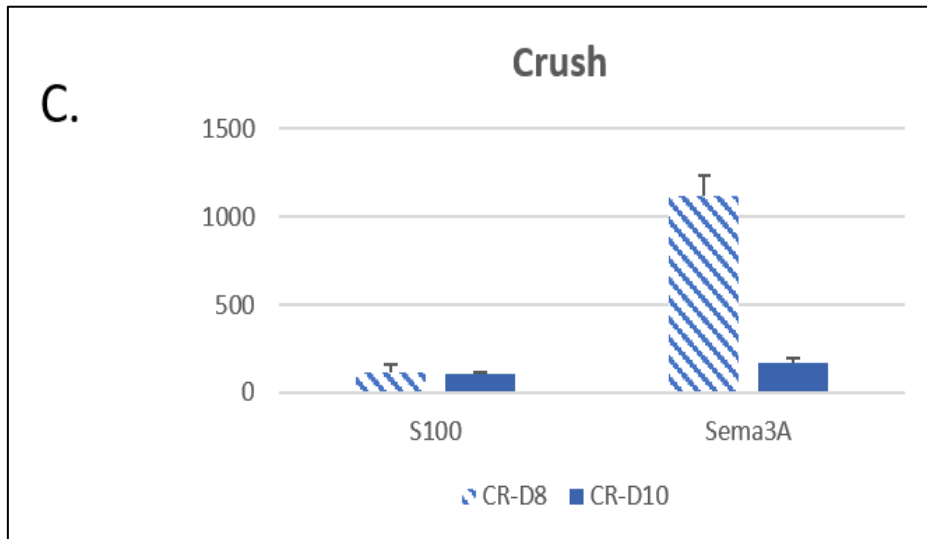
Day

Independent variables



Dependent variables

Region: Diameter (area %)



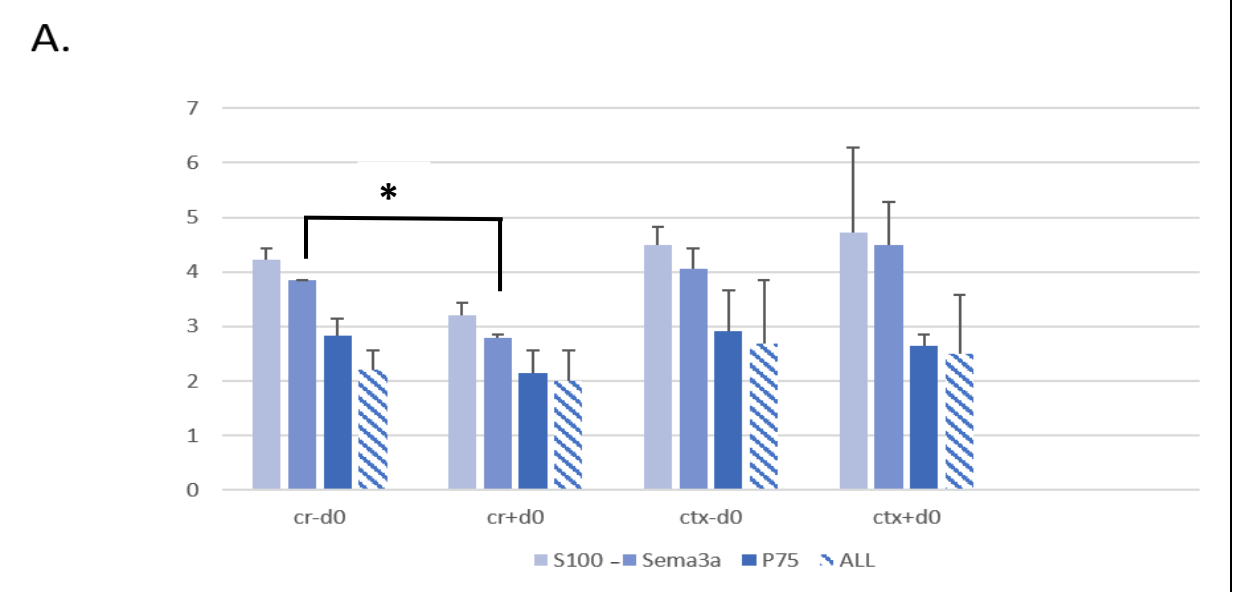
Day

Figure 9. Diameter of mRNA expression sites. (N=20 animals in the ISH staining experiments) on samples collected after crush (CR) or cardiotoxin (CTX) injury. A. In CTX injury after pretreatment, the diameter of Sema3A mRNA expression sites was higher at D6 vs. the CTX-injured group without pretreatment (similar to expression intensity and western blot findings) B. The diameter of expression sites for both S100 and Sema3A mRNA was negatively correlated with time (day post-CR injury) in animals that received ISDN pretreatment. C. The diameter of Sema3A mRNA expression sites decreased from D8 to D10 during recovery from CR injury (1-way Anova, $p=0.041$).

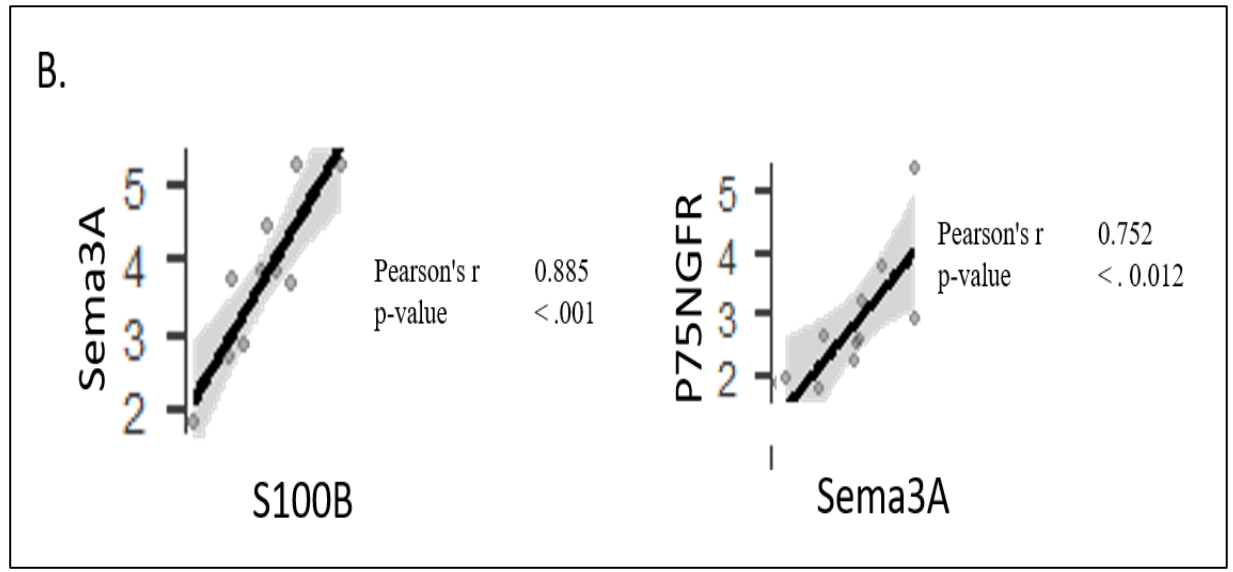
2.5.6 P75 by Immunostaining in combination with ISH

TSCs were identified through the colocalization of the expression of S100B and Sema3A transcripts plus P75NGFR protein, while the cells with the expression of S100B and Sema3A were reported as non-terminal Schwann cells in the presynaptic area. Cells containing only Sema3A expression (i.e., in the absence of S100B expression) in conjunction with P75NGFR protein (detected by immunostaining) were recognized as SCs in muscles at the postsynaptic area. The slope of the linear regression line, significantly different from zero, indicated that with increasing S100B, the level of Sema3A protein also increased. As well, an increase in the number of Sema3A expression sites was accompanied by an increase in the number of P75 expressing cells. Pretreatment to induce premature SC activation before CTX injury increased the level of P75NGFR protein at day 4 after CTX injury, while without pretreatment, the level of P75NGFR was significantly reduced at day 6 post-injury. Pretreatment before CR injury decreased the expression of both S100B and Sema3A transcripts compared to the group without pretreatment, at both day 0 and day 10 (t-test, $p<0.05$, Fig. 10. B) (Table 2).

Dots per field



Independent variables



Dependent variables

Figure 10. Combined assay by in situ hybridization and immunohistochemistry (ISH/ICC assay). A. Colocalization of the expression of S100B and Sema3A (by ISH) and P75NGFR (by immunofluorescence). The ISH/ICC assay was conducted on disrupted myofibers and myotubes at days 0, 6, 8 and 10 in muscles regenerating from cardiotoxin (CTX) or crush (CR) injury in both untreated mice (CTX and CR) and mice pretreated with isosorbide dinitrate (ISDN) 2 days before injury (n=20 mice). The number of Sema3A expression sites was significantly affected by treatment and showed an increase after CR injury at D0 without treatment in comparison to D0 with treatment. B. The slopes of linear regression lines indicated that with increasing S100B, the number of Sema3A expression sites also increased (Pearson's r : 0.885; $p < 0.001$). An increasing number of Sema3A expression sites was also related to increases in the number of P75NGFR expression sites (Pearson's r : 0.752; $p < 0.01$).

Table 2. A summary of statistical comparisons for assays of protein (A) and transcript expression (B) by Western blotting and in situ hybridization assays, respectively.

A Western blotting	Experiments	
	CTX+ vs. CTX-	CR+ vs. CR-
Sema3A protein	↑ D8# ↑ D10#	↑ D0#
γAchR protein	↔	↓ D4# ↓ D8#
S100B protein	↑ D0# ↑ D10#	↑ D6#

B. ISH/ICC	Experiments	
	CTX+ vs. CTX-	CR+ vs. CR-
Sema3A mRNA		
number	↔	↔
intensity	↔	↔
diameter	↔	↔
S100B mRNA		
number	↔	↑ D10#
intensity	↔	↔
diameter	↔	↔
#COLOC P75 (number of TSCs)	↔	↔

Table 2 legend, continued. “CTX+” and “CR+” indicate groups that were pretreated with ISDN; “CTX-” and “CR-” indicate groups that were not pretreated. “M-crush” indicates the group that received muscle-crush injury. “D” indicates day post-injury (D0, 4, 6, and 10). “↔” indicates no significant finding. “COLOC P75” indicates the number of overlapping areas with the RNA expression of S100B, Sema3A and P75NGFR in TSCs. # indicates significant effect (1-way Anova) and pairwise comparison (Tukey’s test) between an indicated pretreatment or transgenic group and its respective control (no pretreatment or non-knockout transgenic group) at a particular day (D) post-injury. Symbols for increase (↑) or decrease (↓) accompany the indication of significance.

2.5.7 Principal Component Analysis (PCA)

The preliminary studies of gene-transcript expression using fluorescence ISH and ISH/ICC staining on crush- or CTX-injured muscles (the same tissues as analyzed in Chapter 2) were also analyzed using PCA which included data generated from ISH staining (P75NGFR, S100B, and Sema3A mRNA expression) and variables for the combined ISH/ICC staining experiments (Fig. 11, Table 3). This PCA was run to examine the localization of P75NGFR expression in TSCs (P75NGFR, S100B and Sema3A) and study the relationships among variables collected from those particular samples that were available.

As shown in Table 3, PCA results showed that the strongest correlations of variables were S100B (loading of 0.987), and S100B diameter (loading of 0.803). F1 in PCA3 represented the levels of S&S com and All3 com. F1 alone, accounted for 55.3% of the total variance in the dataset. F2 represented Sema3A number, intensity and diameter of expression sites, and the S100B intensity and diameter of expression sites. F2 accounted for 19.1% of the total variance. Therefore, these two newly defined dimensions together, accounted for 74.41% of the total variance in the dataset. Bartlett’s test of sphericity had a probability of $p < 0.05$.

In the PCA, the increase in the combined expression for “All3 com” transcripts (Sema3A, S100B and P75) is reflected in an increase in each of the S100, Sema3A and P75 variables, while the All3 com variable decreases with the number of S100B expression sites. Examining the relationships among variables in the PCA S100B & P75 com (loading of 0.987), and S100 diameter

(loading of 0.803) in the PCA run on the limited dataset available for these experiments on crush vs. CTX injury, with or without preactivation of SCs (Table 3).

The correlation circle for the PCA helps interpret the numerous correlations among the many variables and with each of the principal components (Fs, or factors); the greater the value of a correlation, the greater the link with the corresponding dimensions of a PCA (Figure 11). In the P75 PCA, Bartlett's test was significant ($p < 0.05$).

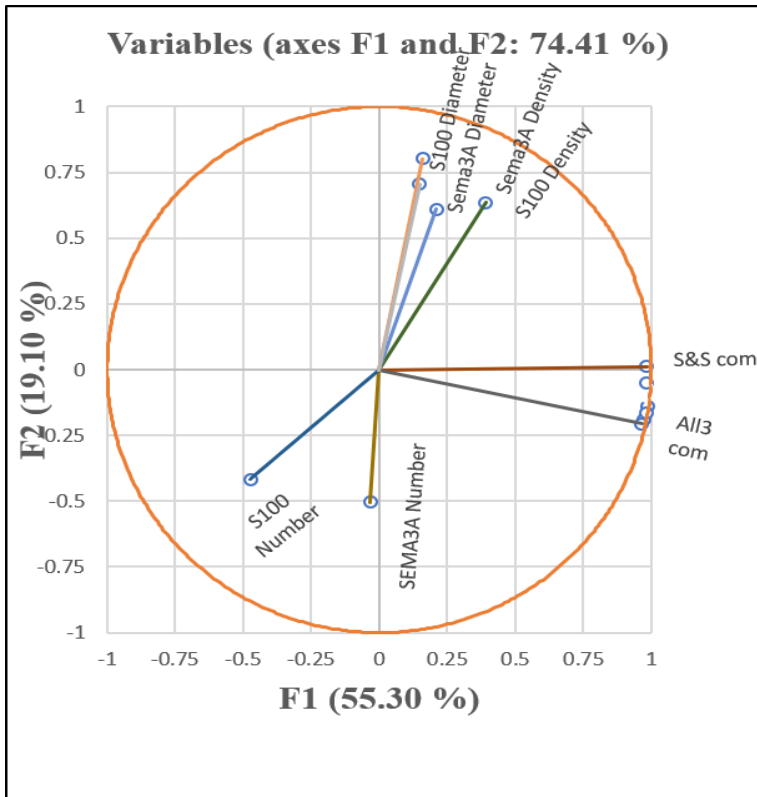


Figure 11. Principal component analysis correlation circle. The PCA correlation circle has 2 dimensions or principal components (also called Factors, Fs) to visualize PCA statistical findings from all variables together (here, ISH and ISH/IHC variables). Vectors (direction and length) represent the coefficients of each of variable with the two factors as orthogonal axes. The endpoint of each vector overlies a position on the x-y grid and represents the loading (or correlation) score of the collected data for that variable (including all control, treatment and injury groups) on each of the two Factors in the PCA plot. When a variable has a short vector length on both F1 (x-axis) and F2 (y-axis) dimensions, the data in that variable are likely better represented on other PCAs dimensions. Variable labels on the vectors are abbreviated as follows: “S&S com” indicates the number of overlapping spots for Sema3A and S100B; and “All3 com” indicates the number of overlapping spots for Sema3A, S100B and P75NGFR.

Table 3. Loading of variables on PCA Factors. Table shows correlation coefficients for the variables (N = 8) loaded on the dimensions of 2 Factors (F1 and F2) as extracted from the analysis of data from muscle-crush injury and CTX injection (N=20 samples). In the row for each variable, numbers show the strength of correlation of that variable with the eigenvector of each F. When the absolute value of correlation coefficients was 0.5, they were considered important (bold font) in identifying that F.

Table 3	F1	F2
S&S com	0.982	0.012
All3 com	0.965	-0.206
Sema3A number	-0.034	-0.503
S100B number	-0.473	-0.417
S100B intensity	0.392	0.635
Sema3A intensity	0.210	0.610
S100B diameter	0.160	0.803
Sema3A diameter	0.149	0.705

2.6 Discussion

The hypothesis for experiments in this chapter was that premature SC activation by a NO-donor drug (ISDN), 2 days before crush or CTX injury would alter the timing of regeneration and Sema3A production, and thus interfere in the establishment of NMJs in regenerating muscle. PCAs were conducted with the aim of combining results of numerous assays on many variables; PCA findings clearly suggested that Sema3A, S100B and P75NGFR are key factors in muscle tissue during both muscle and nerve regeneration after muscle injury.

PCA was run to examine the localization of P75NFR expression in TSCs (P75NFR, S100B and Sema3A) and study the relationships among variables on the limited dataset available for these experiments on crush vs. CTX injury, with or without preactivation of SCs. “All3 com” indicates the number of overlapping spots for Sema3A, S100B and P75NFR and an increase in the combined expression for “All3 com” transcripts, reflected the increase in the mRNA expression of the Sema3A, S100B and P75 variables. The results of ISH/ICC assay also showed that levels of P75NFR protein and Sema3A and S100B mRNAs increased over time in samples without pretreatment in both CTX and CR groups. Moreover, a higher number of S100B mRNA expression sites as well as a decrease in the diameter of Sema3A mRNA expression, smaller myotube diameter and lower expression of Sema3A-65 protein in crush-injured muscles without pre-treatment at day 10 post injury suggest that day 10 is the time when the Wallerian degeneration process ends and initial step of the reinnervation process through the Schwann cell tubes begins. Schwann cells are main mediators in prompting many of the procedures in Wallerian degeneration and changes in expression of their protein at the injury site are crucial to axon regeneration. Schwann cells remove debris through phagocytosis and work to recruit and attract macrophages to the site of nerve injury. Macrophages themselves generate factors that further help Schwann cell proliferation alter. After the removal of myelin debris, the Schwann cells proliferate on the endoneurial tubes which are hollow tube that provide a path for the regenerating axon to regrow [317, 475, 488].

Our finding in chapter 2 showed that the expression of Sema3A-65 protein was lower at day 10 than at day 0 in CR-injured muscles without pretreatment, while the number of mRNA expression sites showed positive correlations of S100B and Sema3A with regeneration time and between S100B and Sema3A which could show that the increase in the expression of Sema3A belonged to TSCs. Induced remodeling of NMJ connections in gastrocnemius muscles which is accompanied by an increase in the expression of Sema3A in TSCs of type IIb/x myofibers. These results revealed that TSCs not only maintain the growth of nerve terminal, but also confine the plasticity of nerve terminal at specific NMJs by releasing a chemorepulsive protein [489].

A coordinated maturation of synapse relies on complex molecular interactions that contain synaptogenic factors from nerve terminals, TSCs and myofibers. TSCs produce and release synaptogenic factors and their own maturation is moderated by pre- and postsynaptic components

[475]. A study showed that the Schwann cells may promote to postsynaptic differentiation by expressing NRG2, which appears to promote the transcription of AchR as well [490]

The assay of P75NGFR was novel for TSC studies, and offers the value of exploring [475] additional proteins that may act as regulators in the deposition and extension of growth cones and the maturation of pre-synaptic and/or post-synaptic areas. While previous findings showed that NO treatment promoted the formation and growth of new myofibers, apparently involving earlier production of Sema3A after CR injury (at D0) and later after CTX injury (D8 and D10) [391], it is not known whether a direct increase in Sema3A would have the same effect on muscle regeneration. However, it is clear from the results of this chapter that premature activation of muscle satellite cells before injury, either by muscle crush or cardiotoxin injury, does interfere with the re-establishment of fiber innervation (NMJ formation) during myotube regeneration. It is also evident from the PCA study of gene expression, that changes in proteins extracted from homogenates of regenerating muscle after both types of injury, were significantly related to changes in gene expression by muscle SCs and also by other types of cell that are in close proximity to NMJ regions on new myotubes. Nonetheless, the detailed timing of reinnervation in relation to the time-course of myofiber regeneration from injury at the cellular level, is still not fully understood.

The results of statistical analysis by PCA prompt several considerations, while being interesting, the interpretation of these complex PCs (each comprising multiple variables) is difficult. The challenge to interpretation arises despite finding that the PCs explained a significant majority of the variance in each dataset that was examined. As a descriptive method, however, PCA is useful for classifying groups of variables and for developing hypotheses for further studies. PCA is also useful in depicting the main variations in a complex dataset using graphical representation of eigenvectors. By finding the most statistically meaningful variables and the important factors that underlie most of the variability in the datasets, our results will now be useful in helping design and analyze future experiments. Although one needs to be cautious in interpreting mathematically extracted components that don't necessarily possess significant biological meaning, it is frequently possible to interpret the composition of the principal components that are determined by PCA.

Genetic and molecular studies in mice and other animal models have thus far, elucidated the current understanding of mechanisms in niche environments of stem/precursor cells during the regeneration of skeletal muscle [491]. For years, there was a controversy as to whether Schwann cells or axons lead the movement of growth cones to their target muscles in the neuromuscular system. Neuregulins and their specific receptors, members of the ErbB family of tyrosine kinases, have been implicated in the control of growth and development of Schwann cells, specialized cells that wrap around nerve axons to provide electrical insulation and physical protection. Development of ErbB3-mutant mice showed an important role for Schwann cells in maintaining axons in the early postnatal stages for mice [492]. Schwann cells undergo mitosis during early development, muscle reinnervation, and nerve sprouting after denervation. While muscle denervation stimulates Schwann cell proliferation, this stimulus is only effective when the Schwann cells actually make contact with axons. More recent research indicates that TSCs extend their processes after both complete and partial denervation and appear to guide the growth of axons during reinnervation and sprouting. As such, TSCs therefore have a key role in the maintenance of structure, function and remodeling of NMJs as well as in development of NMJs in embryogenesis [315].

The above literature suggests that the dynamic relationship among TSCs and motor nerve terminals during development, sprouting and reinnervation may help to generate stronger, larger and more stable NMJs. Thus, it is important to detect those guidance molecules used by TSCs in order to understand the mechanisms of this under-explored system of communication in the nervous and neuromuscular systems.

The application of new techniques such as TSC ablation *in vivo* and transgenic technology to engineer cell-specific markers that can be tracked during a process, has advanced these inquiries [493]. Examples of promising approaches to testing the vital roles of TSCs include: creating mice that express fluorescent reporters such as GFP in TSCs [494] and axons, knockout mice lacking the expression of important molecules associated with the formation and maintenance of NMJs [236], and screening zebrafish mutants for those that show deficiencies in NMJs [495]. The later studies showed that during nerve regeneration, the sprouts of TSCs induce and guide motor neurite terminals, and promote aggregation of post-synaptic AchRs, through production of both agrin and neuregulin. It is not known whether Sema3A produced by one or both of TSCs and SCs, are

mechanistically involved in regulating the maturation of AchR subunits at newly restored NMJ regions in regenerating skeletal muscle.

After axonal injury, Schwann cells participate in Wallerian degeneration and re-express several genes that are initially expressed during embryonic development. This alteration in gene expression leads to phenotypic changes and dedifferentiation in Schwann cells, and transforms them from differentiated into premature Schwann cells. The so-called dedifferentiation process affecting Schwann cells accompanies the appearance of axonal degeneration after a peripheral nerve injury. Schwann cell dedifferentiation is illustrated by a downregulation in the expression of myelin genes and upregulation of others that demonstrate prematurity in Schwann cells during Wallerian degeneration. For instance, p75NGFR increases in Schwann cells after nerve injury [496] and this stimulation is essential for the re-myelination of regenerating axons. Any axonal damage results in the induction of P75NGFR expression in Schwann cells which is then downregulated after axonal regrowth [497, 498]. Furthermore, an older study showed that the level of P75NGFR is upregulated in mature, intact superior cervical ganglion cells (sensory neurons) when they are stimulated to sprout by axonal injury of the contralateral neurons [499]. Therefore, the level of P75NGFR expression in neurons, both motor and sensory, and also in TSCs, is highly responsive to insults in the neuromuscular and nervous systems. The details of this responsiveness are fascinating. Upregulation of P75NGFR is detected in Schwann cells in the distal nerve stump, 36 hrs after nerve transection [500]. Such upregulation of P75NGFR can be used as an indicator of Schwann cell sensitivity to the injury [501].

Future research could extend the current findings by specifically exploring other aspects of NMJ reformation including more detailed timing of denervation/reinnervation, inflammation, the effect of Wallerian degeneration and SC-niche remodeling while examining features such as the RNA and protein levels of TSC and SC markers at different time points post-injury.

More studies are also needed to investigate the interaction of Sema3A (from SCs and other sources) and S100B (from TSCs) in reestablishment of motor and sensory innervation in muscle and awaits careful injury experiments that can disturb the source or level of Sema3A expression in a genetic or disease model to investigate the role of different NMJ compartments on pre- and post-synaptic regions [41, 160] and myofiber typing [228, 397, 420].

3 RESULTS-3

Suppressing Sema3A expression in SCs: is this a good strategy for promoting reinnervation and muscle regeneration?

3.1 Abstract

To extend knowledge about Sema3A expression in satellite cells (SCs) and NMJ reformation, the denervation and reinnervation processes were investigated during recovery from two different injuries, muscle crush or nerve crush, on a SC-specific knockout of Sema3A at different time points post-injury. The hypothesis was that loss of SC-specific Sema3A expression would disrupt TSC gene and protein expression after both nerve and muscle injury. The expression of genes by TSCs (Sema3A, S100B, P75NGFR) and Pax7+ SCs, the level of proteins resulting from that expression (Sema3A, S100B) and γ AchR related to muscle denervation were compared between transgenics with a conditional SC-specific knockout of Sema3A expression during regeneration from injury by muscle crush or nerve crush. Two control groups were constituted: one with the same injury in non-knockout control mice and the other, and a no-surgery control of SC-specific Sema3A-knockout mice. Days 14 and 21 were chosen as time points after a nerve-crush injury to study TSCs and days 21 and 35 were selected to study TSCs after muscle-crush injury.

The ISH results displayed that the intensity of P75NGFR mRNA expression was increased in the SC-Sema3A knockout compared to the non-knockout control group at the same time point after muscle-crush injury; the increase occurred at both time points (time*injury interaction, $F(df)=16$, $P(\text{Tukey's}) < 0.001$, and < 0.001 , respectively). These findings suggest that the loss of SC-derived Sema3A caused an increase in the number of TSCs. Findings for nerve-crush injury experiments also displayed a decrease in the levels of S100B and Sema3A proteins that occurred at day 14 in the non-transgenic control, and had increased again at day 21 (Tukey's test, $P < 0.001$). These results showed that the conditional knock-down of Sema3A expression in SCs accelerated the muscle degeneration and denervation processes, seen after muscle-crush injury. Moreover, Principal Component Analysis performed on the P75 colocalization variable displayed a positive correlation between the colocalizing area representing TSCs, and the intensity of both Sema3A

and S100B expression, and shows the additional importance of variables regarding TSC markers in this study. In summary, results of this study advance our understanding of the pre-synaptic and post-synaptic interactions of TSCs and SCs in vitro and in vivo.

3.2 Introduction

During nervous system development, many types of guidance molecules govern neurite outgrowth. Members of the ephrin, netrin, slit, and semaphorin families of protein show inhibitory effects on neurite growth [305, 502]. Semaphorin proteins not only are expressed by brain tissue, but also by several nonneuronal tissues [417], where they play various roles in processes such as the regulation of inflammation and angiogenesis.

In a 2009 report, Tatsumi and colleagues reported that SCs may control or at least contribute to myofiber innervation during muscle regeneration through secretion of Semaphorin-3A (Sema3A), a member of the secreted group of semaphorins that guides axon outgrowth as well as cell growth and migration. That finding also emphasized the dynamic interaction of SCs with their niche to enable effective muscle regeneration [194]. Another study, slightly earlier and working from a neuropathology model, displayed that during postnatal development of the gastrocnemius muscle, after paralysis was induced by toxin injection, Sema3A expression by TSCs was exclusively located at the NMJs of type Iib/x (fast) myofibers. This finding of Sema3A-expressing TSCs at fast-fiber NMJs revealed that the chemorepellent Sema3A likely plays an important role in restricting anatomical plasticity, specifically at this specific group of NMJs. Moreover, the expression of Sema3A at NMJs on type Iib/x myofibers in a transgenic mouse model for ALS, suggested that Sema3A may contribute to the particular loss of the fast-type neuromuscular synapses that is detected in ALS [303].

Different elements of a synapse have been identified and tracked in previous research using marker proteins such as neurofilament protein (NF) to study nerve endings (axon terminals), S100B and P75NGFR to study TSCs, and α -bungarotoxin to elucidate the post-synaptic or muscle side of the synapses that expresses nAChRs. Expression of S100B is known to vary during TSC development, and different markers of TSCs such as P75 NGFR are used to further illustrate this phenomenon [339, 340, 503]. S100 proteins play a role in a range of processes including apoptosis, energy metabolism, as well as the regulation of inflammation, proliferation and differentiation.

These procedures are interceded through interactions with cytoskeletal subunits, target enzymes, receptors, nucleic acids and transcription factors.

S100 proteins contribute to regulating the activities of neurons, macrophages, neutrophils, myoblasts and Schwann cells, thereby participating in immune responses, tissue development and repair and tumor cell [341]. S100B is a member of calcium binding family of proteins and is identified as having A and B subunits, with only S100B being expressed by TSCs. Note that references to S100 detection or expression, depending on the methods used by researchers, may refer to S100B after specific detection, or S100 after more generic detection, and that this has introduced some confusion in the literature. Antibody to S100 (which, depending on the antibody, may detect S100B and/or S100A) stains Schwannomas, astroglomas, ependymomas and almost all kinds of malignant melanoma. Both these S100 proteins act as extracellular signals and intracellular regulators. Intracellular S100B works as a stimulator of cell migration and proliferation and an inhibitor of apoptosis and differentiation, which might have critical implications in the process of cartilage, brain and skeletal muscle development, restoration and repair. It may also play important roles in the activation of astrocytes during brain damage, cardiomyocyte restoration post-infarction and in tumor development of gliomas and melanomas.

TSCs in denervated muscle are suggested to regulate guidance of regenerating axons to the original site of the NMJ on a myofiber (see Chapter 3). A subgroup of TSCs in NMJ regions of fast, type IIb myofibers, upregulates Sema3A after muscle denervation. This shows that the micro-environment which manages these procedures differs at the single myofiber level depending on fiber type. Studies on muscle regeneration have shown the critical role of Sema3A in guiding intramuscular neuritogenesis during muscle regeneration and those and more recent findings implicate the potential that SCs and TSCs hold for cross-talk at motor nerve terminals regarding Sema3A generation for axon guidance. That work is interestingly related to literature on NMJ stabilization. It is well established that processes acting to stabilize the NMJ include a synaptic signaling system that is mediated by a so-called elimination signal that is generated by post-synaptic cells. That elimination signal in turn, triggers the retraction of some of the nerve terminals, and at the same time, a protective signal stabilizes one terminal to remain at the synaptic site [245].

One explanation for the mechanism of synapse elimination is the idea that active synapses are in opposition to, or competition with inactive synapses. A regular element of competition at CNS as well as PNS neuromuscular synapses, is that temporally correlated nerve activity reduces

or prevents competition, while uncorrelated activity triggers or increases the competition of two incoming (afferent) neurons to synapse with one post-synaptic neuron (CNS) or myofiber (PNS) [504]. While molecular cues included in this process have not been fully characterized so far, it is known that the activity-dependent alteration of BDNF mediates synaptic competition. The activity of motor neurites will cause the proteolytic alteration of pro-BDNF to mature BDNF at motor neurites [245].

Work by De Winter and colleagues [303], studied denervation effects on the expression of *Sema3A* transcripts in TSCs at the NMJs of three different populations of myofibers (postnatal, regenerative, and denervated fibers). That report showed that *Sema3A* expression is selective, as it is present in TSCs at the NMJs of type IIB/x (fast-twitch) but not at those of type I and IIA (slower twitch) myofibers in gastrocnemius muscle after denervation. Using a combination of ISH and quantitative RT-PCR techniques, that report also showed that upregulation of *Sema3A* expression in TSCs was not observed in the denervated slow muscle (soleus) that lacks type IIB/x myofibers. The observation of *Sema3A* upregulation in TSCs of only fast muscle fibers supported the finding of muscle fiber type-specific induction of *Sema3A* by denervation. While many previous reports examined the function of SCs, unfortunately, *Sema3A* expression and the highly likely possibility that TSCs respond to muscle crush injury, especially after muscle denervation, have not been examined. The contributions of TSCs in interactions at the NMJ among various types of reinnervation (during traumatic muscle injury involving nerve damage and during denervation injuries), as well as the role of TSCs in stimulating motor nerve sprouting after injury, through releasing axon guidance proteins remain to be determined.

At least 10% of axons regenerating after nerve crush injury, are able to grow successfully through atrophic nerve stumps after the Wallerian degeneration process [505]; therefore, a small but limited trophic support still lingers in the nerve stumps that remain after long-term denervation. Schwann cells can only travel for 10–20 mm to support nerve regeneration, and some will even synthesize myelin up to 16 months post denervation if they meet regenerating axons. Additional experiments revealed that the clearance of axon debris, myelin and macrophages after Wallerian degeneration induces regeneration-linked gene expression in Schwann cells and allows Schwann cell to dedifferentiate while waiting for axonal and neurite regeneration [506].

Our previous report (Chapter 2) examined the effects of pre-activating SCs before injury on: myogenesis, Sema3A production, and motor neuritogenesis compared to normal regenerating muscle without premature SC activation, assessed at different time points (days 0-10) post-injury in two models of injury (muscle crush and CTX injection). Based on findings suggesting distinct differences in time-dependent changes in NMJ restoration to regenerating myotubes between the CR and CTX muscle injuries, two models of nerve injury, direct sciatic nerve crush and intramuscular nerve damage in the tibialis anterior muscle. The popularity of the sciatic nerve-crush model injury to study nerve injury is undeniable, and likely is due to the surgical availability of this large nerve at the mid-thigh level, which triggers less inconvenience and therefore less surgical distress to the animal. Similar problems balancing muscle-specific denervation and minimal operative stress are also caused in experimental studies of facial nerve injuries, despite its well-characterized central and peripheral projections [507]. In this study, sciatic nerve was chosen as it supplies most of the lower limb muscles; the denervation and reinnervation patterns and morphological features of motor endplates could be studied in the dissected tibialis anterior and also the soleus muscle in a single nerve-crush intervention (data related to soleus muscle is not presented in this research).

Additionally, due to suggested involvement of Sema3A expression in NMJ restoration during regeneration by results reported in Chapter 2 and 3, experiments on Sema3A^{CKO} mice available through collaboration with Dr. Tatsumi at Kyushu University. Experiments were designed to investigate the effect of eliminating Sema3A production specifically by SCs, prior to muscle crush or nerve crush injury, on the terminal Schwann cells (TSCs) and SCs involved in restoration of NMJs on myofibers. The potential to identify TSCs and SCs in high-resolution, high-specificity ISH studies of transcript expression led to additional use of a probe to hybridize to P75^{NGFR} in combination with Sema3A and S100B (to represent TSCs). This was one set of ISH experiments; the second set of ISH experiments was representative of SCs using multiplex hybridization with Pax7, Sema3A, and S100B.

Finally, based on the anticipated differences in restoring nerve supply to fibers in those two models of injury, the end points of experiments on the two models were days 21 and 35 for muscle crush injury, and days 14 and 21 for nerve crush injury. As the time course of nerve degeneration, growth and myofiber reinnervation after nerve crush is not the same as the time course of muscle

regeneration and NMJ restoration after muscle crush, the time points were matched to the particular phases of regeneration/recovery [169, 271]

Some nerve injury models can involve all types of cells and their processes, contained in a nerve bundle and disrupt structures such as the basal lamina around myofibers, connective tissues blood vessels, nerve branches, nerve terminal boutons, TSCs and NMJs. Injury to the nerve supplying the tibialis anterior (TA) muscle via a sciatic nerve crush, did not affect muscle architecture or induce muscle regeneration, although by observation, muscle fibers had a smaller diameter than controls. Thus, the timeline of degenerative and regenerative changes occurring in the different components of muscle tissue depended on the precise insult to the muscle.

The loss of SC-derived Sema3A in the SC-specific Sema3A knockout should affect the response of TSCs (which also make Sema3A) and afferent motor neurites being guided by Sema3A (and other factors) during the process that reinnervates muscle fibers after denervation by nerve crush. Notably, both muscle-crush and nerve-crush models require neurite extension during tissue repair (myotube reinnervation after traumatic muscle-crush injury, and myofiber reinnervation after denervation from sciatic nerve crush).

Therefore, to explore the importance of SC-specific Sema3A on TSCs during motor neurite regrowth toward AchRs and NMJs on fibers and new fibers, the effects of denervation vs. muscle crush injury on gene expression were examined. Additional goals for these experiments were to test whether the loss of SC-derived Sema3A affects motor neurite regrowth as represented by TSC expression of S100B, P75 and Sema3A as neurites grow after traumatic crush injury. TSC expression of Sema3A and S100B during regeneration from muscle vs. nerve injury was also examined.

3.3 Materials and Methods

Experiments were conducted at Kyushu University (Japan) utilizing a transgenic mouse model with tamoxifen-induced SC-specific knockout of Sema3A expression. Generation of Sema3A-Cko. Mice Pax7CreERT2-Sema3A^{flox} (Sema3A-cKO) mice were generated through mating Pax7-CreERT2 with Sema3A-loxP mice, originally developed by Dr. Shahragim Tajbakhsh (Institute Pasteur, France) and Dr. Takeshi Yagi (Osaka University, Japan) and assigned to the Tatsumi lab (Kyushu University, Japan). Transgenic mice were kept in the animal holding

facility at Kyushu University and housed in 22^oC and on a 12-hour light/dark cycle with free access to regular food and deionized water. The Cre recombinase was conditionally activated in adult male mice (8–10 weeks old and under control of the Pax7 promoter by an intra peritoneal injection of tamoxifen (TMX, ERT2 agonist) with a 27-gauge needle for 3 days. This amount of tamoxifen was found to be sufficient to suppress Sema3A in SCs significantly [508]. The mice were then rested for two weeks before undergoing surgery. Sema3A-loxP mice (N=5) were used as non-knockout controls and received the same amount of tamoxifen and at the same age as Sema3A-cKO mice.

3.3.1 Animal treatment and surgery

Male mice 9 weeks old, were weighed and received 10 μ L/gram body weight of TMX by intra peritoneal injection. The injection was repeated daily for 3 consecutive days and at the same time of day.

The plan for animal surgery is shown in Figure 12.

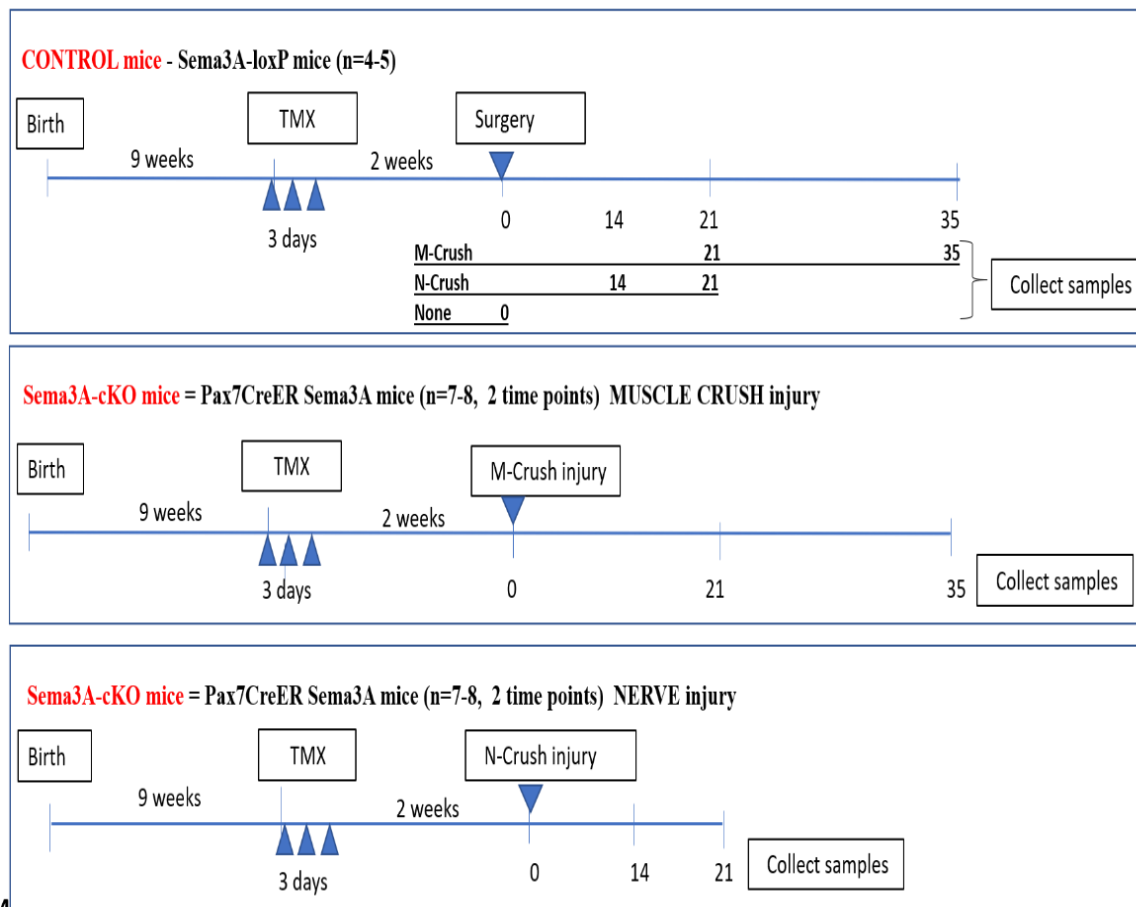


Figure 12. Surgery plan. Samples used for studies of Terminal Schwann cells (TSCs) and muscle satellite cells (SCs) during motor endplate reinnervation after muscle (M) or nerve (N) crush injuries or no surgery (control) in non-transgenic control mice (top panel), and after muscle-crush injury (middle panel) or nerve-crush injury (lower panel) in Sema3A-conditional knockout (cKO) mice in which Sema3A expression and synthesis were knocked down using daily (3X) tamoxifen injections (TMX), 2 weeks before injury.

Surgery was conducted under anesthesia as described [397]. The mice had either a muscle-crush injury (as described in Chapters 2 and 3) or nerve injury, 2 weeks after TMX injection. Sciatic nerve crush was done by exposing the left sciatic nerve posteriorly at the mid-thigh level and crushing it by closing grooved-jaw hemostat forceps around the nerve for 30 seconds. In this study, sciatic nerve was chosen as the target of nerve crush injury instead of peroneal nerve as the sciatic nerve is anatomically simpler and more accessible, and consequently results in less distress

and inconvenience to the animal. Even though an injury to the peroneal nerve seems like it would be a better model for this study, such injury is less commonly used in the literature than a sciatic nerve crush, as it is not as surgically accessible in animal facilities with technical and equipment limitations (such as in Japan) and carries additional issues related to avoiding damage to the vasculature that is closely associated to the peroneal nerve.

In some cases, where mice recovering from surgery interfered with sutures and skin closure, a collar was applied to keep the mice away from the wound until it had healed. Mice were kept in separate cages for 2-4 days and then returned to group housing.

3.3.2 TA Sample collection

All procedures including centrifugation were done at RT. Mice were euthanized under the standard anesthesia protocol at Kyushu University (mice were placed for 10 mins in a closed chamber containing 10 ml isoflurane and then placed in a beaker containing 70% ethanol for another 15 min). The skin was removed, and the TA muscle was dissected and cut to two halves along the long axis. One half was preserved in 4% paraformaldehyde and the other half was directly frozen in liquid nitrogen and kept in Eppendorf tubes at -80C for Genome PCR assay to test the genotype.

3.3.3 Western Blotting

The protein levels of Sema3A, γ AchR, and S100B, and a loading control (β -actin) were determined using Western blots of muscle-protein extracts according to standard protocols for extraction, electrophoresis, blotting, and chemiluminescence detection, as described earlier [391].

3.3.4 Antibody Information

Blocking antibodies in double immunofluorescence staining included: unconjugated Fab Fragment goat anti-mouse IgG (115-007-003, Jackson ImmunoResearch, 1:200), and unconjugated Fab Fragment goat anti-rabbit IgG (11-007-003, Jackson ImmunoResearch, 1:200).

Primary antibodies used for fluorescence staining included: and mouse anti-NGFR P75 antibody (sc-271708, Santa Cruz, 1:1500). Secondary antibodies included: goat anti-rabbit IgG DyLight650 (ab96902, Abcam, 1:200), goat anti-mouse IgG conjugated with DyLight488

(ab96879, Abcam, 1:200) and goat anti-mouse IgG conjugated to horseradish peroxidase (HRP) (A2304, Sigma, 1:200). DAPI was used to counterstain nuclei (D9542 Sigma, 1:10000).

For western blotting, primary antibodies included: rabbit anti-Semaphorin 3A (ab23393-50, Abcam, 1:5000), rabbit anti- γ AchR (sc-13998, Santa Cruz, 1:300), rabbit polyclonal anti-S100B (orb228251, Biorbyt, 1:3000), mouse anti- β -actin (sc-81178, Santa Cruz, 1:1500). Secondary antibodies included: HRP-conjugated goat anti-rabbit IgG H&L (ab97057, Abcam, 1:5000), and HRP-conjugated goat anti-mouse (A-2304, Sigma, 1:5000). Recombinant mouse Semaphorin3A Fc chimera protein (5926-S3-025/CF, R&D Systems) served as a positive control.

3.3.5 In situ hybridization

ISH experiments conducted on (SC-specific Sema3A-knockout transgenics and non-knockout controls with muscle-crush or nerve-crush surgery, and no-surgery transgenic controls) samples to detect transcripts for Sema3A, S100B, P75 or transcripts for Sema3A, S100B, and Pax7 (Table 4). The *in situ* hybridization experiments (ISH) were performed as described in Chapter 3 to detect the level of expression of various mRNA transcripts (S100B, Sema3A, P75, and/or Pax7) in sections of crush or denervated muscle as described at the tissue-collection time points outlined in Fig 13. The various staining combinations available from the above experiments are tabulated below. Cells positive for all three markers of interest in a particular experiment from *in situ* hybridization were identified as follows. Cell positive for S100B, P75NGFR and Sema3A were considered to be TSCs. Cells positive for S100B and P75 (but not Sema3A) were categorized as non-terminal Schwann cells. Cells that showed Sema3A expression (with or without P75) and Pax7, but not S100B were considered to be SCs if they were closely adjacent to myotubes.

3.3.6 Principal Component Analysis (PCA)

All data for every animal in the experiments, regardless of injury type or animal model (transgenic or not, surgery or not), were included in the PCAs (N=48). The term “Coloc” in tables and PCA plots, stands for the number of overlapping spots of mRNA expression for a combination of either: Sema3A, P75NGFR and Pax7 (representing SCs) or Sema3A, S100B and P75NGFR (representing TSCs). The number of areas of colocalization (overlapping areas of expression of transcripts from the respective three genes) that were indicated as “coloc” was tabulated from

analyzing images from the 10 fields that were imaged, and used for PCAs, representing SCs (Sema3A + Pax7 + P75 NGFR, but not S100B) and TSCs (Sema3A + S100B + P75 NGFR).

Table 4. The following summarizes the design of ISH-staining experiments.

assay groups	Sema3A (mRNA)	S100B (mRNA)	Pax7 (mRNA)	P75 (mRNA)
Muscle crush	+	+	+	+
Nerve crush				
No-surgery KO Controls				
non-KO Controls				

3.4 Results

As a first step in understanding the recovery potential in the absence of Sema3A expression in SCs after muscle injury by nerve crush, the level of expression of each transcript (mRNAs of Sema3A, S100B, and P75NGFR and Pax7) was assessed using ISH. Representative images in Figure 13 show the range of variation in the number of expression sites per field, the intensity (areal density) of staining representing expression in that field of muscle tissue, and the size (diameter) of expression sites. Exploring the localization of Sema3A mRNA expression in ISH staining was done through focusing on the co-expression patterns of Sema3A (green) with Pax7 in SCs (white), S100B in TSCs (red), and P75 in both TSCs and SCs (white). Representative areas of colocalization are outlined by white circles in ISH staining (Fig. 13. A-D).

In situ hybridization was used to determine the cellular origin of Sema3A and S100B, P75NGFR and Pax7 mRNA expression in the denervated (muscle-crushed or nerve-crushed) TA muscle. The RNA expression of Sema3A (green) and S100B (red) and Pax7 (white) was observed at day 21 in muscle-crush samples while the number of Pax7 and S100B RNA expression sites. As well the number of colocalized areas for all three RNAs (SCs) increased over time. Moreover, an increase in the number of Sema3A and S100B and P75NGFR (white) colocalized sites over time could be due to an increase in the number of TSCs in the pre-synaptic area over time (Fig. 13. F, H).

In the nerve-crushed muscles, even though the colocalized expression of RNA for Sema3A and S100B and P75NGFR was fewer in the Sema3A knockouts than in both the observed TSCs at the post synaptic area after nerve-crush injury, the number of the sites were fewer than both the non-knockout control groups and the no-surgery knockout control group at day 0 (Fig. 13. D, E, G).

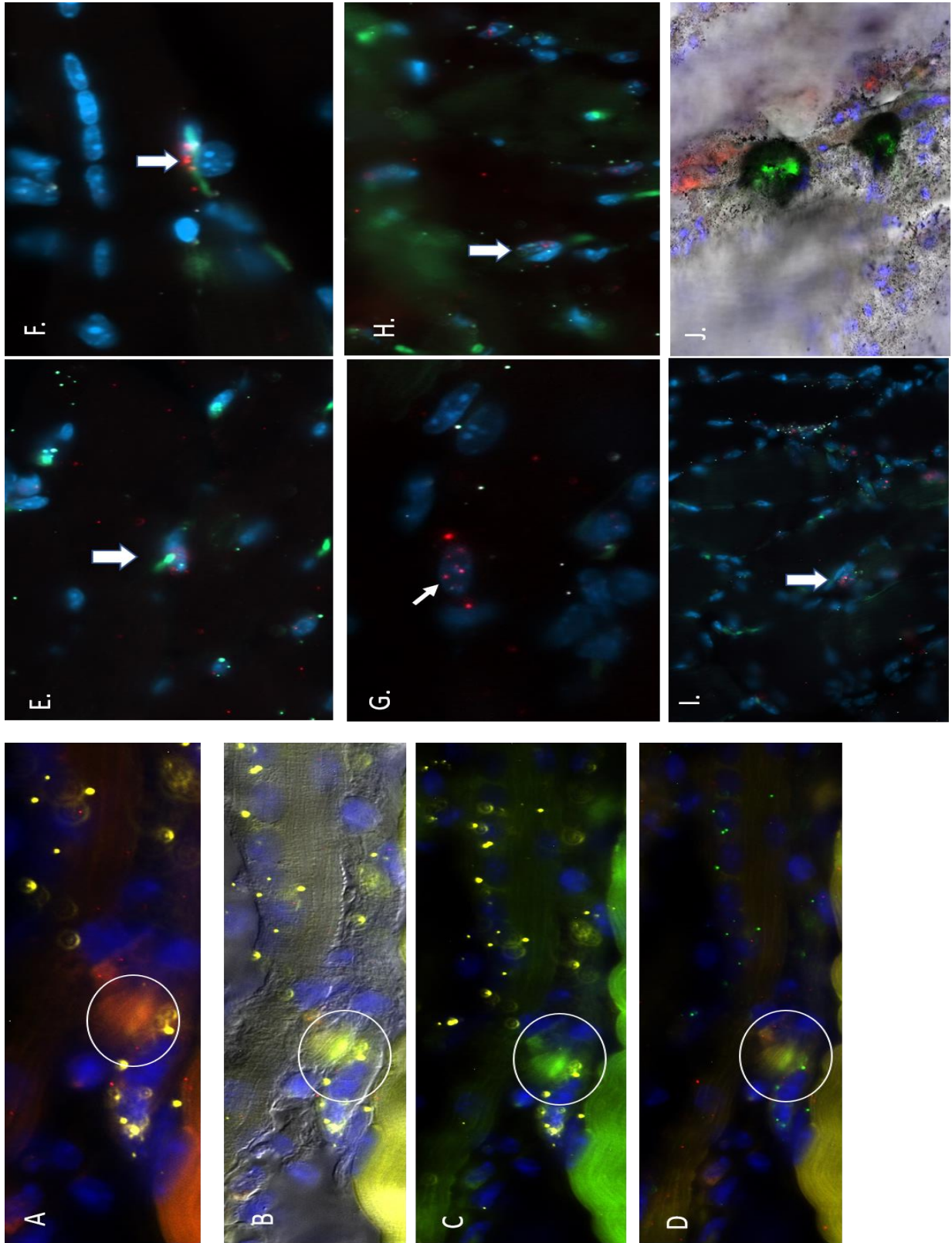


Figure 13. ISH Staining. To explore the localization of Sema3A expression through focusing on the co-expression of Sema3A with pax7 (in SCs) and with S100B (in TSCs) and P75 (in TSCs and SCs). The colocalization (D) of RNA expression of S100B (A), P75NGFR (B) Sema3A (C) in TSCs at D21 post nerve crush injury. E. The colocalization of RNA expression Sema3A, S100, and P75NGFR (white) in TSCs at D14 post nerve injury in non-knockout control group (white arrow). F. The colocalization of RNA expression Sema3A (green), S100B (red) and Pax7 (white) in SCs at D21 post muscle crush injury (white arrow). G. S100-positive cells express the low affinity receptor P75NGFR at 21 days after nerve crush injury (white arrow). H. The colocalization of RNA expression of S100B, Pax7 and Sema3A in SCs at D21 in the non-knockout control group post muscle crush injury I. The colocalization of RNA expression of Sema3A, S100B and P75NGFR in TSCs in no-surgery knockout control group at day 0. J. A combined IF and silver staining method to display the S100B expression (red) at pre-synaptic and AChE (silver staining) and alpha-BTX (green) stained post-synaptic regions at D0 in a control muscle. DAPI staining (blue) shows the nuclei. Original magnification by oil immersion X40 objective lens.

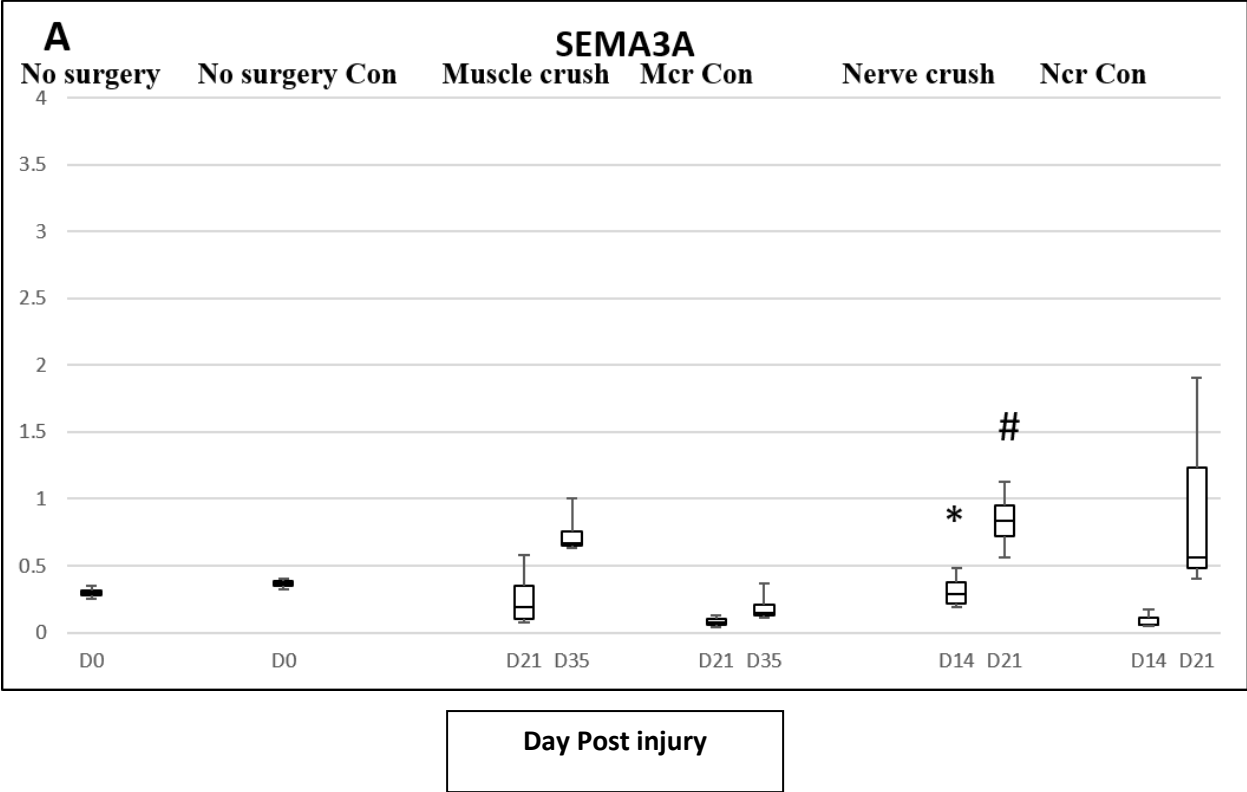
3.4.1 Western Blotting

The levels of Sema3A, γ AchR, and S100B proteins were detected by Western blotting. Band optical density in each blot was normalized to β -actin in the same lane.

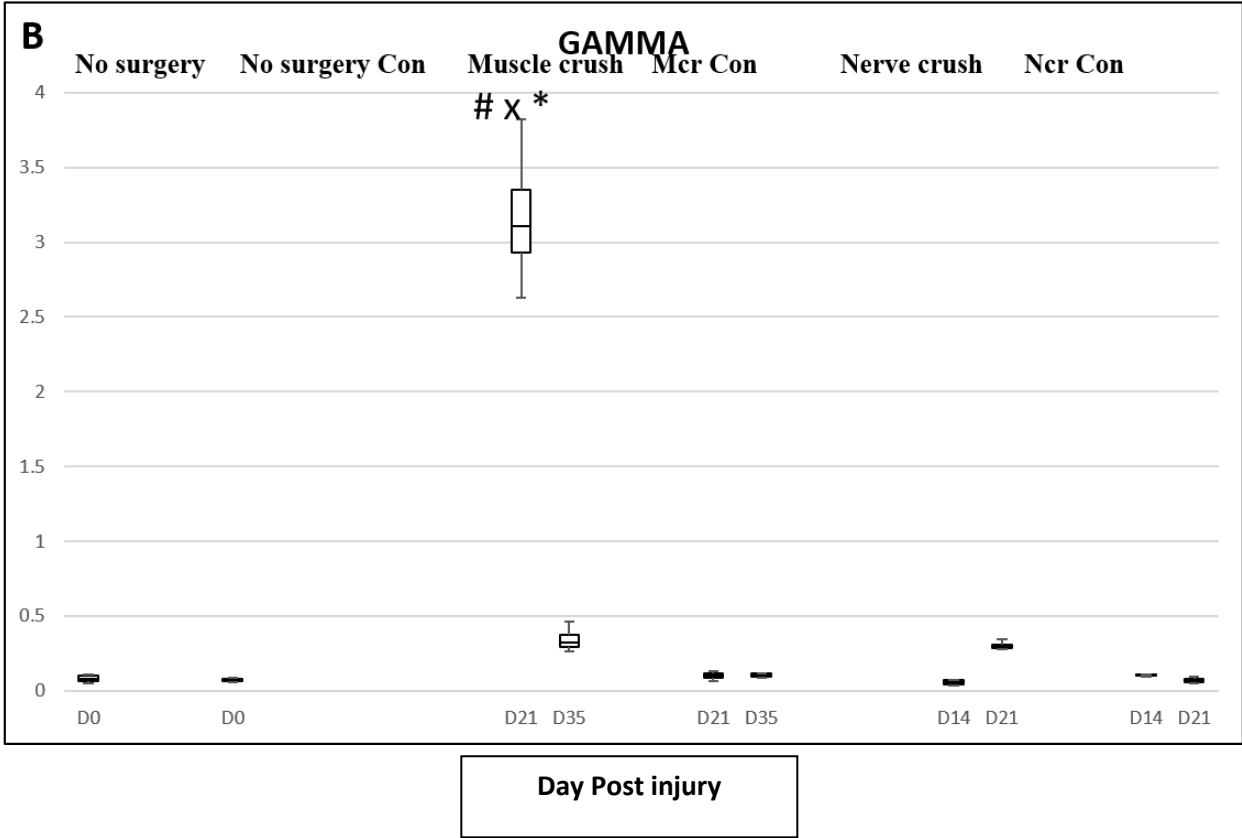
As a first step in understanding the potential impact of injury to nerve vs. muscle on TSCs during the respective regeneration processes, S100B was assayed in the regenerating muscles. S100B was significantly affected by the interaction of injury type*time point (2-way Anova, (df=2), $P < 0.001$). After nerve injury, the expression of S100B protein was lower than non-knockout control group at the same time point at day 14 and then increased at day 21 (Tukey's test, $P < 0.001$, Fig. 14.C). By comparison, after crush injury to muscle, S100B increased enormously at day 35 of regeneration (Tukey's test, df=36, $P < 0.001$).

After nerve-crush injury, S100B and Sema3A showed the highest expression at day 21 in comparison to non-knockout control groups at the same time point (Tukey's test, $P < 0.001$, Figures 14.A&C). The (γ)-subunit of mAChR, indicative of immaturity or denervation, had the highest expression at day 21 in comparison to control group and muscle crush injury groups during regeneration (Tukey's test, df=32, $P < 0.001$, Fig.14. B). The results showed that there is a strong positive association between the expression of S100B and time during regeneration. The slopes of linear regression lines indicated that with increasing time, S100B expression also increased (Tukey's test, df=34, $P < 0.01$). Asterisks (*) indicate significant difference (Tukey's $0.05 < p < 0.001$) from another time with the same injury; # indicates significant difference from NO surgery group; x indicates significant difference from control group with the same time point (n=1-4 male mice per time point in each treatment group) as shown in Table 5. A.

OD/OD β -actin



OD/OD β -actin



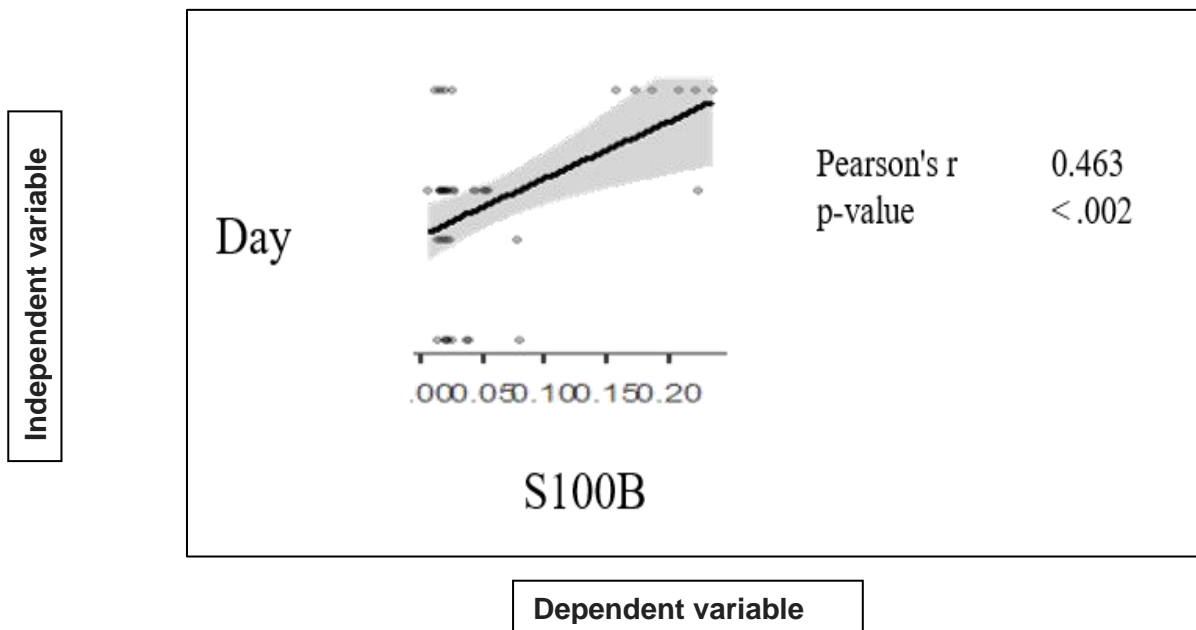
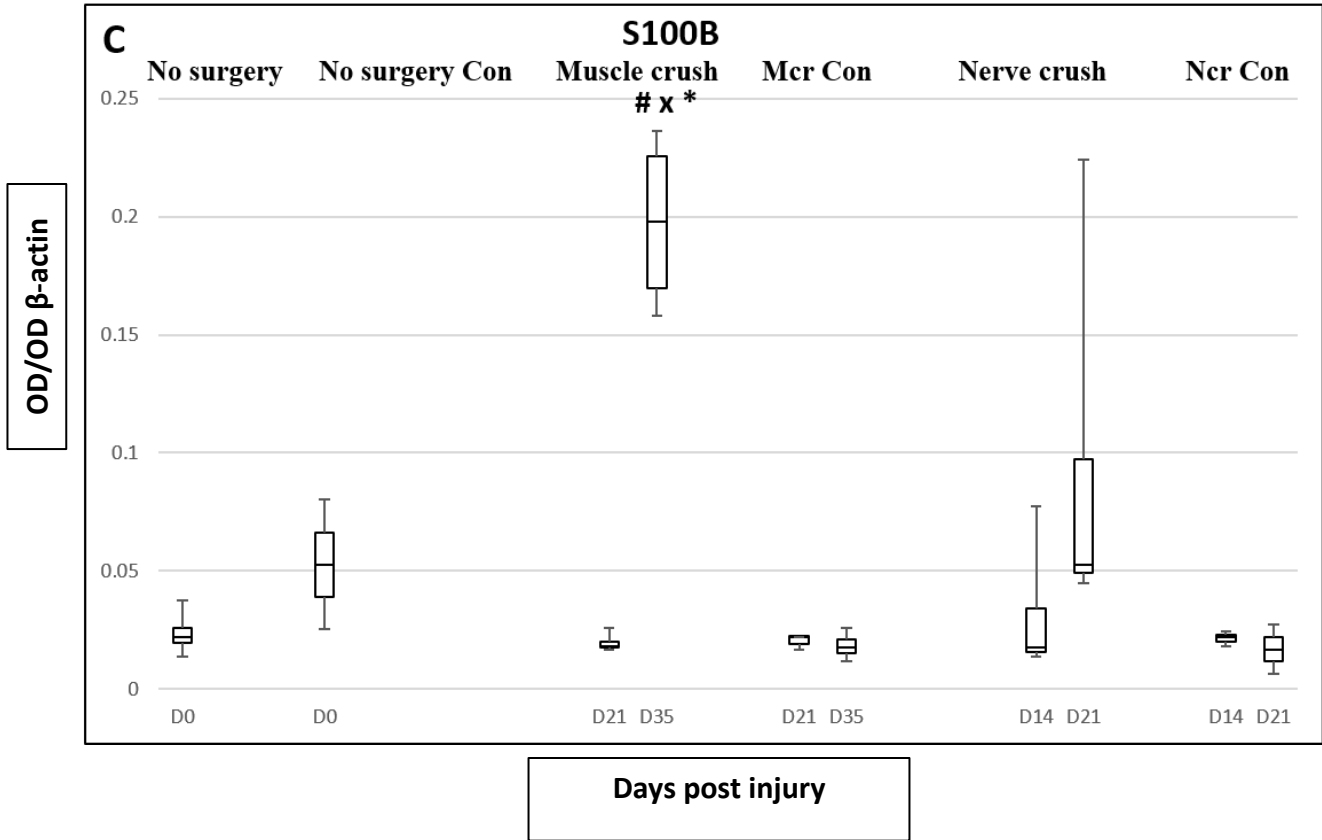


Figure 14. Sema3A, γ AchR, and S100B proteins after injury to nerve (NCr) or muscle (MCr), or control groups. A, C. S100B and Sema3A showed the highest expression at D21 post nerve-crush injury in comparison to control groups (Tukey's test, $df=34$ and 36 , respectively, $P<0.001$). B. Immature gamma (γ)-subunit had the highest expression at D21 in comparison to control group and other muscle crush injury groups during regeneration (Tukey's test, $df=32$, $P<0.001$). C. After crush injury, the expression of S100B protein was increased over time (Tukey's test, $P<0.001$) and increased enormously at D35 of regeneration (Tukey's test, $df=34$, $P<0.001$). Asterisks (*) indicate significant difference from another time point with the same injury. # indicates significant difference from no-surgery group. X indicates significant difference from control group at the same time point.

3.4.2 In situ hybridization (ISH)

Observations of ISH staining displayed details of gene expression that could then be quantified in particular cells of interest.

There were two sets of control groups in these experiments: no-surgery Sema3A-knockouts, and non-knockout controls that had surgery and recovered for the same times as the SC-specific Sema3A-knockout mice. Comparing the Sema3A-knockouts with muscle crush with both control groups showed that even though the RNA expression of the Sema3A was still high, a considerable decrease happened in the number of S100B and the diameter of Pax7 expression sites.

After muscle-crush injury, muscles containing large myotubes (formed since injury to myofibers) contained many central nuclei. Muscles also displayed the RNA expression of Sema3A (green) and S100B (red) in various locations. A few centralized myonuclei displayed a few sites of Pax7 RNA expression (white dots) at day 21, indicating remnant Pax7 RNA expression after fusion into myotubes (Figure 15).

At both time points after nerve-crush injury, muscle sections displayed a high level of Sema3A RNA expression and lower levels of S100B expression. As well, there were very few areas in which Sema3A and S100B were colocalized. It was interesting that the non-knockout control groups for the nerve-crush injury and the no-surgery knockout control group at day 0, showed even

fewer sites of Sema3A expression and very few sites of S100B expression, such that the sites of mRNA expression were not present in every field after ISH staining.

Box-whisker plots for the number of expression sites, the size of those sites (diameter), and their staining intensity are shown for Sema3A, S100B, P75NGFR and Pax7 RNA expression as a function of regeneration time for muscles after muscle crush or nerve crush injury, are presented in Figure 15 for Sema3A knockout mice and for tamoxifen-treated non-knockout transgenic control mice (n=2-4 male mice per group). Overall, measurements of expression sites (number, intensity, and diameter) generally confirmed WB findings for S100B and Sema3A protein expression.

The number of Sema3A expression sites after muscle-crush injury was higher at day 35 than in both the non-knockout control group at the same time point and the no-surgery group at day 0 (time*injury interaction, $F(df)=21$, $P(\text{Tukey's})=0.054$ and $p=0.024$, respectively). The number of Sema3A expression sites after nerve-crush injury muscles was also higher at day 21 than in the no-surgery group at day 0 post-surgery (time*injury interaction, $F(df)=21$, $P(\text{Tukey's})=0.005$; Fig. 15.B). So Sema3A expression overall increases after injury and during regeneration and reinnervation, but that is not in the SCs in the knockouts.

The number of S100B expression sites after muscle-crush injury was higher at day 21 and day 35 than in both the non-knockout control group and the no-surgery group at the same time point. The number of S100B expression sites after nerve-crush injury was also higher at day 14 than in both the non-knockout control group and the no-surgery group at the same time point. Moreover, the number and intensity of Pax7 expression sites after muscle-crush injury did not show any significant difference with the non-knockout control group at the same time points.

The number of P75NGFR expression sites also did not show any significant difference after either muscle-crush or nerve crush injuries in the non-knockout control group or the no-surgery group at the respective time points for each injury. Neither the intensity of Sema3A expression sites nor the intensity of S100B expression sites showed any significant difference after muscle-crush or nerve-crush injury from their respective non-knockout control groups at the same time point. P75NGFR RNA expression intensity in muscle-crush injury was higher in the Sema3A-knockout mice than in the non-knockout control group at the same time point after muscle-crush injury (time*injury interaction, $F(df)=16$, $P(\text{Tukey's}) < 0.001$, and < 0.001 , respectively, and also

higher than in the no-surgery control group at both day 21 and day 35 (time*injury interaction, $F(df)=16$, $P(\text{Tukey's}) < 0.001$, and < 0.001 , respectively; Fig. 15.A).

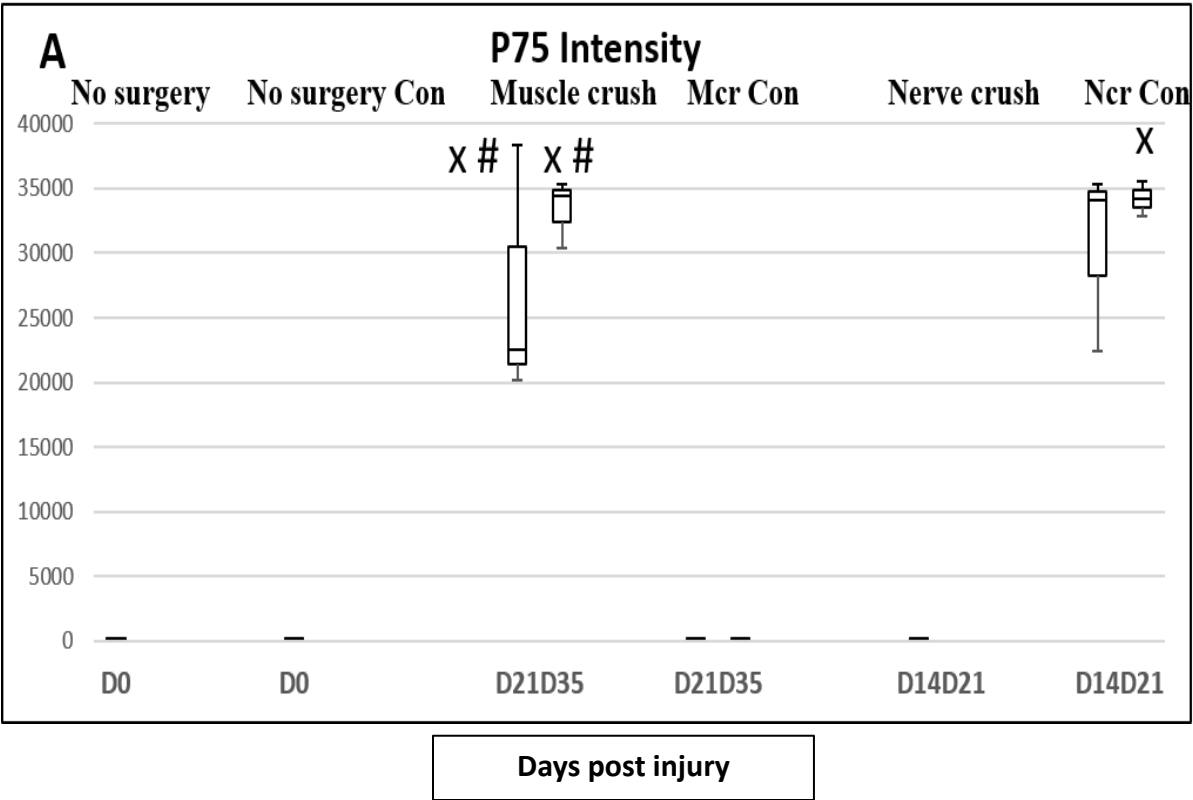
The intensity of P75 RNA showed P75 expression was higher in the Sema3A-knockout mice than the non-knockout control group at the same time point at day 21 after nerve-crush injury (time*injury interaction, $F(df)=16$, $P(\text{Tukey's}) < 0.002$; Fig. 15.A). Moreover, at day 14 after nerve-crush injury, the number of colocalized spots P75NGFR RNA expression with Sema3A and S100B RNA expression was higher in the Sema3A knockout mice than non-knockout control group at the same time point (time*injury interaction, $F(df)=20$, $P(\text{Tukey's}) < 0.033$; Fig. 15.C).

The diameter of Sema3A expression sites was almost the same at all time points for both injuries, and showed no significant difference with either the non-knockout control group or the no-surgery transgenic group at the same time point. The diameter of S100B expression sites after muscle-crush injury was higher at day 21 and day 35 than in both the non-knockout control group and the no-surgery group at the same time point. There were no significant changes in the diameter of Pax7 expression sites. The diameter of P75 expression sites after muscle-crush injury did not show any significant changes from the non-knockout control group at the same time point.

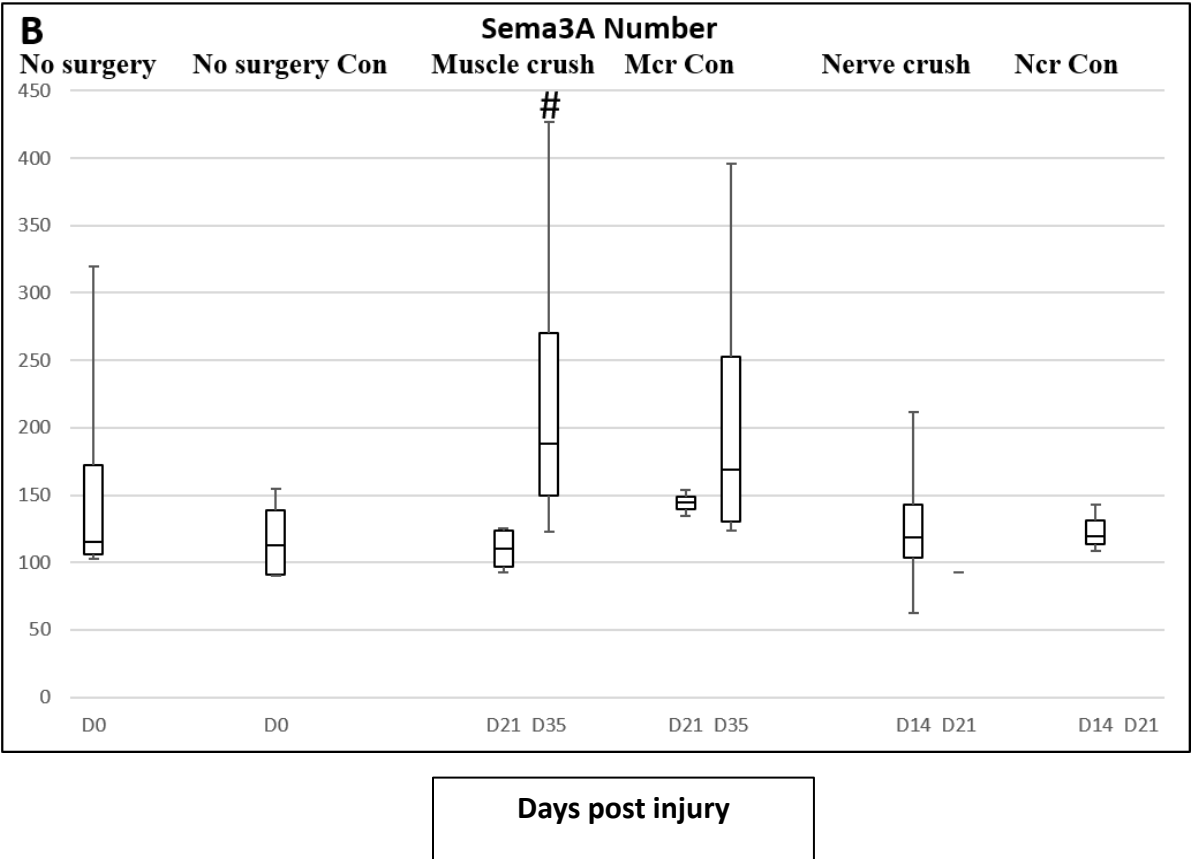
The number of areas where the ISH expression signal for Sema3A was colocalized with P75 and S100B (representing TSCs) after muscle-crush injury was higher at days 21 and 35 than in the no-surgery group at day 0 (time*injury interaction, $F(df)=20$, $P(\text{Tukey's})=0.002$ and $p=0.001$, respectively). The number of these areas after nerve-crush injury was also higher at day 14 than in the non-knockout control group at the same time point (time*injury interaction, $F(df)=20$, $P(\text{Tukey's})=0.033$; Fig. 15.C).

The number of areas where the ISH expression signal for Sema3A was colocalized with expression of P75 and Pax7 (representing SCs) did not change significantly with either nerve or muscle-crush injury compared to their respective non-knockout control groups at the various time points post-surgery (Table 5.B).

Region: Areal Density (Mean)



Dots per field



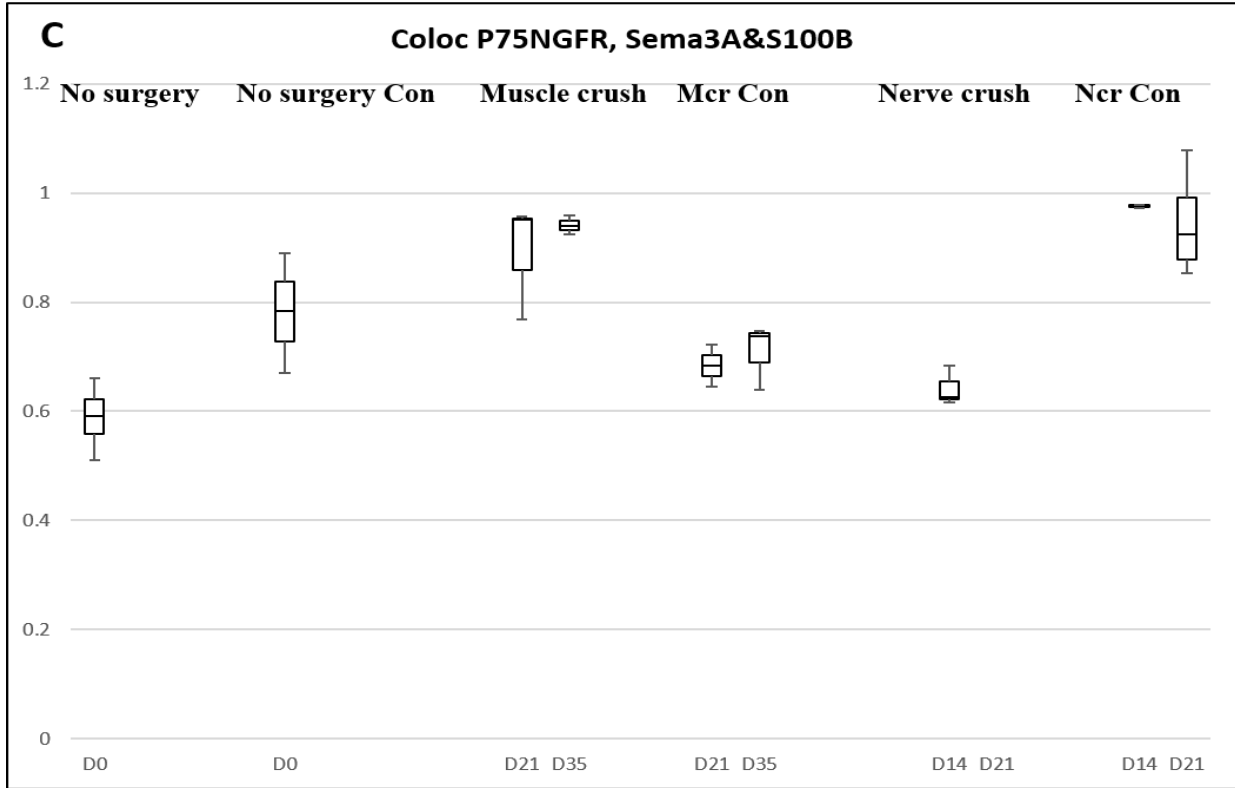


Figure 15. Box-whisker plots for expression studies by ISH. Box-whisker plots for the number of expression sites and their staining intensity are shown for *Sema3A*, *S100B*, *P75* and *PAX7* RNA expression as a function of regeneration time for muscles after crush injury (to muscle, MCr) or nerve (NCr) for *Sema3A* knockout and non-transgenic but tamoxifen-treated Control mice. A. Higher *P75NGFR* RNA expression (intensity), in the *Sema3A*-knockout mice than in the non-knockout control group at the same time point, at both D21 and D35 post muscle crush injury (time*injury interaction, $F(df)=16$, $P(\text{Tukey's}) < 0.001$, and < 0.001 , respectively). The intensity of *P75NGFR* RNA expression was also higher than the no-surgery control group at both time points (time*injury interaction, $F(df)=16$, $P(\text{Tukey's}) < 0.001$, and < 0.001 , respectively). The intensity of *P75* RNA showed *P75* expression was higher in the *Sema3A*-knockout mice than the non-knockout control group at the same time point at D21 after Nerve-crush injury (time*injury interaction, $F(df)=16$, $P(\text{Tukey's}) < 0.002$). B. The number of *Sema3A* expression sites was higher at D35 than in both the non-knockout control group and the no-surgery group (Day0) (time*injury interaction, $F(df)=21$, $P(\text{Tukey's})=0.054$ and $p=0.024$, respectively). The number of *Sema3A* expression sites after nerve-crush injury muscles was also higher at D21 than in the no-surgery group at D0 post-surgery (time*injury interaction, $F(df)=21$, $P(\text{Tukey's})=0.005$). C. The number of colocalized spots *P75NGFR* RNA expression with *Sema3A* and *S100B* RNA expression was higher in the *Sema3A* knockout mice than non-knockout control group at the same time point at D14 post N-crush injury, (time*injury interaction, $F(df)=20$, $P(\text{Tukey's}) < 0.033$). # indicates significant difference from no surgery group; X indicates significant difference from control group with the same time point.

Table 5. A summary of statistical comparisons for assays of protein. (A) and transcript expression (B) by Western blotting and in situ hybridization techniques, respectively. Below, “N-crush” indicates the group that received a nerve-crush injury; “M-crush” indicates the group that received muscle-crush injury. D indicates day post-injury D14, 25, and 31. “↔” indicates there were no significant finding. “Coloc P75NGFR” indicates the number of overlapping areas for the RNA expression of Sema3A, S100B and P75 NGFR in TSCs. “Coloc Pax7” indicates the number of overlapping areas for the RNA expression of Sema3A, Pax7 and P75 NGFR in SCs. # indicates there was a significant effect by 1-way ANOVA and by a pairwise comparison (by Tukey’s test) between the indicated pre-treatment or transgenic group and its respective control group (no pre-treatment or non-knockout transgenic group, respectively) at a particular day (D) post-injury. Symbols for increase (↑) or decrease (↓) accompany the indication of significance.

A Western blotting	Experiments			
	M-Crush vs. M-Cr controls	N-Crush vs. N-Cr controls	M-Crush vs. No-surgery controls	N-Crush vs. No-surgery controls
Sema3A protein	↔	↔	↔	↑D21#
γAChR protein	↔	↔	↑D21#	↔
S100B protein	↑D35#	↔	↑D35#	↔

B. ISH	Experiments			
	M-Crush vs. M-Cr controls	N-Crush vs. N-Cr controls	M-Crush vs. No-surgery controls	N-Crush vs. No-surgery controls
Sema3A mRNA number	↑D35#	↔	↑D35#	↑D21#
intensity	↔	↔	↔	↔
diameter	↔	↔	↔	↔
S100B mRNA number	↔	↔	↔	↔
intensity	↔	↔	↔	↔
diameter	↔	↔	↔	↔
Pax7 mRNA number	↔	↔	↔	↔
intensity	↔	↔	↔	↔
diameter	↔	↔	↔	↔
P75 mRNA number	↔	↔	↔	↔
intensity	↑D35# ↑D21#	↑D21#	↑D35# ↑D21#	↔
diameter	↔	↔	↔	↔
#COLOC P75 (number of TSCs)	↑D21#	↑D21#	↑D35#	↑D14#
#COLOC Pax7 (number of SCs)	↔	↔	↔	↔

3.4.3 Principal Component Analysis

All the variables from analysis of Western blotting and ISH experiments were compiled into Jamovi software and PCA studies were run for: P75NGFR in TSCs (P75NGFR, S100B and Sema3A) and for Pax7 in SCs (P75NGFR, Pax7, Sema3A), and are shown in Figure 16 and Table 6, and Figure 17 and Table 6, respectively.

The number of colocalization sites where the expression of P75NGFR, Sema3A and S100B overlaps, identifies TSCs in post-synaptic areas. The PCA analysis related to TSCs, here named P75NGFR PCA or P75-PCA is shown in Figure 8B. The analysis shows increase of TSC colocalization sites with levels of S100B and Sema3A proteins, and the number and intensity of P75NGFR RNA expression sites.

Examining the relationships of variables with each Factor showed that the strongest correlations of variables were: Sema3A protein (loading of 0.737) and Pax7 intensity (loading of 0.713) in the Pax7 PCA; and S100B intensity (loading of 0.945) and Sema3A protein (loading of 0.736) in the P75-PCA. The correlation circle demonstrates these correlations by showing the line representing their correlation values with the corresponding dimensions of the PCA are longest among all other variables.

The PCA on P75, representing TSCs, used the full dataset on 13 variables, and included all the variables available for ISH and Western blotting assays. As shown in Table 6, in this PCA, F1 accounted for 37.15% of the total variance in the dataset and is defined by colocalization area (representing TSCs), Sema3A and P75NGFR intensity and number, S100B diameter, intensity and number (all from ISH) and S100B protein (from Western blotting). F2 accounts for 14.61% of the total variance and includes Sema3A protein (from Western blotting) and P75 intensity and number (from ISH). Together, the two PCs or Fs accounted for 51.67% of the total variance in the data (Bartlett's sphericity test p-value (0.0001) (Fig. 16 and Table 6).

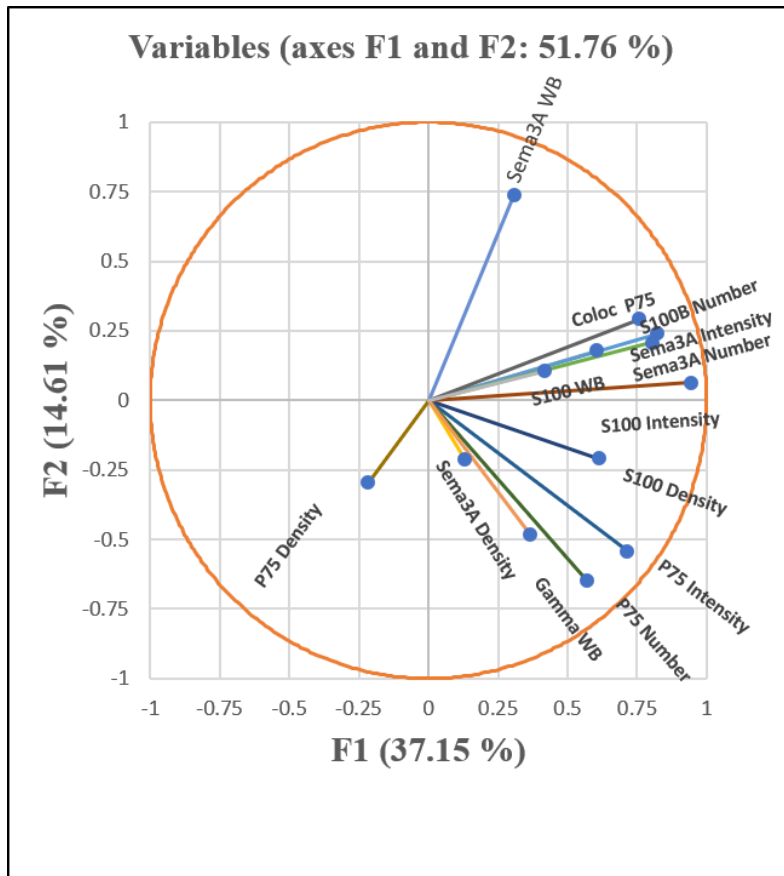


Figure 16. Principal component analysis correlation circle for P75 NGFR, representing TSCs. The plot shows vectors (direction and length) to represent the coefficients of each of the variables with the axes for two Factors (F1, x-axis; F2, y-axis), and the vector endpoints overlaid positions on the x-y grid that represent the loading (or correlation) scores of all the data observations (Controls and injury groups) on each of the Fs in the plot. A variable with a short vector length on both F1 (x-axis) and F2 (y-axis) dimensions indicates that variable is likely better represented on other dimensions. This PCA plot of P75 NGFR includes N = 13 variables. Variable labels on the vectors are abbreviated as follows: Sema3A WB (Western blotting results for Sema3A-protein expression; Gamma WB (Western blotting results for Gamma-protein expression); S100 WB (western blotting results for S100B-protein expression); and “Coloc P75” (the number of overlapping areas with the RNA expression of S100B, Sema3A and P75NGFR in TSCs). Details of loading for each variable in the two Factors appear in Table 6.

Table 6 on data related to P75 in TSCs. Tables show correlation coefficients for the variables (N = 13) loaded on the dimensions of 2 Factors (F1 and F2) as extracted from the analysis of data

from muscle-crush and nerve-crush injuries (N= 48 animals). In the row for each variable, numbers show the strength of correlation of that variable with the eigenvector of each F. When the absolute value of correlation coefficients was 0.5, they were considered important (bold font) in identifying that F.

Table 6 – P75 NGFR PCA	F1	F2
Coloc P75	0.605	0.178
Sema3A diameter	0.131	-0.213
Sema3A intensity	0.824	0.240
Sema3A number	0.803	0.208
S100B diameter	0.612	-0.208
S100B intensity	0.945	0.064
S100B number	0.757	0.291
P75 diameter	-0.216	-0.297
P75 intensity	0.714	-0.543
P75 number	0.568	-0.647
Sema3A WB	0.307	0.736
γ AchR WB	0.366	-0.484
S100B WB	0.416	0.105

The Pax7 PCA, indicative of SCs included variables for both ISH (examining the mRNA expression of Pax7, S100, and Sema3A) and results of Western blotting assays. As indicated in Table 7, F1 on this PCA represented the number of colocalization areas (representing SCs), plus Sema3A diameter and intensity, S100B expression intensity and number, Pax7 number, and Sema3A protein. As a principal component, F1 accounted for 30.94% of the total variance in the dataset. F2 accounted for 18.20% of the total variance. From the Pax7 PCA, therefore, the two new variables, F1 and F2, together accounted for 49.13% of the total variance and the Bartlett's sphericity test p-value was $p < 0.0001$ (Fig. 17 and Table 7).

Table 7 for PCA on data related to Pax7 in SCs. using N =13 variables. Table shows correlation coefficients for the variables loaded on the dimensions of 2 Factors (F1 and F2) as extracted from the analysis of data from muscle-crush and nerve-crush injuries (N= 48). In the row for each variable, numbers show the strength of correlation of that variable with the eigenvector of each F. When the absolute value of correlation coefficients was 0.5, they were considered important (bold font) in identifying that F.

Table 7 – Pax7 PCA	F1	F2
Coloc Pax7	-0.675	0.231
Sema3A diameter	-0.727	0.283
Sema3A intensity	-0.700	-0.626
Sema3A number	-0.486	-0.037
S100B diameter	-0.727	-0.201
S100B intensity	-0.639	-0.676
S100B number	-0.512	0.255
Pax7 diameter	-0.077	0.092
Pax7 intensity	-0.326	-0.713
Pax7 number	-0.597	0.447
Sema3A WB	0.737	0.093
γ AchR WB	-0.223	0.705
S100B WB	0.226	0.233

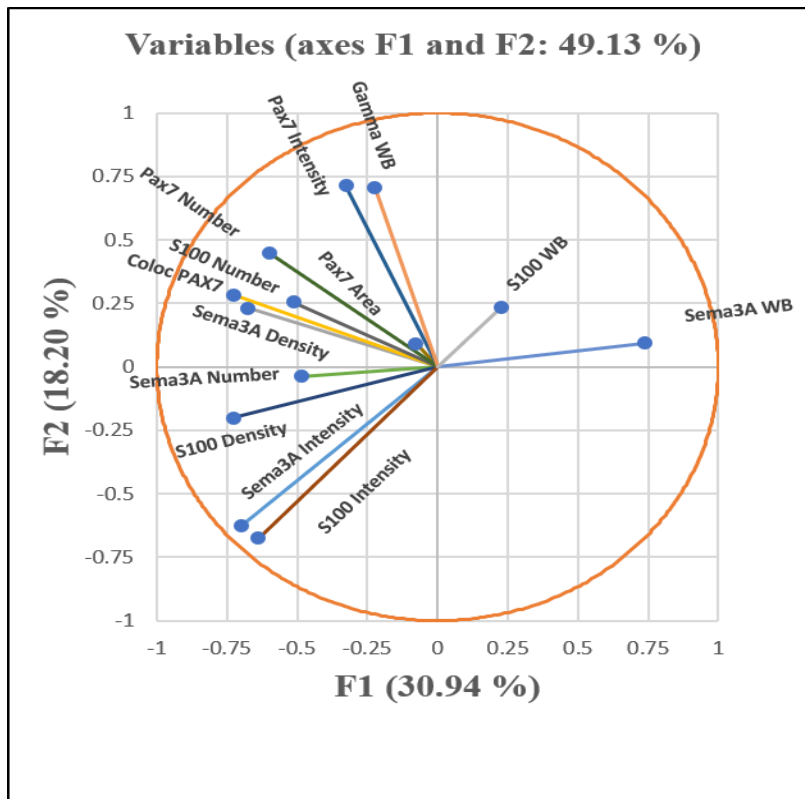


Figure 17. Principal component analysis correlation circle for Pax7, representing SCs. The plot shows vectors (direction and length) to represent the coefficients of each of the variables with the axes for two Factors (F1, x-axis; F2, y-axis), and the vector endpoints overlie positions on the x-y grid that represent the loading (or correlation) scores of all the data observations (Controls and injury groups) on each of the Fs in the plot. A variable with a short vector length on both F1 (x-axis) and F2 (y-axis) dimensions indicates that variable is likely better represented on other dimensions. This PCA plot of Pax7 includes N = 13 variables. Variable labels on the vectors are abbreviated as follows: Sema3A WB (western blotting results for Sema3A-protein expression; Gamma WB (western blotting results for γ AchR-subunit protein expression); S100 WB (western blotting results for S100B-protein expression); and “ColocPax7” (the number of overlapping areas with the RNA expression of Sema3A, Pax7 and P75 NGFR in SCs). Details of loading for each variable in the two Factors appear in Table 7.

3.5 Discussion

The current report extends the information available on *Sema3A* expression in satellite cells (SCs) and terminal Schwann cells (TSCs) during NMJ reformation by investigating the impact of SC-specific knockout of *Sema3A* following two different injuries, muscle crush or nerve crush. Gene and protein expression were examined during changes in the denervation and reinnervation status at different time points post-injury. The primary hypothesis of this study was that changes in γ AchR, TSC markers such as *S100B* and *P75*, and the expression of other indicator proteins accompany NMJ reformation after muscle and crush injuries, and that these variables are affected by the loss of *Sema3A* expression by SCs. Results of the ISH experiments showed that the intensity of *P75* RNA expression was increased in the SC-*Sema3A* knockout compared to the non-knockout control group at the same time point after muscle-crush injury. *P75* expression intensity was also higher in knockouts after muscle crush injury at days 21 and 35 than in no surgery *Sema3A* knockout controls. *P75*NGFR mRNA expression in muscle was also increased in the *Sema3A*-knockout at day 21 after nerve injury compared to the non-knockout group at the same time-point and to the no-surgery control groups. These findings suggest that the number of TSCs was increased only with the loss of SC-derived *Sema3A*. Moreover, the intensity of *P75*NGFR expression was also positively correlated to *Sema3A* intensity (from non-SC sources including TSCs), *S100B* intensity (another gene expressed by TSCs) and γ AchR protein (expressed by muscle fibers during denervation). The level of *Pax7* expression by ISH (intensity) was also positively correlated to the level of the γ AchR protein, suggesting that there is an increase in the number of muscle SCs during denervation or that each SC increases its level of *Pax7* expression after injury.

In this study, the expression of genes relevant to motor neuritegenesis and axon guidance (*Sema3A*, *S100B*, *P75*NGFR) by TSCs and *Pax7*⁺ SCs was investigated, as well as the level of proteins resulting from the expression *Sema3A*, *S100B* and γ AchR related to muscle denervation. The loss of SC-specific *Sema3A* expression was anticipated to disrupt TSC gene and protein expression after both nerve and muscle injury. The parameters were compared between transgenics with a conditional SC-specific knockout of *Sema3A* expression (starting from before the time of injury, and continuing) during regeneration from injury by muscle crush or nerve crush (denervation). Expression results for studies of crush injury to either muscle or nerve in transgenic

knockout mice were compared to two groups of controls: one with the same injury in non-knockout control mice (that received tamoxifen but did not have the cre/loxP insertion), and the other, a no-surgery control of SC-specific Sema3A-knockout mice (that illustrated the day-0 time point in the injured knockout mice).

Days 14 and 21 were selected as time points for studying TSCs after a nerve-crush injury, while days 21 and 35 were time points selected for studying TSCs after muscle-crush injury. These time points were selected on the basis of literature related to understanding the patterns of motor endplate reinnervation after the two types of injury [344]. The large TA muscle, innervated by the deep peroneal branch of the sciatic nerve, was identified as the muscle of choice as it was large enough to provide many samples for additional assessments (not included in the text of this thesis), and results could be compared to the previous experiments on TA muscle-tissue regeneration and NMJ restoration that are reported in Chapters 2 and 3 of this thesis.

The results of Western blot experiments showed a higher level of Sema3A at day 21 than day 14 after nerve crush. This seems puzzling, since one would expect to see denervation and higher γ AchR after nerve crush than was observed, a notion that is based on a report from double-fluorescent transgenic mice [423]. In that study, authors found that one week after sciatic nerve-crush injury, all the motor endplates are denervated. The blood-nerve barrier breaks down within 2 days of nerve crush injury which accompanies a combination of proliferation of the Schwann cells and endogenous fibroblasts and the infiltration of inflammatory cells that participate in Wallerian degeneration, neurotrophin synthesis and phagocytosis. Motor endplate recovery in the TA was noted to start at two weeks following nerve-crush injury, with hyperinnervation of the endplates at week 3, alongside deficient function; Magill *et al* (2007) interpreted this to signify an immaturity of endplates together with continuing synaptic competition. Restoration of axons to motor endplates to a state similar to uninjured controls was detected at six weeks after nerve crush [423]. Most research on synapse formation, stabilization, elimination, and activity suggest the developmental pattern is reinstated by endplate recovery after nerve injury in the adult [507, 509].

Schwann cells are activated during the first 24 hours after nerve injury and their first role is phagocytosis of the myelin and axonal debris. Macrophages infiltrate into the injury area and stimulate proliferation of fibroblasts and Schwann cells. Macrophages and Schwann cells work together to clean up the injury area which may take between 1 week to quite a few months. This timing depends on the type of the injury and area, for example it is dramatically slower in the

mammalian CNS and could take months [345]. Empty endoneural tubes lead the return of some nerve fibers to motor endplates, while other axons continue to extend along TSC networks. These axonal projections outside the NMJ region are known as “escaped fibers” and are strongly influenced by Schwann cell guidance during denervation or even shortly after reinnervation [510]. This bridging by Schwann cells was accompanied by the proliferation of peripheral Schwann cells close to motor endplates two weeks after nerve-crush injury.

A mature, one-to-one ratio of terminal axons to motor endplates is formed within six weeks after sciatic nerve crush injury, when associated Schwann cells establish the phenotypic morphology of stabilized NMJs. This seems puzzling, since one would expect to see denervation and higher γ AchR after nerve crush than was observed [423]. However, studying the reinnervation process following nerve crush over time in living mice [511], displayed that the gradual loss of the nerve terminal boutons inside a NMJ is coordinated with a gradual loss of AchRs by the myofibers at corresponding areas.

Normally, one axon reinnervates the primary endplate by growing through the old Schwann-cell-derived tube whereas another endplate sprouts from an adjacent endplate. Within 2 weeks after reinnervation, most of the sprouts regress and the transient state of multiple innervation returns to the normal low level. At some endplates, nerve terminal boutons were permanently eliminated as they did not receive sprouts from the axons remaining at the endplates. There was also a corresponding permanent loss of AchRs within the myofiber membrane just beneath the eliminated nerve boutons. This finding showed that the reduction in receptors at areas of synapse elimination occurred because of both a selective loss of AchRs already integrated into these sites and the absence of new receptors inserting at the same sites. Interestingly, these regions of pre- and postsynaptic loss do not interfere with cholinesterase staining, which is preserved in the basal lamina for a long period of time. The control experiments in that study also illustrated that endplates with permanent denervation, incomplete reoccupation with reinnervating axons, or stained several times in normal muscle do not lose postsynaptic receptor areas. Interestingly, receptors seem to be eliminated before there is any noticeable alteration in the staining of the nerve terminals [509, 511]. One interpretation is that the redistribution or removal or related postsynaptic molecules by one innervating axon may stimulate the removal of matching terminals.

Another aspect of this reinnervation process, synaptic competition, results in the elimination of some synaptic terminals and the removal of the respective post-synaptic areas that

were occupied by those eliminated axon terminals. The reoccupation is not always stable, as some reoccupied areas become vacant during the synapse-elimination period following reinnervation. Even though there are some protein cues that make synaptic areas exclusively attractive to axons, the interactions that happen during synapse elimination trigger loss of some of these nascent synaptic areas, possibly through eliminating synaptic markers [511]. Due to those findings, the consistent expression of Sema3A between Sema3A-knockout groups and their controls over time suggests the role of Sema3A expression at the postsynaptic area is to guide those axons entering an endplate via the original Schwann cell sheath during reinnervation. In muscle-crush injury, the higher expression of γ AchR at day 21 in comparison to the no-surgery Sema3A-knockout group (day 0) is taken to indicate the highest level of denervation occurred at that time. The higher expression of S100B protein, and transcript expression of Sema3A and Pax7 at day 35 in comparison to the no-surgery group (day 0) could be due to the activation of SCs and reinnervation through reestablishment of TSCs at the pre-synaptic area. It might show that SCs either increase Pax7 expression at that point, or there is a round of SC proliferation late after the muscle injury.

The approach to studying transcript expression using ISH has long served as a valuable tool for exploring mechanisms of cellular pathology since the 1970s. ISH is a powerful and sensitive technique for studying gene expression in cells in a way that is analogous to immunocytochemistry (ICC) which is utilized to localize specific proteins within cells (often selected so they are unique to one type of cell in a particular tissue). This is of importance as using other approaches, the simultaneous recognition of proteins and mRNAs in the cells of adjacent, serial sections requires conditions where (a) cell morphology is highly retained in the same manner on adjacent sections, and (b) the reactivity of nucleic acids and antigens to probing by both ISH and ICC approaches, is preserved. In situ hybridization and immunocytochemistry are the techniques of preference to verify and localize in a tissue (i.e., in situ) the expression of biomarkers. Both methods, especially ICC, present a semi-quantitative detection of target moieties (nucleic acids or proteins) by protecting topological information of the expression inside cells within the surrounding tissue structures. Such evidence is lost with identification techniques, such as flow cytometry or quantitative polymerase chain reaction assays (qPCR) for which tissues need to be dissociated and for which the yield is a cell or tissue “average” of expression.

ICC provides visualization of protein antigens inside cells and tissues. So, ISH and ICC are gold standards for studying biomarkers in their location in tissues. The combination of those

two techniques can overcome the limitations related to a single ISH or ICC method. Quantification of ISH/ICC corresponded closely to use of other semi-quantitative techniques, such as RT-qPCR and flow cytometry, although with additional benefits including the possibility to assess cell morphology, expression of both mRNA and protein in the same cell population in a single staining experiment, and information about the subcellular localization of a protein or transcript [512]. Notably, the RNAScope technology employs the double-Z target probe designs, pre-amplifications, and amplifications, and multiplex (multiple transcript) procedures for highly specific and sensitive detection of individual transcripts [513-515]. These methods further improve the already sensitive approaches by digoxigenin-labeled ISH [135].

The results of this study therefore confirm the dynamic nature of the TSC populations at the nerve terminal after injury. TSCs are closely connected to motor endplates and provide a “cap” that bridges the fiber and the nerve terminal, protects the extracellular environment at NMJs and moderates their function [493]. Following denervation, the morphology and populations of Schwann cells changes at the endplate region, as Schwann cells display the ability to revert from their mature phenotype to more immature, even phagocytic shape and function [339]. During this time, the modified morphology of the limited number of TSCs presents widespread formation Schwann-cell processes among adjacent motor endplates.

P75 NGFR is one of several molecules that have been examined in the distal nerve stump. The genes that encode for P75, cell adhesion molecules, NGF, epidermal growth factor (EGF), BDNF, and extracellular matrix proteins are all upregulated after nerve injury, and their later downregulation is associated with the establishment of reinnervation [506]. Poor regeneration of nerve axons after a long interval of denervation is generally accompanied by deterioration of denervated organs. However, there are reports that deterioration of the distal stumps, rather than the failure of denervated muscles themselves, to recover from denervation atrophy, can account for the reduced regenerative ability of long-term denervated muscles [516]. This failure to regenerate after long-term denervation may be due to the inability of the non-neural cells inside the distal nerve stumps to preserve their expression of growth proteins, such as those that would bind to P75NGFR.

One particularly interesting study compared changes in P75NGFR expression after short-term (1 week) vs. long-term (1–12 months) transection of the distal sciatic nerve [506]. Cell behaviour was examined using double immunocytochemistry for P75NGFR and the S100B

protein. That study revealed that P75NGFR immunoreactivity was confined to Schwann cells. Unfortunately, this study did not distinguish TSCs from other types of Schwann cell. Moreover, quantitative analysis of the *in situ* hybridization assays conducted by the same authors, revealed that the upregulation of P75NGFR mRNA after denervation, matched closely with the increased synthesis of the related P75 protein and reached a peak within 1 month after the nerve transection[506]. These findings were interpreted by authors as indicating that, based on the expression of P75NGFR, Schwann cells provide a most suitable environment for the regenerating axons up to the first month after nerve transection, by guiding nerve terminal extensions by growth cones, toward the distal nerve stump and ultimately, an NMJ region. However, at later stages of reinnervation following denervation, the capability of Schwann cells to generate P75 NGFR and cell adhesion proteins such as N-CAM actually decreases. This was considered as one of the possible features that reduce functional recovery after long-term denervation, if regenerating axons reach the distal stump too late to find the necessary composition of N-CAM and P75 NGFR needed to sustain the guidance function toward the target NMJs and myofibers [506].

In the current study, the RNA intensity of the TSC marker P75 NGFR was stronger at week 3 (day 21) after sciatic nerve crush and at 5 weeks (day 35) after muscle-crush injury than in their respective control groups, a result that may be related to migration of TSCs as well as expressing more P75 per cell. Reduced expression of S100B protein at day 14 after nerve crush and day 21 after muscle-crush injury could be due to the migration of TSCs from denervated NMJ regions, cell death among TSCs or a complete lack of S100B promoter activity [344].

The upregulation of P75 is known to occur with cellular proliferation during Wallerian degeneration [500]. Another study [423] used a double-fluorescent transgenic mouse to demonstrate regenerating axons (thy1-CFP) and migrating Schwann cells (S100-GFP) as they grew through an acellular nerve graft that bridged a transected sciatic nerve. In that study, entire motor endplates were denervated, whereas axons were preserved for 1 week during Wallerian degeneration one week after sciatic nerve crush. Also shown in that study, GFP intensity representing S100 over-expression was diminished in TSCs at 2 weeks following nerve-crush injury (similar to results of the present study), suggesting that TSCs may have dedifferentiated into a more immature phenotype that did not express S100B as intensely as in controls. The decrease in the intensity of expression by Schwann cells, 2 weeks after nerve-crush injury in that study, corresponded to muscle denervation and Schwann cell dedifferentiation into a hyperinnervation

phenotype at three and four weeks after nerve-crush injury. The timing of the current findings at 21 and 35 days after nerve-crush injury is consistent with the timing and features of S100 expression in the earlier study [423].

TSCs are known to play several roles and are important for the long-term maintenance, development and repair of synaptic construction and function at the adult NMJ [316]. The distance from the area of a nerve-crush to the relevant motor endplates, and consequently the amount of time needed for the reinnervation process may be a factor in data variations [423]. After nerve-crush injury and consequent muscle denervation, nerve terminals degenerate and TSCs spread processes to guide the regeneration of axons and fill the primary synaptic-cleft areas. Also, shortly after denervation, inactive myofibers release factors such as neural adhesion molecules and neurotrophins which diffuse over long distances to reach regenerating axons as they approach the fiber.

For example, Marques and colleagues [517] showed that TSC processes develop a widespread network away from the motor endplates by day 16 after nerve injury, to orientate regenerated axons. My findings for nerve-crush injury experiments displayed a decrease in the levels of S100B and *Sema3A* proteins occurred in the non-transgenic control, at day 14 which increased again at day 21.

Together with the increase in both S100B and *Sema3A* proteins at day 35 after muscle-crush injury, results of comparisons between knockdown transgenic and controls showed that the conditional knock-down of *Sema3A* expression in SCs accelerated the processes of both denervation and muscle degeneration seen after muscle-crush injury. The knockdown of *Sema3A* in SCs also accelerated the process of Wallerian degeneration seen in nerve-crush injury, compared to controls. The expression of *Sema3A*, *Sema3F* and their receptors neuropilin (NRP) 1 and NRP2 is stimulated during degeneration of axon distal stumps; this denervation-dependent stimulation illustrates the positive role of semaphorins and their receptors during Wallerian degeneration in peripheral nerves (affected by both muscle and nerve crush), since cells were prompted to increase expression in apparent compensation for the lack of SC-derived *Sema3A*. Since *Sema3A* also contributes to regulation of cell migration [348], loss of *Sema3A* would also be anticipated to affect both myogenic regeneration and reinnervation processes during recovery from both nerve- and muscle-crush injuries, although this was not examined in the experiments reported here.

In considering the PCs extracted from PCAs run on samples from Sema3A-knockout project (nerve-crush and muscle-crush injuries with Sema3A knockout transgenic mice), the colocalizing area in Pax7 PCA (representing the number or cytoplasmic extent of SCs) was more positively correlated (a stronger correlation) to the level of γ AchR-subunit protein than levels of Sema3A and S100B proteins. The positive correlations between the number, intensity and diameter measures of S100B, Sema3A and Pax7 suggest these variables are informative and usefully retained in analyses by PCA. On the other hand, in the PCA performed on the P75 colocalization variable, the positive correlations between the colocalizing area and the intensity of both Sema3A and S100B expression in the F1 dimension, shows the additional importance of variables regarding TSC markers in this study.

For PCAs on samples in this chapter, the horizontal axis (or F1) included all the variables related to intensity, diameter, and number of transcript expression sites, and also the protein expressions suggesting the value of these ISH/ICC variables for further investigation. Present results would also be practically applied in follow-up clinical applications such as use in tracking whether a particular therapy might accelerate the recovery process and increase the function of that recovery. The current findings also suggest the ISH technique could be used as a method for helping to predict the chance of successful recovery; for example, by studying the degree of involvement of particular molecular markers of TSCs and SCs such as P75 and Pax7, colocalized with S100B and Sema3A.

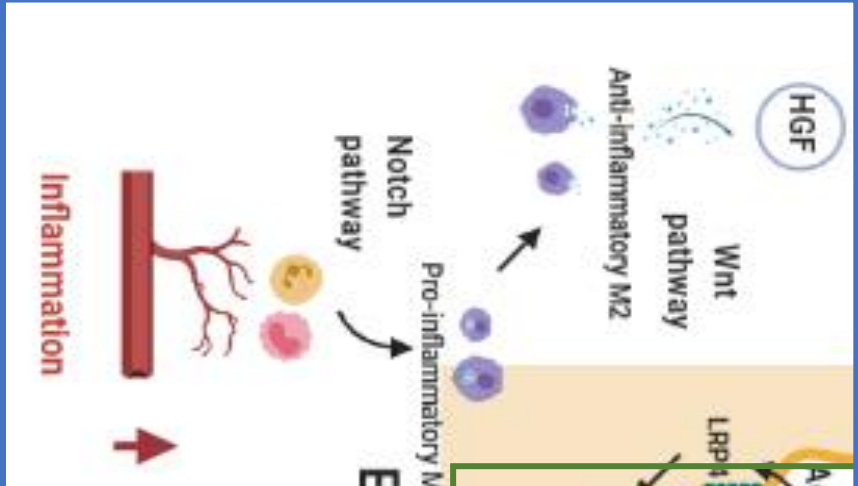
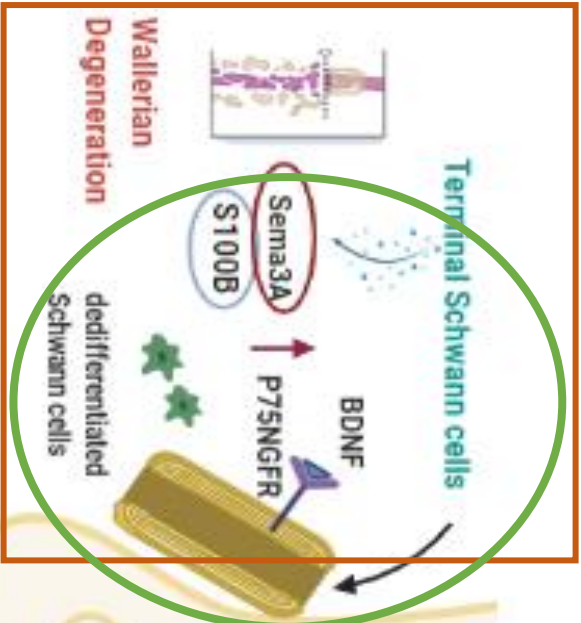
A longer study of recovery after the two types of surgery would have allowed use of information on functional recovery of skeletal muscle and NMJ reformation (with more variables assessed). That information could be provided, for example by measuring factors such as muscle contraction responsiveness and muscle mass. As a descriptive method, PCA is not a hypothesis-based statistical technique, and does not provide enough information on statistical significance on its own. Rather, PCA can be used as an aside to hypothesis-based analysis, since given the many variables that can theoretically affect every process, PCA is helpful in understanding the main sources of variation in a dataset. In the case of findings for nerve and muscle crush, the PCAs clearly showed the significance of S100B, P75, Pax7 and Sema3A expression during recovery responses and the colocalized expression of Sema3A with S100B and Pax7 in SCs during muscle regeneration in the samples from muscle-crush injury (with and without premature SC activation).

4 CONCLUDING DISCUSSION

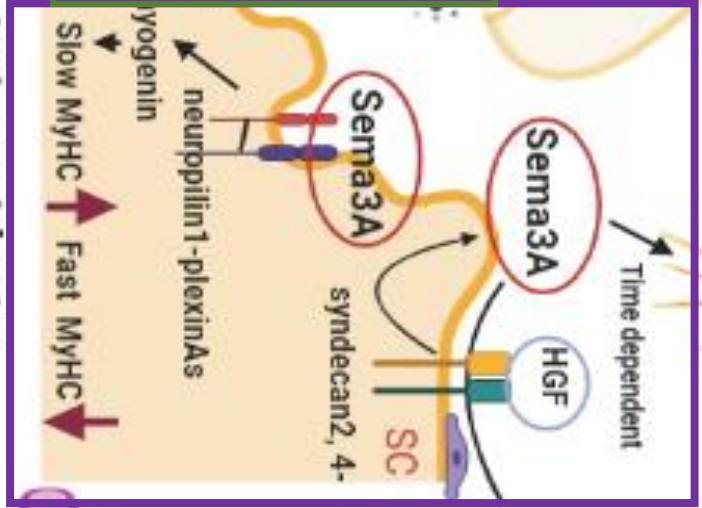
The main findings of this thesis research project can be summarized as follows.

1. TSCs are important in guiding motor axons to reconstitute NMJs in the region of original synapses after nerve injury.
2. NMJ patterns of neurites and AchE plaques, shown by silver-staining histochemistry, and colocalized distribution of pre- and post-synaptic NMJ specializations, were both immature after ISDN pretreatment to induce premature SC activation before muscle injury.
3. Concurrent effects of ISDN pretreatment on Sema3A-65 and S100B that differed between CTX and CR injuries, suggested that both the guidance by TSCs and the elongation of neurites may be affected by premature activation of SCs, and secondary effects on the multiple sources of Sema3A during NMJ restoration.
4. NMJ regions matured earlier after CTX than after CR injury, including AchE plaques, AchR configuration, neurite branching, and colocalization of pre- and post-synaptic structures, likely due to injury-related changes that are distinct from those induced by a traumatic injury by muscle crush.
5. Pretreatment by ISDN also decreased NMJ maturation during myogenic repair in both models, especially after CR injury.
6. Differential effects of the type of muscle injury on S100B protein, implicated both TSCs and SCs in the spatiotemporal synchrony of NMJ/synaptic remodeling and myogenic repair.
7. P75NGFR mRNA expression in muscle was increased in the Sema3A-knockout at day 21 after nerve injury compared to P75 expression in both the non-knockout and no-surgery control groups, so the state of SCs (activated or not at the time on injury) the expression of Sema3A by SCs and the type of injury all affect the number of TSCs and their expression features, as well as NMJ restoration and their timing.

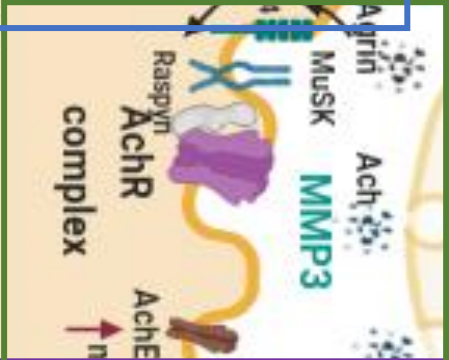
8. The consistent expression of Sema3A between Sema3A-knockout groups and their controls over time, showed the role of Sema3A expression from non-SC sources at the postsynaptic area to guide axons during reinnervation.
9. The higher expression of γ AchR at day 21 in the Sema3A knockout transgenic mice after muscle-crush injury compared to the no-surgery Sema3A-knockout group, showed that denervation is greatest at that time.
10. The knockdown of Sema3A in SCs accelerated the process of Wallerian degeneration seen in nerve-crush injury, compared to controls.
11. PCA analyses showed the importance of SC-derived Sema3A in TSC activities related to Wallerian degeneration after nerve-crush injury and reinnervation patterns of gene/protein expression during NMJ regrowth after muscle-crush injury.



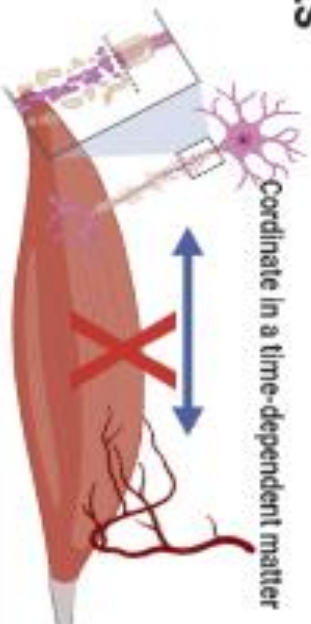
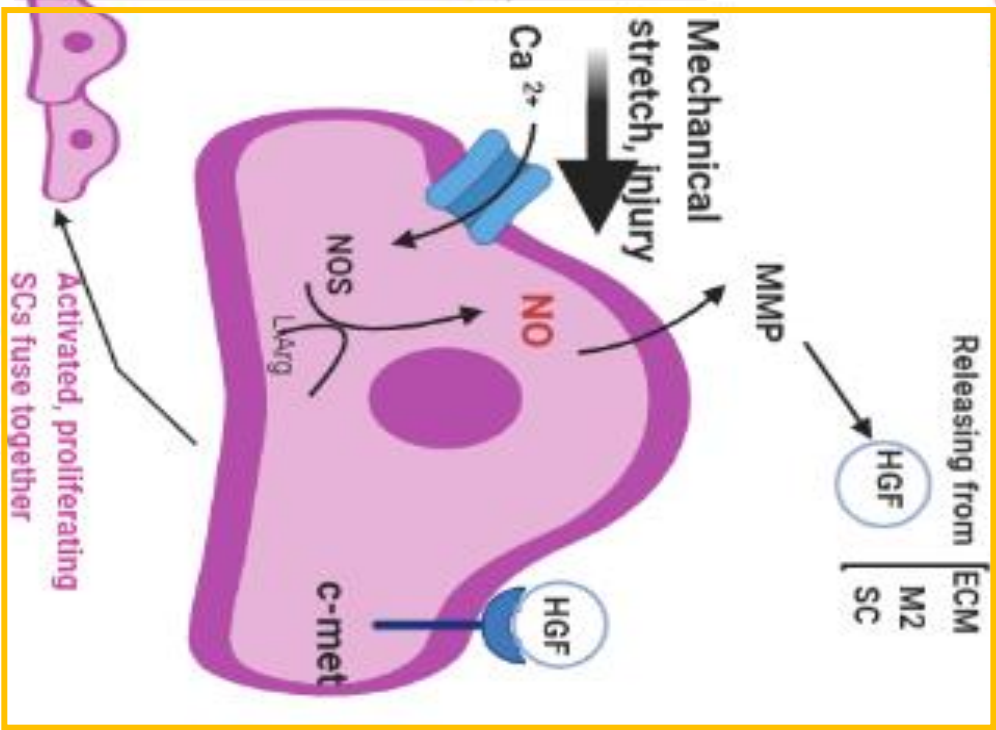
Repelling motor neurite axon terminals



Early-differentiated myoblasts



Upregulated angiogenesis
Blood capillaries for oxygen & Fatty acids



Schematic representation of changes in NMJ involvement during real steps in muscle regeneration. A muscle injury contains damages to motor neuron branches and the loss of the integrity of the basal lamina and sarcolemma. Injury models indicate distinct diversities in the levels of degeneration and regeneration chapters, related to the nature, timing and/or extent of each of the damage, the immune response, and the need for nerve and vessel formation. Injuries crush the myofiber sarcolemma and cause an interruption of the calcium equilibrium; this initiates the degeneration in an injured muscle. After mechanical or injury-induced signals, an increase in intracellular calcium ions, triggers the generation of Nitric oxide (NO) by NO synthase (NOS). The burst of NO into the ECM causes the activation of matrix metalloproteinases (MMP), which prompts the release of HGF from the ECM. HGF is able to stimulate SC activation and inhibit muscle differentiation through binding to its receptor, c-Met. The shift from SC proliferation to differentiation is regulated by Wnt and Notch signaling. Notch signaling is prevalent during the proliferation phase while Wnt signaling is activated throughout the differentiation phase (yellow rectangle). HGF also induces the secretion of Semaphorin 3A from activated SCs via HGF/syndecan2, 4-dependent pathway. Semaphorin 3A upregulation by HGF, peaks in early differentiation phase and mediate the timing of axons ingrowth to regenerating myofibers. Semaphorin 3A perform via the neuropilin2-plexinA3- myogenin pathway, which is especially active in slow muscle and promote fast-MyHC expression while suppress fast-MyHC expression (purple rectangle, the SC activation and Semaphorin 3A generation and their effect on the structures in the niche were investigated in chapter 1). Semaphorin 3A is anti-angiogenic and prevents the activity of integrin in vessel formation receptor. It is also an agonist of neuropilin-1 and its secretion repels endothelial cells and functions to decrease endothelial cell survival through preventing the activity of VEGF. Angiogenesis is organized in a time-dependent way via Semaphorin 3A expression that increases and decreases throughout muscle regeneration. MMP3 activity also causes the cleavage of agrin and therefore the removal of unstable AchRs. Such mechanisms could play a role to the transition of the endplate into a pretzel-like structure, and are consistent with the shift of PSCs from a 'fried-egg' morphology to a branched shape throughout postnatal development (green square). BDNF is initially

synthesized as its precursor form (pro-BDNF), which is then cleaved to produce the mature form (mBDNF). The conversion from pro-BDNF to mBDNF is regulated by synaptic MMP3 and the activity of motor neurons and influence presynaptic maturation. The pro-BDNF promotes synapse elimination via various receptor interactions, while mBDNF favours the maintenance of synapses (green circle). At the same time as muscle reformation, scar tissue after repair of the connective tissues in the muscle, develops connections among the residual functional myofibers. In less severe injuries, this tissue scar acts like a channel or scaffold that can assist myofiber formation. In more severe injuries, the tissue scar is large, and its maturation can block migration of the myoblasts, vascular endothelial cells, and axons that are required for effective regeneration. Inflammation is triggered by cytokines that are released from the myofiber following a alteration in the sarcolemma. During muscle degeneration, injured and necrotic myofibers are degraded and primarily removed by immune cells such as monocytes and neutrophils. Monocytes differentiate into pro-inflammatory macrophages (M1) after they infiltrate the injured region from residence in non-injured tissue. Another group of monocytes travel into the interstitium (endocrine system) and differentiates into anti-inflammatory (M2) macrophages and secrete growth factors including HGF. The HGF released from M2 macrophages also plays a role in stimulating SCs proliferation and early differentiation to generate Sema3A (blue square). The NMJ exhibits a pretzel-like structure which comprised a presynaptic motor nerve terminals, postsynaptic endplates in the membrane of myofibers, The ECM in the synaptic cleft and terminal Schwann cells (TSCs), which cap the nerve-muscle junctions. TSCs have a key role in the maintenance of configuration, function and remodeling of NMJs as well as NMJ development during embryogenesis. Wallerian degeneration occurs after axonal injury and contains many issues such as an increase in the permeability of blood vessels; the degeneration of the distal axon; the dedifferentiation and proliferation of Schwann cells, the engagement of macrophages; and the restructuring of the ECM. The general purpose of all of these actions is to create an innervation-permissive environment to allow regenerated axons to reinnervate the muscle endplate as soon as Wallerian degeneration is finished. During reinnervation, the sprouts of TSCs lead motor neurite terminals through bridges or escaped fibers. These processes present a substrate that directs regenerating axons to vacant synaptic areas and guides them to develop beyond

these spots. TSCs reacting to denervation gradually leave parts of the synaptic area and some of these abandoned areas are never reinnervated. The lack of reinnervation of these areas and the reinnervation of other sites conducts lossing AChRs at the unreinnervated areas. Therefore, a significant portion of the remodeling of synaptic areas is correlated with alterations in SC coverage of synaptic areas throughout denervation (brown square). During nerve retraction, TSCs on fast-twitch myofibers express Sema3A and S100B. TSCs also upregulate several proteins engaged in cell structure and cell junctions such as low-affinity p75NTR. An upregulation in P75NGFR can be used as an indicator of Schwann cell sensitivity to the injury and is important for the re-myelination of regenerating axons. The absence of p75NTR decreases apoptosis of the proliferating Schwann cell during Wallerian degeneration. The p75NTR is also essential for motoneuronal survival during development, but p75NTR expression post injury prevent motor axonal regeneration. TSCs not only support the growth of nerve terminal, but also inhibit nerve terminal plasticity at specific NMJs through secreting a Sema3A chemorepulsive proteins. Therefore, downregulation of p75NTR is required for guiding myogenic cells towards terminal differentiation (green circle, which are assessed and discussed in chapters 3 and 4 of this thesis).

This research is significant because the complex interaction between TSCs and SCs during the response to muscle or nerve injury, and during muscle growth, muscle development, and genetic diseases affecting muscle and/or nerve, is a new area of study, despite the close proximity of TSCs and SCs at NMJs. This project aimed to integrate fields of research on muscle biology and neurobiology; in the long term, the goal is that results may have applications as broad as muscle growth (e.g., in aging or meat production) and advancing our understanding of different neurodegenerative disorders such as spinal muscular atrophy [518]. Additional importance could be derived from the potential to help prevent serious medical conditions such as progressive and debilitating changes in age-related atrophy (sarcopenia). By understanding the timing, the sequence, and the extent of regeneration, and the reconnection of NMJs on fibers with innervating neurites, we will be better able to address questions about the role of many factors that contribute to the regeneration of these tissues and muscle reinnervation. These advances have potential to help in finding new approaches to understand and possibly reduce the lethal impact of declining nerve-muscle interactions in neuromuscular disease conditions such as amyotrophic lateral sclerosis.

The present study addressed important questions related to the role of TSCs in restoring NMJs and reinnervation. One major, as yet unsolved issue, is the lack of genes that could be used as unique markers for TSCs and their function, since many potential markers are not specifically or solely expressed in TSCs. However, current research evaluated the expression of Schwann cell markers that are relatively specific and additionally, combined that evaluation with studies of Sema3A expression by both or either skeletal muscle SCs and TSCs in fast-twitch TA muscle. Experiments were designed to study TSC expression during regeneration and reinnervation in two different models of injury, nerve and muscle crush. Further insight into screens of genetic or molecular markers for NMJ defects, and monoclonal antibody screens for proteins unique to TSCs could provide additional useful methods for selectively manipulating TSCs. Those experiments would have even better potential to advance our understanding of the pre-synaptic and post-synaptic interactions of TSCs and satellite cells *in vitro* and *in vivo*. Moreover, experiments to measure the conduction velocity of motor nerves, quantify Ach release from motor nerve terminals using electrophysiological techniques, and/or use approaches with micro-dialysis and high-pressure liquid chromatography (HPLC) methods to collect samples from specific regions of a

muscle-NMJ complex (for instance using vital imaging or co-culture systems) would be very useful for verifying the functional adjustments of motor nerves after injuries such as muscle crush and nerve crush.

This thesis project was aimed to study the involvement of *Sema3A* expression by TSCs and SCs in reinnervation of motor endplate regions following traumatic muscle and nerve injuries. Here, I report findings related to the timing and extent of axonal reinnervation, SC activities in myogenic regeneration, and the expression of available markers for TSCs, such as S100B and P75 NGFR expression during NMJ reformation regeneration in the PNS. These molecular studies have encouraged further interest in investigating the role of *Sema3A* in motor-axon pathfinding and in finding new ways to identify how the modifications in molecular signaling at the post-synaptic area influence reinnervation in nerve and muscle injuries and the survival and growth of myofibers regenerating from muscle damage.

Further experiments such as the combination of BTX staining for post-synaptic AchRs, silver staining histochemistry for pre-synaptic neurite branches and AchE plaques, and morphometry at the histological (or ultrastructural) level, comparing those features in the *Sema3A*-knockout transgenic mice with no-surgery and non-knockout controls, would further advance our understanding of the overall role of SC-derived *Sema3A* in muscle regeneration and myofiber reinnervation. However, the differences between SC-specific knockout transgenic mice and their controls shown by ISH and PCA analyses, showed the importance of SC-derived *Sema3A*, in TSC activities related to Wallerian degeneration (after nerve-crush injury) and reinnervation patterns of gene/protein expression during NMJ regrowth (after muscle-crush injury). Unfortunately, it was not possible to include a cardiotoxin-injury group of transgenic mice, with and without pretreatment with ISDN in this research. If preactivation of non-*Sema3A*-expressing SCs before muscle injury was found to accelerate the peak of *Sema3A* synthesis, that treatment approach could be a potential way to manipulate the timing of re-innervation after muscle damage. It is possible that such manipulation might enable muscle regeneration to advance further before reinnervation occurs, to improve the outcome of overall tissue repair from traumatic injury.

The NMJ structures are remarkably stable in young animals (1–12 months old), [308]; however, these synapses in muscle change dramatically under several circumstances including early development [519], aging, [520, 521] and reinnervation [258]. When motoneurons are disconnected from their myofibers by damage to a peripheral nerve, they frequently sprout and

reconnect with myofibers by following Schwann-cell endoneurial tubes that they occupied earlier [312]. Terminal Schwann cells extend away from the old synaptic site during denervation [328], and supply a substrate that guides re-growing axons to synaptic sites that are vacant of innervation [259]. These findings show that a considerable portion of the remodeling of synaptic sites depends on changes in TSCs during denervation. Major questions that remain after analysis of my results relate to how synaptic remodeling relates to effects of the loss of cellular components such as terminal Schwann cells and postsynaptic AchRs. The answers to these questions about the structural changes at synaptic sites and the stability of the synaptic connection during reinnervation await future research.

Despite the fact that some research has been done on the influence of motor innervation on the regeneration capacity of injured myofibers, the effects of muscle injury itself, on its own innervation has been neglected. This neglect may be related to the complexity of separating the trauma (crushing) of myofibers from the accompanying damage it does to axons and NMJs. Thus, it was of interest to earlier authors, to examine whether cardiotoxin had any effect on axon terminals. Chang and Lee [522] reported that the cardiotoxin from *Naja naja atra* venom caused loss of conduction in the axon terminals and muscle depolarization. Results in that report demonstrated that some degree of axonal depolarization may occur in what is typically understood to be a solely myotoxic injury (only to myofibers). Other experiments indicated that the cardiotoxin does selective damage to myofibers and leaves their motor innervation intact, while showing how secondary morphological abnormalities in motor end-plates may progress because of a primary lesion of the myofibers after cardiotoxin damage [523]. Except for the Chang and Lee report, the repair of muscle has not been examined separately from nerve repair after cardiotoxin injury. My research therefore, revisited reports of damage by CTX and support the early results of Couteaux and colleagues [296].

This research thus, separated SCs driving Sema3A from TSCs or other cell sources, as an important aspect of the process of reinnervation and muscle regeneration. Pre-activation by ISDN was a nonspecific way of approaching the aim to change the timing of NMJ restoration via changes in Sema3A. The use of the SC-specific Sema3A-knockout transgenics allowed further dissection of the importance of SC-derived Sema3A from production of Sema3A by TSCs at the same nerve-muscle junctions. Changes in Sema3A production by SCs, the stem cells in skeletal muscle,

changed the timing of muscle regeneration by manipulating SC proliferation behavior, and myogenesis, and likely also affected production of *Sema3A* by other sources, since the timing of nerve retraction was also delayed by premature SC activation.

Different procedures in the experiments reported here, may have provided variance in the current dataset, such as: the variability of sampling across mice (e.g., dissecting the whole TA muscle in Japan experiments and a longitudinally bisected TA), the injections of CTX (into the muscle) and TMX (to induce conditional knockdown of *Sema3A* or in no-surgery transgenic controls), and selective study of the injury site (showing myotube formation) in crushed muscles. These procedures may have influenced whether additional or different changes between injured and control muscles could have been detected but were not identified by the PCAs that were performed in this research.

4.1 Future research

The detailed timing of NMJ restoration in CTX, muscle-crush, and nerve-crush injuries, with and without *Sema3A* expression by muscle SCs, still requires further investigation. In life, injuries to muscle may occur from surgical treatment or accidental trauma. Such injuries and trauma carry a massive social and financial burden, including costs related to decreased productivity, co-morbidities, disability and premature death. Therefore, further collaborative research using cell and molecular, clinical and epidemiological approaches are needed to challenge and address these important quality-of-life issues, with the aim to develop innovative procedures, upgrade the healing process and modify social policy.

Even though my research did not have access to facilities that would enable physiology studies as part of this project, measures of conduction and contractility during the injury-recovery processes (regeneration of fibers and reinnervation of their NMJs) would be important in following up on the results reported in this thesis project. Further exploration of different models of injury, and studies of SC and TSC behavior and expression at additional time points (both shorter and longer-term after injury) will help to determine the impact of SCs production of *Sema3A*, and the apparent attempt by SCs from SC-specific *Sema3A*-knockout muscle to compensate for their deficient production of the chemorepellent. Further insight into genetic screens for NMJ defects, monoclonal antibody screens for TSC factors and Schwann-cell lineage would provide useful

methods for selectively manipulating TSCs and thereby adding to our knowledge of pre- and post-synaptic interactions *in vivo*. As noted above, measuring conduction velocity of motor nerves and Ach release from motor nerve terminals using the electrophysiological techniques and microdialysis/HPLC methods, respectively, would be useful in verifying the functional adjustments of motor nerves after injury.

As always seems the case in research, further investigation is now needed to explore the impact of reinnervation specificity and different neuro-regenerative therapies on SCs and TSCs, and the pattern of Schwann-cell differentiation after disruptive injuries to nerve axons and myofibers. Such work will continue to expand our knowledge of Schwann cell function in muscle regeneration and the functional restoration of nerve supply during muscle growth in development and repair. Application of this information could also be extended to applications in meat production and conditions that affect muscle innervation and atrophy, such as amyotrophic lateral sclerosis and aging.

5 REFERENCES

1. Ostrovidov, S., et al., *Skeletal muscle tissue engineering: methods to form skeletal myotubes and their applications*. Tissue Engineering Part B: Reviews, 2014. **20**(5): p. 403-436.
2. Seene, T., P. Kaasik, and E.-M. Riso, *Review on aging, unloading and reloading: changes in skeletal muscle quantity and quality*. Archives of gerontology and geriatrics, 2012. **54**(2): p. 374-380.
3. Clark, J., *Tendons, ligaments, and capsule of the rotator cuff*. *Gross and microscopic anatomy*. The Journal of bone and joint surgery. American volume, 1992. **74**(5): p. 713-725.
4. Allen, D.L., et al., *Cardiac and skeletal muscle adaptations to voluntary wheel running in the mouse*. J.Appl.Physiol, 2001. **90**(5): p. 1900-1908.
5. Bittner, R.E., et al., *Recruitment of bone-marrow-derived cells by skeletal and cardiac muscle in adult dystrophic mdx mice*. Anatomy and embryology, 1999. **199**(5): p. 391-396.
6. Duxson, M., J. Ross, and A. Harris, *Transfer of differentiated synaptic terminals from primary myotubes to new-formed muscle cells during embryonic development in the rat*. Neuroscience letters, 1986. **71**(2): p. 147-152.
7. Denetclaw, W. and C.P. Ordahl, *The growth of the dermomyotome and formation of early myotome lineages in thoracolumbar somites of chicken embryos*. Development, 2000. **127**(4): p. 893-905.
8. Zierath, J.R. and J.A. Hawley, *Skeletal muscle fiber type: influence on contractile and metabolic properties*. PLoS biology, 2004. **2**(10): p. e348.
9. MacIntosh, B.R., P.F. Gardiner, and A.J. McComas, *Skeletal muscle: form and function*. Vol. 2nd. 2006, Champaign, IL: Human Kinetics. 1-423.
10. Butler-Browne, G.S., D. Herlicoviez, and R.G. Whalen, *Effects of hypothyroidism on myosin isozyme transitions in developing rat muscle*. FEBS letters, 1984. **166**(1): p. 71-75.
11. Soukup, T. and V. Smerdu, *Effect of altered innervation and thyroid hormones on myosin heavy chain expression and fiber type transitions: a mini-review*. Histochemistry and cell biology, 2015. **143**(2): p. 123-130.
12. Bottinelli, R. and C. Reggiani, *Human skeletal muscle fibres: molecular and functional diversity*. Progress in biophysics and molecular biology, 2000. **73**(2): p. 195-262.
13. Schiaffino, S. and T. Partridge, *Skeletal muscle repair and regeneration*. Vol. 3. 2008: Springer Science & Business Media.
14. Borg, T.K. and J.B. Caulfield, *Morphology of connective tissue in skeletal muscle*. Tissue and Cell, 1980. **12**(1): p. 197-207.
15. Mukund, K. and S. Subramaniam, *Skeletal muscle: A review of molecular structure and function, in health and disease*. Wiley Interdisciplinary Reviews: Systems Biology and Medicine, 2020. **12**(1): p. e1462.
16. Laing, N.G. and K.J. Nowak, *When contractile proteins go bad: the sarcomere and skeletal muscle disease*. Bioessays, 2005. **27**(8): p. 809-822.
17. Ervasti, J.M., *Dystrophin, its interactions with other proteins, and implications for muscular dystrophy*. Biochim.Biophys.Acta, 2007. **1772**(2): p. 108-117.
18. Le Rumeur, E., S.J. Winder, and J.-F. Hubert, *Dystrophin: more than just the sum of its parts*. Biochimica et Biophysica Acta (BBA)-Proteins and Proteomics, 2010. **1804**(9): p. 1713-1722.
19. Gumerson, J.D. and D.E. Michele, *The dystrophin-glycoprotein complex in the prevention of muscle damage*. BioMed Research International, 2011. **2011**.

20. Petrof, B.J., et al., *Dystrophin protects the sarcolemma from stresses developed during muscle contraction*. Proceedings of the National Academy of Sciences, 1993. **90**(8): p. 3710-3714.
21. Wozniak, A.C. and J.E. Anderson, *The dynamics of the nitric oxide release-transient from stretched muscle cells*. Int.J.Biochem.Cell Biol., 2009. **41**(3): p. 625-631.
22. Grozdanovic, Z. and H.G. Baumgarten, *Nitric oxide synthase in skeletal muscle fibers: a signaling component of the dystrophin-glycoprotein complex*. Histol.Histopathol., 1999. **14**(1): p. 243-256.
23. Anderson, J.E., *A role for nitric oxide in muscle repair: nitric oxide-mediated activation of muscle satellite cells*. Mol.Biol.Cell, 2000. **11**(5): p. 1859-1874.
24. Anderson, J.E. and A.C. Wozniak, *Satellite cell activation on fibers: modeling events in vivo - an invited review*. Can J Physiol Pharmacol, 2004. **82**(5): p. 300-310.
25. Wozniak, A.C. and J.E. Anderson, *Single-fiber isolation and maintenance of satellite cell quiescence*. Biochem.Cell Biol., 2005. **83**(5): p. 674-676.
26. Wozniak, A.C., et al., *C-met expression and mechanical activation of satellite cells on cultured muscle fibers*. J.Histochem.Cytochem., 2003. **51**(11): p. 1437-1445.
27. Wozniak, A.C. and J.E. Anderson, *Nitric oxide-dependence of satellite stem cell activation and quiescence on normal skeletal muscle fibers*. Dev.Dyn., 2007. **236**(1): p. 240-250.
28. Braun, T., et al., *MyoD expression marks the onset of skeletal myogenesis in Myf-5 mutant mice*. Development, 1994. **120**(11): p. 3083-3092.
29. Olson, E., et al., *Know your neighbors: three phenotypes in null mutants of the myogenic bHLH gene MRF4*. Cell, 1996. **85**(1): p. 1-4.
30. Rudnicki, M.A., et al., *MyoD or Myf-5 is required for the formation of skeletal muscle*. Cell, 1993. **75**(7): p. 1351-1359.
31. Patapoutian, A., et al., *Disruption of the mouse MRF4 gene identifies multiple waves of myogenesis in the myotome*. Development, 1995. **121**(10): p. 3347-3358.
32. Rudnicki, M.A. and R. Jaenisch, *The MyoD family of transcription factors and skeletal myogenesis*. Bioessays, 1995. **17**(3): p. 203-209.
33. Buckingham, M., *Skeletal muscle formation in vertebrates*. Current opinion in genetics & development, 2001. **11**(4): p. 440-448.
34. Olson, E.N., et al., *Molecular control of myogenesis: antagonism between growth and differentiation*, in *Molecular Mechanisms of Cellular Growth*. 1991, Springer. p. 7-13.
35. Burke, R.E., *Motor Units: Anatomy, Physiology and Functional Organization*, in *Comprehensive Physiology*, V.B. Brookhart, V.B. Mountcastle, and V.B. Brooks, Editors. 2011, American Physiological Society: Bethesda, MD. p. 345-422.
36. Buller, A.J., J.C. Eccles, and R.M. Eccles, *Interactions between motoneurons and muscles in respect of the characteristic speeds of their responses*. J.Physiol, 1960. **150**: p. 417-439.
37. Navarrette, R. and G. Vrbova, *Activity-dependent interactions between motoneurons and muscles: their role in the development of the motor unit*. Prog.Neurobiol., 1993. **41**(1): p. 93-124.
38. Ontell, M., *Evidence for myoblastic potential of satellite cells in denervated muscle*. Cell Tissue Res., 1975. **160**(3): p. 345-353.
39. Washabaugh, C.H., et al., *Role of the nerve in determining fetal skeletal muscle phenotype*. Dev.Dyn., 1998. **211**(2): p. 177-190.
40. Ishikawa, H., H. Sawada, and E. Yamada, *Surface and internal morphology of skeletal muscle*, in *Skeletal Muscle, Section 10*, L.D. Peachey, Editor. 1983, American Physiological Society: Bethesda. p. 1-21.
41. Buller, A., J. Eccles, and R.M. Eccles, *Interactions between motoneurons and muscles in respect of the characteristic speeds of their responses*. The Journal of physiology, 1960. **150**(2): p. 417-439.

42. Mars, T., et al., *Functional innervation of cultured human skeletal muscle proceeds by two modes with regard to agrin effects*. Neuroscience, 2003. **118**(1): p. 87-97.
43. Fong, P., et al., *Increased activity of calcium leak channels in myotubes of Duchenne human and mdx mouse origin*. Science, 1990. **250**(4981): p. 673-676.
44. Alderton, J.M. and R.A. Steinhardt, *Calcium influx through calcium leak channels is responsible for the elevated levels of calcium-dependent proteolysis in dystrophic myotubes*. Journal of Biological Chemistry, 2000. **275**(13): p. 9452-9460.
45. Yin, H., F. Price, and M.A. Rudnicki, *Satellite cells and the muscle stem cell niche*. Physiological reviews, 2013. **93**(1): p. 23-67.
46. Huxley, H., *The mechanism of muscular contraction*. Science, 1969. **164**(3886): p. 1356-1366.
47. Tidball, J.G. and T.L. Daniel, *Myotendinous junctions of tonic muscle cells: structure and loading*. Cell and tissue research, 1986. **245**(2): p. 315-322.
48. Bugera, E.M., et al., *The systemic myokine response of decorin, interleukin-6 (IL-6) and interleukin-15 (IL-15) to an acute bout of blood flow restricted exercise*. European Journal of Applied Physiology, 2018. **118**(12): p. 2679-2686.
49. Cornish, S.M. and S.T. Johnson, *Systemic cytokine response to three bouts of eccentric exercise*. Results in immunology, 2014. **4**: p. 23-29.
50. Ryall, J.G., J.D. Schertzer, and G.S. Lynch, *Cellular and molecular mechanisms underlying age-related skeletal muscle wasting and weakness*. Biogerontology., 2008. **9**(4): p. 213-228.
51. Yin, H., F. Price, and M.A. Rudnicki, *Satellite cells and the muscle stem cell niche*. Physiol Rev, 2013. **93**(1): p. 23-67.
52. Jiménez-Maldonado, A., et al., *Chronic exercise increases plasma brain-derived neurotrophic factor levels, pancreatic islet size, and insulin tolerance in a TrkB-dependent manner*. PLoS One, 2014. **9**(12): p. e115177.
53. Delezie, J. and C. Handschin, *Endocrine crosstalk between skeletal muscle and the brain*. Frontiers in neurology, 2018. **9**: p. 698.
54. McIntosh, L.M., A.N. Pernitsky, and J.E. Anderson, *The effects of altered metabolism (hypothyroidism) on muscle repair in the mdx dystrophic mouse*. Muscle Nerve, 1994. **17**(4): p. 444-453.
55. Standring, S., et al., *Gray's anatomy: the anatomical basis of clinical practice*. American journal of neuroradiology, 2005. **26**(10): p. 2703.
56. Slaughter, K., H. Li, and A.J. Sokoloff, *Neuromuscular organization of the superior longitudinalis muscle in the human tongue. 1. Motor endplate morphology and muscle fiber architecture*. Cells Tissues Organs, 2005. **181**(1): p. 51-64.
57. Figeac, N., *Satellite cells delivered in their niche efficiently generate functional myotubes in three-dimensional cell culture*. 2018.
58. Hawke, T.J. and D.J. Garry, *Myogenic satellite cells: physiology to molecular biology*. J.Appl.Physiol, 2001. **91**(2): p. 534-551.
59. Forcina, L., et al., *An overview about the biology of skeletal muscle satellite cells*. Current genomics, 2019. **20**(1): p. 24-37.
60. Song, T. and S. Sadayappan, *Featured characteristics and pivotal roles of satellite cells in skeletal muscle regeneration*. Journal of muscle research and cell motility, 2019: p. 1-13.
61. Chen, B. and T. Shan, *The role of satellite and other functional cell types in muscle repair and regeneration*. Journal of muscle research and cell motility, 2019: p. 1-8.
62. Conboy, I.M. and T.A. Rando, *Heterochronic parabiosis for the study of the effects of aging on stem cells and their niches*. Cell cycle, 2012. **11**(12): p. 2260-2267.

63. Alway, S.E., M.J. Myers, and J.S. Mohamed, *Regulation of satellite cell function in sarcopenia*. *Frontiers in aging neuroscience*, 2014. **6**: p. 246.
64. Mashinchian, O., et al., *The muscle stem cell niche in health and disease*, in *Current topics in developmental biology*. 2018, Elsevier. p. 23-65.
65. Brack, A.S. and T.A. Rando, *Tissue-specific stem cells: lessons from the skeletal muscle satellite cell*. *Cell Stem Cell*, 2012. **10**(5): p. 504-14.
66. Perandini, L.A., et al., *Chronic inflammation in skeletal muscle impairs satellite cells function during regeneration: can physical exercise restore the satellite cell niche?* *The FEBS journal*, 2018. **285**(11): p. 1973-1984.
67. Velleman, S.G. and Y. Song, *Development and growth of the avian pectoralis major (breast) muscle: function of Syndecan-4 and Glypican-1 in adult myoblast proliferation and differentiation*. *Frontiers in physiology*, 2017. **8**: p. 577.
68. Riederer, I., et al., *Laminin therapy for the promotion of muscle regeneration*. *FEBS letters*, 2015. **589**(22): p. 3449-3453.
69. Morrissey, J.B., et al., *Biomechanical origins of muscle stem cell signal transduction*. *Journal of molecular biology*, 2016. **428**(7): p. 1441-1454.
70. Brancaccio, A. and D. Palacios, *Chromatin signaling in muscle stem cells: interpreting the regenerative microenvironment*. *Frontiers in aging neuroscience*, 2015. **7**: p. 36.
71. Parker, M.H., *The altered fate of aging satellite cells is determined by signaling and epigenetic changes*. *Frontiers in genetics*, 2015. **6**: p. 59.
72. Thomas, K., A.J. Engler, and G.A. Meyer, *Extracellular matrix regulation in the muscle satellite cell niche*. *Connective tissue research*, 2015. **56**(1): p. 1-8.
73. Bentzinger, C.F., et al., *Cellular dynamics in the muscle satellite cell niche*. *EMBO reports*, 2013. **14**(12): p. 1062-1072.
74. Mounier, R., F. Chretien, and B. Chazaud, *Blood vessels and the satellite cell niche*, in *Current topics in developmental biology*. 2011, Elsevier. p. 121-138.
75. Gopinath, S.D. and T.A. Rando, *Stem cell review series: aging of the skeletal muscle stem cell niche*. *Aging cell*, 2008. **7**(4): p. 590-598.
76. Snow, M.H., *Myogenic cell formation in regenerating rat skeletal muscle injured by mincing II. An autoradiographic study*. *The Anatomical Record*, 1977. **188**(2): p. 201-217.
77. Konigsberg, U.R., B.H. Lipton, and I.R. Konigsberg, *The regenerative response of single mature muscle fibers isolated in vitro*. *Developmental biology*, 1975. **45**(2): p. 260-275.
78. Bischoff, R., *A satellite cell mitogen from crushed adult muscle*. *Dev.Biol.*, 1986. **115**(1): p. 140-147.
79. Allen, R.E. and L.K. Boxhorn, *Regulation of skeletal muscle satellite cell proliferation and differentiation by transforming growth factor-beta, insulin-like growth factor I, and fibroblast growth factor*. *J.Cell Physiol*, 1989. **138**(2): p. 311-315.
80. Allen, R.E. and L.K. Boxhorn, *Inhibition of skeletal muscle satellite cell differentiation by transforming growth factor-beta*. *J.Cell Physiol*, 1987. **133**(3): p. 567-572.
81. Mulvaney, D., D. Marple, and R. Merkel, *Proliferation of skeletal muscle satellite cells after castration and administration of testosterone propionate*. *Proceedings of the society for experimental biology and medicine*, 1988. **188**(1): p. 40-45.
82. d'Albis, A., et al., *Regulation by thyroid hormones of terminal differentiation in the skeletal dorsal muscle: I. Neonate mouse*. *Developmental biology*, 1987. **123**(1): p. 25-32.
83. Jirmanová, I. and S. Thesleff, *Ultrastructural study of experimental muscle degeneration and regeneration in the adult rat*. *Zeitschrift für Zellforschung und mikroskopische Anatomie*, 1972. **131**(1): p. 77-97.

84. McGeachie, J.K. and M.D. Grounds, *Initiation and duration of muscle precursor replication after mild and severe injury to skeletal muscle of mice. An autoradiographic study.* Cell Tissue Res., 1987. **248**(1): p. 125-130.
85. Mauro, A., *Satellite cell of skeletal muscle fibers.* J.Biophys.Biochem.Cytology, 1961. **9** p. 493-495.
86. Yablonka-Reuveni, Z., *The skeletal muscle satellite cell: still young and fascinating at 50.* J.Histochem.Cytochem., 2011. **59**(12): p. 1041-1059.
87. Tajbakhsh, S., *Stem cells to tissue: molecular, cellular and anatomical heterogeneity in skeletal muscle.* Current opinion in genetics & development, 2003. **13**(4): p. 413-422.
88. Péault, B., et al., *Stem and progenitor cells in skeletal muscle development, maintenance, and therapy.* Molecular therapy, 2007. **15**(5): p. 867-877.
89. Beauchamp, J.R., et al., *Dynamics of myoblast transplantation reveal a discrete minority of precursors with stem cell-like properties as the myogenic source.* J.Cell Biol., 1999. **144**(6): p. 1113-1122.
90. Gibson, M.C. and E. Schultz, *The distribution of satellite cells and their relationship to specific fiber types in soleus and extensor digitorum longus muscles.* The Anatomical Record, 1982. **202**(3): p. 329-337.
91. Mackey, A.L., et al., *Assessment of satellite cell number and activity status in human skeletal muscle biopsies.* Muscle & Nerve: Official Journal of the American Association of Electrodiagnostic Medicine, 2009. **40**(3): p. 455-465.
92. Okada, S., I. Nonaka, and S. Chou, *Muscle fiber type differentiation and satellite cell populations in normally grown and neonatally denervated muscles in the rat.* Acta neuropathologica, 1984. **65**(2): p. 90-98.
93. Tidball, J.G., *Inflammatory cell response to acute muscle injury.* Medicine and science in sports and exercise, 1995. **27**(7): p. 1022-1032.
94. Folker, E. and M. Baylies, *Nuclear positioning in muscle development and disease.* Frontiers in physiology, 2013. **4**: p. 363.
95. Buttgereit, A., C. Weber, and O. Friedrich, *A novel quantitative morphometry approach to assess regeneration in dystrophic skeletal muscle.* Neuromuscular Disorders, 2014. **24**(7): p. 596-603.
96. González-Sánchez, J., et al., *Improvement of Duchenne muscular dystrophy phenotype following obestatin treatment.* Journal of cachexia, sarcopenia and muscle, 2018. **9**(6): p. 1063-1078.
97. Mancio, R.D., et al., *Dystrophic phenotype improvement in the diaphragm muscle of mdx mice by diacerhein.* PloS one, 2017. **12**(8).
98. Briguët, A., et al., *Histological parameters for the quantitative assessment of muscular dystrophy in the mdx-mouse.* Neuromuscul.Disord., 2004. **14**(10): p. 675-682.
99. van Velthoven, C.T. and T.A. Rando, *Stem cell quiescence: dynamism, restraint, and cellular idling.* Cell Stem Cell, 2019. **24**(2): p. 213-225.
100. Heslop, L., J.E. Morgan, and T.A. Partridge, *Evidence for a myogenic stem cell that is exhausted in dystrophic muscle.* J.Cell Sci., 2000. **113 (Pt 12)**: p. 2299-2308.
101. Day, K., et al., *The depletion of skeletal muscle satellite cells with age is concomitant with reduced capacity of single progenitors to produce reserve progeny.* Dev.Biol., 2010. **340**(2): p. 330-343.
102. Mourikis, P., et al., *A critical requirement for notch signaling in maintenance of the quiescent skeletal muscle stem cell state.* Stem cells, 2012. **30**(2): p. 243-252.
103. Brack, A.S., et al., *A temporal switch from notch to Wnt signaling in muscle stem cells is necessary for normal adult myogenesis.* Cell stem cell, 2008. **2**(1): p. 50-59.
104. Liu, L., et al., *Impaired notch signaling leads to a decrease in p53 activity and mitotic catastrophe in aged muscle stem cells.* Cell stem cell, 2018. **23**(4): p. 544-556. e4.

105. Rodgers, J.T., et al., *HGFA is an injury-regulated systemic factor that induces the transition of stem cells into GAlert*. Cell reports, 2017. **19**(3): p. 479-486.
106. Bischoff, R., *Interaction between satellite cells and skeletal muscle fibers*. Development, 1990. **109**(4): p. 943-952.
107. Jones, S.A., et al., *The soluble interleukin 6 receptor: mechanisms of production and implications in disease*. The FASEB Journal, 2001. **15**(1): p. 43-58.
108. Tatsumi, R., et al., *HGF/SF is present in normal adult skeletal muscle and is capable of activating satellite cells*. Dev.Biol., 1998. **194**(1): p. 114-128.
109. Wen, Y., et al., *Constitutive Notch activation upregulates Pax7 and promotes the self-renewal of skeletal muscle satellite cells*. Molecular and cellular biology, 2012. **32**(12): p. 2300-2311.
110. Bröhl, D., et al., *Colonization of the satellite cell niche by skeletal muscle progenitor cells depends on Notch signals*. Developmental cell, 2012. **23**(3): p. 469-481.
111. Watt, D.J., et al., *The movement of muscle precursor cells between adjacent regenerating muscles in the mouse*. Anat.Embryol.(Berl), 1987. **175**(4): p. 527-536.
112. Alfaro, L.A.S., et al., *CD34 promotes satellite cell motility and entry into proliferation to facilitate efficient skeletal muscle regeneration*. Stem cells, 2011. **29**(12): p. 2030-2041.
113. Stark, D.A., et al., *Eph/ephrin interactions modulate muscle satellite cell motility and patterning*. Development, 2011. **138**(24): p. 5279-5289.
114. Cornelison, D., et al., *MyoD^{-/-} satellite cells in single-fiber culture are differentiation defective and MRF4 deficient*. Developmental biology, 2000. **224**(2): p. 122-137.
115. Füchtbauer, E.M. and H. Westphal, *MyoD and myogenin are coexpressed in regenerating skeletal muscle of the mouse*. Developmental dynamics, 1992. **193**(1): p. 34-39.
116. Grounds, M.D., et al., *Identification of skeletal muscle precursor cells in vivo by use of MyoD1 and myogenin probes*. Cell Tissue Res., 1992. **267**(1): p. 99-104.
117. Cooper, R.N., et al., *In vivo satellite cell activation via Myf5 and MyoD in regenerating mouse skeletal muscle*. J.Cell Sci., 1999. **112 (Pt 17)**: p. 2895-2901.
118. Rantanen, J., et al., *Satellite cell proliferation and the expression of myogenin and desmin in regenerating skeletal muscle: evidence for two different populations of satellite cells*. Lab Invest, 1995. **72**(3): p. 341-347.
119. Zammit, P.S., et al., *Kinetics of myoblast proliferation show that resident satellite cells are competent to fully regenerate skeletal muscle fibers*. Experimental cell research, 2002. **281**(1): p. 39-49.
120. Cornelison, D.D. and B.J. Wold, *Single-cell analysis of regulatory gene expression in quiescent and activated mouse skeletal muscle satellite cells*. Dev.Biol., 1997. **191**(2): p. 270-283.
121. Megeney, L.A., et al., *MyoD is required for myogenic stem cell function in adult skeletal muscle*. Genes & development, 1996. **10**(10): p. 1173-1183.
122. Sabourin, L.A., et al., *Reduced differentiation potential of primary MyoD^{-/-} myogenic cells derived from adult skeletal muscle*. The Journal of cell biology, 1999. **144**(4): p. 631-643.
123. Gayraud-Morel, B., et al., *A role for the myogenic determination gene Myf5 in adult regenerative myogenesis*. Developmental biology, 2007. **312**(1): p. 13-28.
124. Rudnicki, M.A., et al., *The molecular regulation of muscle stem cell function*. Cold Spring Harb.Symp.Quant.Biol., 2008. **73**: p. 323-331.
125. Montarras, D., et al., *Cultured myf5 null and myoD null muscle precursor cells display distinct growth defects*. Biology of the Cell, 2000. **92**(8-9): p. 565-572.
126. Kitzmann, M., et al., *The muscle regulatory factors MyoD and myf-5 undergo distinct cell cycle-specific expression in muscle cells*. The Journal of cell biology, 1998. **142**(6): p. 1447-1459.

127. Day, K., et al., *Nestin-GFP reporter expression defines the quiescent state of skeletal muscle satellite cells*. Dev.Biol., 2007. **304**(1): p. 246-259.
128. Riuzzi, F., et al., *HMGB1–RAGE regulates muscle satellite cell homeostasis through p38-MAPK-and myogenin-dependent repression of Pax7 transcription*. J Cell Sci, 2012. **125**(6): p. 1440-1454.
129. Olguin, H.C., et al., *Reciprocal inhibition between Pax7 and muscle regulatory factors modulates myogenic cell fate determination*. J.Cell Biol., 2007. **177**(5): p. 769-779.
130. Cornelison, D.D., et al., *MyoD(-/-) satellite cells in single-fiber culture are differentiation defective and MRF4 deficient*. Dev.Biol., 2000. **224**(2): p. 122-137.
131. Grounds, M.D., et al., *Identification of skeletal muscle precursor cells in vivo by use of MyoD1 and myogenin probes*. Cell and tissue research, 1992. **267**(1): p. 99-104.
132. Smith, C.K., M.J. Janney, and R.E. Allen, *Temporal expression of myogenic regulatory genes during activation, proliferation, and differentiation of rat skeletal muscle satellite cells*. J.Cell Physiol, 1994. **159**(2): p. 379-385.
133. Cao, Y., et al., *Global and gene-specific analyses show distinct roles for Myod and Myog at a common set of promoters*. The EMBO journal, 2006. **25**(3): p. 502-511.
134. Benchaouir, R., et al., *Restoration of human dystrophin following transplantation of exon-skipping-engineered DMD patient stem cells into dystrophic mice*. Cell stem cell, 2007. **1**(6): p. 646-657.
135. Garrett, K.L. and J.E. Anderson, *Colocalization of bFGF and the myogenic regulatory gene myogenin in dystrophic mdx muscle precursors and young myotubes in vivo*. Dev.Biol., 1995. **169**(2): p. 596-608.
136. Li, L., et al., *Cyclic AMP-dependent protein kinase inhibits the activity of myogenic helix-loop-helix proteins*. Molecular and cellular biology, 1992. **12**(10): p. 4478-4485.
137. Benezra, R., et al., *The protein Id: a negative regulator of helix-loop-helix DNA binding proteins*. Cell, 1990. **61**(1): p. 49-59.
138. Spicer, D.B., et al., *Inhibition of myogenic bHLH and MEF2 transcription factors by the bHLH protein Twist*. Science, 1996. **272**(5267): p. 1476-1480.
139. Dey, B.K., J. Gagan, and A. Dutta, *miR-206 and-486 induce myoblast differentiation by downregulating Pax7*. Molecular and cellular biology, 2011. **31**(1): p. 203-214.
140. Chen, J.-F., et al., *microRNA-1 and microRNA-206 regulate skeletal muscle satellite cell proliferation and differentiation by repressing Pax7*. The Journal of cell biology, 2010. **190**(5): p. 867-879.
141. Yan, D., et al., *MicroRNA-1/206 targets c-Met and inhibits rhabdomyosarcoma development*. Journal of Biological Chemistry, 2009. **284**(43): p. 29596-29604.
142. Shen, X., et al., *Circular RNA profiling identified an abundant circular RNA circTMTTC1 that inhibits chicken skeletal muscle satellite cell differentiation by sponging miR-128-3p*. International journal of biological sciences, 2019. **15**(10): p. 2265.
143. Yue, B., et al., *Biogenesis and ceRNA role of circular RNAs in skeletal muscle myogenesis*. The International Journal of Biochemistry & Cell Biology, 2019. **117**: p. 105621.
144. Legnini, I., et al., *Circ-ZNF609 is a circular RNA that can be translated and functions in myogenesis*. Molecular cell, 2017. **66**(1): p. 22-37. e9.
145. Hong, L., et al., *Genome-wide analysis of circular RNAs mediated ceRNA regulation in porcine embryonic muscle development*. Frontiers in Cell and Developmental Biology, 2019. **7**: p. 289.
146. Partridge, T., *Myoblast transplantation*. Neuromuscular Disorders, 2002. **12**: p. S3-S6.
147. Chen, X. and Y. Li, *Role of matrix metalloproteinases in skeletal muscle: migration, differentiation, regeneration and fibrosis*. Cell adhesion & migration, 2009. **3**(4): p. 337-341.

148. Camirand, G., et al., *COMBINED IMMUNOSUPPRESSION OF MYCOPHENOLATE MOFETIL AND FK506 FOR MYOBLAST TRANSPLANTATION IN mdx MICE1*. Transplantation, 2001. **72**(1): p. 38-44.
149. Suzuki, K., et al., *Single fibers of skeletal muscle as a novel graft for cell transplantation to the heart*. The Journal of Thoracic and Cardiovascular Surgery, 2002. **123**(5): p. 984-992.
150. Suzuki, K., et al., *Intracoronary infusion of skeletal myoblasts improves cardiac function in doxorubicin-induced heart failure*. Circulation, 2001. **104**(suppl_1): p. I-213-I-217.
151. Suzuki, K., et al., *Cell transplantation for the treatment of acute myocardial infarction using vascular endothelial growth factor-expressing skeletal myoblasts*. Circulation, 2001. **104**(suppl_1): p. I-207-I-212.
152. Menasché, P., *Skeletal myoblasts as a therapeutic agent*. Progress in cardiovascular diseases, 2007. **50**(1): p. 7-17.
153. Camargo, F.D., et al., *Single hematopoietic stem cells generate skeletal muscle through myeloid intermediates*. Nature medicine, 2003. **9**(12): p. 1520.
154. Abedi, M., et al., *Robust conversion of marrow cells to skeletal muscle with formation of marrow-derived muscle cell colonies: a multifactorial process*. Experimental hematology, 2004. **32**(5): p. 426-434.
155. Negroni, E., et al., *Invited review: Stem cells and muscle diseases: advances in cell therapy strategies*. Neuropathology and applied neurobiology, 2015. **41**(3): p. 270-287.
156. Popescu, L., et al., *Identification of telocytes in skeletal muscle interstitium: implication for muscle regeneration*. Journal of cellular and molecular medicine, 2011. **15**(6): p. 1379-1392.
157. Gussoni, E., et al., *Dystrophin expression in the mdx mouse restored by stem cell transplantation*. Nature, 1999. **401**(6751): p. 390-394.
158. Lapan, A.D., A. Rozkalne, and E. Gussoni, *Human fetal skeletal muscle contains a myogenic side population that expresses the melanoma cell-adhesion molecule*. Human molecular genetics, 2012. **21**(16): p. 3668-3680.
159. Charge, S.B. and M.A. Rudnicki, *Cellular and molecular regulation of muscle regeneration*. Physiological reviews, 2004. **84**(1): p. 209-238.
160. Leiter, J.R., R. Upadhaya, and J.E. Anderson, *Nitric oxide and voluntary exercise together promote quadriceps hypertrophy and increase vascular density in female 18-mo-old mice*. Am.J.Physiol Cell Physiol, 2012. **302**(9): p. C1306-C1315.
161. Lee, A.S., et al., *Aged skeletal muscle retains the ability to fully regenerate functional architecture*. Bioarchitecture, 2013. **3**(2): p. 25-37.
162. Anderson, J.E., L.M. McIntosh, and R. Poettcker, *Deflazacort but not prednisone improves both muscle repair and fiber growth in diaphragm and limb muscle in vivo in the mdx dystrophic mouse*. Muscle Nerve, 1996. **19**(12): p. 1576-1585.
163. Pernitsky, A.N., L.M. McIntosh, and J.E. Anderson, *Hyperthyroidism impairs early repair in normal but not dystrophic mdx mouse tibialis anterior muscle. An in vivo study*. Biochem.Cell Biol., 1996. **74**(3): p. 315-324.
164. Arnold, L., et al., *Inflammatory monocytes recruited after skeletal muscle injury switch into antiinflammatory macrophages to support myogenesis*. J.Exp.Med., 2007. **204**(5): p. 1057-1069.
165. Kaneko, S., et al., *A selective Sema3A inhibitor enhances regenerative responses and functional recovery of the injured spinal cord*. Nature medicine, 2006. **12**(12): p. 1380-1389.
166. Carlson, B.M. and J.A. Faulkner, *The regeneration of skeletal muscle fibers following injury: a review*. Medicine and science in sports and exercise, 1982. **15**(3): p. 187-198.
167. Charge, S.B. and M.A. Rudnicki, *Cellular and molecular regulation of muscle regeneration*. Physiol Rev., 2004. **84**(1): p. 209-238.

168. Schultz, E. and K.M. McCormick, *Skeletal muscle satellite cells*. Rev.Physiol Biochem.Pharmacol., 1994. **123**: p. 213-257.
169. Lee, A.S., et al., *Aged skeletal muscle retains the ability to fully regenerate functional architecture*. Bioarchitecture., 2013. **3**(2): p. 25-37.
170. Mendler, L., et al., *Regeneration of reinnervated rat soleus muscle is accompanied by fiber transition toward a faster phenotype*. J Histochem Cytochem, 2008. **56**(2): p. 111-23.
171. Zimowska, M., et al., *Distinct patterns of MMP-9 and MMP-2 activity in slow and fast twitch skeletal muscle regeneration in vivo*. International Journal of Developmental Biology, 2008. **52**(2): p. 307.
172. Yang, X., et al., *Patterning of muscle acetylcholine receptor gene expression in the absence of motor innervation*. Neuron, 2001. **30**(2): p. 399-410.
173. Tidball, J.G. and S.A. Villalta, *Regulatory interactions between muscle and the immune system during muscle regeneration*. Am.J.Physiol Regul.Integr.Comp Physiol, 2010. **298**(5): p. R1173-R1187.
174. Anderson, J.E., M. Weber, and C. Vargas, *Deflazacort increases laminin expression and myogenic repair, and induces early persistent functional gain in mdx mouse muscular dystrophy*. Cell Transplant., 2000. **9**(4): p. 551-564.
175. Alfaro, L.A., et al., *CD34 promotes satellite cell motility and entry into proliferation to facilitate efficient skeletal muscle regeneration*. Stem Cells, 2011. **29**(12): p. 2030-2041.
176. Turner, N.J. and S.F. Badylak, *Regeneration of skeletal muscle*. Cell and tissue research, 2012. **347**(3): p. 759-774.
177. Anderson, J., et al., *The time course of basic fibroblast growth factor expression in crush-injured skeletal muscles of SJL/J and BALB/c mice*. Experimental cell research, 1995. **216**(2): p. 325-334.
178. ROBERTS, P., J.K. McGEACHIE, and M.D. GROUNDS, *The host environment determines strain-specific differences in the timing of skeletal muscle regeneration: Cross-transplantation studies between SJL/J and BALB/c mice*. Journal of anatomy, 1997. **191**(4): p. 585-594.
179. Peake, J.M., et al., *Muscle damage and inflammation during recovery from exercise*. Journal of applied physiology, 2017. **122**(3): p. 559-570.
180. Pimorady-Esfahani, A., M.D. Grounds, and P.G. McMenamin, *Macrophages and dendritic cells in normal and regenerating murine skeletal muscle*. Muscle & Nerve: Official Journal of the American Association of Electrodiagnostic Medicine, 1997. **20**(2): p. 158-166.
181. Weller, A.H., et al., *Spontaneous myopathy in the SJL/J mouse: pathology and strength loss*. Muscle & Nerve: Official Journal of the American Association of Electrodiagnostic Medicine, 1997. **20**(1): p. 72-82.
182. Grounds, M.D. and J.K. McGeachie, *A comparison of muscle precursor replication in crush-injured skeletal muscle of Swiss and BALBc mice*. Cell Tissue Res., 1989. **255**(2): p. 385-391.
183. Shono, J.i., et al., *Preliminary time-course study of antiinflammatory macrophage infiltration in crush-injured skeletal muscle*. Animal Science Journal, 2013. **84**(11): p. 744-750.
184. Sakaguchi, S., et al., *Implication of anti-inflammatory macrophages in regenerative motoneuritogenesis: promotion of myoblast migration and neural chemorepellent semaphorin 3A expression in injured muscle*. Int J Biochem Cell Biol, 2014. **54**: p. 272-85.
185. Serrano, A.L. and P. Muñoz-Cánoves, *Regulation and dysregulation of fibrosis in skeletal muscle*. Experimental cell research, 2010. **316**(18): p. 3050-3058.
186. Tatsumi, R., et al., *Possible implication of satellite cells in regenerative motoneuritogenesis: HGF upregulates neural chemorepellent Sema3A during myogenic differentiation*. American Journal of Physiology-Cell Physiology, 2009. **297**(2): p. C238-C252.

187. Lu, H., et al., *Macrophages recruited via CCR2 produce insulin-like growth factor-1 to repair acute skeletal muscle injury*. The FASEB Journal, 2011. **25**(1): p. 358-369.
188. Ceafalan, L.C., B.O. Popescu, and M.E. Hinescu, *Cellular players in skeletal muscle regeneration*. Biomed Res Int, 2014. **2014**(957014).
189. Campion, D.R., *The muscle satellite cell: a review*, in *International review of cytology*. 1984, Elsevier. p. 225-251.
190. Snow, M.H., *An autoradiographic study of satellite cell differentiation into regenerating myotubes following transplantation of muscles in young rats*. Cell and tissue research, 1978. **186**(3): p. 535-540.
191. Anderson, J.E., *The satellite cell as a companion in skeletal muscle plasticity: currency, conveyance, clue, connector and colander*. J Exp.Biol., 2006. **209**(Pt 12): p. 2276-2292.
192. Mauro, A., *Satellite cell of skeletal muscle fibers*. The Journal of biophysical and biochemical cytology, 1961. **9**(2): p. 493-495.
193. Scharner, J. and P.S. Zammit, *The muscle satellite cell at 50: the formative years*. Skeletal muscle, 2011. **1**(1): p. 28.
194. Tatsumi, R., et al., *Possible implication of satellite cells in regenerative motoneuritogenesis: HGF upregulates neural chemorepellent Sema3A during myogenic differentiation*. Am.J.Physiol Cell Physiol, 2009. **297**(2): p. C238-C252.
195. Lefaucheur, J.P. and A. Sébille, *The cellular events of injured muscle regeneration depend on the nature of the injury*. Neuromuscular Disorders, 1995. **5**(6): p. 501-509.
196. Sonnet, C., et al., *Human macrophages rescue myoblasts and myotubes from apoptosis through a set of adhesion molecular systems*. Journal of cell science, 2006. **119**(12): p. 2497-2507.
197. Karpati, G., et al., *Reinnervation is followed by necrosis in previously denervated skeletal muscles of dystrophic hamsters*. Exp.Neurol., 1983. **82**(2): p. 358-365.
198. Karpati, G., et al., *Hypophysectomy mitigates skeletal muscle fiber damage in hamster dystrophy*. Annals of Neurology: Official Journal of the American Neurological Association and the Child Neurology Society, 1985. **17**(1): p. 60-64.
199. Garry, D.J., et al., *Persistent expression of MNF identifies myogenic stem cells in postnatal muscles*. Developmental biology, 1997. **188**(2): p. 280-294.
200. Archer, J.D., C.C. Vargas, and J.E. Anderson, *Persistent and improved functional gain in mdx dystrophic mice after treatment with L-arginine and deflazacort*. FASEB J, 2006. **20**(6): p. 738-740.
201. Behar, O., et al., *Semaphorin III is needed for normal patterning and growth of nerves, bones and heart*. Nature, 1996. **383**(6600): p. 525-528.
202. Prior, B.M., et al., *Exercise-induced vascular remodeling*. Exercise and sport sciences reviews, 2003. **31**(1): p. 26-33.
203. d'Albis, A., et al., *Regeneration after cardiotoxin injury of innervated and denervated slow and fast muscles of mammals: myosin isoform analysis*. European journal of biochemistry, 1988. **174**(1): p. 103-110.
204. Turner, N.J., et al., *Xenogeneic extracellular matrix as an inductive scaffold for regeneration of a functioning musculotendinous junction*. Tissue Engineering Part A, 2010. **16**(11): p. 3309-3317.
205. Bassaglia, Y. and J. Gautron, *Fast and slow rat muscles degenerate and regenerate differently after whole crush injury*. Journal of Muscle Research & Cell Motility, 1995. **16**(4): p. 420-429.
206. Järvinen, M., *Healing of a crush injury in rat striated muscle: 2. A histological study of the effect of early mobilization and immobilization on the repair processes*. Acta Pathologica Microbiologica Scandinavica Section A Pathology, 1975. **83**(3): p. 269-282.

207. Vracko, R. and E.P. Benditt, *Basal lamina: The scaffold for orderly cell replacement: Observations on regeneration of injured skeletal muscle fibers and capillaries*. The Journal of cell biology, 1972. **55**(2): p. 406-419.
208. Whalen, R.G., et al., *Expression of myosin isoforms during notexin-induced regeneration of rat soleus muscles*. Developmental biology, 1990. **141**(1): p. 24-40.
209. Carlson, B.M. *Regeneration of entire skeletal muscles*. in *Federation proceedings*. 1986.
210. Sommer, A. and D.B. Rifkin, *Interaction of heparin with human basic fibroblast growth factor: protection of the angiogenic protein from proteolytic degradation by a glycosaminoglycan*. Journal of cellular physiology, 1989. **138**(1): p. 215-220.
211. Judson, R.N., et al., *Isolation, culture, and differentiation of fibro/adipogenic progenitors (FAPs) from skeletal muscle*, in *Skeletal Muscle Development*. 2017, Springer. p. 93-103.
212. Low, M., C. Eisner, and F. Rossi, *Fibro/adipogenic progenitors (FAPs): isolation by FACS and culture*, in *Muscle Stem Cells*. 2017, Springer. p. 179-189.
213. Fiore, D., et al., *Pharmacological blockage of fibro/adipogenic progenitor expansion and suppression of regenerative fibrogenesis is associated with impaired skeletal muscle regeneration*. Stem cell research, 2016. **17**(1): p. 161-169.
214. Lefaucheur, J.P., C. Pastoret, and A. Sebillle, *Phenotype of dystrophinopathy in old mdx mice*. Anat.Rec., 1995. **242**(1): p. 70-76.
215. Fink, E., et al., *Recovery of contractile and metabolic phenotypes in regenerating slow muscle after notexin-induced or crush injury*. Journal of Muscle Research & Cell Motility, 2003. **24**(7): p. 421-429.
216. Ceafalan, L.C., B.O. Popescu, and M.E. Hinescu, *Cellular players in skeletal muscle regeneration*. BioMed research international, 2014. **2014**.
217. Turgeman, T., et al., *Prevention of muscle fibrosis and improvement in muscle performance in the mdx mouse by halofuginone*. Neuromuscul.Disord., 2008. **18**(11): p. 857-868.
218. Huebner, K.D., et al., *Functional resolution of fibrosis in mdx mouse dystrophic heart and skeletal muscle by halofuginone*. Am.J.Physiol Heart Circ.Physiol, 2008. **294**(4): p. H1550-H1561.
219. Allen, M.D., et al., *Skeletal muscle morphology and contractile function in relation to muscle denervation in diabetic neuropathy*. Journal of Applied Physiology, 2014. **116**(5): p. 545-552.
220. Leiter, J.R.S. and J.E. Anderson, *Satellite cells are increasingly refractory to activation by nitric oxide and stretch in aged mouse-muscle cultures*. International Journal of Biochemistry and Cell Biology, 2010. **42**(1): p. 132-136.
221. Carraro, U., et al., *Recovery from muscle weakness by exercise and FES: lessons from Masters, active or sedentary seniors and SCI patients*. Aging clinical and experimental research, 2017. **29**(4): p. 579-590.
222. Larrick, J. and A.R. Mendelsohn, *Exercise partially rejuvenates muscle stem cells*. Rejuvenation Research, 2020(ja).
223. Franco, I., et al., *Healthy skeletal muscle aging: the role of satellite cells, somatic mutations and exercise*. Int Rev Cell Mol Biol, 2019. **346**: p. 157-200.
224. Brett, J.O., et al., *Exercise rejuvenates quiescent skeletal muscle stem cells in old mice through restoration of Cyclin D1*. Nature Metabolism, 2020. **2**(4): p. 307-317.
225. Horowitz, A.M., et al., *Blood factors transfer beneficial effects of exercise on neurogenesis and cognition to the aged brain*. Science, 2020. **369**(6500): p. 167-173.
226. Cornish, S.M., et al., *A focused review of myokines as a potential contributor to muscle hypertrophy from resistance-based exercise*. European Journal of Applied Physiology, 2020: p. 1-19.

227. Mizunoya, W., et al., *Improvement of Endurance Based on Muscle Fiber-Type Composition by Treatment with Dietary Apple Polyphenols in Rats*. Plos One, 2015. **10**(7): p. e0134303.
228. Mizunoya, W., et al., *Fast-to-slow shift of muscle fiber-type composition by dietary apple polyphenols in rats: Impact of the low-dose supplementation*. Anim Sci J, 2017. **88**(3): p. 489-499.
229. Snijders, T., et al., *Satellite cells in human skeletal muscle plasticity*. Front Physiol, 2015. **6**: p. 283.
230. Hall, J.K., et al., *Prevention of muscle aging by myofiber-associated satellite cell transplantation*. Science translational medicine, 2010. **2**(57): p. 57ra83-57ra83.
231. Hindi, S., et al., *Matrix Metalloproteinase-9 Inhibition Improves Proliferation and Engraftment of Myogenic Cells in*. 2013.
232. Vinel, C., et al., *The exerkin apelin reverses age-associated sarcopenia*. Nature medicine, 2018. **24**(9): p. 1360-1371.
233. Ricchetti, M., *How stem cells manage to escape senescence and ageing—while they can: A recent study reveals that autophagy is responsible for senescence-dependent loss of regenerative potential of muscle stem cells during ageing*. Bioessays, 2016. **38**(9): p. 857-862.
234. Sanes, J.R. and J.W. Lichtman, *Development of the vertebrate neuromuscular junction*. Annual review of neuroscience, 1999. **22**(1): p. 389-442.
235. Zhu, Z., et al., *Abnormal spreading and subunit expression of junctional acetylcholine receptors of paraspinal muscles in scoliosis associated with syringomyelia*. Spine (Phila Pa 1976), 2007. **32**(22): p. 2449-54.
236. Sanes, J.R. and J.W. Lichtman, *Development of the vertebrate neuromuscular junction*. Annu.Rev.Neurosci., 1999. **22**: p. 389-442.
237. Missias, A.C., et al., *Maturation of the acetylcholine receptor in skeletal muscle: regulation of the AChR gamma-to-epsilon switch*. Dev.Biol., 1996. **179**(1): p. 223-238.
238. Witzemann, V., *Development of the neuromuscular junction*. Cell Tissue Res., 2006. **326**(2): p. 263-271.
239. 辰巳隆一, et al., *筋線維型の新規制御機構の理解と食品機能学的調節*. 2016.
240. Gigliotti, D., et al., *Atrophy, inducible satellite cell activation, and possible denervation of supraspinatus muscle in injured human rotator-cuff muscle*. Am.J.Physiol Cell Physiol, 2015. **309**(6): p. C383-C391.
241. Burke, R. and P. Tsairis, *Anatomy and innervation ratios in motor units of cat gastrocnemius*. The Journal of physiology, 1973. **234**(3): p. 749-765.
242. Comai, G. and S. Tajbakhsh, *Molecular and cellular regulation of skeletal myogenesis*, in *Current topics in developmental biology*. 2014, Elsevier. p. 1-73.
243. Schiaffino, S., et al., *How is muscle phenotype controlled by nerve activity?* The Italian Journal of Neurological Sciences, 1999. **20**(6): p. 409-412.
244. Hernández-Hernández, J.M., et al. *The myogenic regulatory factors, determinants of muscle development, cell identity and regeneration*. in *Seminars in cell & developmental biology*. 2017. Elsevier.
245. Bloch-Gallego, E., *Mechanisms controlling neuromuscular junction stability*. Cellular and molecular life sciences, 2015. **72**(6): p. 1029-1043.
246. Le Grand, F., et al., *Wnt7a activates the planar cell polarity pathway to drive the symmetric expansion of satellite stem cells*. Cell Stem Cell, 2009. **4**(6): p. 535-547.
247. Zhang, Q., et al., *Nesprin-1 and -2 are involved in the pathogenesis of Emery Dreifuss muscular dystrophy and are critical for nuclear envelope integrity*. Hum.Mol.Genet., 2007. **16**(23): p. 2816-2833.
248. Macpherson, P.C., D. Cieslak, and D. Goldman, *Myogenin-dependent nAChR clustering in aneural myotubes*. Molecular and Cellular Neuroscience, 2006. **31**(4): p. 649-660.

249. Kozeka, K. and M. Ontell, *The three-dimensional cytoarchitecture of developing murine muscle spindles*. *Developmental biology*, 1981. **87**(1): p. 133-147.
250. Ontell, M., D. Bourke, and D. Hughes, *Cytoarchitecture of the fetal murine soleus muscle*. *American journal of anatomy*, 1988. **181**(3): p. 267-278.
251. Ontell, M. and K. Kozeka, *Organogenesis of the mouse extensor digitorum longus muscle: a quantitative study*. *American Journal of Anatomy*, 1984. **171**(2): p. 149-161.
252. Hughes, D.S., R.R. Schade, and M. Ontell, *Ablation of the fetal mouse spinal cord: the effect on soleus muscle cytoarchitecture*. *Dev.Dyn.*, 1992. **193**(2): p. 164-174.
253. Weydert, A., et al., *Developmental pattern of mouse skeletal myosin heavy chain gene transcripts in vivo and in vitro*. *Cell*, 1987. **49**(1): p. 121-129.
254. Dickson, G., et al., *Distinct dystrophin mRNA species are expressed in embryonic and adult mouse skeletal muscle*. *FEBS letters*, 1988. **242**(1): p. 47-52.
255. Russell, S.D., N.A. Cambon, and R.G. Whalen, *Two types of neonatal-to-adult fast myosin heavy chain transitions in rat hindlimb muscle fibers*. *Developmental biology*, 1993. **157**(2): p. 359-370.
256. Kummer, T.T., et al., *Nerve-independent formation of a topologically complex postsynaptic apparatus*. *The Journal of cell biology*, 2004. **164**(7): p. 1077-1087.
257. van Ooyen, A. and D.J. Willshaw, *Poly- and mononeuronal innervation in a model for the development of neuromuscular connections*. *Journal of theoretical biology*, 1999. **196**(4): p. 495-511.
258. Rich, M. and J.W. Lichtman, *Motor nerve terminal loss from degenerating muscle fibers*. *Neuron*, 1989. **3**(6): p. 677-688.
259. Son, Y.-J. and W.J. Thompson, *Schwann cell processes guide regeneration of peripheral axons*. *Neuron*, 1995. **14**(1): p. 125-132.
260. Kang, H. and J.W. Lichtman, *Motor axon regeneration and muscle reinnervation in young adult and aged animals*. *J.Neurosci.*, 2013. **33**(50): p. 19480-19491.
261. MacIntosh, B.R., P.F. Gardiner, and A.J. McComas, *Skeletal muscle: form and function*. 2006: Human kinetics.
262. Shi, L., A.K. Fu, and N.Y. Ip, *Molecular mechanisms underlying maturation and maintenance of the vertebrate neuromuscular junction*. *Trends in neurosciences*, 2012. **35**(7): p. 441-453.
263. Trappe, S., et al., *Single muscle fiber adaptations with marathon training*. *Journal of applied physiology*, 2006. **101**(3): p. 721-727.
264. Andersen, J.L. and P. Aagaard, *Effects of strength training on muscle fiber types and size; consequences for athletes training for high-intensity sport*. *Scandinavian journal of medicine & science in sports*, 2010. **20**: p. 32-38.
265. Balagopal, P., et al., *Age effect on transcript levels and synthesis rate of muscle MHC and response to resistance exercise*. *American Journal of Physiology-Endocrinology And Metabolism*, 2001. **280**(2): p. E203-E208.
266. Häkkinen, K., et al., *Neuromuscular adaptations during concurrent strength and endurance training versus strength training*. *European journal of applied physiology*, 2003. **89**(1): p. 42-52.
267. Hughes, D.C., S. Ellefsen, and K. Baar, *Adaptations to endurance and strength training*. *Cold Spring Harbor perspectives in medicine*, 2018. **8**(6): p. a029769.
268. Hawley, J.A., *Molecular responses to strength and endurance training: are they incompatible?* *Applied physiology, nutrition, and metabolism*, 2009. **34**(3): p. 355-361.
269. Zierath, J.R. and J.A. Hawley, *Skeletal muscle fiber type: influence on contractile and metabolic properties*. *PLoS Biol*, 2004. **2**(10): p. e348.

270. Norman, T.L., et al., *Aerobic exercise as a countermeasure for microgravity-induced bone loss and muscle atrophy in a rat hindlimb suspension model*. *Aviat.Space Environ.Med.*, 2000. **71**(6): p. 593-598.
271. Gordon, T. and G.H. Borschel, *The use of the rat as a model for studying peripheral nerve regeneration and sprouting after complete and partial nerve injuries*. *Experimental neurology*, 2017. **287**: p. 331-347.
272. Gordon, T., J. Hegedus, and S.L. Tam, *Adaptive and maladaptive motor axonal sprouting in aging and motoneuron disease*. *Neurol.Res.*, 2004. **26**(2): p. 174-185.
273. Jang, Y.C., et al., *Increased superoxide in vivo accelerates age-associated muscle atrophy through mitochondrial dysfunction and neuromuscular junction degeneration*. *The FASEB Journal*, 2010. **24**(5): p. 1376-1390.
274. Barrett, E.F., J.N. Barrett, and G. David, *Mitochondria in motor nerve terminals: function in health and in mutant superoxide dismutase 1 mouse models of familial ALS*. *Journal of bioenergetics and biomembranes*, 2011. **43**(6): p. 581-586.
275. Duregotti, E., et al., *Mitochondrial alarmins released by degenerating motor axon terminals activate perisynaptic Schwann cells*. *Proceedings of the National Academy of Sciences*, 2015. **112**(5): p. E497-E505.
276. Tudoraşcu, I., et al., *Motor unit changes in normal aging: a brief review*. *Rom J Morphol Embryol*, 2014. **55**(4): p. 1295-1301.
277. Jang, Y.C. and H. Van Remmen, *Age-associated alterations of the neuromuscular junction*. *Experimental gerontology*, 2011. **46**(2-3): p. 193-198.
278. Lepore, E., et al., *Neuromuscular Junction as an Entity of Nerve-Muscle Communication*. *Cells*, 2019. **8**(8): p. 906.
279. Carnio, S., et al., *Autophagy impairment in muscle induces neuromuscular junction degeneration and precocious aging*. *Cell reports*, 2014. **8**(5): p. 1509-1521.
280. Anagnostou, M.-E. and R.T. Hepple, *Mitochondrial Mechanisms of Neuromuscular Junction Degeneration with Aging*. *Cells*, 2020. **9**(1): p. 197.
281. Mizunoya, W., et al., *Improvement of endurance based on muscle fiber-type composition by treatment with dietary apple polyphenols in rats*. *PloS one*, 2015. **10**(7): p. e0134303.
282. D'Souza, D.M., et al., *Diet-induced obesity impairs muscle satellite cell activation and muscle repair through alterations in hepatocyte growth factor signaling*. *Physiol Rep*, 2015. **3**(8).
283. Cornish, S.M. and P.D. Chilibeck, *Alpha-linolenic acid supplementation and resistance training in older adults*. *Applied Physiology, Nutrition, and Metabolism*, 2009. **34**(1): p. 49-59.
284. Cornish, S.M., et al., *Conjugated linoleic acid combined with creatine monohydrate and whey protein supplementation during strength training*. *International journal of sport nutrition and exercise metabolism*, 2009. **19**(1): p. 79-96.
285. Chrusch, M.J., et al., *Creatine supplementation combined with resistance training in older men*. *Medicine & Science in Sports & Exercise*, 2001. **33**(12): p. 2111-2117.
286. Lewis, M.I., S.A. Monn, and G.C. Sieck, *Effect of corticosteroids on diaphragm fatigue, SDH activity, and muscle fiber size*. *Journal of Applied Physiology*, 1992. **72**(1): p. 293-301.
287. Bacou, F., et al., *Expression of myosin isoforms in denervated, cross-reinnervated, and electrically stimulated rabbit muscles*. *European journal of biochemistry*, 1996. **236**(2): p. 539-547.
288. Snoj-Cvetko, E., et al., *Regenerated rat fast muscle transplanted to the slow muscle bed and innervated by the slow nerve, exhibits an identical myosin heavy chain repertoire to that of the slow muscle*. *Histochemistry and cell biology*, 1996. **106**(5): p. 473-479.
289. Aravamudan, B., et al., *Denervation effects on myonuclear domain size of rat diaphragm fibers*. *Journal of applied physiology*, 2006. **100**(5): p. 1617-1622.

290. Blaauw, B., S. Schiaffino, and C. Reggiani, *Mechanisms modulating skeletal muscle phenotype*. Compr.Physiol, 2013. **3**(4): p. 1645-1687.
291. Gunning, P. and E. Hardeman, *Multiple mechanisms regulate muscle fiber diversity*. The FASEB Journal, 1991. **5**(15): p. 3064-3070.
292. Wigmore, P.M. and D.J. Evans, *Molecular and cellular mechanisms involved in the generation of fiber diversity during myogenesis*, in *International review of cytology*. 2002, Elsevier. p. 175-232.
293. Schiaffino, S. and A. Serrano, *Calcineurin signaling and neural control of skeletal muscle fiber type and size*. Trends in pharmacological sciences, 2002. **23**(12): p. 569-575.
294. Schiaffino, S. and C. Reggiani, *Fiber types in mammalian skeletal muscles*. Physiological reviews, 2011. **91**(4): p. 1447-1531.
295. Stockdale, F.E., *Mechanisms of formation of muscle fiber types*. Cell structure and function, 1997. **22**(1): p. 37-43.
296. Couteaux, R., J.-C. Mira, and A. d'Albis, *Regeneration of muscles after cardiotoxin injury I. Cytological aspects*. Biology of the Cell, 1988. **62**(2): p. 171-182.
297. Do, M.K., et al., *Growth factor regulation of neural chemorepellent Sema3A expression in satellite cell cultures*. Am.J.Physiol Cell Physiol, 2011. **301**(5): p. C1270-C1279.
298. Suzuki, T., et al., *Comparative analysis of semaphorin 3A in soleus and EDL muscle satellite cells in vitro toward understanding its role in modulating myogenin expression*. Int J Biochem Cell Biol, 2013. **45**(2): p. 476-82.
299. Suzuki, T., et al., *Comparative analysis of semaphorin 3A in soleus and EDL muscle satellite cells in vitro toward understanding its role in modulating myogenin expression*. The international journal of biochemistry & cell biology, 2013. **45**(2): p. 476-482.
300. Bruusgaard, J.C. and K. Gundersen, *In vivo time-lapse microscopy reveals no loss of murine myonuclei during weeks of muscle atrophy*. The Journal of clinical investigation, 2008. **118**(4): p. 1450.
301. Kamath, S., et al., *MRI appearance of muscle denervation*. Skeletal radiology, 2008. **37**(5): p. 397-404.
302. Hsu, M. and F.F. Stevenson, *Wallerian degeneration and recovery of motor nerves after multiple focused cold therapies*. Muscle & nerve, 2015. **51**(2): p. 268-275.
303. De Winter, F., et al., *The expression of the chemorepellent Semaphorin 3A is selectively induced in terminal Schwann cells of a subset of neuromuscular synapses that display limited anatomical plasticity and enhanced vulnerability in motor neuron disease*. Mol.Cell Neurosci., 2006. **32**(1-2): p. 102-117.
304. Schmidt, E.R., R.J. Pasterkamp, and L.H. van den Berg, *Axon guidance proteins: novel therapeutic targets for ALS?* Progress in neurobiology, 2009. **88**(4): p. 286-301.
305. Tessier-Lavigne, M. and C.S. Goodman, *The molecular biology of axon guidance*. Science, 1996. **274**(5290): p. 1123-1133.
306. Kang, H. and J.W. Lichtman, *Motor axon regeneration and muscle reinnervation in young adult and aged animals*. The Journal of Neuroscience, 2013. **33**(50): p. 19480-19491.
307. Koirala, S., L.V. Reddy, and C.-P. Ko, *Roles of glial cells in the formation, function, and maintenance of the neuromuscular junction*. Journal of neurocytology, 2003. **32**(5-8): p. 987-1002.
308. Balice-Gordon, R.J., *Dynamic roles at the neuromuscular junction. Schwann cells*. Current biology: CB, 1996. **6**(9): p. 1054.
309. Araque, A., et al., *Tripartite synapses: glia, the unacknowledged partner*. Trends in neurosciences, 1999. **22**(5): p. 208-215.

310. Robitaille, R., *Multi-level regulation of synaptic efficacy by perisynaptic Schwann cells at the vertebrate neuromuscular junction*. The tripartite synapse: glia in synaptic transmission. Oxford University Press, New York, 2002: p. 224-236.
311. Volterra, A., P.J. Magistretti, and P.G. Haydon, *The tripartite synapse: glia in synaptic transmission*. 2002: Oxford University Press.
312. Nguyen, Q.T., J.R. Sanes, and J.W. Lichtman, *Pre-existing pathways promote precise projection patterns*. Nature neuroscience, 2002. **5**(9): p. 861.
313. Gutmann, E. and J.Z. Young, *The re-innervation of muscle after various periods of atrophy*. Journal of Anatomy, 1944. **78**(Pt 1-2): p. 15.
314. Lubischer, J.L. and D.M. Bebinger, *Regulation of terminal Schwann cell number at the adult neuromuscular junction*. Journal of Neuroscience, 1999. **19**(24): p. RC46-RC46.
315. Love, F.M. and W.J. Thompson, *Schwann cells proliferate at rat neuromuscular junctions during development and regeneration*. Journal of Neuroscience, 1998. **18**(22): p. 9376-9385.
316. Feng, Z. and C.P. Ko, *The role of glial cells in the formation and maintenance of the neuromuscular junction*. Annals of the New York Academy of Sciences, 2008. **1132**(1): p. 19-28.
317. Kang, H., et al., *Terminal Schwann cells participate in neuromuscular synapse remodeling during reinnervation following nerve injury*. Journal of Neuroscience, 2014. **34**(18): p. 6323-6333.
318. Kawabuchi, M., et al., *The spatiotemporal relationship among Schwann cells, axons and postsynaptic acetylcholine receptor regions during muscle reinnervation in aged rats*. The Anatomical Record: An Official Publication of the American Association of Anatomists, 2001. **264**(2): p. 183-202.
319. Verdú, E., et al., *Influence of aging on peripheral nerve function and regeneration*. Journal of the Peripheral Nervous System, 2000. **5**(4): p. 191-208.
320. Narici, M.V. and N. Maffulli, *Sarcopenia: characteristics, mechanisms and functional significance*. British medical bulletin, 2010. **95**(1): p. 139-159.
321. Koirala, S., H. Qiang, and C.P. Ko, *Reciprocal interactions between perisynaptic Schwann cells and regenerating nerve terminals at the frog neuromuscular junction*. Journal of neurobiology, 2000. **44**(3): p. 343-360.
322. Kawabuchi, M., H. Tan, and S. Wang, *Age affects reciprocal cellular interactions in neuromuscular synapses following peripheral nerve injury*. Ageing research reviews, 2011. **10**(1): p. 43-53.
323. Apel, P.J., et al., *How age impairs the response of the neuromuscular junction to nerve transection and repair: an experimental study in rats*. Journal of Orthopaedic Research, 2009. **27**(3): p. 385-393.
324. Park, K.H., *Mechanisms of muscle denervation in aging: insights from a mouse model of amyotrophic lateral sclerosis*. Aging and disease, 2015. **6**(5): p. 380.
325. Gigliotti, D., et al., *Altered Satellite Cell Responsiveness and Denervation Implicated in Progression of Rotator-Cuff Injury*. PLoS One, 2016. **11**(9): p. e0162494.
326. Zorick, T.S. and G. Lemke, *Schwann cell differentiation*. Current opinion in cell biology, 1996. **8**(6): p. 870-876.
327. Jessen, K. and R. Mirsky, *Signals that determine Schwann cell identity*. Journal of anatomy, 2002. **200**(4): p. 367-376.
328. Reynolds, M. and C. Woolf, *Terminal Schwann cells elaborate extensive processes following denervation of the motor endplate*. Journal of neurocytology, 1992. **21**(1): p. 50-66.
329. Jessen, K.R., R. Thorpe, and R. Mirsky, *Molecular identity, distribution and heterogeneity of glial fibrillary acidic protein: an immunoblotting and immunohistochemical study of Schwann cells, satellite cells, enteric glia and astrocytes*. Journal of neurocytology, 1984. **13**(2): p. 187-200.

330. Nieke, J. and M. Scbachner, *Expression of the neural cell adhesion molecules L1 and N-CAM and their common carbohydrate epitope L2/HNK-1 during development and after transection of the mouse sciatic nerve*. Differentiation, 1985. **30**(2): p. 141-151.
331. Curtis, R., et al., *GAP-43 is expressed by nonmyelin-forming Schwann cells of the peripheral nervous system*. The Journal of cell biology, 1992. **116**(6): p. 1455-1464.
332. Georgiou, J., et al., *Synaptic regulation of glial protein expression in vivo*. Neuron, 1994. **12**(2): p. 443-455.
333. Woolf, C., et al., *Denervation of the motor endplate results in the rapid expression by terminal Schwann cells of the growth-associated protein GAP-43*. Journal of Neuroscience, 1992. **12**(10): p. 3999-4010.
334. Taniuchi, M., H.B. Clark, and E.M. Johnson, *Induction of nerve growth factor receptor in Schwann cells after axotomy*. Proceedings of the National Academy of Sciences, 1986. **83**(11): p. 4094-4098.
335. Yoshikami, D. and L.M. Okun, *Staining of living presynaptic nerve terminals with selective fluorescent dyes*. Nature, 1984. **310**(5972): p. 53.
336. Chen, L., D.B. Folsom, and C.-P. Ko, *The remodeling of synaptic extracellular matrix and its dynamic relationship with nerve terminals at living frog neuromuscular junctions*. Journal of Neuroscience, 1991. **11**(9): p. 2920-2930.
337. Macleod, G.T., P.A. Dickens, and M.R. Bennett, *Formation and function of synapses with respect to Schwann cells at the end of motor nerve terminal branches on mature amphibian (*Bufo marinus*) muscle*. Journal of Neuroscience, 2001. **21**(7): p. 2380-2392.
338. Jessen, K.R. and R. Mirsky, *Negative regulation of myelination: relevance for development, injury, and demyelinating disease*. Glia, 2008. **56**(14): p. 1552-1565.
339. Jessen, K.R. and R. Mirsky, *The origin and development of glial cells in peripheral nerves*. Nature Reviews Neuroscience, 2005. **6**(9): p. 671-682.
340. Wanner, I.B., et al., *Role of N-cadherin in Schwann cell precursors of growing nerves*. Glia, 2006. **54**(5): p. 439-459.
341. Donato, R., et al., *Functions of S100 proteins*. Current molecular medicine, 2013. **13**(1): p. 24.
342. Banerjee, S.S., et al., *Malignant melanoma showing smooth muscle differentiation*. Journal of clinical pathology, 1996. **49**(11): p. 950-951.
343. Thomas, P., *Changes in the endoneurial sheaths of peripheral myelinated nerve fibres during Wallerian degeneration*. Journal of anatomy, 1964. **98**(Pt 2): p. 175.
344. Weinberg, H.J. and P.S. Spencer, *The fate of Schwann cells isolated from axonal contact*. Journal of neurocytology, 1978. **7**(5): p. 555-569.
345. Vargas, M.E. and B.A. Barres, *Why is Wallerian degeneration in the CNS so slow?* Annu. Rev. Neurosci., 2007. **30**: p. 153-179.
346. Fawcett, J. and R.J. Keynes, *Peripheral nerve regeneration*. Annual review of neuroscience, 1990. **13**(1): p. 43-60.
347. Wong, K.M., E. Babetto, and B. Beirowski, *Axon degeneration: make the Schwann cell great again*. Neural regeneration research, 2017. **12**(4): p. 518.
348. Roth, L., et al., *The many faces of semaphorins: from development to pathology*. Cellular and Molecular Life Sciences, 2009. **66**(4): p. 649.
349. Kumanogoh, A. and H. Kikutani, *Semaphorins and their receptors: novel features of neural guidance molecules*. Proceedings of the Japan Academy. Series B, Physical and biological sciences, 2010. **86**(6): p. 611.
350. De Winter, F., et al., *The expression of the chemorepellent Semaphorin 3A is selectively induced in terminal Schwann cells of a subset of neuromuscular synapses that display limited anatomical*

- plasticity and enhanced vulnerability in motor neuron disease*. Molecular and Cellular Neuroscience, 2006. **32**(1): p. 102-117.
351. Do, M.-K.Q., et al., *Growth factor regulation of neural chemorepellent Sema3A expression in satellite cell cultures*. American Journal of Physiology-Cell Physiology, 2011. **301**(5): p. C1270-C1279.
352. Do, M.-K.Q., et al., *Transmembrane proteoglycans syndecan-2, 4, receptor candidates for the impact of HGF and FGF2 on semaphorin 3A expression in early-differentiated myoblasts*. Physiological Reports, 2015.
353. Sato, Y., et al., *Satellite cells produce neural chemorepellent semaphorin 3A upon muscle injury*. Animal Science Journal, 2013. **84**(2): p. 185-189.
354. Gallo, G., *RhoA-kinase coordinates F-actin organization and myosin II activity during semaphorin-3A-induced axon retraction*. Journal of cell science, 2006. **119**(16): p. 3413-3423.
355. Okubo, M., et al., *Semaphorin 3A is expressed in human osteoarthritic cartilage and antagonizes vascular endothelial growth factor 165 promoted chondrocyte migration: An implication for chondrocyte cloning*. Arthritis & Rheumatism, 2011. **63**(10): p. 3000-3009.
356. Gomez, C., et al., *Expression of Semaphorin-3A and its receptors in endochondral ossification: Potential role in skeletal development and innervation*. Developmental Dynamics, 2005. **234**(2): p. 393-403.
357. Taniguchi, M., et al., *Disruption of semaphorin III/D gene causes severe abnormality in peripheral nerve projection*. Neuron, 1997. **19**(3): p. 519-530.
358. Kawasaki, T., et al., *Requirement of neuropilin 1-mediated Sema3A signals in patterning of the sympathetic nervous system*. Development, 2002. **129**(3): p. 671-680.
359. Henningsen, J., et al., *Dynamics of the skeletal muscle secretome during myoblast differentiation*. Mol.Cell Proteomics., 2010. **9**(11): p. 2482-2496.
360. Anderson, J.E., et al., *The role of semaphorin3A in myogenic regeneration and the formation of functional neuromuscular junctions on new fibres*. Biological Reviews, 2017. **92**(3): p. 1389-1405.
361. Roth, L., et al., *The many faces of semaphorins: from development to pathology*. Cell Mol.Life Sci., 2009. **66**(4): p. 649-666.
362. Tatsumi, R., et al., *Slow-Myofiber Commitment by Semaphorin 3A Secreted from Myogenic Stem Cells*. Stem Cells, 2017. **35**(7): p. 1815-1834.
363. Gigliotti, D., et al., *Atrophy, inducible satellite cell activation and possible denervation of supraspinatus muscle in injured human rotator-cuff muscle*. American Journal of Physiology-Cell Physiology, 2015: p. ajpcell. 00143.2015.
364. クイ, ド.コ., *Regenerative motoneuritogenesis promoted by axon-guidance cue semaphorin 3A secretion from resident myogenic stem cells*. 2015, 九州大学.
365. Wozniak, A.C. and J.E. Anderson, *Nitric oxide-dependence of satellite stem cell activation and quiescence on normal skeletal muscle fibers*. Developmental Dynamics, 2007. **236**(1): p. 240-250.
366. Sheehan, S.M., et al., *HGF is an autocrine growth factor for skeletal muscle satellite cells in vitro*. Muscle & nerve, 2000. **23**(2): p. 239-245.
367. Anderson, J.E., *A role for nitric oxide in muscle repair: nitric oxide-mediated activation of muscle satellite cells*. Molecular biology of the cell, 2000. **11**(5): p. 1859-1874.
368. Anderson, J.E., *The satellite cell as a companion in skeletal muscle plasticity: currency, conveyance, clue, connector and colander*. Journal of Experimental Biology, 2006. **209**(12): p. 2276-2292.
369. Torrente, Y., et al., *Identification of a putative pathway for the muscle homing of stem cells in a muscular dystrophy model*. The Journal of cell biology, 2003. **162**(3): p. 511-520.

370. Sellman, J.E., et al., *In vivo inhibition of nitric oxide synthase impairs upregulation of contractile protein mRNA in overloaded plantaris muscle*. Journal of Applied Physiology, 2006. **100**(1): p. 258-265.
371. Anderson, J. and O. Pilipowicz, *Activation of muscle satellite cells in single-fiber cultures*. Nitric Oxide, 2002. **7**(1): p. 36-41.
372. Zhang, H. and J.E. Anderson, *Satellite cell activation and populations on single muscle-fiber cultures from adult zebrafish (Danio rerio)*. J.Exp.Biol., 2014. **217**(Pt 11): p. 1910-1917.
373. Tatsumi, R., et al., *Release of hepatocyte growth factor from mechanically stretched skeletal muscle satellite cells and role of pH and nitric oxide*. Molecular biology of the cell, 2002. **13**(8): p. 2909-2918.
374. Yablonka-Reuveni, Z. and J.E. Anderson, *Satellite cells from dystrophic (mdx) mice display accelerated differentiation in primary cultures and in isolated myofibers*. Developmental Dynamics, 2006. **235**(1): p. 203-212.
375. Tatsumi, R., et al., *Mechanical stretch induces activation of skeletal muscle satellite cells in vitro*. Experimental cell research, 2001. **267**(1): p. 107-114.
376. Leiter, J.R., R. Upadhaya, and J.E. Anderson, *Nitric oxide and voluntary exercise together promote quadriceps hypertrophy and increase vascular density in female 18-mo-old mice*. American Journal of Physiology-Cell Physiology, 2012. **302**(9): p. C1306-C1315.
377. Mizunoya, W., et al., *Nitric oxide donors improve prednisone effects on muscular dystrophy in the mdx mouse diaphragm*. American Journal of Physiology-Cell Physiology, 2011. **300**(5): p. C1065-C1077.
378. Anderson, J.E., A. Zhu, and T.M. Mizuno, *Nitric oxide treatment attenuates muscle atrophy during hind limb suspension in mice*. Free Radic Biol Med, 2017. **115**: p. 458-470.
379. Timpani, C.A., A. Hayes, and E. Rybalka, *Therapeutic strategies to address neuronal nitric oxide synthase deficiency and the loss of nitric oxide bioavailability in Duchenne Muscular Dystrophy*. Orphanet journal of rare diseases, 2017. **12**(1): p. 1-11.
380. Hofer, H.R. and R.S. Tuan, *Secreted trophic factors of mesenchymal stem cells support neurovascular and musculoskeletal therapies*. Stem Cell Research & Therapy, 2016. **7**(1): p. 1-14.
381. Danna, N.R., et al., *Therapeutic approaches to skeletal muscle repair and healing*. Sports Health, 2014. **6**(4): p. 348-355.
382. Vasilaki, A. and M.J. Jackson, *Role of reactive oxygen species in the defective regeneration seen in aging muscle*. Free Radical Biology and Medicine, 2013. **65**: p. 317-323.
383. De Palma, C. and E. Clementi, *Nitric oxide in myogenesis and therapeutic muscle repair*. Mol.Neurobiol., 2012. **46**(3): p. 682-692.
384. Filippin, L.I., et al., *Nitric oxide and repair of skeletal muscle injury*. Nitric Oxide, 2009. **21**(3-4): p. 157-63.
385. Allen, D.G., N.P. Whitehead, and S.C. Froehner, *Absence of dystrophin disrupts skeletal muscle signaling: roles of Ca²⁺, reactive oxygen species, and nitric oxide in the development of muscular dystrophy*. Physiological reviews, 2016. **96**(1): p. 253-305.
386. Sellman, J.E., et al., *In vivo inhibition of nitric oxide synthase impairs upregulation of contractile protein mRNA in overloaded plantaris muscle*. J Appl.Physiol, 2006. **100**(1): p. 258-265.
387. Filippin, L.I., et al., *Nitric oxide regulates the repair of injured skeletal muscle*. Nitric Oxide, 2011. **24**(1): p. 43-49.
388. Archer, J.D., C.C. Vargas, and J.E. Anderson, *Persistent and improved functional gain in mdx dystrophic mice after treatment with L-arginine and deflazacort*. The FASEB Journal, 2006. **20**(6): p. 738-740.

389. Marques, M.J., et al., *Muscle regeneration in dystrophic mdx mice is enhanced by isosorbide dinitrate*. Neuroscience letters, 2005. **382**(3): p. 342-345.
390. Wang, G., et al., *Development of a nitric oxide-releasing analogue of the muscle relaxant guaifenesin for skeletal muscle satellite cell myogenesis*. Molecular pharmaceutics, 2009. **6**(3): p. 895-904.
391. Daneshvar, N., et al., *Premature satellite cell activation before injury accelerates myogenesis and disrupts neuromuscular junction maturation in regenerating muscle*. American Journal of Physiology-Cell Physiology, 2020.
392. Wosczyzna, M.N. and T.A. Rando, *A Muscle Stem Cell Support Group: Coordinated Cellular Responses in Muscle Regeneration*. Dev Cell, 2018. **46**(2): p. 135-143.
393. Bodine-Fowler, S., *Skeletal muscle regeneration after injury: an overview*. J.Voice, 1994. **8**(1): p. 53-62.
394. Duchen, L.W., et al., *Changes in motor end-plates resulting from muscle fibre necrosis and regeneration. A light and electron microscopic study of the effects of the depolarizing fraction (cardiotoxin) of Dendroaspis jamesoni venom*. J.Neurol.Sci., 1974. **21**(4): p. 391-417.
395. Aartsma-Rus, A., et al., *Comparative analysis of antisense oligonucleotide analogs for targeted DMD exon 46 skipping in muscle cells*. Gene Ther., 2004. **11**(18): p. 1391-1398.
396. Grounds, M.D. and J.K. McGeachie, *A model of myogenesis in vivo, derived from detailed autoradiographic studies of regenerating skeletal muscle, challenges the concept of quantal mitosis*. Cell Tissue Res., 1987. **250**(3): p. 563-569.
397. Tatsumi, R., et al., *Slow-Myofiber Commitment by Semaphorin 3A Secreted from Myogenic Stem Cells*. Stem Cells, 2017. **35**(7): p. 1815-1834.
398. Lepper, C., T.A. Partridge, and C.M. Fan, *An absolute requirement for Pax7-positive satellite cells in acute injury-induced skeletal muscle regeneration*. Development, 2011. **138**(17): p. 3639-46.
399. Filippin, L.I., et al., *The role of nitric oxide during healing of trauma to the skeletal muscle*. Inflamm.Res., 2011. **60**(4): p. 347-356.
400. Anderson, J.E., *Hepatocyte Growth Factor and Satellite Cell Activation*. Adv Exp Med Biol, 2016. **900**: p. 1-25.
401. Sakaguchi, S., et al., *Implication of anti-inflammatory macrophages in regenerative motoneuritegenesis: promotion of myoblast migration and neural chemorepellent semaphorin 3A expression in injured muscle*. Int.J.Biochem.Cell Biol., 2014. **54**: p. 272-285.
402. Tatsumi, R., et al., *Satellite cell activation in stretched skeletal muscle and the role of nitric oxide and hepatocyte growth factor*. Am.J Physiol Cell Physiol, 2006. **290**(6): p. C1487-C1494.
403. Wozniak, A.C., et al., *Signaling satellite-cell activation in skeletal muscle: Markers, models, stretch, and potential alternate pathways*. Muscle Nerve, 2005. **31**(3): p. 283-300.
404. Constantin, B., *Dystrophin complex functions as a scaffold for signalling proteins*. Biochim Biophys Acta, 2014. **1838**(2): p. 635-42.
405. Mizunoya, W., et al., *Nitric oxide donors improve prednisone effects on muscular dystrophy in the mdx mouse diaphragm*. Am.J.Physiol Cell Physiol, 2011. **300**(5): p. C1065-C1077.
406. Marques, M.J., et al., *Muscle regeneration in dystrophic mdx mice is enhanced by isosorbide dinitrate*. Neurosci.Lett., 2005. **382**(3): p. 342-345.
407. Sato, Y., et al., *Satellite cells produce neural chemorepellent semaphorin 3A upon muscle injury*. Anim Sci.J., 2013. **84**(2): p. 185-189.
408. Zhu, Z., Y. Qiu, and B. Wang, *Gamma subunits expression of junctional acetylcholine receptor of paraspinal muscles in scoliosis associated with syringomyelia*. Stud Health Technol Inform, 2006. **123**: p. 605-9.

409. Vignaud, A., et al., *Differential recovery of neuromuscular function after nerve/muscle injury induced by crude venom from Notechis scutatus, cardiotoxin from Naja atra and bupivacaine treatments in mice*. *Neurosci Res*, 2007. **58**(3): p. 317-23.
410. Couteaux, R., J.C. Mira, and A. d'Albis, *Regeneration of muscles after cardiotoxin injury. I. Cytological aspects*. *Biol Cell*, 1988. **62**(2): p. 171-82.
411. McIntosh, L.M. and J.E. Anderson, *Hypothyroidism prolongs and increases mdx muscle precursor proliferation and delays myotube formation in normal and dystrophic limb muscle*. *Biochem.Cell Biol.*, 1995. **73**(3-4): p. 181-190.
412. McIntosh, L.M., R.E. Baker, and J.E. Anderson, *Magnetic resonance imaging of regenerating and dystrophic mouse muscle*. *Biochem.Cell Biol.*, 1998. **76**(2-3): p. 532-541.
413. McIntosh, L., et al., *Nuclear magnetic resonance spectroscopy study of muscle growth, mdx dystrophy and glucocorticoid treatments: correlation with repair*. *NMR Biomed.*, 1998. **11**(1): p. 1-10.
414. Kelly, A.M., *Satellite cells and myofiber growth in the rat soleus and extensor digitorum longus muscles*. *Dev Biol*, 1978. **65**(1): p. 1-10.
415. Slater, C.R. and S. Schiaffino, *Innervation of regenerating muscle*, in *Skeletal Muscle Repair and Regeneration*, S. Schiaffino and T. Partridge, Editors. 2008, Springer: Dordrecht, The Netherlands. p. 303-334.
416. Grunwald, I.C. and R. Klein, *Axon guidance: receptor complexes and signaling mechanisms*. *Curr Opin Neurobiol*, 2002. **12**(3): p. 250-9.
417. Anderson, J.E., et al., *The role of semaphorin3A in myogenic regeneration and the formation of functional neuromuscular junctions on new fibres*. *Biol Rev Camb Philos Soc*, 2016.
418. de Wit, J. and J. Verhaagen, *Role of semaphorins in the adult nervous system*. *Prog.Neurobiol.*, 2003. **71**(2-3): p. 249-267.
419. Nakamura, F., R.G. Kalb, and S.M. Strittmatter, *Molecular basis of semaphorin-mediated axon guidance*. *J Neurobiol*, 2000. **44**(2): p. 219-29.
420. Suzuki, T., et al., *Comparative analysis of semaphorin 3A in soleus and EDL muscle satellite cells in vitro toward understanding its role in modulating myogenin expression*. *Int.J.Biochem.Cell Biol.*, 2013. **45**(2): p. 476-482.
421. Do, M.K., et al., *Transmembrane proteoglycans syndecan-2, 4, receptor candidates for the impact of HGF and FGF2 on semaphorin 3A expression in early-differentiated myoblasts*. *Physiol Rep*, 2015. **3**(9).
422. Riuzzi, F., et al., *Cellular and molecular mechanisms of sarcopenia: the S100B perspective*. *J Cachexia Sarcopenia Muscle*, 2018. **9**(7): p. 1255-1268.
423. Magill, C.K., et al., *Reinnervation of the tibialis anterior following sciatic nerve crush injury: a confocal microscopic study in transgenic mice*. *Experimental neurology*, 2007. **207**(1): p. 64-74.
424. Donato, R., et al., *Functions of S100 proteins*. *Curr Mol Med*, 2013. **13**(1): p. 24-57.
425. Wang, G., et al., *Development of a nitric oxide-releasing analogue of the muscle relaxant guaifenesin for skeletal muscle satellite cell myogenesis*. *Mol.Pharm.*, 2009. **6**(3): p. 895-904.
426. Anderson, J.E., L. Liu, and E. Kardami, *The effects of hyperthyroidism on muscular dystrophy in the mdx mouse: greater dystrophy in cardiac and soleus muscle*. *Muscle Nerve*, 1994. **17**(1): p. 64-73.
427. Suzuki, T., et al. *Semaphorin 3A secreted from myogenic stem cells promotes slow-twitch muscle fiber generation*.
428. Young, H.S., L.G. Herbet, and V. Skita, *Alpha-bungarotoxin binding to acetylcholine receptor membranes studied by low angle X-ray diffraction*. *Biophys J*, 2003. **85**(2): p. 943-53.
429. Barik, A., et al., *Schwann Cells in Neuromuscular Junction Formation and Maintenance*. *J Neurosci*, 2016. **36**(38): p. 9770-81.

430. Upadhaya, R., W. Mizunoya, and J.E. Anderson, *Detecting multiple proteins by Western blotting using same-species primary antibodies, precomplexed serum, and hydrogen peroxide*. *Anal.Biochem.*, 2011. **419**(2): p. 342-344.
431. *The jamovi project, in jamovi (Version 1.2) [Computer Software]*. Retrieved from <https://www.jamovi.org>. 2020.
432. Adams, R.H., et al., *The chemorepulsive activity of secreted semaphorins is regulated by furin-dependent proteolytic processing*. *EMBO J*, 1997. **16**(20): p. 6077-86.
433. Schafer, B.W. and C.W. Heizmann, *The S100 family of EF-hand calcium-binding proteins: functions and pathology*. *Trends Biochem Sci*, 1996. **21**(4): p. 134-40.
434. Baudier, J., J.C. Deloulme, and G.S. Shaw, *The Zn(2+) and Ca(2+) -binding S100B and S100A1 proteins: beyond the myths*. *Biol Rev Camb Philos Soc*, 2020.
435. Banuls, C., et al., *The pivotal role of nitric oxide: effects on the nervous and immune systems*. *Curr Pharm Des*, 2014. **20**(29): p. 4679-89.
436. McAllister, R.M., S.C. Newcomer, and M.H. Laughlin, *Vascular nitric oxide: effects of exercise training in animals*. *Appl Physiol Nutr Metab*, 2008. **33**(1): p. 173-8.
437. Tonello, F., et al., *A Lys49-PLA2 myotoxin of *Bothrops asper* triggers a rapid death of macrophages that involves autocrine purinergic receptor signaling*. *Cell Death Dis*, 2012. **3**: p. e343.
438. Hei Yuan, H., K. S, and J. Anderson, *A mechanism for semaphorin-induced apoptosis: DNA damage of endothelial and myogenic cells in primary cultures from skeletal muscle*. *Oncotarget*, 2018. **9**(32): p. 22618-22630.
439. Zheng, Y., et al., *Increased BrdU incorporation reflecting DNA repair, neuronal de-differentiation or possible neurogenesis in the adult cochlear nucleus following bilateral cochlear lesions in the rat*. *Exp Brain Res*, 2011. **210**(3-4): p. 477-87.
440. Chan, A.C. and I.G. Walker, *Reduced DNA repair during differentiation of a myogenic cell line*. *J Cell Biol*, 1976. **70**(3): p. 685-91.
441. Kuan, C.Y., et al., *Hypoxia-ischemia induces DNA synthesis without cell proliferation in dying neurons in adult rodent brain*. *J Neurosci*, 2004. **24**(47): p. 10763-72.
442. Boor, P.J. and N. Kretschmer, *Increased DNA synthesis in the heart during acute allylamine cardiotoxicity*. *Res Commun Chem Pathol Pharmacol*, 1990. **68**(1): p. 3-11.
443. Stockdale, F.E., *DNA synthesis in differentiating skeletal muscle cells: initiation by ultraviolet light*. *Science*, 1971. **171**(3976): p. 1145-7.
444. Miyazawa, K., T. Shimomura, and N. Kitamura, *Activation of hepatocyte growth factor in the injured tissues is mediated by hepatocyte growth factor activator*. *J Biol Chem*, 1996. **271**(7): p. 3615-8.
445. Anderson, J. and O. Pilipowicz, *Activation of muscle satellite cells in single-fiber cultures*. *Nitric.Oxide.*, 2002. **7**(1): p. 36-41.
446. Sadeh, M., L.Z. Stern, and K. Czyzewski, *Changes in end-plate cholinesterase and axons during muscle degeneration and regeneration*. *J Anat*, 1985. **140 (Pt 1)**: p. 165-76.
447. Merte, J., et al., *A forward genetic screen in mice identifies *Sema3A*(K108N), which binds to *neuropilin-1* but cannot signal*. *J Neurosci*, 2010. **30**(16): p. 5767-75.
448. Moloney, E.B., et al., *Expression of a Mutant *SEMA3A* Protein with Diminished Signalling Capacity Does Not Alter ALS-Related Motor Decline, or Confer Changes in NMJ Plasticity after BotoxA-Induced Paralysis of Male Gastrocnemius Muscle*. *PLoS One*, 2017. **12**(1): p. e0170314.
449. White, F.A. and O. Behar, *The development and subsequent elimination of aberrant peripheral axon projections in *Semaphorin3A* null mutant mice*. *Dev.Biol.*, 2000. **225**(1): p. 79-86.

450. Klitgaard, H., et al., *Function, morphology and protein expression of ageing skeletal muscle: a cross-sectional study of elderly men with different training backgrounds*. Acta Physiol Scand., 1990. **140**(1): p. 41-54.
451. Arbour, D., C. Vande Velde, and R. Robitaille, *New perspectives on amyotrophic lateral sclerosis: the role of glial cells at the neuromuscular junction*. J Physiol, 2017. **595**(3): p. 647-661.
452. Xia, C., et al., *S100 Proteins As an Important Regulator of Macrophage Inflammation*. Front Immunol, 2017. **8**: p. 1908.
453. O'Malley, J.P., M.T. Waran, and R.J. Balice-Gordon, *In vivo observations of terminal Schwann cells at normal, denervated, and reinnervated mouse neuromuscular junctions*. J Neurobiol, 1999. **38**(2): p. 270-86.
454. McCleary, R.J. and R.M. Kini, *Non-enzymatic proteins from snake venoms: a gold mine of pharmacological tools and drug leads*. Toxicon, 2013. **62**: p. 56-74.
455. Yano, H. and M.V. Chao, *Neurotrophin receptor structure and interactions*, in *Pharmacochimistry library*. 2000, Elsevier. p. 253-260.
456. Klein, R., et al., *The trkB tyrosine protein kinase is a receptor for brain-derived neurotrophic factor and neurotrophin-3*. Cell, 1991. **66**(2): p. 395-403.
457. Rodríguez-Tébar, A., et al., *Binding of neurotrophin-3 to its neuronal receptors and interactions with nerve growth factor and brain-derived neurotrophic factor*. The EMBO journal, 1992. **11**(3): p. 917-922.
458. Tucker, K.L., M. Meyer, and Y.-A. Barde, *Neurotrophins are required for nerve growth during development*. Nature neuroscience, 2001. **4**(1): p. 29-37.
459. Schmalbruch, H. and D. Lewis, *Dynamics of nuclei of muscle fibers and connective tissue cells in normal and denervated rat muscles*. Muscle & Nerve: Official Journal of the American Association of Electrodiagnostic Medicine, 2000. **23**(4): p. 617-626.
460. Chen, W., D. Datzkiw, and M.A. Rudnicki, *Satellite cells in ageing: use it or lose it*. Open Biology, 2020. **10**(5): p. 200048.
461. Parker, M.H., P. Seale, and M.A. Rudnicki, *Looking back to the embryo: defining transcriptional networks in adult myogenesis*. Nature Reviews Genetics, 2003. **4**(7): p. 497-507.
462. Balemans, W. and W. Van Hul, *Extracellular regulation of BMP signaling in vertebrates: a cocktail of modulators*. Developmental biology, 2002. **250**(2): p. 231-250.
463. Ip, F.C., J. Cheung, and N.Y. Ip, *The expression profiles of neurotrophins and their receptors in rat and chicken tissues during development*. Neuroscience letters, 2001. **301**(2): p. 107-110.
464. Toti, P., et al., *Nerve growth factor expression in human dystrophic muscles*. Muscle & nerve, 2003. **27**(3): p. 370-373.
465. Küst, B., et al., *Elevated levels of neurotrophins in human biceps brachii tissue of amyotrophic lateral sclerosis*. Experimental neurology, 2002. **177**(2): p. 419-427.
466. Ruberti, F., et al., *Phenotypic knockout of nerve growth factor in adult transgenic mice reveals severe deficits in basal forebrain cholinergic neurons, cell death in the spleen, and skeletal muscle dystrophy*. Journal of Neuroscience, 2000. **20**(7): p. 2589-2601.
467. Baron, P., et al., *Expression of the low-affinity NGF receptor during human muscle development, regeneration, and in tissue culture*. Muscle & Nerve: Official Journal of the American Association of Electrodiagnostic Medicine, 1994. **17**(3): p. 276-284.
468. Mousavi, K. and B.J. Jasmin, *BDNF is expressed in skeletal muscle satellite cells and inhibits myogenic differentiation*. J Neurosci., 2006. **26**(21): p. 5739-5749.
469. Seidl, K., C. Erck, and A. Buchberger, *Evidence for the participation of nerve growth factor and its low-affinity receptor (p75^{NTR}) in the regulation of the myogenic program*. Journal of cellular physiology, 1998. **176**(1): p. 10-21.

470. Deponti, D., et al., *The low-affinity receptor for neurotrophins p75NTR plays a key role for satellite cell function in muscle repair acting via RhoA*. *Molecular biology of the cell*, 2009. **20**(16): p. 3620-3627.
471. Roux, P.P. and P.A. Barker, *Neurotrophin signaling through the p75 neurotrophin receptor*. *Progress in neurobiology*, 2002. **67**(3): p. 203-233.
472. Schor, N.F., *The p75 neurotrophin receptor in human development and disease*. *Progress in neurobiology*, 2005. **77**(3): p. 201-214.
473. Tintignac, L.A., H.-R. Brenner, and M.A. Rüegg, *Mechanisms regulating neuromuscular junction development and function and causes of muscle wasting*. *Physiological reviews*, 2015. **95**(3): p. 809-852.
474. Domingues-Faria, C., et al., *Skeletal muscle regeneration and impact of aging and nutrition*. *Ageing research reviews*, 2016. **26**: p. 22-36.
475. Darabid, H., A.P. Perez-Gonzalez, and R. Robitaille, *Neuromuscular synaptogenesis: coordinating partners with multiple functions*. *Nature Reviews Neuroscience*, 2014. **15**(11): p. 703-718.
476. McMahan, U., D. Edgington, and D. Kuffler, *Factors that influence regeneration of the neuromuscular junction*. *Journal of Experimental Biology*, 1980. **89**(1): p. 31-42.
477. Grumbles, R.M., et al., *Motoneuron replacement for reinnervation of skeletal muscle in adult rats*. *Journal of Neuropathology & Experimental Neurology*, 2012. **71**(10): p. 921-930.
478. Kirsch, M., et al., *Wallerian degeneration and axonal regeneration after sciatic nerve crush are altered in ICAM-1-deficient mice*. *Cell and tissue research*, 2009. **338**(1): p. 19-28.
479. Boyd, J. and T. Gordon, *The neurotrophin receptors, trkB and p75, differentially regulate motor axonal regeneration*. *Journal of neurobiology*, 2001. **49**(4): p. 314-325.
480. Ferri, C.C., F.A. Moore, and M.A. Bisby, *Effects of facial nerve injury on mouse motoneurons lacking the p75 low-affinity neurotrophin receptor*. *Journal of neurobiology*, 1998. **34**(1): p. 1-9.
481. Amano, T., et al., *Production of nerve growth factor in rat skeletal muscle*. *Neuroscience letters*, 1991. **132**(1): p. 5-7.
482. Tatsumi, R., *Mechano-biology of skeletal muscle hypertrophy and regeneration: Possible mechanism of stretch-induced activation of resident myogenic stem cells*. *Animal Science Journal*, 2010. **81**(1): p. 11-20.
483. Brojatsch, J., et al., *CAR1, a TNFR-related protein, is a cellular receptor for cytopathic avian leukosis-sarcoma viruses and mediates apoptosis*. *Cell*, 1996. **87**(5): p. 845-855.
484. AMP. *The Journal of Molecular Diagnostics* 2020; Available from: <https://jmd.amjpathol.org/>.
485. Thermo Fisher. *Introduction to Celleste™ Imaging Analysis Software*. 2019; Available from: file:///C:/Users/Owner/Desktop/Celleste_Training_Guide_UG.pdf.
486. Navarro, D. and D. Foxcroft, *Learning statistics with jamovi: A tutorial for psychology students and other beginners (Version 0.70)*. 2018.
487. Mukaka, M.M., *A guide to appropriate use of correlation coefficient in medical research*. *Malawi medical journal*, 2012. **24**(3): p. 69-71.
488. Menorca, R.M., T.S. Fussell, and J.C. Elfar, *Peripheral nerve trauma: mechanisms of injury and recovery*. *Hand clinics*, 2013. **29**(3): p. 317.
489. Pasterkamp, R.J. and J. Verhaagen, *Semaphorins in axon regeneration: developmental guidance molecules gone wrong?* *Philos.Trans.R.Soc.Lond B Biol.Sci.*, 2006. **361**(1473): p. 1499-1511.
490. Sugiura, Y. and W. Lin, *Neuron-glia interactions: the roles of Schwann cells in neuromuscular synapse formation and function*. *Bioscience reports*, 2011. **31**(5): p. 295-302.
491. Feige, P., et al., *Orienting muscle stem cells for regeneration in homeostasis, aging, and disease*. *Cell stem cell*, 2018. **23**(5): p. 653-664.

492. Riethmacher, D., et al., *Severe neuropathies in mice with targeted mutations in the ErbB3 receptor*. Nature, 1997. **389**(6652): p. 725-730.
493. Reddy, L.V., et al., *Glial cells maintain synaptic structure and function and promote development of the neuromuscular junction in vivo*. Neuron, 2003. **40**(3): p. 563-580.
494. Kang, H., et al. *In vivo imaging of terminal Schwann cells using GFP expressing transgenic mice*. in Society for Neuroscience Abstracts. 2000.
495. Panzer, J.A., Y. Song, and R.J. Balice-Gordon, *In vivo imaging of preferential motor axon outgrowth to and synaptogenesis at prepatterned acetylcholine receptor clusters in embryonic zebrafish skeletal muscle*. Journal of Neuroscience, 2006. **26**(3): p. 934-947.
496. Lemke, G. and M. Chao, *Axons regulate Schwann cell expression of the major myelin and NGF receptor genes*. Development, 1988. **102**(3): p. 499-504.
497. Saika, T., et al., *Effects of nerve crush and transection on mRNA levels for nerve growth factor receptor in the rat facial motoneurons*. Molecular brain research, 1991. **9**(1-2): p. 157-160.
498. Lee, H.K., et al., *Proteasome inhibition suppresses Schwann cell dedifferentiation in vitro and in vivo*. Glia, 2009. **57**(16): p. 1825-1834.
499. Hassan, S., et al., *GAP-43 and p75 NGFR immunoreactivity in presynaptic cells following neuromuscular blockade by botulinum toxin in rat*. Journal of neurocytology, 1994. **23**(6): p. 354-363.
500. Toma, J., et al., *Spatiotemporal increases in epidermal growth factor receptors following peripheral nerve injury*. Journal of Neuroscience, 1992. **12**(7): p. 2504-2515.
501. Roberson, M., et al., *NGFR-mRNA expression in sciatic nerve: a sensitive indicator of early stages of axonopathy*. Molecular brain research, 1995. **28**(2): p. 231-238.
502. Kolodkin, A.L., et al., *Neuropilin is a semaphorin III receptor*. Cell, 1997. **90**(4): p. 753-762.
503. Liu, W., et al., *Inducible depletion of adult skeletal muscle stem cells impairs the regeneration of neuromuscular junctions*. Elife., 2015. **4**.
504. Je, H.S., et al., *Role of pro-brain-derived neurotrophic factor (proBDNF) to mature BDNF conversion in activity-dependent competition at developing neuromuscular synapses*. Proceedings of the National Academy of Sciences, 2012. **109**(39): p. 15924-15929.
505. Fu, S.Y. and T. Gordon, *Contributing factors to poor functional recovery after delayed nerve repair: prolonged denervation*. Journal of Neuroscience, 1995. **15**(5): p. 3886-3895.
506. You, S., et al., *The expression of the low affinity nerve growth factor receptor in long-term denervated Schwann cells*. Glia, 1997. **20**(2): p. 87-100.
507. Savastano, L.E., et al., *Sciatic nerve injury: a simple and subtle model for investigating many aspects of nervous system damage and recovery*. Journal of Neuroscience Methods, 2014. **227**: p. 166-180.
508. Young, P., et al., *Single-neuron labeling with inducible Cre-mediated knockout in transgenic mice*. Nature neuroscience, 2008. **11**(6): p. 721-728.
509. Lichtman, J.W. and H. Colman, *Synapse elimination and indelible memory*. Neuron, 2000. **25**(2): p. 269-278.
510. Kang, H., L. Tian, and W. Thompson, *Terminal Schwann cells guide the reinnervation of muscle after nerve injury*. Journal of neurocytology, 2003. **32**(5-8): p. 975-985.
511. Rich, M.M. and J.W. Lichtman, *In vivo visualization of pre-and postsynaptic changes during synapse elimination in reinnervated mouse muscle*. Journal of Neuroscience, 1989. **9**(5): p. 1781-1805.
512. Chan, S., et al., *A method for manual and automated multiplex RNAscope in situ hybridization and immunocytochemistry on cytospin samples*. PloS one, 2018. **13**(11): p. e0207619.

513. Kann, A.P. and R.S. Krauss, *Multiplexed RNAscope and immunofluorescence on whole-mount skeletal myofibers and their associated stem cells*. *Development*, 2019. **146**(20): p. dev179259.
514. Chermahini, G.A., A. Rashnonejad, and S.Q. Harper, *RNAscope in situ hybridization-based method for detecting DUX4 RNA expression in vitro*. *Rna*, 2019. **25**(9): p. 1211-1217.
515. Hildyard, J.C., et al., *Single-transcript multiplex in situ hybridisation reveals unique patterns of dystrophin isoform expression in the developing mammalian embryo*. Wellcome Open Research, 2020. **5**(76): p. 76.
516. Fu, S.Y. and T. Gordon, *Contributing factors to poor functional recovery after delayed nerve repair: prolonged denervation*. *J.Neurosci.*, 1995. **15**(5 Pt 2): p. 3886-3895.
517. Marques, M.J., et al., *Nerve-terminal and Schwann-cell response after nerve injury in the absence of nitric oxide*. *Muscle & Nerve: Official Journal of the American Association of Electrodiagnostic Medicine*, 2006. **34**(2): p. 225-231.
518. Mech, A.M., et al., *Post-synaptic morphology of mouse neuromuscular junctions is linked to muscle fibre type*. *bioRxiv*, 2020.
519. Marques, M.J., J.-A. Conchello, and J.W. Lichtman, *From plaque to pretzel: fold formation and acetylcholine receptor loss at the developing neuromuscular junction*. *Journal of Neuroscience*, 2000. **20**(10): p. 3663-3675.
520. Li, Y., Y. Lee, and W.J. Thompson, *Changes in aging mouse neuromuscular junctions are explained by degeneration and regeneration of muscle fiber segments at the synapse*. *J.Neurosci.*, 2011. **31**(42): p. 14910-14919.
521. Valdez, G., et al., *Attenuation of age-related changes in mouse neuromuscular synapses by caloric restriction and exercise*. *Proceedings of the National Academy of Sciences*, 2010. **107**(33): p. 14863-14868.
522. Chang, C. and C. Lee, *Electrophysiological study of neuromuscular blocking action of cobra neurotoxin*. *British journal of pharmacology and chemotherapy*, 1966. **28**(2): p. 172.
523. Duchon, L.W., *The effects of tetanus toxin on the motor end-plates of the mouse. An electron microscopic study*. *J.Neurol.Sci.*, 1973. **19**(2): p. 153-167.

Appendix

6 EXPERIMENTAL METHODS AND MATERIALS

6.1 Mice and surgery

Adult male C57BL6 mice (10 weeks old, n=84) were housed and handled according to regulations set by the Canadian Council on Animal Care as approved by the University of Manitoba, protocol F14-015. Half the mice received a daily oral dose of ISDN (66 mg/kg in canola oil; at a volume of 2.7 μ l/g body weight) for 2 days [378, 405] as “pretreatment” before surgery (24hr after the second dose). Animals were assigned to receive either crush (CR, n=40) or cardiotoxin injury (CTX, n=40) such that half of each injury group received pretreatment with ISDN and the other half did not.

Crush injury: This caused injury to the entire tissue contained in a muscle “belly” through a focal region (approx. 1mm wide) across the mid-region of the tibialis anterior muscle (TA). At this region of the TA, muscle myofibers, blood vessels and nerves were damaged and need to regenerate; SCs survived the trauma and began the process of muscle regeneration. The pre-surgical administration of analgesia through subcutaneous injection of meloxicam (1mg/kg, Boehringer Ingelheim, Japan) 20-30 minutes prior to surgery and 1mg/kg at 24 and 48 hr post-surgery helped to mitigate the surgery pain. After injection with meloxicam (subcutaneous, 2mg/kg) for analgesia 20-30 minutes prior to surgery, mice were anesthetized (isoflurane (2-3% concentration) inhalation for induction in a chamber, then maintained under anesthesia using a nose cone and Bupivacaine (B5274, Sigma Aldrich, USA). Eye lubricant (Optixcare, AVENTIX, Canada) was used as adjunctive support to dry eye and then mice were ear-punched in order to facilitate record keeping.

Surgery was conducted using aseptic technique. The hair over the front of the left hind limb was clipped and the skin was cleaned by chlorhexidine scrubs and betadine swabs, then were dried. After preparing the area, the mouse was draped (88VCSTF5, Gepco, INC., USA) then a skin incision was made using autoclaved surgical scissors, approximately 7 mm long along the length

of the leg, to expose the TA muscle. The connective tissue over the TA was carefully opened using surgical scissors to avoid damage to the muscle and blunt-end forceps were passed beneath the mid-belly of the TA (below its attachment to the tibia), to separate it from surrounding and deeper muscles, avoiding damage to the nerve and blood supply at the proximal aspect, deep to the TA. After withdrawing the forceps, one blade of a small hemostat was passed beneath the mid-belly of the TA and the hemostat was closed (to one click) over the TA for 5 seconds. The hemostat was released, 30 seconds were allowed to pass (to check for the blood loss), and the skin was closed using 3-4 absorbable monofilament sutures (3-0 monocryl, Ethicon, USA). Animals were placed on a clean paper towel under a warming light and observed until fully mobile (approx. 15-20 min).

Animals were monitored for the next hour, and then at 2 and 3 hours post-surgery, before returning (in single cages) to the animal room. At both 24 and 48 hours after surgery, mice received repeated injections of meloxicam analgesic. After the third injection, and following examination of body weight, animal movement and physical signs, mice were returned to group housing, in a cage of 2 or 3 mice together, as they are social animals. Mouse behavior and muscle use were monitored after crush injury and CTX injection (see below) all during the post-surgical period to make sure any possible behavioral abnormalities were observed. This served as a concrete monitor of post-surgery animal condition and we were able to sacrifice the few mice in emergency cases, to avoid excessive inflammation and suffering, as required under animal care guidelines.

Mice were maintained after surgery for up to 10 days. Two hours before euthanizing, mice received an injection of bromodeoxyuridine (BrdU, subcutaneously, 100 mg/kg in 0.1 ml, *intra peritoneal*, B5002, Sigma Aldrich, USA) to label dividing cells. Mice were euthanized by cervical dislocation under isoflurane anesthesia at 0, 2, 4, 6, 10 days post-injury. All the animal procedures were approved in the animal protocol F14-015, at the University of Manitoba.

Cardiotoxin (CTX) injection: The basis of this mode of injury is that it selectively injures muscle fibers, leaving muscle SCs, nerves and blood vessels intact in position in the muscle, for myofiber regeneration. The muscle regeneration that is induced by this injury, therefore provides a comparator for the coordinated regeneration of muscle and non-muscle tissues that are induced by the crush-injury procedure.

Mice were anesthetized with isoflurane (as above) and were injected with meloxicam (2 mg/kg) for analgesia post-operatively. Surgery was conducted using an aseptic technique. The skin over the lower left hind limb was cleaned by chlorhexidine scrubs and betadine swabs, then was wiped dry. A syringe (309626, BD, USA) equipped with a 25-gauge needle (305122, BD, USA) was used to inject cardiotoxin (CTX, a potent polypeptide snake venom from the *Naja mossambica* snake) through the skin and into the TA.

To administer CTX, a needle was inserted into the TA at 4 locations from proximal to distal, and CTX (0.1 ml of a 10 mM stock solution) was slowly injected into the muscle in each location. Mice were monitored post-surgery for recovery of locomotion, and during the time-course of regeneration (0-10 days) a record of behavior and muscle use was used as a 'clinical' indicator of muscle damage. CTX tends to produce rapid disuse of muscle, although both models of injury result in very mild overt disuse or change in behavior after 2 days. Euthanasia by cervical dislocation under isoflurane anesthesia occurred at 0, 2, 4, 6, 10 days post-injury.

In the CTX-injured muscles, most of the TA, if not the whole TA muscle, is damaged by exposure to the myotoxin (by 4 injections along the length of the muscle). By comparison, after crush injury, the mid-section of the muscle is directly damaged, and then the region of injury is secondarily extended by the inflammatory response to the necrotic fibers; this leaves both proximal and distal segments of the muscle that survive the injury. For comparison with processes in CTX-injured muscles, only the damaged and regenerating segment of the TA in crush-injured muscles was used for study of protein or gene expression, while full-length longitudinal sections of the other half of each muscle (including proximal and distal surviving regions) were used for sectioning and staining, to help orient observations of the regeneration and reinnervation processes.

6.1.1 Tissue handling

TA muscle samples were dissected out of the limb, cut in half longitudinally. Half of each muscle was transferred to 4% paraformaldehyde (P6148, Sigma Aldrich, USA) in phosphate-buffered saline (PFA) and kept at 4°C for 24 hours for fixation and then transferred to cryoprotectant (4°C for 2-3 days) until they were embedded in optimal temperature control medium and flash frozen for sectioning. The right hind limb TA muscle was collected as the non-injured control. Muscle samples were removed from cryoprotectant, first blotted on a filter paper

and transferred into Tissue-Tek® Cryomold® Biopsy molds 10 x 10 x 5 mm (4565, Sakura Finetek, Torrance, California, USA) filled with Shandon cryomatrix medium (28-600-51, Fisher, Pittsburgh, Pennsylvania, USA) and immersed in -50°C isopentane (AC126470010, Fisher, New Jersey, USA) for 4-6 minutes to freeze.

Eight sections of right and left TA muscle for each sample were collected on gelatin coated slides using cryostat at -20°C [160, 405] and 10 slides were prepared for each sample. Cryosections were subjected to staining for routine histology, and histochemistry and/or immunostaining for protein markers of myogenesis, synapse formation and function, receptors, etc. The other half of the TA muscle samples were collected into 1.5 mL of RNA-later solution (AM7024, Life Technologies, Burlington, Ontario, Canada) and stored at -20°C before processing for protein extraction and western blotting to quantify the proteins of interest.

6.2 Hematoxylin and Eosin staining

Hematoxylin and eosin staining (H&E staining) was used as a principal histology method. H&E staining involves application of hemalum (a complex formed from aluminum ions-based complex) and hematein (an iron-based hematoxylin product). Hematoxylin is basic (positively charged), and binds to basophilic elements which are negatively charged and acidic, including DNA and RNA. Hemalum therefore, colors nuclei, calcified material and keratohyalin granules blue. Eosin is acidic and binds to acidophilic elements which are positively charged, such as basic proteins. It colors eosinophilic structures in different shades of pink, orange and red. Immunostaining is a method utilized to define in which cells a specific protein is located. These stains utilize the protein-binding feature of antibodies to bind to particular antigens in a cell or tissue, and antibodies are detected using conjugated molecules such as colored or fluorescent markers, or enzymes such as horseradish peroxidase (HRP).

One slide per mouse (total of 10 slides) was brought to room temperature for 30 minutes. Next, slides went through sequential incubations in different solutions, each for a various period. Slides were first submerged in 100% ethanol (A405P-4, Fairlawn, New Jersey, Fisher, USA) for two episodes of five minutes, following submersing in 95% ethanol for 2 minutes. Slides were then rinsed through soaking in distilled water for 5 minutes (mentioned as “rinse” hereafter), following incubation in Harris’ Hematoxylin (SH26-5001, Fisher, Fairlawn, New Jersey, USA) for 4.5 minutes to stain nuclei and then rinsed. Afterward, slides were immersed in 1% acid alcohol

five times and then rinsed. Slides were incubated in saturated lithium carbonate (L119500, Fisher, Fairlawn, New Jersey, USA) for 2 minutes, followed by another rinse. At the next step, slides were immersed in Eosin (SE23-5001, Fisher, Fairlawn, New Jersey, USA) for 2 minutes to stain fiber cytoplasm, and then were dipped ten times in distilled water, ten times in 70% ethanol and fifteen times in 95% ethanol. Lastly, slides were incubated in 100% alcohol solution for two, 2-minute phases followed by two, 2 minute phases in Slide Brite™ (Sasco of Georgia Inc., Albany, Georgia). Slides were then air dried briefly, followed by mounting with coverslips by means of Permount mounting medium (Fisher, Hampton, New Hampshire).

Myotubes were photographed within the mid-belly of the TA after CTX injury and in the regenerating zone of CR muscles, one 20X field proximal to the directly-crushed region [54]. Ten non-overlapping fields (200X) were photographed using an Olympus BH-2 microscope and a UC-50 digital camera (Olympus, Richmond Hill, ON Canada). Myotube diameter was measured in the first 100 myotubes in each section using calibrated NIH Image J software. Muscle fiber diameter was also measured in day-0 injured muscles and in TAs of untreated control animals, as a baseline.

6.3 NMJ maturation

An overview of post-synaptic configurations on new myotubes was examined using coded slides of regenerating muscle and direct-fluorescent staining for AchRs [428], as reported for developing [429] and pathological muscle [240]. Alpha-bungarotoxin (α -BTX) is a neurotoxic protein, discovered in the venom of the krait snake; it binds specifically to acetylcholine receptors at NMJs and can be utilized to analyze the arrangement of AchRs via the direct fluorescence approach [428]. Fluorescent-tagged α -BTX was utilized to display the morphological characteristics of NMJs and to clarify whether myofibers are normally innervated or denervated.

To perform α -BTX fluorescence staining, muscle sections were brought to RT for 30 minutes and then incubated in 0.01M phosphate buffered saline (PBS) for 2 minutes (mentioned as “wash” hereafter). After fixation with acetone for 1 minute, they were air dried for 10 minutes, washed again with PBS and then incubated at 4°C overnight with 200 μ L of fluorescein-conjugated α -BTX (F1176, Invitrogen, Carlsbad California) in PBS (dilution of 1:200) per slide. The day after, slides were washed with PBS in dark and then mounted with Vectashield (H-1000, Cedarlane, Burlington, ON, Canada) and visualized. Ten non-overlapping images per section were captured using a 40X objective lens through systematic scanning across the sections.

Pre-synaptic regions of AchE activity and the configuration of motor neurites and nerve terminals were detected with histochemistry and silver staining in sections of muscle. AchE sites form a plaque on the fiber membrane in mature NMJs while silver staining of intramuscular pre-synaptic motor neurites typically shows one or more branches emanating from an axon toward a smaller AchE plaque [56, 429].

Sections were incubated in fresh 2.6 mM acetyl-thiocholine iodide (A5751, Sigma Aldrich, USA) mixed in 0.1 M sodium hydrogen maleate buffer (pH 6.0) containing 0.1 M sodium citrate, 30 mM copper sulphate and 5 mM potassium ferricyanide. After rinsing in distilled water, sections were incubated in 0.5 M potassium ferricyanide, rinsed again, and incubated (60 min) in aqueous 10% silver nitrate. Sections were rinsed, saturated with Bodian's developer (5.0 g sodium sulfite and 1.0 g hydroquinone in 100 ml distilled water), rinsed in 1% glacial acetic, dehydrated in ethanols, and coverslipped. Images from 10 non-overlapping fields were captured using a 40X objective lens on a Zeiss Apotome (Jena, Germany). The number of silver-stained plaques, either mature ovals of AchE plus neurites (\pm terminal boutons) or smaller, immature AchE plaques with neurite branches, was counted in each field of regenerating fibers. The mature proportion of all silver-stained plaques was compared among groups.

A combination of BTX direct-fluorescent staining and silver-staining histochemistry (processed in that order) was applied to sections from approximately half the mice per group and used as a further assessment of NMJ maturity. NMJ regions were scored according to the presence or absence of colocalized post-synaptic AchRs (BTX+) plus pre-synaptic silver staining for AchE plaques and motor neurites. The distribution of NMJ regions with BTX+ regions, silver staining (neurites+AchE), or both (neurites+AchE+BTX) was determined by counting all stained regions in 10 non-overlapping fields of regenerating myotubes photographed using a 40X objective lens.

6.4 Protein-expression studies using Western Blotting

The levels of Sema3A, γ AchR, S100, and a loading control (β -actin) were assayed using Western blots of muscle-protein extracts using standard protocols for extraction, electrophoresis, blotting, and chemiluminescence detection, as reported [160, 240, 405]. Membranes were probed with primary antibody mixed in Immunoreaction Enhancer Solution-1 then secondary antibodies mixed in Immunoreaction Enhancer Solution-2 (NKB-101, Toyobo, Osaka, Japan) to detect the

protein of interest [352] before probing for the loading control to standardize quantification. In one lane of each gel, 3 μL of Western protein molecular weight standards (MagicMark XP, LC5602, Fisher) was loaded to provide direct visualization of the standard on the blot.

6.4.1 Protein Isolation and Assay

The western blotting procedure was done based on a standard lab protocol [160, 430]. Tissue samples kept at -80°C thawed on ice and removed from RNA-later storage solution. Sample muscles were then weighed and chopped with a razor blade into small pieces, in a petri dish on ice. Samples were added to Matrix D lysing tubes (116913500, MP Biomedicals, Solon, OH, USA) containing ceramic spheres. Lysis buffer was pipetted into the tubes (200 μL for every 0.01g). Samples were homogenized two times at 4.0m/s for 20 seconds each time in the Fast-Prep 24 homogenizer (MP Biomedicals, Solon, OH, USA). Afterwards, tubes were vortexed for 30 seconds and incubated on ice for 1 hour, followed by another vortexing for 30 seconds. Muscle samples were then centrifuged at 10,000 rpm for 5 minutes and the protein extract of each sample (the supernatant) was transferred into Eppendorf® tubes (22363352, Fisher) to be stored at -80°C for further use or be processed for protein assay.

A protein assay was performed utilizing the BCA Pierce Protein Assay Kit (23227, Pierce, Fisher), to adjust the concentration of protein in each sample so 20 μg of protein could be loaded into each well of gels. A 2.0g/mL stock solution of bovine serum albumin (BSA) was diluted to different concentrations of 2000, 1500, 1000, 750, 500, 250, 125, 25, and 0 $\mu\text{g}/\text{mL}$ (blank) for use in calibrating sample concentration. Working reagent was then made in a 50:1 ratio of Reagents A: B, and 1.0 mL of working reagent was added into labeled tubes containing 50 μL of each of the BSA standard dilutions. In other tubes, 2.5 μL of each prepared protein sample was added to 47.5 μL sterile distilled water (DW) plus 1.0mL of the working reagent. All labelled tubes (standards and samples) were incubated together for 1 hour in a water bath at 37°C and then cooled for 10 minutes to RT. The absorbance of the fluid in each tube was measured by means of a spectrophotometer set to 562nm. Absorbance values for each of the standards were plotted against their protein concentration and utilized to make a standard curve; the equation of the linear-fit line (in Microsoft Excel 2010) was applied to absorbance of the samples to determine the concentration of unknown proteins in the samples. Appropriate sample volumes containing 20 μg of protein were aliquoted and stored at -80°C until further use for Western blotting.

6.4.2 Protein Sample Preparation

Aliquoted protein of each sample was thawed from -80°C , mixed with $3\ \mu\text{L}$ loading sample buffer (S3401, Sigma Aldrich, ON, Canada), and centrifuged for 1 minute before being incubated in a block heater for 9-10 minutes at 98°C . Tubes were then quenched for 1 minute on ice and centrifuged for 3 minutes before being loaded into gels.

6.4.3 Gel Electrophoresis

Following preparation and pouring of separating gel from 9% polyacrylamide, gels were polymerized for 30 minutes. A stacking gel solution was added on the top of the solid separating gel. The stacking gel was polymerized for 30 minutes while a 15-tooth comb was embedded at the top of the gel. Running buffer was prepared and poured in an assembled electrophoresis apparatus (BioRad Inc., Mississauga, Ontario) before loading the samples into wells. A molecular weight marker (1610374, BioRad Inc.) was also loaded into the first well of each gel. Gels were first run at 80V for 10 minutes until the dye in the sample buffer reached the top of the separating gel, and then run at 120-130V until the dye moved off the end of the gel.

Polyvinylidene fluoride (PVDF) membranes (PV4HY00010, Immobilon Millipore Corporation, Billerica, MA) were soaked in methanol for 10 min, rinsed with DW and used to blot the gels. Transfer buffer was made to fill a BioRad blotting apparatus (Mississauga, Ontario) and a transfer sandwich was assembled for each membrane using two different types of sponges, the filter, the gel, and a PVDF membrane, according to manufacturer's instructions. The process of protein transfer to the membrane was done at 100V for 1 hour. Following 3 rinses with DW, the membranes were blocked for an hour in 5% milk powder (w/v) in PBS-Tween 20 (PBS-T) and then incubated at 4°C in a primary antibody solution prepared in 5% milk powder in PBS-T overnight. The membranes were washed in PBS-T three times the next day and incubated for one hour at RT in a secondary antibody solution prepared in 5% milk powder in PBS-T. The membranes were then washed with PBS-T three times and analyzed utilizing the VersaDoc method, described below.

6.4.4 Developing the Membrane

The chemiluminescence exposure method used with Santa Cruz Western blotting luminol-detection technique for using horseradish peroxidase (HRP) to quantify proteins. Prepared

membrane blots were first incubated in luminol (2048, Santa Cruz Biotechnology, Inc., Dallas, TX, USA) for 1 minute and then placed on a plastic film inside the VersaDoc chamber (BioRad Inc.). Images were captured from the membranes via the QuantityOne program over a period of 600 seconds with increasing exposure increments of 100 seconds. Captured images were then opened in ImageOne software to measure the density of the relevant bands and band intensity was tabulated in Excel 2010 for further analysis.

6.4.5 Quenching the Membranes

As the last step, membranes were re-probed for a loading control (β -actin) to standardize quantification of the above-mentioned proteins. Subsequent to probing for a given protein of interest, each membrane was quenched as described before [430]. In brief, after washing with PBS-T three times (10 minutes each time), membranes were quenched with 27% H_2O_2 (H1009, Sigma, Canada) for 20 minutes; this was followed by three additional washes with PBS-T. Afterwards, membranes were incubated overnight at 4°C in the primary anti- β -actin prepared in 5% milk powder (weight/volume) in PBS-T. The membranes were washed with PBS-T the next day, and incubated at RT for one hour in a HRP-conjugated secondary antibody solution, prepared in 5% milk powder in PBS-T. The membranes were then washed with PBS-T and developed for luminol detection and analyzed for β -actin concentration, by means of the VersaDoc software as already described.

6.5 Immunostaining

The sample slides were brought from -20°C to RT for 30 minutes, washed with 0.01M PBS and then processed for antigen retrieval (incubating in 2N hydrochloric acid (HCl) for 10-15-minute followed by 10 min air drying) when required. Another set of three washes with 0.01M PBS was performed before sections were incubated 30 minutes in 1% Triton-X 100 (Mallinckrodt, Pointe-Claire, Quebec) at RT. Slides were then incubated in blocking solution for 1 hour at RT containing the serum of the host animal of the secondary antibody plus 2M glycine and unconjugated antibody against the host of the primary antibody at a ratio of 20:1:1, as previously reported [240], to decrease non-specific background staining. Slides were then further washed 3 times with 0.01M tris-buffered saline with Tween-20 (TBS-T), followed by blocking with 0.001% avidin solution at RT for 15 minutes. The slides were rinsed again with PBS then blocked for

another 15 minutes at RT in 0.001% biotin solution to further decrease background staining. Following three washes in TBS-T, slides were then incubated at 4°C with a primary antibody solution overnight. The day after, slides were incubated with a fluorescent secondary antibody in dark for 1 hour to visualize through the HRP staining method. In some instances, slides were incubated in multiple primary antibodies together, rinsed thoroughly and then incubated in the appropriate secondary antibodies for double, or triple immunostaining.

6.6 Antibody Information

Blocking antibodies in double immunofluorescence staining included: unconjugated Fab Fragment goat anti-mouse IgG (115-007-003, Jackson ImmunoResearch, 1:200), and unconjugated Fab Fragment goat anti-rabbit IgG (11-007-003, Jackson ImmunoResearch, 1:200).

Primary antibodies used in double fluorescence staining included: rabbit anti-Pax7 (ab34360, Abcam, 1:150), Mouse anti-NGFR p75 Antibody (sc-271708, Santa Cruz, 1:500) and mouse anti-BrdU (11170376001, Roche, 1:200). Secondary antibodies included: goat anti-rabbit IgG DyLight650 (ab96902, Abcam, 1:200), goat anti-mouse IgG conjugated with DyLight488 (ab96879, Abcam, 1:200) and goat anti-mouse IgG conjugated to horseradish peroxidase (HRP) (A2304, Sigma, 1:200). DAPI was used to counterstain nuclei (D9542 Sigma, 1:10000).

For western blotting, primary antibodies included: rabbit anti-Semaphorin 3A (ab23393-50, Abcam, 1:5000), rabbit anti- γ AchR (sc-13998, Santa Cruz, 1:300), rabbit polyclonal anti-S100B (orb228251, Biorbyt, 1:3000), mouse anti- β -actin (sc-81178, Santa Cruz, 1:1500). Secondary antibodies included: HRP-conjugated goat anti-rabbit IgG H&L (ab97057, Abcam, 1:5000), and HRP-conjugated goat anti-mouse (A-2304, Sigma, 1:5000). Recombinant mouse Semaphorin3A Fc chimera protein (5926-S3-025/CF, R&D Systems) served as a positive control.

6.7 Fluorescence immunostaining

To visualize the BrdU incorporation in activated SCs (Pax7+), the muscle samples were developed with fluorescent antibodies. After an incubation with primary antibody solution (anti-Pax7 and anti-BrdU) overnight, slides were washed three times with TBS-T before incubation with a fluorescent secondary antibody solution for 1 hour at RT. Following incubation for 1 hour at RT and in dark with the secondary antibody solution, slides were washed again with TBS-T and mounted further with Vectashield mounting medium (H-1000, Cedarlane, Burlington, ON,

Canada) and visualized on the Zeiss ApoTome (Jena, Germany). A maximum of 10 non-overlapping images per section was taken with a 100X oil immersion lens for fluorescence, differential interference contrast (DIC) and 4',6'-Diamidino-2-phenylindole dihydrochloride ((DAPI), D9542, Sigma) imaging. Fluorescent SCs were identified by Pax7+ fluorescence overlapping DAPI nuclear staining in each image. The number of Pax7+ SCs was counted and compiled in Excel 2010 (Microsoft) as activated (Pax7+ and BrdU+) or not (Pax7+ and BrdU-), and the proportion of active SCs (BrdU+/Pax7+ over the total number of Pax7+ cells) was compared between groups using Student's t-tests.

6.8 The generation of Sema3A-Cko Mice

Pax7CreER^{T2}-Sema3A^{flox} (Sema3A-cKO) mice were generated through mating Pax7-CreER^{T2} with Sema3A-loxP mice, a method originally developed by Dr. Shahragim Tajbakhsh (Institute Pasteur, France) and Dr. Takeshi Yagi (Osaka University, Japan) and assigned to Dr. Tatsumi (Kyushu University). Transgenic mice were kept in the animal holding facility at the Kyushu University and housed in 22°C and on a 12-hour light/dark cycle with free access to regular food and deionized water. The Cre recombinase was conditionally activated in adult male mice (8–10 weeks old) and under control of the Pax7 promoter by a daily i.p. injection of tamoxifen (TMX, ER^{T2} agonist) with a 27-gauge needle for 3 days. This amount of tamoxifen was found to be sufficient to significantly suppress Sema3A expression by SCs [297]. The mice were then rested for two weeks before undergoing surgery. Sema3A-loxP mice (N=5) were used as controls and received the same amount of tamoxifen and at the same age as Sema3A-cKO mice.

6.8.1 Tamoxifen preparation

To prepare 20 ml TMX solution, 400 mg tamoxifen (T5648, sigma) has be weighed and transfer to a 50 ml falcon tube, wrapped with aluminum foil and be kept on ice. Then, 1000 ul of ethanol was added on top of the TMX and repeatedly vortexed (3 mins.) and inverted to ensure the mixture was dissolved. As the next step, 19 ml of sunflower oil (S5007, Sigma) was added on top of that and the lid was sealed with parafilm tightly to keep it away from air and then again covered with aluminum foil. A beaker was filled with tap water and ice and was kept in a sonicator. The tube was vortexed for 3 mins and then shaken in the sonicator for another 3 mins to cool down. This step was continued for three and a half hours and then the tube was left aside for 30 mins to

make sure no bubbles were in the solution and then the solution was distributed in microcentrifuge tubes and was kept in -20°C for a month. The 9 weeks old male mice (n=15) were weighed and received 10 µl/gram weight of TMX (wrapped in foil and kept on ice) and through intraperitoneal injection. The injection was repeated for 3 days in row and at the same every day. Pre-surgery TMX injections were done under anesthesia [362]. The solution was kept at 4°C in the dark until use.

Mice had muscle crush injury (as described above) or nerve crush injury 2 weeks after TMX injection. Sciatic nerve crush was performed by exposing the left sciatic nerve at the mid-thigh level and crushing it for 30 seconds in hemostatic forceps with grooved jaws before closing the skin with sutures. In some cases, mice that chewed sutures had a collar applied to prevent their access to the wound. Mice were kept in separate cages for 2-4 days, and then returned to the group cages. TA samples for sectioning were collected and prepared as described above.

6.9 In situ hybridization

Fluorescence in situ hybridization was conducted to detect multiple gene transcripts using RNAScope technology available from Advanced Cell Diagnostics (ACD, Hayward, CA). At a low concentration, the threshold levels of detection per cell are approximately 10-20 copies of mRNA using this technology, with variation attributable to potential masking of the sequence of interest by an associated protein or cellular structure. Thus, the type of probe is an important parameter.

The ACD technology employs a double-Z design model which utilizes a series of target probes to hybridize to a single target mRNA molecule. This novel strategy improves the signal-to-noise ratio through amplifying target-specific signals, but does not amplify potential background signals from non-specific hybridization. Each target probe comprises an 18- to 25-base region complementary to the target RNA, plus a spacer sequence, and a tail sequence that contains 14 bases (known as Z). A pair of target probes (double-Z), with different types of tail sequence, hybridize to a 50-base target region in the RNA of interest. The two tail sequences shape a 28-base hybridization spot for the preamplifier, which holds 20 binding spots for the amplifier, which in turn, has 20 binding spots for the target probe. Normally, a 1-kb section on the RNA molecule is labeled with 20 probe pairs. This means that sequential hybridizations containing preamplifier, amplifier, and target probe theoretically produce 8000 labels for every target RNA molecule. The

HRP-labeled or alkaline phosphatase probes can also be used for chromogenic reactions, for detection by bright-field microscopy. In this study, the target probes were fluorescently labeled for direct visualization under an epifluorescence microscope (Apotome, Zeiss).

Multiple RNA species were determined concurrently in two different ways by using the same tail sequence in target probes for different mRNAs, and several signal-amplification steps with multiple-label probes were used to find each RNA species; this aspect of the technology allows for complex recognition of various target RNAs. NIH ImageJ software was used to determine two-probe pairs (labelling with two fluorochromes) that generated visibly colocalized signals. Ten pairs were selected for each probe, for ideal signals and to add robustness against partial RNA degradation and variable target accessibility.

The sequences for target probes, preamplifier, amplifier, as well as label probes were sourced through <http://jmd.amjpathol.org> and supplied by Advanced Cell Diagnostics (Hayward, CA). The probes were labeled to detect Sema3A, S100, Pax7 and P75NGFR for fluorescent detection (Molecular Probes; Invitrogen, Eugene, OR). Assays were done along with positive and negative controls in each staining run for *in situ* hybridization, to ensure results were appropriately interpreted. Based on the finding from earlier studies on NMJ maturation, *in situ* hybridization was conducted on slides from animals after crush and CTX injury (with and without pre-treatment) at day 0 (crush and CTX), day 6 (CTX), and days 8 and 10 (crush). Other *in situ* hybridization experiments were conducted on all samples collected from Japan.

The assay was started by turning the HyBEZ™Oven (Advanced Cell Diagnostics, Hayward, CA) on and setting the temperature on 40°C. The tray was warmed for 30 minutes at 40°C before use. A humidifying paper was placed in the Humidity Control Tray and wet completely with DW. The covered tray was inserted into oven and the oven door was closed to keep the temperature constant. Then, 200 mL of fresh RNAscope® 1X Target Retrieval Reagent was prepared by adding 180 mL DW to 20 mL 10X Target Retrieval Reagent. The slides were laid on the bench and about 1 drop (100µL) of RNAscope® Hydrogen Peroxide was applied to cover the entire section before slides were incubated for 10 minutes at RT. The RNAscope® Hydrogen Peroxide solution was removed from one slide at a time by tapping and/or flicking the slide on absorbent paper. The slide was taken immediately into an autoclaved slide rack submerged in a staining dish filled with DW.

A steamer (4 qt, Black & Decker, Canadian Tire, Winnipeg MB) was used to perform target retrieval and two slide holders were placed in the steam bowl (each filling with 200 mL of RNAscope® 1X Target Retrieval Reagent and 200 mL of distilled H₂O). The steamer timer was set to heat for 95 minutes and temperature was allowed to rise to at least 99°C. The slides were added to the container containing DW for 10 seconds to acclimate slides and then moved to the container containing RNAscope® 1X Target Retrieval Reagent. The slides were removed from the steamer after 5 minutes, transferred to a separate rinse container with 200 mL of DW and rinsed for 15sec. The slides were then transferred into 100% alcohol for 30 minutes and then dried in 60°C incubator (or at RT). A barrier was drawn 2–4 times around each section with an Immedge™ hydrophobic barrier pen and the barrier was allowed to dry completely (1 minute or overnight) at RT.

Dried slides were placed on the ACD EZ-Batch™ Slide Rack, and about 1 drop (100 µL) of RNAscope Protease Plus was added to entirely cover each section. The HybEZ™ Humidity Control Tray was removed from the HybEZ™ Oven and the slide rack was placed in the tray. The lid was closed, sealed, and the tray was inserted back into the oven and incubated at 40°C for 10–15 minutes. Each slide, one at a time, was taken from the slide rack and tapped and/or flicked to remove excess liquid before being placed immediately in an autoclaved slide rack submerged in a staining dish filled with DW. The slides were then washed 3–5 times by moving the slide rack up and down in the distilled water.

Excess liquid was again removed from the slides, and slides were placed in the HybEZ™ or EZ-Batch™ Slide Rack. One drop (100µL) of the probe mix was added to entirely cover each slide and the slide rack containing the slides was inserted into the HybEZ™Oven for 2 hrs at 40°C. The slides were washed in 1X Wash Buffer for 2 minutes at RT. Around 1drop (100µL) RNAscope® Multiplex FL v2 Amp 1 (amplifier 1) was added to entirely cover each slide and then returned back into the HybEZ™Oven for 30 minutes at 40°C. Next, around 1drop (100µL) RNAscope® Multiplex FL v2 Amp 2 was added to entirely cover each slide, the slides were returned into the HybEZ™Oven for 30 minutes at 40°C. The slides were washed in 1X Wash Buffer for 2 minutes at RT. Around 1 drop (100µL) RNAscope® Multiplex FL v2 Amp 3 was added to entirely cover each slide, the slides were returned to the HybEZ™Oven for 15 minutes at 40°C and then were washed in 1X Wash Buffer for 2 minutes at RT.

To develop the HRP-C1 signal, one drop (100 μ L) of the RNAscope® Multiplex FL v2 HRP-C1 solution was added to entirely cover each slide before slides were inserted into the HybEZ™Oven for 15 minutes at 40°C. Slides were then washed in 1X Wash Buffer for 2 minutes, excess liquid was removed and 150–200 μ L diluted TSA® Plus fluorescein was added to each slide followed by a 30-minute incubation at 40°C. After a 2-minute wash in 1X Wash Buffer around 1 drop (100 μ L) RNAscope® Multiplex FL v2 HRP blocker was added to each slide, and slides were incubated at 40°C for 30 minutes, and then washed with 1X Wash Buffer for 2 minutes at RT.

During the next step and to develop HRP-C2 signal, around 1 drop (100 μ L) RNAscope® Multiplex FL v2 HRP-C2 was added to each slide, and slides were incubated for 15 minutes at 40°C in the oven and then were washed in 1X Wash Buffer for 2 minutes at RT. Next, 150–200 μ L diluted TSA® Plus TMR was added to each slide, and slides were incubated for 30 minutes at 40°C before being washed in 1X Wash Buffer for 2 minutes at RT. This was followed by adding 1 drop (100 μ L) RNAscope® Multiplex FL v2 HRP blocker to each slide, for a 15-minute incubation at 40°C. Slides were then washed for 2 minutes at RT in 1X Wash Buffer. After the last step, excess liquid was removed from slides, and 100 μ L of DAPI was added to each slide and incubated for 30 minutes at RT. Then, 1–2 drops of ProLong Gold Antifade Mountant were placed on each slide and slides were covered with 24 mm x 50 mm glass coverslips and dried for 30 minutes to overnight in the dark.

The morphology of cells was examined under fluorescence microscope with DIC optics (Olympus, Tokyo, Japan) using 40X objective lenses. The number of mRNA transcripts revealed by the RNAscope protocol was recorded as the fluorescent-spot counts in microscopic images. The per-cell copy number was determined by dividing the total spot count by the number of cells counted. Images were taken using an Olympus IX71 fluorescent microscope and a PXL37 CCD camera (Photometrics, Tucson, AZ).

This system has far greater ability to detect the expression of a transcript than earlier methods using digoxigenin-labeled probe sequences that were novel in the 1990s [26, 135].

4 % Paraformaldehyde

Dissolve 4 g Paraformaldehyde in 100ml preheated 1X PBS (~ 50-70 °C), turn off the heat. Paraformaldehyde will take a while to dissolve. Stir continuously, heat gently and add a couple of drops of 1M NaOH to assist dissolution, pH to 7 using pH strip. Leave it in fume hood to cool down, filter using filter paper, store solution at 4°C. This solution is good for 2 weeks.

Cryoprotectant protocol for storage of frozen sections

To prepare 500 ml 0.1M PB, first add 500 ml of distilled water in a suitable container, then add 5.1 g of Sodium phosphate dibasic heptahydrate and 1.6 g of Sodium phosphate monobasic monohydrate to the solution. Next, add 150 g Sucrose to be dissolved and as the last step add 500 µL Sodium Azide to the solution.

Working Lysis Buffer Solution

Solution	Final Concentration in Solution	Stock Concentration
Pepstatin A	1.0µM	0.001M (1mM)
Dithiothreitol (DTT)	0.5mM	1M

To make up 10mL working Lysis Buffer Solution

10mL pre-lysis buffer

5µL stock DTT (Make fresh daily, see below)

10µL Pepstatin A (25µL aliquots in -20 hallway)

Stock DTT

0.015425g DTT (in 4C RNA freeze)

250µL ddH₂O

Pepstatin A stock

Mix 9mL methanol and 1 mL acetic acid

Add 7.29mL to 5mg pepA, concentration = 0.001M

Recipe for 9% gels

Separating gel solution (10ml)

4.3 ml dH₂O
3 ml acrylamide (30%T, 2.7% C)
2.5 ml 1.5M Tris (pH 8.8)
100 µL 10% SDS

Stacking gel solution (2ml)

2.4 ml dH₂O
500 µL acrylamide
1000 µL 1.0M Tris, pH 6.8
40 µL 10% SDS

1) Acrylamide (30%) 14.6 g Acrylamide

0.4 g N'N'-bis-methylene-acrylamide

Dissolve in 30 mL ddH₂O. Make up to 50 mL with ddH₂O. Filter. Cover bottle with aluminum foil and store at 4° C for a Maximum of 30 days.

2) Tris buffers (500ml) 1.5M Tris buffer

90.8 g Tris

Dissolve Tris in 250ml milliQ water, adjust to pH 8.8, then bring to 500ml don't autoclave. Store in 4 °C.

1 M Tris buffer

60.55 g Tris

Dissolve Tris in 250ml milliQ water, adjust to pH pH6.8, then bring to 500ml don't autoclave. Store in 4 °C.

3) 10% Ammonium Persulfate (APS)

Dissolve 100 mg (0.1 g) of ammonium persulfate in 1 mL ddH₂O (can be done in weighing boat). Prepare fresh daily or we can prepare early and freeze it. One Aliquot can be used three times.

4) 10 % SDS

10g SDS dissolved in 70 mL ddH₂O with gentle stirring; May

need to heat to 68° C to aid dissolution, bring to 100 mL with ddH₂O.

5) 2X Sample Prep Buffer (SPB)

For 50 ml 2XSPB

100mM DDT	0.77 g
4% SDS	2 gram
0.16 M Tris-HCl (pH 6.8)	8 ml (1M Tris, pH 6.8)
43% glycerol	21.5 ml
0.2% Bromophenol Blue	0.1 g

6) Running buffer (10X) 32.5 g Tris Base

144 g Glycine

10 g SDS

Dissolve in 500ml ml milliQ water, then bring to 1000ml.

7) Transfer buffer OR Blot Buffer (1X)

5.82 g of Tris

2.93 g of Glycine

200 ml of methanol

Add methanol after dissolving everything and make up to 1L by adding ddH₂O

8) 10X PBS

To make up 1 liter

NaCl 80 g

KCl 2 g

Na₂HPO₄·7H₂O 26.8 g

KH₂PO₄ 2.4 g

Dissolve in 800 ml Milli-Q H₂O

Adjust pH to 7.4

Bring volume to 1 liter, autoclave or sterile filter

Working Solution (0.01M or 1X): For 1 liter of 1X PBS, mix 100ml 10XPBS with 900ml ddH₂O).

9) PBS-T

1 x PBS (Dilute if form 10 x PBS with milliQ water)

Add 0.1% Tween 20 (1000 μ L/1L 1X PBS)